MULTI-SCALE MODELLING OF LONG-SPAN BRIDGES FOR HEALTH ASSESSMENT IN STRUCTURAL HEALTH MONITORING

Yang YU

Ph.D

THE HONG KONG POLYTECHNIC UNIVERSITY

2012

THE HONG KONG POLYTECHNIC UNIVERSITY

DEPARTMENT OF CIVIL AND ENVIRONMENTAL

ENGINEERING

Multi-scale Modelling of Long-span Bridges for Health Assessment in Structural Health Monitoring

by

Yang YU

A thesis submitted in partial fulfillment of the requirements for the

Degree of **Doctor of Philosophy**

March 2011

To my family

CERTIFICATE OF ORIGINALITY

I hereby declare that this thesis is my own work and that, to the best of my knowledge and belief, it reproduces no material previously published or written, nor material that has been accepted for the award of my other degree or diploma, except where due acknowledgement has been made in the text.

_____ (Signed)

YU Yang (Name of student)

ABSTRACT

Nowadays long-span bridges are usually modeled in different length scale levels for various research purposes. An accurate model should concurrently use the different theories at the respective scale level. The work described in this thesis aims to develop the effective strategies and methodologies for multi-scale finite element modeling of long-span steel bridges for health assessment and demonstrate its efficiency through analytical and experimental case studies as well as the practical engineering applications.

The strategy and methodology of multi-scale modeling is successfully proposed and numerically implemented using mixed dimensional coupling through multi-point constraint equations. The reduced-scale specimen of the longitudinal steel truss has been studied in analytical computation and laboratory test. The comparison between the calculated results by different models and measurements data as well as the analytical results comparison with ones by other modeling methods suggest the proposed multi-scale model is the most efficient and accurate. All the strategies and implementation methods have been generalized and considered as applicable to full-scale long-span bridge structure.

As an actual engineering application, a multi-scale model of long-span bridge of Tsing Ma Bridge is then developed by incorporating local detailed model of concerned location into structural global model based on proposed multi-scale

modeling strategy. Structural global response at component scale and the hot-spot stress distribution of critical locations at local scale are then obtained simultaneously that can be used for structural health assessment and damage-related analyses. After performing sensitivity-based model updating and verification, the comparison results indicates that the developed multi-scale model is superior as compared to traditional two-step analyzing method.

To demonstrate the developed multi-scale model can be further extended for nonlinear analysis, the linear and nonlinear seismic responses of the bridge under El-Centro ground motion are investigated considering geometric nonlinearity and bilinear hysteretic constitutive model. There are no universal principles to describe the influence pattern of traveling wave, so such effects should be specifically investigated for an individual bridge. The implementation schemes for nonlinear damage-related analyzing procedures are finally explored and outlined by introducing a nonlinear computing algorithm of constitutive equations combined with proper damage laws to consider the structural deterioration process.

LIST OF PUBLICATIONS

Yu, Y., Chan, T. H. T., Sun, Z. H. and Li, Z. X. (2012), "Mixed-dimensional consistent coupling by multi-point constraint equations for efficient multi-scale modeling", *Journal of Advances in Structural Engineering*, 15(5), 837-853.

Yu, Y., Yin, A. G., Qian, F. and Li, Z. X. (2008), "Experimental research on static and dynamic responses of steel truss with local welding details", *Journal of Experimental Mechanics*, 23(5), 377-386 (in Chinese).

Yu, Y., Chan, T. H. T. and Li, Z. X. (2006), "Typhoon-induced accumulated fatigue damage evaluation using health monitoring data", *Proceedings of 3rd International Conference on Protection of Structures Against Hazards*, Sept.28-29, 2006, Venice, Italy, 293-302.

Chan, T. H. T., Li, Z. X., **Yu, Y.** and Sun, Z. H. (2009), "Concurrent multi-scale modeling of civil infrastructures for analyses on structural deteriorating-Part II: model updating and verification", *Journal of Finite Element in Analysis and Design*, 45(11), 795-805.

Chan, T. H. T., Ashebo, D. B., Tam, H. Y., **Yu, Y.**, Chan, T. F., Lee, P. C. and Gracia, E. P. (2009), "Vertical displacement measurements for highway bridges using optical fiber sensors and CCD cameras: a preliminary study",

Structural Health Monitoring, 8(3), 243-247.

Chan, T. H. T., **Yu, Y.**, Wong, K. Y. and Li, Z. X. (2008), "Condition-assessment-based finite element modeling of long-span bridge by mixed dimensional coupling method", *Proceedings of the 3rd World Congress on Engineering Asset Management and Intelligent Maintenance System* (WCEAM-IMS 2008), October 27-30, 2008, Beijing China, 260-270.

Chan, T. H. T, **Yu, Y.**, Wong, K. Y. and Guo, L. (2007), "A multi-scale finite element model of Tsing Ma Bridge for hot spot stress analysis", *Proceeding of International Conference on Health Monitoring of Structure, Material and Environment*, Oct.16-18, 2007, Southeast University, Nanjing, China, 130-140.

Li, Z. X., Chan, T. H. T., **Yu, Y.** and Sun, Z. H. (2009), "Concurrent multi-scale modeling of civil infrastructures for analyses on structural deteriorating-Part I: modeling methodology and strategy", *Journal of Finite Element in Analysis and Design*, 45(11), 782-794.

Li, Z. X., Zhou, T. Q., Chan, T. H. T. and **Yu, Y.** (2007), "Multi-scale numerical analysis on dynamic response and local damage in long-span bridges", *Engineering Structures*, 29(7), 1507-1524.

Li, Z. X., Sun, Z. H., Guo, L., Chan, T. H. T. and **Yu, Y.** (2007), "Concurrent multi-scale modeling of structures and damage analyses", *Journal of Southeast University* (Natural Science Edition) 37(2), 251-260 (in Chinese).

Yu, Y., Li, Z. X. and Chan, T. H. T., "Concurrent multi-scale modeling of civil infrastructures for analyses on structural deterioration and its application to a large-span bridge" (to be submitted).

ACKNOWLEDGEMENTS

First of all, my deepest gratitude goes to my chief supervisor, Prof. Tommy H.T. Chan for his valuable guidance and high sense of his responsibility, and dedication of his time throughout my studying periods staying in both Hong Kong and Nanjing. I deeply appreciate his effort to providing the unique opportunity and freedom to pursue my study. I have been impressed by his deep insights into scientific problems, his conscientious and meticulous attitudes to research and his professional ethics, which benefit me inexhaustibly in my future career. I also wish to express my heartfelt gratitude to my co-supervisor, Prof. LI Zhaoxia of Southeast University for her continuous support and persistent encouragement throughout the course of this research. Her valuable suggestion, profound insight and high dedication have been the constant source of inspiration for my study.

Secondly, sincere appreciation goes to the Highways Department of Hong Kong SAR Government for their continuous support throughout the project. Special thanks are also due to Dr. K.Y. Wong of the Department for his valuable and useful advices. The kind assistance and helpful suggestions of Mr. HUANG Yueping when performing laboratory test in Southeast University are also gratefully acknowledged.

In addition, I am very grateful to Post-doctor YU Ling for his continuous advice

and encouragement. Special thanks are also extended to my friends and fellow colleagues. I particularly thank Prof. SHI Zhiyu, Dr. HUA Fengling, Dr. FEI Qingguo, Dr. YANG Jie, Dr. CHEN Bo, Dr. HUA Xugang, Dr. DUAN Yuanfeng, Dr. CHEN Juan, Dr. ZHAO Xing, Dr. LUO Chunling for their constructive discussion and kind assistances during my stay in Hong Kong. Also special thanks would be given to the Prof. HAN Xiaoling, Dr. GUO Li, Dr. SUN Zhenghua for their helpful discussions when I continued my research in Southeast University.

I appreciate to the financial supports from the RGC project and additional research funding for years throughout the whole studying period. The kind help of staff in the university library, relevant administrative offices, and general office of Department of Civil and Structural Engineering are also appreciated.

Last but not least, I especially express my deepest gratitude to my wife, WANG Yizhou, for her understanding, encouragement and patience for these years. Also I am deeply grateful to my family members for their constant love and strong support throughout my study.

TABLE OF CONTENTS

LIST OF FIGURES

LIST OF TABLES

CHAPTER 1

INTRODUCTION

1.1 BACKGROUND AND MOTIVATION

Served as a symbol of our present highly industrialized society, civil infrastructures, which include bridges and building structures, begin to deteriorate once they are built and used. It is then important to determine the integrity of a structure in term of its age and usage, and level of safety and reliability for daily use in order to prevent catastrophic events (Chang *et al*. 2003). The primary objective of engineers is to ensure the safety and health conditions of those facilities that are constructed for the general public. Much work has been carried out towards this objective. Structural Health Monitoring (SHM) (Aktan *et al*. 1998; Farrar, Sohn and Doebling 2000a; Housner *et al*. 1997), earlier defined as a process that could involve a damage detection strategy for aerospace, civil and mechanical engineering infrastructures, has attracted considerable attentions in recent years. Here structural damage is usually defined as changes of the material and/or geometric properties of these systems, including those changes of the boundary conditions and system connectivity, which would adversely affect the current or future performance of that system. However, the damage detection

strategy may not be necessarily included in the SHM strategy. Chan *et al*. (2011) further defines SHM as "the use of on-structure sensing system to monitor the performance of the structure and evaluate its health state" to distinguish SHM from damage detection.

As for extracting damage-sensitive features from measurement and determining the structural state or detecting damage, there has been many works, including some review papers (Doebling *et al*. 1996, 1998; Farrar and Sohn 2001a; Friswell and Mottershead 2001) and several conferences dedicated to this topic (Dublin 1999; Newport Beach 2001; Palo Alto 2001). Advances in damage detection methods utilizing measurements from SHM have been proposed over the last two decades, as for the global SHM of bridges, could be divided into two major categories: 1) damage detection from changes in the vibration characteristics of the structure (Doebling *et al*. 1998), and 2) damage detection based on vibration-based model updating (Fritzen and Jennewein 1998; Friswell and Mottershead 1995). Most of those damage detection techniques related to global SHM proposed in these references examine changes in modal properties (frequencies and mode shapes), or changes in quantities derived from modal properties. Other common features using vibration-based detection studies include changes in structural model parameters (elemental stiffness values) resulting from model updating procedures, non-model based time-history and spectral pattern methods, and methods based on the nonlinear and/or non-stationary response introduced by the onset of damage.

As well known amongst researchers working in this field, the damage state in a structure can be described in terms of five different levels (Stubbs *et al*. 2000) as follows: 1) Is there damage in the structure (existence)? 2) Where is the damage in the structure (location)? 3) What kind of damage is present (type)? 4) How severe is the damage (extent)? and 5) What about the impact of the damage on the structure, or How much useful life remains (prediction)? Answering these questions in the presented order represents increasing knowledge of the damage state. There are many methods developed for damage detection which can detect the existence of damage in a structure. Vibration-based damage identification methods that do not make use of a structural model can only address the first two questions. When vibration-based methods are coupled with a structural model, question 4 can be obtained in some cases, while the solution to questions 3 and 5 is generally associated with more accurate and physical-based modeling of structural damage behavior by applying the theory of continuum damage mechanics, fracture mechanics, and so on (Krazig and Petryna 2001).

The basic assumption of these vibration-based damage detection methods is that damage will significantly change the stiffness, mass or energy dissipation properties of the system, which will in turn alter the measured dynamic responses of that system. Although the basis appears to be intuitive and there have been many works for damage detection methods, many issues are still controversial and the researchers are still working on exploring reliable SHM strategies which are robust enough to be put into practical use in the large-scale civil engineering

structures. Some problems with structural damage detection have been found in the existing methods, such as identifying damage-sensitive features from the measured responses using sparsely-instrumented sensing system, and most of studies assume that the structure can be modeled as a linear system before and after damage; and so on (Farrar and Sohn 2001b). Among these serious limitations on the practical use of existing methodologies, the most fundamental challenge is the fact that damage is typically a local phenomenon and may not significantly influence the lower frequency of global response of structures, which is normally measured and identified through ambient vibration tests.

In spite of the fact that some advances have been achieved for structural damage detection with SHM in the past years, more and more researchers come to realize that the damage detection method has stepped into the “bottleneck” stage and only effective for the user-defined case-special scenario instead of universal purpose for the complicated large-scale engineered systems. Its actual application in large structures still poses many significant technical challenges, some of which are related to the inherent properties of structures and have become serious limitations on the practical use of the methods. For instance, linear techniques based on modal properties are usually used to detect local damage whereas the global nature of the structure associated with lower frequency is somewhat insensitive to local damage. In fact, many damage mechanisms, such as cracks, the degradation of material, and geometric properties as well will produce non-linear effects. Anyway, structural failure is a consequence of accumulated

structural damage originating from local material damage. All these indicate that the damage detection approach may not be effective in the SHM of large complicated civil structures.

As an important component of civil infrastructure, the modern large-span cable-supported bridges with increasing span length, are normally designed to have a long service life. More and more in-service or to be built long-span bridges are subjected to different variable-amplitude traffic loadings in complicated patterns everyday. Moreover, service loads, environmental and accidental actions may cause damage to bridge structures. Meanwhile, we need to recognize the distinctions between such "constructed" and "manufactured" engineering systems in term of size, cost, lifecycle, and variability in material properties, and also the uncertainties in identification of operating and loading environment. In addition, the material deterioration and structural damage could make bridge components unserviceable and even might lead to the collapse of a bridge if damage develops to a significant level at last. The potential possibilities such as improper design and consideration, lack of inspection and maintenance, natural and man-made disasters of a bridge have been widely addressed and acknowledged in the literature by the bridge engineering community (e.g. Shepherd and Frost 1995). All those factors make continuous health monitoring or regular condition assessment of these important bridges absolutely necessary so that early identification and localization of any potential damage and condition assessment can be performed for structural health evaluation.

Current efforts on long-term SHM for large-span steel bridges are still considered as to limit to the observations and measurements on the operational environment and structural response. For instance, the SHM systems developed for Skarnsundet Bridge in Norway, New HaengJu Bridge in Korea, Storck's Bridge in Switzerland. The Wind And Structural Health Monitoring System (WASHMS) designed for the three bridges in Hong Kong, namely, the Tsing Ma Bridge, the Kap Shui Mun Bridge, and the Ting Kau Bridges, is probably the most heavily instrumented bridge project around the world, in which total of about 774 various kinds of sensors are permanently installed in bridges (Lau, Wong and Flint 2000).

Civil engineers are especially cognizant of the limitations in their current practice for condition assessment based on visual inspections. Besides regular condition assessment, typical routine applications of condition assessment are carried out on bridges or buildings for evaluating seismic vulnerability or post-earthquake damage, and to all types of facilities after overloading of accidents. However, the community has been aware of the limitations and shortcomings of visual inspection are that it is often very difficult to establish the correlation between visual appearance and structural reliability for safety (Catbas *et al*. 2002a). Engineers need to know more about the actual cause of damage or distress and its impacts on structural reliability in order to make meaningful management decisions. Therefore, the practical procedure of condition assessment is usually considered as largely relying on a constructed finite element model as closest to real condition as possible so that it is capable of considering the major effect of

the damage, locally deteriorating processes and nonlinear influence on structural response. From this point of view, a nonlinear model for the damaged structure is imperatively needed so as to accurately simulate damage-related behavior since the small changes due to damage are likely to be more identifiable for nonlinear effects (Friswell and Mottershead 2001).

On the other hand, the long-span bridge modeling is usually of the order of magnitude of kilometres while welded details vulnerable to damage and cracks initiated locations due to localized stress concentration are modeled in meters. It is obviously unreasonable to numerically model and analyze the global and local behaviors of response and damage in a unified spatial scale. In practical numerical analysis of such a large structure on the global level, the majority of finite element models are usually constructed as a "fish-bone" model which treats one component as one element with the lower dimensional type. However, for the purposes of fatigue analysis and condition assessment, more attentions should be paid on the local detailed characteristics with the higher dimensional type elements which are not represented in the aforementioned global model. In this sense, it would be desirable to construct the global model at the structural scale with reduced or lower dimensional elements and incorporate model of local concerned details at the local scale with the higher dimensional ones in a single model to simultaneously account for the structural responses at different spatial scale levels.

Therefore it is essential to develop a numerical method in multiple spatial scales

for the damage analysis and condition assessment of civil infrastructure considering structural deteriorating process. An efficient multi-scale modeling strategy is firstly proposed in this thesis. The mixed dimensional coupling method by constraint equations for the effective connection is then introduced. The experimental and numerical studies on the steel truss specimen which is scaled down model of critical section extracted from an existing long-span bridge, have been carried out to verify and validate the developed multi-scale modeling strategy and implementation methods. After successful application on the scaled down model, the general multi-scale modeling procedure has also been proposed and applied to the full-scale bridge structure. Finally a multi-scale model of a long-span suspension bridge of Tsing Ma Bridge (TMB) is thus developed accordingly. The developed multi-scale model is further updated on the basis of sensitivity-based model updating method with parameter constraints, and then verified on dynamic characteristics and static responses by comparing the calculated values with measurement data in terms of the first few natural frequencies and the vertical displacement influence line. After updating and validating the multi-scale model, the structural global response at component scale and the hot-spot stress distribution of critical locations at local scale level could then be obtained simultaneously to serve the respective research purposes. Moreover, this multi-scale model could be further extended for nonlinear analyzing process by incorporating the various constitutive equations to describe the different mechanical behaviors. Also the constitutive formulation combined

with the different damage laws could be considered for structural deterioration process to obtain the real stress values closer to the actual situation. In addition, with the help of monitoring data acquired from the SHM, the multi-scale model is able to predict the stresses at those critical locations where there are no sensors installed. Finally, those stresses information-obtained from SHM and predicted stresses, could be further used for future research of evaluating the health status of the engineering structure.

1.2 OBJECTIVES

The main objectives of this Ph.D study are to develop a simulation strategy for multi-scaled modeling of long-span steel bridges to simultaneously output the structural responses at the different length scales for the purpose of health assessment in structural health monitoring. The developed multi-scale model is able to concurrently provide the structural overall response at the structural level and hot-spot stress distribution at the local level. This multi-scale model can be further extended for nonlinear analysis by introducing the nonlinear computing algorithm. With the help of monitoring data from the SHM, the developed multi-scale model and the approach will be applied to the state assessment of an existing suspension steel bridge, and further to the development of the structural health monitoring of a future suspension steel bridge.

All the research work within this scope will be focused on multi-scale modeling

of long-span steel bridge which would be achieved by completion of the following objectives:

Objective 1 – Development of a multi-scale modeling strategy and implementation method

For large civil infrastructure, the structural model is usually constructed on the basis of the component level while the damage is prone to be occurred at the local details that are at the different length scale levels. It is well known that many damage mechanisms, such as cracks or degradation of structural connections, occur locally at material points which will in turn influence the entire structural behavior, contribute to global structural damage, and possibly cause structural failure subsequently. An accurate model for simulating such behavior should incorporate the physical mechanism of local damage into global structural analysis. Multi-scale modeling is then considered as absolutely necessary for accurate representation of system response on both length scales.

Objective 2 – Study of concurrent structural component response on global scale and local hot-spot stress distribution on material scale

The correspondingly developed multi-scale model could be used for multi-scale numerical analysis for global dynamic response and local damage of long-span bridges. Structural component responses on the global scale can be obtained by linear computation. Meanwhile, the local hot-spot stress distribution could be simultaneously acquired. The hot-spot stress distribution would be the basis for

the subsequent fatigue damage analysis and condition assessment of engineering structures.

Objective 3 – Feasibility study on the extension of the developed multi-scale model for nonlinear analysis

After completing the multi-scale modeling strategy and methods combined with developed TMB multi-scale model, this multi-scale model could be extended for nonlinear analysis. Geometrical and material nonlinearities could be considered in the local detailed model when applying the nonlinear computing algorithm. Damage-related analysis is also able to be performed with introducing the constitutive formulations with damage variable to simulate the structural deterioration process. The corresponding nonlinear computing algorithms and implementation method are eventually explored and attempted to propose for future research.

The multi-scale model of TMB could be developed based on the proposed multi-scale modeling strategy as stated as the first objective. Structural overall response at the structural level and hot-spot stress distribution at the local level could be then simultaneously obtained by the developed multi-scale model for achieving the second objective. The approaches used in nonlinear numerical analysis for simulating structural deterioration behavior would be illustrated by objective three. The first two objectives are the main objectives to be achieved in this study while the third one clearly outlines an implementation method of

extending the developed multi-scale model for nonlinear analysis for the future research.

1.3 SIGNIFICANCE AND VALUE

The possible outcomes of the study and its relevance, significance and value are summarized below:

(1) The proposed multi-scale modeling strategy and implementation method will provide a framework for close attentions to structural responses at one or more length scale levels.

(2) The verification and updating procedures on scaled-down steel truss specimen can also be summarized as the general procedure for application to the full-scale long-span bridge structure.

(3) The structural overall response at the global scale and hot-spot stress distribution could be obtained simultaneously with the developed multi-scale model, which is considered as superior as compared to the traditional two-step analysis.

(4) The developed multi-scale model could be further extended for nonlinear analyzing procedure with proper introducing nonlinear computing algorithm, and it can also be used to simulate the structural deterioration

process by incorporating the constitutive formulation combined with desirable damage law for future research.

1.4 OUTLINE OF THE THESIS

This dissertation comprises seven chapters and the outline is given as follows:

Chapter 1 introduces the background and motivation for the present study and states the objectives to be achieved in this Ph.D program. Also the possible significance and values of this study are proposed.

Chapter 2 contains the literature review on existing research work related to following topics: structural health monitoring, damage identification methods, finite element modeling and model updating methods, multi-scale modeling and simulation, fatigue damage analysis of steel bridges and mixed dimensional coupling in finite element analysis. After an introduction of general concept of structural health monitoring, damage identification methods are briefly surveyed. Subsequently finite element modeling and fatigue damage analysis of long-span bridges are reviewed. Multi-scale modeling and simulation are then briefly introduced. Lastly the mixed dimensional coupling methods for multi-scale modeling are presented. In the end, the critical issues and shortcomings of existing methods are discussed.

Chapter 3 focuses on the development of multi-scale modeling strategy and

implementation methods. Concept of concurrent multi-scale modeling is firstly introduced with necessity and physical description. Multi-scale modeling implemented by mixed dimensional coupling between beam and shell elements is then investigated and implemented through constraint equations on the interface. Preliminary numerical simple case studies in both determinate and indeterminate structures are finally performed to verify and validate the proposed multi-scale modeling strategy and methods.

Chapter 4 presents the experimental and analytical case study of a typical steel truss section. A scale-down steel truss section of prototype from an existing long-span bridge structure is experimentally tested in the laboratory for dynamic characteristics and static response tests. The results comparison of different analytical models and measurements are in good agreement at the aspects of dynamic characteristics, nominal stress and hot-spot stress distribution. The developed FE model is then further updated and verified on the basis of measurement data. At last the general procedures of multi-scale updating and verification are stated.

Chapter 5 describes the development of a multi-scale model of the long-span suspension Tsing Ma Bridge on the basis of aforementioned multi-scale modeling strategy. A 3D FE model on the global scale is firstly constructed, and identified critical component at the longitudinal truss with connection details is then modeled in details and incorporated into the structural global model to obtain the multi-scale model. After model updating and verification procedure, the

comparison result indicates that the proposed multi-scale model is more accurate and efficient for the simultaneous output of structural global response on component scale and hot-spot stress distribution of critical region on local component.

Chapter 6 states the extension of the developed multi-scale model of TMB for nonlinear analyzing procedure. Nonlinear computing algorithm is proposed on the basis of multi-scale model for dynamic response of long-span bridges. Geometric nonlinearity could be considered in calculation while material nonlinearity is taken into account by introducing the constitutive equations for steel. The linear and nonlinear seismic responses of TMB by multi-scale model under the El-Centro earthquake wave are studied. Traveling wave effect on the seismic response is also investigated. Constitutive relationship associated with various damage laws could be incorporated into the nonlinear computing algorithm to consider the structural deterioration process through damage variable for future research. Nonlinear response analysis by multi-scale model is eventually summarized in general procedure.

Chapter 7 summarizes the contribution, findings and conclusions from the present work in this study. Due to the limitation of time and author's research scope, there are still many aspects of research work should be further investigated. Some recommendations for the future work are finally presented.

CHAPTER 2

LITERATURE REVIEW

2.1 GENERAL CONCEPTS AND OVERVIEW

2.1.1 Overview of Structural Health Monitoring

Civil infrastructures, which include building and bridge structures, begin to deteriorate once they are built and used. Maintaining safety and reliability of civil infrastructures for daily use is important to all of us. Knowing the integrity of a structure in terms of its age and usage, and its level of safety to withstand infrequent but high forces such as overweight trucks, earthquakes, tornadoes, and hurricanes seems to be important and necessary.

The process of implementing a damage detection strategy for aerospace, civil and mechanical engineering infrastructure is referred to as Structural Health Monitoring (SHM). Here damage is defined as changes to the material and/or geometric properties of these systems, including changes to the boundary conditions and system connectivity, which adversely affect the system's performance (Farrar *et al*. 2001a). According to the definition by Housner *et al*. (1997), structural health monitoring is defined as "the use of *in-situ*,

nondestructive sensing and analysis of structural characteristics, including the structural response, for the purpose of identifying if damage has occurred, determining the location of damage, estimating the severity of damage and evaluating the consequences of damage on the structures".

Ideally, health monitoring of civil infrastructure consists of determining, by measured parameters, the location and severity of damage in the structures as they happen. Currently, these methods that can only determine whether or not damage is present in the entire structure are referred to as "global health monitoring" methods. They are very important because whether or not the damage has occurred is all that one needs to know in the first place, based on which further examination of the structure to find the exact location and severity of the damage can be taken. Most global health monitoring methods are centered on either finding shifts in resonant frequencies or changes in structural mode shapes. The premise that changes in the dynamic characteristics of a structure indicates damage is masked by the fact that temperature changes, moisture and other environmental factors also produce changes in dynamic characteristics. If the causes of changes in dynamic characteristics other than damage are considered to be noise in the measurement, then the changes due to damage must be significantly larger than the noise in order for the techniques to work.

Assessing the structural condition without removing the individual structural components is known as Nondestructive Evaluation (NDE) or nondestructive inspection. NDE techniques include those involving acoustics, dye penetrating,

eddy current, emission spectroscopy, fiber - optic sensors, fiber - scope, hardness testing, isotope, leak testing, optics, magnetic particles, magnetic perturbation, X-ray, noise measurements, pattern recognition, pulse-echo, radiography, and visual inspection, etc. (Zong *et al*. 2002). Most of these techniques have been used successfully to detect location of certain elements, cracks or weld defects, corrosion/erosion, and so on. These methods are "local health monitoring" methods. NDE is often time consuming and expensive, and access is not always possible. Therefore, both global and local health monitoring methods are necessary. In a word, global methods attempt to simultaneously assess the condition of whole structure whereas local methods focus NDE tools on specific structural components. These two approaches are complementary to each other.

Another important use of health monitoring is to estimate the service condition and the remaining service life of a structure. Recorded data for strain on supporting members of a bridge can be used to obtain vehicle weight (weigh-in-motion), vehicle count, environment conditions such as wind load and temperature variations (Chang *et al*. 2003). These data in turn can be used to help estimate the structure's safety and reliability. Currently in the US, more bridges are being replaced because of their functionally obsolete than being structurally unsound.

Structural health monitoring is primarily for owners and clients of bridges but also will be useful to designers, contractors, researchers, and management and maintenance organizations. The general objectives and potential benefits of

establishing a SHM system are summarized as (Moss and Matthews 1995a, 1995b; McGown *et al*. 1997a, 1997b; Maguire 1999): (i) to validate the assumptions and parameters adopted during design of bridges with the potential benefit to improve design standards, specifications, codes, and guidelines; (ii) to monitor geometrical configuration and the stress of bridges during their construction with potential benefits to improve construction method, construction material, and workmanship; (iii) to ensure structural and operational safety during the service life of bridges and provide real-time data and information on structural condition during natural and man-made disasters for timely and effective response; (iv) to facilitate and optimize the maintenance and rehabilitation of bridges when necessary; and finally (v) to provide large amounts of raw data for leading-edge research fields of bridge engineering, such as wind resistant design, seismic resistant design.

The development of structural health monitoring for surveillance, evaluation and assessment, maintenance and management of existing or newly-built bridges has now attained some degree of maturity. Furthermore, structural health monitoring has evolved from monitoring paradigm to go far beyond data collection and limited processing to include smart or intelligent sensors, local data storage and transmission systems, central data management systems, local (embedded) or central data analysis, reporting and alarming, diagnosis with respect to structural knowledge and prognosis on future performance, providing powerful means to maintenance and management of bridges.

Due to the great promising and potential benefits of SHM, this emerging and

fertile research field has brought together worldwide researchers, customers, industrial partners, and government agencies who have responsibilities to manage and maintain bridges from diverse disciplines including civil, mechanical, electrical, material, and computer engineering to study various issues of structural health monitoring including smart/intelligent sensor, wireless communication, information technology, data management and data mining, system identification, damage identification, reliability assessment, and bridge condition assessment through the increasing numbers of international journals, conferences, workshops, proceedings, publications and research projects. Some of them are Journal of Structural Health Monitoring, Journal of Structural Durability and Health Monitoring, Journal of Intelligent Material Systems and Structures, International Workshops on Structural Health Monitoring (Chang, F. K. edt. 1997, 1999, 2001, 2003), European Workshops on Structural Health Monitoring (Balageas 2002; Boller and Staszewski 2004), International Workshop of Structural Health Monitoring of Innovative Structures (Mufti 2002), International Conference on Structural Health Monitoring and Intelligent Infrastructure (Wu and Abe 2003), Annual Symposia on Smart Structures and Materials, European Conferences on Smart Structures and Materials, World Conferences on Structural Control, International Modal Analysis Conferences, and others (Cheung 2000; Auweraer and Peeters 2003), Structural Health Monitoring: Current Status and Perspectives (Chang, F. K. edt. 1997), Structural Health Monitoring: Advancements and Challenges for Implementation (Chang, F. K. edt. 2005) and etc.

Although the development in SHM systems for large-span bridges only lasts for few decades, successful implementation of innovative SHM system would lead to significant safety reliability improvement, downtime minimization, effective evacuation during natural and man-made disasters, operation and maintenance cost reduction, avoidance of catastrophic structural failure, development and improvement in design standards, specifications, codes, and guidelines. Development of reliable SHM systems for large-span bridges is a challenging task and requires advancement through innovative techniques.

2.1.2 Structural Health Monitoring Process

The SHM process involves the observation of a system over time using periodically sampled dynamic response measurements from an array of sensors, the extraction of damage-sensitive features from these measurements, and the statistical analysis of these features to determine the current state of system health (Farrar *et al*. 2001a). For long-term SHM, the output of this process is periodically updated information regarding the ability of the structure to perform its intended function in light of the inevitable aging and degradation resulting from operational environments. After extreme events, such as earthquakes or blast loading, SHM is used for rapid condition screening and aims to provide, in near real time, reliable information regarding the integrity of the structure. In general, a structural health monitoring system has the potential to provide both damage detection and condition assessment of a structure (Farrar *et al*. 2001b).

Current SHM methods are either visual or localized experimental methods such as acoustic or ultrasonic methods, magnetic field methods, radiograph, eddy-current methods and thermal field methods (Doherty 1987). All of these experimental techniques require that the vicinity of the damage is known a priori and that the portion of the structure being inspected is readily accessible. The need for quantitative global damage detection methods that can be applied to complex structures has led to research into damage detection methods that examine changes in the vibration characteristics of the structure. The basic premise of these global SHM methods is that damage will alter the stiffness, mass or energy dissipation properties of a system, which, in turn, alter the measured dynamic response of the system. Summaries of this research can be found in recent review articles (Doebling *et al*. 1998; Housner *et al*. 1997). To date, most global SHM techniques proposed in these references examine changes in modal properties (resonant frequencies, mode shapes), or changes in quantities derived from modal properties.

Taken as a whole, the aforementioned characteristics pose serious limitations on the practical use of existing methodologies. Indeed, there are actually no real examples of reliable strategies for SHM that are robust enough for practical use. The goal of SHM research effort is to identify an appropriate application for SHM technology and then to develop a robust and cost-effective SHM system specific to particular civil infrastructure by integrating and extending technologies from various engineering and information technology disciplines (Farrar *et al*. 2000a).

The SHM problem is acknowledged fundamentally as a statistical pattern recognition. Therefore, the damage detection studies are summarized in the context of a statistical pattern recognition paradigm. In this paradigm, the SHM process can be divided into four parts: (1) operational evaluation, (2) data acquisition and cleansing, (3) feature extraction and information condensing, and (4) statistical model development for feature discrimination (Farrar and Doebling 2001c). When one attempts to apply this paradigm to data from real world structures, it seems to be apparent that the ability to cleanse, compress, normalize and fuse data to account for operational and environmental variability is a key implementation issue when addressing parts 2-4 of this paradigm. These processes can be implemented through hardware or software and, in general, some combination of these two approaches will be used.

However, SHM is a relatively new term for civil engineering application, and even a single definition has yet to be standardized. According to Aktan's suggestion (Aktan *et al*. 2002), SHM is the tracking of any aspect of a bridge's health status by reliably measured data and analytical simulations in conjunction with heuristic experience so that the current and expected performance of the bridge at least the most critical limit-events, can be described in a pro-active manner.

In Hong Kong, a sophisticated on-structure instrumentation system, Wind And Structural Health Monitoring System (WASHMS), has been devised and deployed by the Hong Kong SAR Government Highways Department to monitor

the structural condition and performance as well as evaluate condition of three long-span cable-supported bridges, namely Tsing Ma Bridge, Kap Shui Mun Bridge, and Ting Kau Bridge, under in-service conditions (Flint *et al*. 1995; Yeung *et al*. 1995; Lau *et al*. 2000; Wong *et al*. 2000a, 2000b, 2000c; Wong 2004), and two newly-installed SHM systems deployed for the cable-stayed Western Corridor and Stonecutters Bridges have been completed in Hong Kong (Wong 2004; Ko *et al*. 2005). The on-line monitoring system for the existing three bridges consists of over 800 sensors of different types, including accelerometers, strain gauges, displacement transducers, level sensors, anemometers, temperature sensors, weigh-in-motion sensors and global positioning systems, permanently installed on the bridges. This system accomplishes 24-hour continuous monitoring per day and the raw data is acquired at a rate of 63.46MB per hour for the Tsing Ma Bridge and Kap Shui Mun Bridge, and 55.87MB per hour for the Ting Kau Bridge, storing over one terabyte of data every year. Diagnosis and prognosis of structural condition of the bridges with continuous measurement data is one of major objectives to deploy such a system, which also provides the research background for this Ph.D study. It is worth mentioning that a gap between structural health monitoring and bridge management and maintenance still exists.

2.1.3 Condition Assessment of Civil Infrastructure Systems

Recently, there has been significant attention on structural health monitoring of

civil infrastructure systems (Chang 1997, 1999; Atkan and Gosselin 2000). To achieve the objectives, we may still expect a generic framework sharing many technologies and algorithms serving for health monitoring of all those systems. Civil engineers are especially cognizant of the limitations in their current practice for condition assessment based on visual inspections. Typical routine applications of condition assessment are carried out on civil infrastructure systems such as bridges, dams, and river navigational facilities, on buildings for evaluating seismic vulnerability or post-earthquake damage, and to all types of facilities after overloading, accidents, or when codes or use modes change. However, the community has long been aware of the limitations and shortcomings of visual inspection, and a recent investigation by the Federal Highway Administration (FHWA) on its lack of reliability has been especially conducted (FHWA 2001).

It seems to be difficult for the inspections to find signs of damage such as cracks, chemical deterioration, and corrosion before these become visible. However, the relation between such visible signs of damage and the corresponding “condition” or “reliability” of the structure is often very difficult to establish. There might be a dramatic difference in the meaning of a certain ‘‘visual damage’’ for a steel, pre-stressed, or an ordinary reinforced concrete bridge, and often, the effect may be observed but the decision making has to be carried out based on heuristics and experience. The cause may not be identified definitively. Engineers need to know the actual cause of certain damage or distress and its impacts on structural reliability in order to make meaningful management decisions. Most importantly,

discovery of deterioration before or at its onset, and not after it takes its course, is needed for cost-effective management (Enright and Frangopol 2000).

Many existing bridges have been deemed structurally deficient (Aktan *et al*. 1996). Despite the extent of the problem, the condition assessment of bridges is largely based on visual observations and described by subjective indices which do not permit accurate evaluation of bridge dynamics, serviceability and safety by incorporating the bridges' existing state and actual behavior. A significant amount of research has been performed on the condition assessment of existing bridges and relevant studies have accelerated in recent years. Aktan *et al*. (1996, 1997, 1998) describe an integrated experimental and analytical methodology for structural identification and field testing aimed at condition assessment of bridges, through consideration of defects, deterioration, damage, bridge state and performance. Saraf (1998) uses nondestructive load testing methods to evaluate three existing reinforced concrete bridges. Wahab and Roeck (1999) investigate the damage detection in bridges using curvatures of mode shapes. These investigations are carried out on the basis of the field testing and numerical analysis while the conditions of these bridges are still difficult to assess quantitatively because the deterioration and damage in the structure are difficult to describe mathematically. As a result, since the reliable assessment depends on quantitative rather than qualitative information, there is an urgent need and essential motivation to develop methodologies for objective and accurate condition assessment and reliability evaluation. The finite element (FE) model

updating method (Mottershead and Friswell 1993) which integrates finite element analysis (FEA) and experimental modal analysis (EMA) has emerged in the 1990s as a subject of great importance for mechanical and aerospace structures. This model updating techniques can produce a systematically validated FE model by correcting uncertainties form modeling, geometry, physical parameters, and analysis to improve the analytical results closing to the real values based on dynamically measured data. However, it is difficult to apply as an engineering tool because of the difficulties in prototype testing and experimental data analysis resulting from the nature, size, location and usage of these structures. Recently, the civil engineering community has begun to apply the FE model updating methods. Its successful application to bridge condition assessment mainly depends on the interdisciplinary experience and skills of the analyst and its especial application to bridge structure is becoming more and more popular (Brownjohn *et al*. 2001).

Although considerable researches on condition assessment have been conducted, there are still fundamental issues to be resolved. Most research has been in the area of manufactured systems, and the distinctions between manufactured and constructed systems may not be well understood by researchers from mechanical and aerospace fields. Consensus definitions, measures and indices for performance, condition, damage, and health over the lifecycle of common types of constructed facilities and complete infrastructure systems are necessary for reliable condition assessment. Although drift, span deflection, crack width, and

stress level have been typically used for defining the onset of serviceability and damageability limit states for common constructed facilities, proven relationships between such measurable indices, and actual facility performance have not been established (Catbas and Atkan 2002b).

2.2 DAMAGE IDENTIFICATION METHODS

2.2.1 Classification of Damage and Damage Identification Methods

The effects of damage on a structure can be classified as linear or nonlinear (Doebling *et al*. 1998). A linear damage situation is defined as the case when an initially linear-elastic structure remains linear-elastic after damage. The changes in modal properties are a result of changes in the geometry and/or the material properties of the structure, but the structural response can still be modeled using linear equations of motion. Linear methods can be further classified as model-based and non-model based. Model-based methods assume that the monitored structure responds in some predetermined manner that can be accurately discretized by finite element analysis. Up to now, majority of the researches and their work mainly focus on the damage cases in linear manner.

Nonlinear damage is defined as the case when the initially linear-elastic structure behaves in a nonlinear manner after the damage has been introduced. These non-linear behaviors in structural response can also be attributed to the changes in geometry and material properties caused by damage. A typical example of

geometrically nonlinear damage is the formation of a fatigue crack that subsequently opens and closes under the normal operating vibration environment. Moreover, material nonlinear damage examples include nonlinear behavior exhibited by damaged polymers and delaminated multi-layer plates. If a structure exhibits moderate or severe nonlinearities, traditional damage identification methods are proved not to yield satisfactory results.

Another classification system for damage-identification methods defines four levels of damage identification, as follows (Rytter 1993):

• Level 1: Determination that damage is present in the structure

• Level 2: Level 1 plus determination of the geometric location of the damage

• Level 3: Level 2 plus quantification of the severity of the damage

• Level 4: Level 3 plus prediction of the remaining service life of the structure

The four levels reveal a proper sequence to assess the damage state step by step. To date, vibration-based damage identification methods that do not make use of some structural model primarily provide Level 1 and Level 2 damage identification. When vibration-based methods are coupled with a structural model, Level 3 damage identification can be obtained in some cases. Level 4 prediction is generally associated with the fields of fracture mechanics, fatigue-life analysis, or structural design assessment. Comparing with the five different stages defined in damage state by Stubbs (Stubbs *et al*. 2000) aforementioned, Rytter corresponds

his four levels to four stages and answers the corresponding questions respectively except for the damage type. Therefore, most of damage detection methods developed to date limit themselves to Level 1 to Level 3. For the further study, Level 4 requires the multi-discipline knowledge but they are still very limited.

Another category of classification for damage identification techniques makes the distinction between methods that are used for continuous monitoring of structural performance and methods that are applicable to the detection of damage caused by extreme events. As an example, a system that uses continuous or intermittent accelerometer measurements from sensors mounted permanently to a bridge is different in terms of instrumentation and data acquisition requirements from a system that does not acquire data except during and immediately following an earthquake or a hurricane. It should be noted that the primary distinction between these situations has to do with the sensors and data acquisition system requirements. Typically, the same types of analytical techniques can be applied to the data to determine the integrity of the structure.

2.2.2 Vibration-based Damage Identification Methods

According to the type of measurement data, damage detection methods can be classified as static-based methods and vibration-based methods. The commonly used vibration-based methods evaluate structural damage on the basis of the measurement changes in modal properties before and after damage occurrence.

As the modal properties can be identified through vibration tests, the vibration-based methods are therefore considered to be showing great promise for on-line SHM and have been studied extensively. According to Farrar and Doebling (Farrar *et al*. 1999), the most mature and successful application of vibration-based damage detection technology has been in the monitoring of rotating machinery. In efforts to extend this pattern recognition approach more widely, they suggest that the vibration-based damage detection problem is fundamentally one of statistical pattern recognition (Carden and Fanning 2004). All of these experimental techniques require that the vicinity of the damage is known a priori and that the portion of the structure being inspected is readily accessible. Subject to these deficiencies, the above methods can only detect damage on or near the surface of structures. In addition, these methods are inefficient when applied to large and complex structures. The need for global damage detection methods that can be applied to large and complex structures, such as cable-supported bridges, high-rise buildings, and offshore platforms, has led to the development and continued research of methods that examine changes in the global characteristics of structures (Doebling *et al.*1998), such as basic modal properties (resonant frequencies, modal damping and mode shape vectors), dynamically measured flexibility and updating structural model parameters (mass, stiffness, and damping).The basic idea remains that commonly measured modal parameters (notably frequencies, mode shapes, and modal damping) are functions of the physical properties of the structure (mass, damping, and stiffness).

Therefore, changes in the physical properties, such as reductions in stiffness resulting from the onset of cracks or loosening of a connection, will cause detectable changes in these modal properties. Because changes in modal properties or properties derived from these quantities are being used as indicators of damage, the process of vibration-based damage detection eventually reduces to some form of a pattern recognition problem.

As for the vibration-based damage detection methodologies, there have been developed various techniques ranging from the simple and straightforward comparison of damage index to the complicated statistical pattern recognition algorithms such as artificial neural networks (ANNs) and support vector machines (SVMs). Doebling *et al.* (1998) and Sohn *et al.* (2004) present a comprehensive review of the existing global damage detection methods. Other review papers include those of Mottershead and Friswell (1993) who extensively study the model updating methods and the accessory techniques, which has been cited so many times and also are considered as fundamental of model updating techniques. Moreover, Carden and Fanning (2004) summarize the state-of-the-art in vibration-based condition monitoring with the emphasis on structural engineering applications.

Damage index methods make use of the test modal data from the undamaged and damaged structure, such as natural frequencies, mode shapes, modal damping, etc. The changes in these modal parameters due to damage are correlated with other relevant information, such as a mathematical model of the structure and output

responses predicted from the model, to implement damage indicators for localizing the damage site in the structure. The damage index methods are relatively simple and straightforward, and do not require complex computations. However, these methods generally do not provide the information regarding damage severity. Nevertheless, in many practical applications, it is sufficient that the location of damage is indicated and this damage can be investigated subsequently by visual inspection or other non-destructive test methods for further quantification. According to the type of modal properties used to synthesize damage indicators, the existing approaches may be roughly classified into the following five categories: (i) methods using modal frequencies; (ii) methods using mode shapes; (iii) methods using curvature or strain modes; (iv) methods using modal strain energy; and (v) methods using modal flexibility. Since the existing damage index methods are just briefly introduced in review, they are not elaborated more in details.

Although there have been many research works for damage detection methods, there are several confounding factors making vibration-based damage identification difficult to implement in practice. First, standard modal properties represent a form of data compression. Modal properties are estimated experimentally from measured response time histories. Intuitively, information about the current state of a structure must be lost in this data reduction and system identification process. The loss of information occurs primarily from the fact that for a linear system the modal properties are independent of the excitation signal

characteristics (amplitude and frequency content) and the location of the excitation, whereas the time histories are not. In addition, if the input excites response at frequencies greater than those that can be resolved with the specified data sampling parameters, the identified modes will not provide any information regarding the higher frequency response characteristics of the structure that are contributing to the measured time-history responses. Within the measured frequency range of response, it is often difficult to identify all the modes contributing to the measured response because of coupling between the modes that are closely spaced in frequency. This difficulty is observed more commonly at the higher frequency portions of the spectrum where the modal density is typically greater. Also, the introduction of bias (or systematic) errors, such as those that arise from windowing of the data, finite frequency resolution, and those that arise from changing environmental conditions during the test, will tend to make the identified modal parameters less representative of the true dynamic properties of the structure.

Another confounding factor is the fact that damage typically is a local phenomenon. Local response is captured by higher frequency modes whereas lower frequency modes tend to capture the global response of the structure and are less sensitive to local changes in a structure. From a testing standpoint it is more difficult to excite the higher frequency response of a structure, as more energy is required to produce measurable response at these higher frequencies than at the lower frequencies. These factors coupled with the loss of information

resulting from the necessary reduction of time-history measurements to modal properties add difficulties to the process of vibration-based damage identification. These factors also contribute to the limitation of this technology to the research arena with only limited practice by the engineering community.

There are still many of issues which are critical and still to be resolved in the field of vibration-based structural damage identification. One issue of primary importance is the dependence on prior analytical models and/or prior test data for the detection and location of damage. Many algorithms presume access to a detailed FEM of the structure, while others presume that a data set from the undamaged structure is available. Often, the lack of availability of this type of data can make a method impractical for certain applications. While it is doubtful that all dependence on prior models and data can be eliminated, certainly steps can and should be taken to minimize the dependence on such information.

Almost all of the damage-identification methods rely on linear structural models. Further development of methods that have the ability to account for the effects of nonlinear structural response has the potential to enhance this technology significantly. An example of such a response would be the opening and closing of a fatigue crack during cyclic loading, in either an operational situation or in the case of a forced-vibration test. Many methods are inherently limited to linear model forms and, therefore, cannot account for the nonlinear effects of such a damage scenario. Another advantage of methods that detect nonlinear structural response is that they can often be implemented without detailed prior models.

The number and location of measurement sensors is another important issue. Many techniques that appear to work well in example cases actually perform poorly when subjected to the measurement constraints imposed by actual testing. Techniques that are to be seriously considered for implementation in the field should demonstrate that they can perform well under the limitations of a small number of measurement locations, and under the constraint that these locations be selected as priori without knowledge of the damage location.

An issue that is a point of controversy among many researchers is the general level of sensitivity that modal parameters have to small flaws in a structure. Much of the evidence on both sides of this disagreement is anecdotal because it is only demonstrated for specific structures or systems and not proven in a fundamental sense. This issue is important for the development of health monitoring techniques because the user of such methods needs to have confidence that the damage will be recognized while the structure still has sufficient integrity to allow repair.

In summary, most global damage detection techniques proposed in these references examine changes in modal properties (resonant frequencies, mode shapes), or changes in quantities derived from modal properties. Drawbacks of these investigations could be described as follows (Farrar *et al*. 2000a):

(1) The use of relatively expensive off-the-shelf, wired instrumentation and data processing hardware not designed specifically for SHM. The relative

expense of these sensing systems currently dictates that a structure is sparsely instrumented.

(2) Excitation has, in general, been from ambient sources inherent to the operating environment. These ambient sources typically excite the system's lower frequency global modes that are insensitive to local damage.

(3) When identifying damage sensitive features from the measured responses, data reduction is usually based on classical linear modal analysis. Therefore, most studies assume that the structure can be modeled as a linear system before and after damage.

(4) Trending and threshold detection are the primary tools used to determine when a system change has occurred. Statistical methods have not been used to quantify when changes in the dynamic response are significant and caused by damage. Varying environmental and operational conditions produce changes in the system's dynamic response that can be easily mistaken for damage.

Taken as a whole, the aforementioned characteristics place serious limitations on the practical use of existing methodologies. Indeed, with the exception of applications to rotating machinery, it has been found that there are almost no effective examples of reliable general strategies for damage detection that are robust enough to be of practical use.

2.3 FINITE ELEMENT MODELING OF LARGE-SPAN BRIDGE

As the important component of civil infrastructure, the more and more modern large-span cable-supported bridges with increasing span lengths are in-service or to be built. Subjected to different and complicated variable-amplitude traffic loadings everyday, those bridges are normally designed to have long life span. Service loads, environmental and accidental actions may cause damage to bridges. Continuous health monitoring or regular condition assessment of important bridges is obviously necessary so that early identification and localization of any potential damage can be made to prevent the potential catastrophic events.

Due to the structural complexity of large span cable-supported bridges, the finite element (FE) method with its long history continues to be the predominant strategy employed by engineers to perform the modal analysis and dynamic response analysis under earthquake, wind and vehicle loadings (Fleming *et al*. 1980; Nazmy *et al*. 1990a, 1990b; Wilson *et al*. 1991a; Karoumi 1999; Zhu *et al*. 2000). Starting from the knowledge of the structure geometry, the boundary conditions and material properties, the mass, stiffness and damping distribution of the structure are expressed in a matrix form. To identify changes in the dynamic characteristics of a bridge, a baseline finite element is often required. Bridge health then can be monitored or assessed when the "baseline model" is compared against a finite element model of the updated bridge. However, the success of finite element method application strongly depends on the reliability of the model

since many simplifying assumptions are made in modeling the complicated structures, and there are many uncertainties in the material and geometric properties. The calculated results are often questionable if the finite element model is not properly validated by the field test results. Therefore, the general procedure for constructing the "baseline model" on the basis of features of dynamic characteristics could be summarized as follows:

(1) Firstly, an initial full three-dimensional FE model would be usually established according to the information from blue prints.

(2) The initial FE model is then verified with the field test results in terms of frequencies and mode shapes with clarifying the important modeling issues.

(3) The experimentally verified FE model would be eventually used as "baseline" for the dynamic health monitoring and succeeding dynamic response of the bridge.

The conventional FE model construction usually introduces plenty of simplifications on the tower, cable, suspension and decking systems for two-dimensional or three-dimensional model by using beam or link type elements in the structural analysis involved in the aforementioned studies. As shown in Figure 2.1, FE modeling of long-span bridge decking system could be mainly divided into four categories, namely the bridge of single-girder beam model, Π-girder beam model, double-girder beam model and triple-girder beam model, respectively.

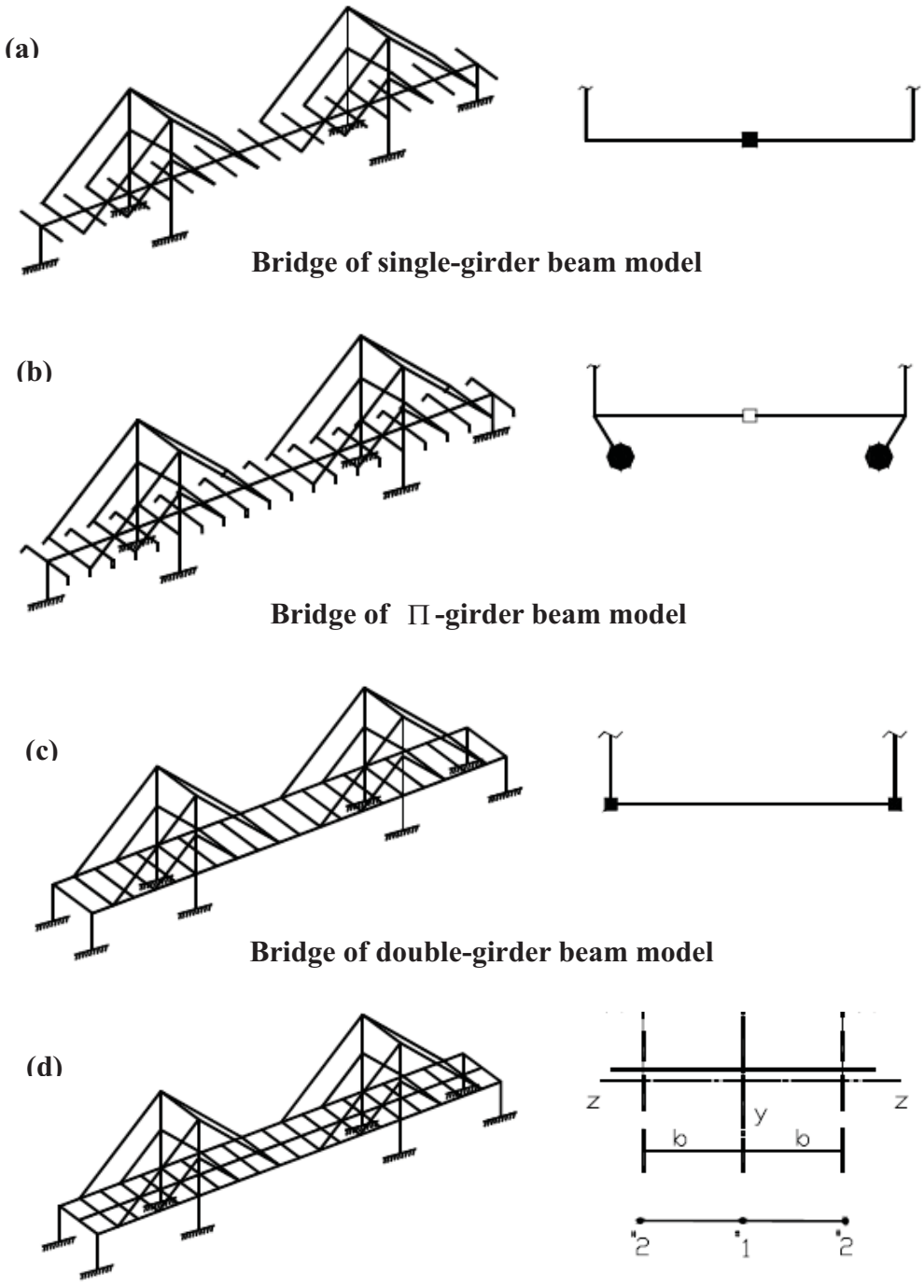

Figure 2.1 Schematic diagrams of various simulation models of decking systems of long-span bridge: (a) single-girder beam model; (b) Π-girder beam model; (c) double-girder beam model; (d) triple-girder beam model

The single-girder (spine) model is probably the earliest three-dimensional finite element model of cable-stayed bridges in structural dynamics. The bridge deck is

modeled using a single central spine with offset rigid links to accommodate cable anchor points. The deck stiffness is assigned to the spine, and mass (translational and rotational) is assigned to the spine nodes. This simplified model neglects the floor beam stiffness and girder warping, so it is suitable for a box section girder with relatively large pure torsional stiffness but small warping stiffness.

To take the warping stiffness of the bridge deck into account in the single-girder beam element model, Wilson and Gravelle (1991b) present a $\prod$-type model where the deck stiffness and mass are separately treated. Due to the distribution of lumped mass on both sides, the rotation effect of deck mass can be automatically included. This model may produce coupling between torsional and lateral motions of the deck using an equivalent pure torsional stiffness.

For cable-stayed bridges with double cable planes and open-section deck systems, the double-girder model seems more natural. The double-girder beam element model consists of two girders located in each cable plane coupled to floor beams. This model may include part of torsional stiffness through the opposite vertical bending of the two girders. Nazmy and Abdel-Ghaffar (1990a, 1990b) successfully apply the model to the three-dimensional nonlinear earthquake-response analysis of long-span cable-stayed bridge.

The warping stiffness of the open-section decks is one of the most difficult parameters to estimate in developing a model of cable-stayed bridges. Zhu *et al*. (2000) present a triple-girder beam element model consisting of one central girder

and two side girders to include the warping stiffness properly. If deck stiffness and mass are correctly equalized and distributed to three girders, the warping stiffness can be effectively considered. The model is verified through a comparison with the measured dynamic results of the Nanpu cable-stayed bridge.

Apart from the decking system, the tower is usually modeled using linear elastic beam element and the cable with truss or link element while the rigid or elastic links for the connection and the boundary constraints. Combined with the appropriate boundary conditions simulations, all components of the bridge can be modeled properly and incorporated together to produce the three-dimensional FE model of long-span bridge. Constructing a good three-dimensional finite element of long-span bridge is not an easy task. Many different modeling strategies (i.e., what kind of element types, how many degrees of freedom, etc.) are possible. The choice of modeling strategy depends on the skill and experience of the analyst and on the intended application of the model. The baseline finite element model for structural dynamics needs an accurate representation of the bridge dynamic behavior. However, extremely large computational effort is required depending on the number of degrees of freedom in the model.

All those developed model based on the girder beam would be regarded as the “spine model” of the bridge structures which is enough for the design purpose of the bridge. Moreover, this kind of model could be used to determine the overall structural responses such as dynamic characteristics and stress-strain features of the certain cross-section level on the global structural scale instead of those of

detailed locations, which is far beyond the modeling requirement for the purpose of structural health monitoring and condition assessment.

As the bridge model for the purposes of structural health monitoring and condition assessment, it should meet the basic requirements that the structural static and dynamic responses on global scale and hot-spot stress distribution of identified critical components should be collected as the analyzing basis under the actual service loading. However, the overall structural analysis is usually carried out on the global length scale on the basis of theory of structures while hot-spot stress distribution of fatigue analysis on the more detailed model with continuum damage mechanics. Both of those procedures are performed on the different length scale levels and applied with the different theories to serve the respective objective. On the basis of the finding, it is obviously inappropriate that the finite element modeling of a long-span bridge is performed on the single length scale. Nevertheless, after realizing the intrinsic deficiency of structural modeling, Peng (2003) and Guo (2005) propose the modeling methods simulating the bridge deck with the shell element model to get closer to the real structural configuration. As for the steel girder bridge structure, it is easy to construct the bridge model by shell element through equalizing the stiffness of steel stiffener while the equivalence procedure is relatively complicated. Meanwhile, it is still simulated as a node at the critical location which can not present the characteristics of local phenomena such as hot-spot stress distribution or stress concentration. Duan *et al*. (2006) develops a full three-dimensional finite element model that major

structural components such as bridge deck and towers, are modeled in details and the connections and boundary conditions are modeled properly so that the stresses/strains in major structural components can be directly computed and validated. The huge model containing approximate half million elements results in tremendous calculation costs so that all the modeling and simulation work are executed in a 64-bit Itanium Server with 8 CPUs, each of 1.5 GHz. From this point of view, it is unnecessary and impractical to model the every components of large span bridge in details. Only those regions that are commonly identified as the areas of stress concentration and vulnerable to fatigue and fracture-related damage are focused. To keep the balance between the computation costs and simulation efficiency for the purpose of structural condition assessment, an accurate idealized model should express the features of both critical component response at global structural scale and nonlinear fatigue damage of crucial region at local detailed scale simultaneously.

2.4 MODEL UPDATING METHODS

Another large class of previous researches on damage identification methods is based on the modification of a structural model to reproduce as closely as the measured static or dynamic responses from the damaged structure. The model is usually constructed by the stiffness, mass, and/or damping matrices assembled on the basis of finite element theory. The algorithms solving for the updated matrices

(or perturbations to the original model that produce the updated matrices) based on the governing equations of structural motion, the original model and the measured data are called as “model updating algorithms”. Majority of previous research work suggest that comparisons of the updated matrices to original model correlated to the intact structure provide an indication of the location and extent of damage.

It should be noted that the model updating algorithms are usually applied in both damage detection applications and model improvement applications in a similar way, namely, to seek an analytical model that is as close to the real structure as possible. The purpose of model improvement is to seek an accurate model correlated to the real structure for predicting the response of the structure to disturbances and suggesting the design modifications in the structural configuration for performance advances. The updated model is then used for response prediction and structural modification. The model improvement is eventually performed under the circumstances of numerous simplifications in finite element modeling. Usually there are complex geometrical features that cannot be modeled accurately. Moreover, boundary conditions and joint parameters between components are seldom fully understood. In such cases the analyst may, according to his engineering judgment, manage to find a compromise with acceptable results. Mottershead and Friswell (1993) summarize three common modeling errors that could lead to significant discrepancies between analytical predictions and testing values as: 1) model structure errors,

which are liable to occur when there is uncertainty concerning the governing physical equations; 2) model parameter errors, which typically include inappropriate boundary conditions and inaccurate assumptions used in order to simplify the model; and 3) model order errors, which typically include inappropriate boundary conditions, inaccurate assumptions in order to simplify the model and inconsistent material properties. These model errors may exist only in a few locations or be extensively distributed in the structure (Law, Chan and Wu 2001).

On the other hand, the damage detection applications aim to detect and identify the changes in stiffness, mass and damping matrices due to damage but not by modeling errors. Generally the damage only causes loss in local stiffness of the structure. To distinguish damage from previously mentioned artificial errors in model construction, a good quality original model that accurately represents the structure of intact stage is required. This is accomplished by a first-stage model improvement procedure for correlating the original model with testing data of intact structure (Titurus *et al.* 2003a). The improved model is commonly used as the baseline model and can be then further correlated with testing data of possibly damaged structures for damage detection by using a similar updating procedure (Titurus *et al.* 2003b). Therefore a two-step scheme is generally required for damage detection application using model updating methods with the first step correcting the modeling errors and the second step detecting structural damage. Comparisons of the updated matrices to the correlated original ones provide an

indication of damage location and extension. For a large-scale structure, the modeling errors could spread over the whole structure while the damage generally tends to concentrate on several critical locations.

Model updating is a rapidly developing technology and considerable research efforts have been devoted to propose numerous methods, e.g., in Zimmerman and Widengren (1990), Farhat and Hemez (1993), Friswell and Mottershead (1995), and Fritzen *et al.* (1998). A comprehensive survey on the model updating techniques can be found in Mottershead and Friswell (1993) and Natke *et al.* (1994). A literature review on the finite-element model updating techniques and their applications to damage detection and structural health monitoring can also be found in Doebling *et al.* (1998). The finite element model updating methods, either for model improvement application or for damage detection application, could be generally classified into three categories: 1) Optimal matrix updating algorithms; 2) Eigenstructure assignment algorithms; and 3) Sensitivity-based updating methods.

2.4.1 The Optimal Matrix Updating Methods

Optimal matrix updating methods include methods that use a closed-form direct solution to find the updated model matrices (stiffness and/or mass) to produce the measured modal data as close as possible. Several reviews on these methods have been published (Smith and Beattie 1991; Zimmerman and Smith 1992). The problem is generally formulated by Lagrange multiplier, penalty-based

optimization, which could be expressed in the following format:

$$\underset{\Delta M,\Delta C,\Delta K}{Min} = \{J(\Delta M,\Delta C,\Delta K) + \lambda R(\Delta M,\Delta C,\Delta K)\} \tag{2.1}$$

where $\Delta M = M - M_A$ is the correction to original mass matrix, $\Delta C = C - C_A$ is the correction to original damping matrix, $\Delta K = K - K_A$ is the correction to original stiffness matrix, J is the objective function, R is the constraint function, λ is the Lagrange multiplier or penalty constant.

The commonly used minimization constraints for the updating of the stiffness matrix include symmetry, orthogonality, eigen-dynamics, rigid body check, the details as follows. Similar constraints can be used for the mass matrix.

Symmetry: $$[K] - [K]^T = 0 \tag{2.2}$$

Orthogonality: $$\{\phi_i\}^T [K] \{\phi_i\} - \omega_i^2 = 0, \quad (i = 1, \cdots, n) \tag{2.3}$$

Eigen-dynamics: $$[K]\{\phi_i\} - [M]\{\phi_i\}\omega_i{}^2 = 0, \quad (i = 1, \cdots, n) \tag{2.4}$$

Rigid body check: $$[K]\{\phi_i{}^R\} == 0, \quad (i = 1, \cdots, r) \tag{2.5}$$

where ω_i is the ith natural frequency of a structural system with n DOFs (Degree of Freedom) and $\{\phi_i^R\}$ is one of the r rigid body modes of the structure. Often there is another regularization-based consideration that aims to minimize the perturbation to the original structural matrices such that the updated matrices are as close as possible to the original ones.

Early work in the area of optimal matrix updating for structural matrix

identification using measured modal data dates back to 1960's. Rodden (1967) uses the measured vibration modes to determine the structural influential coefficients of an effectively unconstrained structure. Hall (1970) presents an approach to optimize the stiffness matrix by minimizing the least-squares formed difference between the analytical modes and experimental modes. A similar procedure has been also proposed by Ross (1971) and Zak (1983) that they determine both the mass and stiffness matrix from measured natural frequencies and mode shape vectors respectively supplemented by arbitrary linearly independent vectors and analytical predicted modal vectors.

Constrained minimization theory has also been applied to the optimal matrix updating algorithms and the problem of model updating is formulated as a Lagrange-multiplier-based optimization problem with various constraints. Brock (1968) proposes an approach to optimize linear structural matrices by minimizing modal force errors with a property matrix symmetry constraint, which helps to preserve the reciprocity condition in the updated model. Baruch (1978) assumes the mass matrix is correct and formulated a stiffness optimization method to acquire improved eigenvectors by minimizing the mass-weighted Frobenius norm of perturbations to global modal parameter matrix. Berman and Nagy (1983) question the assumption of the exact mass matrix, and develop a so-called analytical model improvement (AMI) procedure to adjust the stiffness and mass matrix simultaneously for model refinement. Based on the methods from Baruch and Berman's work, researchers find the fact that one of three quantities, either

the analytical mass, stiffness and the measured modes, should be assumed to be exact, or as the reference, and then the other two can be updated. A new class of structural matrix updating methods, titled as the model reference basis methods, is subsequently introduced and attracted considerable attention in structural dynamics.

The previous approaches will produce a model where the analytical modes agree exactly with the measured ones. However, as demonstrated by Chen *et al*. (1983), the updated mass and stiffness matrices can be dramatically modified, e.g., a stiffness coefficient of zero value in original matrix could be altered to a very large number. The load paths that do not exist in real structure are thus introduced by these undesirable alterations. It is because that the aforementioned constraints still lack adequate mechanisms to control parameter changes in matrix updating procedure. Kabe (1985) introduces a method that uses structural connectivity information as constraint to optimally adjust stiffness matrix. The adjustment is performed so that the percentage change to each stiffness matrix coefficient is minimized. The physical configuration is preserved by keeping the sparsity pattern of the original stiffness matrix and the updated model exactly reproduces the measured modes. Smith and Beattie (1991) extend Kabe's formulation and solve the problem as the minimization of both the perturbation matrix norm and modal force error subjected to symmetry and sparsity constraints. McGowan *et al*. (1990) also use structural connectivity information in their stiffness adjustment algorithms applied to damage identification, in which mode shape expansion

algorithms are employed to extrapolate the incomplete measured mode shapes to be comparable with analytical predicted modes.

Zimmerman and Kaouk (1994) observe that perturbation matrices tend to be of small rank because damage is usually located in a few structural members rather than distributed all over the structure. They present the basic minimum rank perturbation theory algorithm (MRPT). A non-zero entry in the damage vector is interpreted as an indication of the location of damage. The resulting perturbation has the same rank as the number of modes used to compute the modal force error. Further research is subsequently conducted by them and their colleagues to extend and improve the algorithm (Kaouk and Zimmerman 1994a, 1994b, 1994c, 1995; Zimmerman *et al*. 1995). A method is further presented by Doebling (1996) to compute a minimum rank update for elemental parameter vector rather than for global or elemental stiffness matrices. This approach adopts the same basic formulation as MRPT but constrains the global stiffness matrix perturbation to be an explicit function of the diagonal elemental stiffness parameter perturbation matrix. A limitation of this method, as with all minimum rank procedures, is that the rank of perturbation matrix is always equal to the number of modes used in the computation of modal force residuals. In addition, as pointed out by Friswell and Penny (1997), MRPT does not necessarily ensure that the change in stiffness will be local, as the stiffness change could be global but of low rank.

The optimal matrix update methods, with constraints based on structural vibration mechanics and physical connectivity may be useful for the model improvement

problem to obtain improved modal responses by analytical prediction. However, its capability for damage detection is doubtful. Damage typically caused local changes in structural matrices (only stiffness matrix usually), whereas the matrix update methods tend to make modification throughout the entire matrices. Therefore, the subsequent results of damage identification suffer from a lack of persuasive proof with physical meaning.

2.4.2 The Eigenstructure Assignment Methods

Another group of matrix updating methods, known as eigenstructure assignment methods, is developed on the basis of the design of a fictitious controller that would minimize the modal force residuals. The controller gains are then interpreted as the perturbation to the system matrices. The procedure of eigenstructure assignment is originally developed for structural control to force a structure to respond in a pre-determined way, and is adapted to model updating by Minas and Inman (1988).

In eigenstructure assignment approaches, the model updating problem is formulated as a closed loop system, in which state feedback is used to describe the right-hand side of the dynamic equation of motion in terms of the displacement and velocity states. The feedback gains matrix is then determined so that the eigenvalues and eigenvectors of the closed loop system are identical to the measured modal data. This procedure typically results in modifications to the stiffness and damping matrices but the analytical mass matrix remains unchanged.

The updated stiffness and damping matrices are given by

$$[K]=[K_A]+[B][G][C_0], \qquad [C]=[C_A]+[B][G][C_1] \tag{2.6}$$

where $[B]$ is an input distribution matrix which may be chosen arbitrarily, $[C_0]$ and $[C_1]$ are the matrices relating the outputs and states and $[G]$ is the feedback gain matrix determined by the eigenstructure assignment method, $[K]$ and $[C]$ are the updated stiffness and damping matrices respectively, $[K_A]$ and $[C_A]$ are the original stiffness and damping matrices respectively. Because the obtained correction matrices $[B][G][C_0]$ and $[B][G][C_1]$ are usually asymmetric, a further process of determining $[C_0]$ and $[C_1]$ iteratively may be needed until the symmetric correction matrices are required. Minas and Inman (1990) has developed two-step, iterative scheme that formulates the problem as a non-linear optimization procedure with enforced symmetry constraint, in which $[C_0]$ and $[C_1]$ are fixed, and both eigenvalues and eigenvectors are assigned to produce the updated stiffness and damping matrices. Therefore，the eigenstructure assignment process is repeated by replacing the original stiffness and damping matrices with the symmetric updated matrices. Zimmerman and Widengren (1990) develop another method to enforce the symmetry of stiffness and damping matrices that uses a generalized algebraic Riccati equation to calculate symmetric corrections to the stiffness and damping matrices directly.

The study on the implementation of global eigenstructure assignment technique for damage detection has been performed by Zimmerman and Kaouk (1992).

They use a subspace rotation algorithm to improve the assignability of the eigenvectors and preserve matrix sparsity in the updated model. Lindner and Goff (1993) use an eigenstructure assignment technique to identify the damage coefficient defined for each structural member. Lim and Kashangaki (1994) and Lim (1995) propose a damage detection approach using eigenstructure assignment that directly identifies change of element-level stiffness. The best achievable eigenvector is expressed in terms of measured eigenvectors and then related to the measured eigenvectors as indicators of damage location. The localized damage is quantified using eigenstructure assignment technique so that the best achievable eigenvectors, intact structural matrices and the control gains satisfy the modal force error equation. Other studies regarding the use of eigenstructure assignment methods include the work of Cobb and Liebst (1997) who develop an optimization strategy to minimize the deviations between measured and analytical modal data for determining the diagonal control gain matrix which directly related to the damage coefficients, and the work of Kiddy and Pines (1998) who adapt the eigenstructure assignment approach to account for the centrifugal forces for damage detection in rotating structures.

As indicated by Lim (1995), one special merit of eigenstructure assignment methods is that they can be not only used for damage detection and health monitoring of structures, but also for monitoring the sensor and actuator performance in a unified manner. However, the eigenstructure structure assignment methods for damage detection and model refinement suffer from the

same drawbacks as the optimal matrix updating methods. Furthermore they may require a large amount of computation in particular for nonlinear optimization. In addition, there are no physical meanings of the assigned matrices.

2.4.3 The Sensitivity-Based Updating Methods

The sensitivity-based methods are another class of model updating methods based on the solution of first-order Taylor series that minimizes an error function of the matrix perturbations. Hemez (1993) presents an exhaustive classification of various sensitivity-based updating techniques. The theoretical basis of these methods is the eigen-sensitivity analysis, i.e., the study of relations between changes in modal parameters of a structure and the structural design variables. In this approach, model updating problem reduces to the solution of an optimization problem which minimizes a penalty function of either the equation errors or the output errors. In the equation-error-based model updating methods, the errors in eigenvalue equations expressed in terms of measured modes are minimized (Fritzen 1986; Fritzen and Zhu 1991; Friswell and Mottershead 1995). The disadvantage of the equation error approach is that it requires the measurement data at all modeled DOFs; otherwise either a modal expansion or a model reduction procedure is necessary. In addition, the estimated parameters are biased because of both sides of system of equations are contaminated with measurement errors (Fritzen 1986). The instrumental variable method (Fritzen 1986) and total least squares method (Ziaei-Rad and Imregun 1996) have been applied to mitigate

the biasness of parameter estimator.

In contrast to model updating on the basis of equation error, the output error approaches for model updating minimize the output errors between analytical modal data and experimental ones. The virtues of the approaches encompass the unbiased estimation as well as the fact that the match between analytical and measurement DOFs is not required. As modal parameters are nonlinear functions of updating parameters, the output error approaches generally give rise to nonlinear optimization problems in which the problems of convergence and computation time could appear. Furthermore, the iterative scheme requires the evaluation of eigenvalue problem and eigensensitivity at each iteration step. Nevertheless, the sensitivity-based methods have been widely accepted and have been proven very promising due to the fact that they can be readily applied to practical cases where measured coordinates are incomplete.

Jahn (1948) has derived the complete formula for eigenvalue and eigenvector sensitivities in first-order Taylor series for a standard eigen-problem. The theory is then extended by Fox and Kappor (1968) in structural dynamics to solve the eigen-derivatives of a generalized symmetric eigen-problem with respect to physical variable changes. Eigen-sensitivity analysis, that is, the calculation of changes in modal properties with respect to physical parameter variation is considered to be very useful and indispensable in the calculation of sensitivity when solving the nonlinear optimization problem.

Taking the derivative of the ith mode undamped structural vibration equation with respect to the jth parameter p_j, one can obtain

$$\left(\frac{\partial[K]}{\partial p_j}-\lambda_i\frac{\partial[M]}{\partial p_j}\right)\{\phi_i\}-\frac{\partial\lambda_i}{\partial p_j}[M]\{\phi_i\}+([K]-\lambda_i[M])\frac{\partial\{\phi_i\}}{\partial p_j}=0 \qquad (2.7)$$

Pre-multiplying the transpose of $\{\phi_i\}$ to both sides of the equation, applying the mass orthogonal relationship to the mode shapes, and taking advantage of the symmetry of the vibration equation, the derivative of the ith eigenvalue can be written as

$$\frac{\partial\lambda_i}{\partial p_j}=\{\phi_i\}^T\left(\frac{\partial[K]}{\partial p_j}-\lambda_i\frac{\partial[M]}{\partial p_j}\right)\{\phi_i\} \qquad (2.8)$$

The eigenvector derivative could be simply expressed as a linear combination of the eigenvectors. However, the calculation of eigenvector derivatives is found to be much more complicated. Fox and Kapoor (1968) present two approaches for the determination of eigenvector derivatives. In the first approach, the eigenvector derivative is expressed as a linear function of all the eigenvectors. Although analytically simple and mathematically elegant, this approach becomes prohibitively expensive for large-scale structures as it requires the calculation of all eigenvectors. The second approach involves the use of eigenvalue equations together with an equation derived from the mass orthogonality equation to generate $n+1$ equations with the n unknown element of eigenvector derivatives. The solution of this set of equations by a pseudo-inverse technique is also computationally expensive due to loss of symmetry and banded form of the

equations. To essentially avoid such difficulties, Nelson (1976) develops efficient method for the calculation of derivatives of the ith eigenvector by just using the modal data of that mode. In order to improve the computational efficiency, an improved approach that utilizes the calculated lower modes and the known flexibility matrix to approximate the required eigenvector derivatives have been proposed by Lim *et al*. (1987) and Ting (1992) suggests an accelerated subspace iteration method to improve computation efficiency. Works that address the eigenvalue and eigenvector sensitivities of the systems with repeated eigenvalues are stated by Dailey (1988) and Lee and Jung (1997).

The earliest application of eigen-sensitivity analysis to finite element model updating is proposed by Collins *et al*. (1974). The solution is obtained by successively linearizing modal data as a function of structural parameters

$$\begin{Bmatrix} \Delta f \\ \Delta \phi \end{Bmatrix} \approx \begin{Bmatrix} \dfrac{\partial f(p)}{\partial p} \\ \dfrac{\partial \phi(p)}{\partial p} \end{Bmatrix} \Delta p \tag{2.9}$$

where Δp is the perturbation in the parameters; Δf and $\Delta \phi$ are the discrepancies in eigenvalues and eigenvectors between analytical predictions and testing results, respectively; and $\partial f / \partial p$ and $\partial \phi / \partial p$ are the sensitivities of eigenvalues and eigenvectors with respect to updating parameters evaluated at the linearization point respectively. Furthermore they incorporate the Bayesian theorem for parameter estimation in which confidence levels in the analytical models and the measurement data are considered. Both the measurements and the

current parameter estimates are assumed to have uncertainties given in terms of their estimated variances, namely $V_{\varepsilon\varepsilon}$ and V_{pp}. The updated parameters with the minimum variance are then calculated as

$$\Delta p = V_{pp} S^T \left[S^T V_{pp} S + V_{\varepsilon\varepsilon} \right]^{-1} \varepsilon \tag{2.10}$$

and the variance of this updated parameter is estimated as

$$V_{pp}^* = V_{pp} - V_{pp} S^T \left[S^T V_{pp} S + V_{\varepsilon\varepsilon} \right]^{-1} S V_{pp} \tag{2.11}$$

where ε is the combined vector of discrepancies in eigenvalues and eigenvectors, $\varepsilon = \left\{ \Delta f^T \Delta \phi^T \right\}^T$ and similarly S is the combined vector of eigenvalues and eigenvector derivatives. However, this derivation is based on the assumption that the measured data and the analytical data are statistically independent. In general, this will be true only for the first iteration. After the first iteration, the measured data have been used to update the parameters, and therefore the assumption of statistical independence is a gross simplification. Friswell (1989) calculate the correlation between the measurements and the updated parameter estimates at each of iteration and the correlation matrix is used to calculate the next parameter vector estimate. This improvement seems to converge more quickly.

Chen and Garba (1980) then modify the method proposed by Collins by introducing matrix perturbation technique to avoid the eigen-solution required for each iterative step. Zhang *et al*. (1987) further improve the solution condition of the inverse problem by reducing the number of unknowns through early

localization of the significant model errors. Lin *et al*. (1995) propose an improvement in which the computation of sensitivity matrix is accomplished using the combined analytical and experimental modal data, and the advantage of the improved method over the traditional method in terms of fast convergence and convergence region is demonstrated. Such accurately determined eigen-sensitivity coefficients are then used in the classical model updating procedure to overcome the existing difficulties of identifying small magnitude model errors and slow convergence. Jung and Ewins (1992) suggest dividing the model updating procedure into two sessions, with the first session to locate major errors in grouped macro elements, then to refine the analytical model in the second session. Based on a similar consideration, Law *et al*. (2001) employ the super-element modeling technique to improve the finite element model of a bridge deck structure. The large number of DOFs in the original analytical model is dramatically reduced so that the solution condition is improved accordingly.

The main difference among the various sensitivity-based methods is the modal parameters used for estimating the sensitivity matrix. The selection of residuals to be minimized is a crucial step since the residuals should be sensitive to local and small modeling errors or slight structural damage. Basically, in addition to the commonly used modal data such as natural frequencies and mode shapes, any type of data, e.g. frequency response functions (FRFs), time series of response, or the combination of these, can be selected. Abdel Wahab (2001) presents a damage detection method based model updating, in which the sensitivity of the natural

frequencies, mode shapes and modal curvatures to damage are combined to construct the sensitivity matrix and also indicate that the inclusion of curvature mode shapes does not improve the convergence of sensitivity-based model updating algorithms. In addition, one recent paper by Worden *et al.* (2005) argues that the quantities that are sensitive to local structural damage will also be sensitive to environmental conditions and measurement noises. As modal data are indirect measurement data, they could be contaminated by measurement errors as well as modal extraction errors. To avoid the modal extraction errors, the FRF data in frequency domain may be used directly to update the FE model without extracting the natural frequencies and mode shapes (Fritzen and Zhu 1991; Friswell and Penny 1992; Fritzen *et al.* 1998; Zimmerman *et al.* 2005). One problem associated with model updating using FRF data is that the damping must be considered in the analytical FE model to achieve good updating results. The system identification and model updating can also be accomplished with the direct use of time domain data (Choi and Stubbs 2005; Kang *et al.* 2005).

Parameter selection is regarded as a key issue in FE model updating (Friswell *et al.* 2001) because it is important that the chosen updating parameters should be able to clarify the ambiguity of the model, and it is also necessary for the model output to be sensitive to these parameters. It is usually found that selection of elements in the mass and stiffness matrices as candidate parameters performs very poorly, which is one reason why the direct methods of model updating such as optimal matrix updating methods and eigenstructure assignment methods are not

favored (Friswell and Mottershead 1995). The strategy of selecting physical parameters such as the flexural rigidity of a beam element, Young's modulus, and geometrical dimension, is commonly used in model refinement and damage detection applications. Despite the clear physical meanings, these methods are difficult to model the joint stiffness and cannot correct both the model structure and model order errors. A new parameter selection strategy for finite element updating has been proposed by Gladwell and Ahmadian (1995), in which they introduce the concept of generic element stiffness and mass matrices that shows a good balance between the matrix-element updating scheme and physical-parameter updating strategy. The model updating consists of two parts: defining the generic families among which the "real" model exists, and finding the appropriate parameter values to specify the model in these families. The updated model could then predict modal behave accurately, and simultaneously satisfy the required positivity and connectivity conditions. The main obstacle is that one cannot give physical explanations of updated generic parameters, which hinders the wide application of generic element theory to damage detection and model refinement (Ahmadian *et al.* 2002).

2.5 FATIGUE DAMAGE ANALYSES OF STEEL BRIDGES

Steel bridges are very common in the world and they are expected to be vulnerable to fatigue and fracture-related damage. Durability of the bridge

structures is mainly dominated by the fatigue behavior of the critical elements of the bridge. On the other hand, fatigue design of bridges according to the BSI 1982 code is limited by design loading which may have a significant effect on the service of bridges. Moreover, highway bridges are subjected to a large number of repetitive loadings of different magnitudes caused by the passage of vehicles. For long-span bridges, they are subjected to different and complicated variable-amplitude traffic loadings everyday so that fatigue of the members is accumulated in the bridge members. Fisher (1984) has made extensive investigations on the fatigue and fracture behavior of steel bridges and bridge failure accidents. He has discovered that fatigue is one of the most important bridge failure modes and that fatigue of even the secondary member can sometimes cause the whole steel bridge to collapse. All of these suggest that the fatigue analysis is absolutely significant for the safety of these bridges.

There have been a lot of studies on fatigue damage analysis and life prediction theories (Schijve 1996; Sjostrom 1997; Fatemi 1998). The basic concept and relative law of cumulative fatigue damage have been proposed by Miner in 1945 which gives a linear estimation of cumulative fatigue damage. Miner's law is recommended for fatigue analysis in almost all codes for fatigue design and evaluation of steel bridges because it has the advantage of simplicity with mathematical elegance, making them attractive to practicing structural engineers. However, the life prediction based on this rule is often unsatisfactory for fatigue under variable-amplitude loading (Schijve 1996) and this approach does not

directly associate fatigue damage with its physical mechanism such as fatigue crack initiation and growth. There are so many factors that are not considered in Miner's rule: (1) load cycles below the fatigue limit which can propagate microcracks if the cracks are initiated by load cycles with amplitude higher than the fatigue limit; (2) the load sequence effect. It has been proved by Zhao and Haldar (1996) and Agerskov and Nielsen (1999) that the traditional Miner's law is more applicable to the design of new bridges than to the evaluation of the fatigue damage as well as the remaining life of existing bridges. Therefore, it is really necessary to seek an efficient approach for accurately evaluating fatigue conditions of existing steel bridges. This approach should be based on the fatigue theory associated with damage mechanism in accumulative fatigue process directly, and should also be easy to apply to bridge fatigue assessment.

After the work by Miner, many different fatigue damage models have been developed, which include: (1) the work as an improvement of Miner's rule, such as the double linear damage rule (Manson 1966), the damage curve approach, refined double linear damage rule (Manson *et al*. 1986) and the double damage curve approach (Manson *et al*. 1981); (2) fatigue damage theories based on plastic strain energy or total strain energy (Golos and Ellyin 1988; Halford 1966); and (3) fatigue damage theory based on the new subject of mechanics, continuum damage mechanics (CDM) models (Kachanov 1986; Krajcinovic *et al*. 1987; Lemaitre 1996; Lemaitre and Chaboche 1990; Chaboche and Lesne 1988). These fatigue models have advantages in describing the deterioration on accumulative fatigue

process. However, they are still at a primary stage to investigate the material specimens in the laboratory and have a long way to go before practical engineering applications.

As for the research on fatigue analysis method for engineering structures, bridge fatigue behaviors and available approach for evaluating fatigue are studied. Systematical works have been carried out by National Cooperative Highway Research Program (NCHRP) such as Schilling *et al*. (1978a), Fisher *et al*. (1980), Fisher *et al*. (1983) and Moses *et al*. (1986), in which fatigue behaviors of welded steel bridges under variable-amplitude loading are experimentally investigated for different bridge members and different classes of weld details. Since steel bridges are manufactured with many components jointed by welding, special attentions must be paid to these connections because they are commonly identified as the critical locations for fatigue damage and failure. These experimental results are applied to develop the current specifications of bridge fatigue in which $S-N$ curves for components and details grouped into several categories are given according to their fatigue resistance.

Fatigue damage under a variable amplitude stress spectrum has been shown to be a process of nonlinear cumulative damage. A nonlinear fatigue model based on Continuum Damage Mechanics (CDM) has been proven to be more reliable than the linear Miner's model, by the fatigue tests conducted on different materials (Krajcinovic *et al*. 1987, Chaboche *et al*. 1988; Bhattacharya *et al*. 1998), and it can be used for precisely modeling a damaged structure with clear physical

meaning.

Chan *et al*. (2000b, 2001a) propose a model constructed by elastic members and welded connections with possible initiated cracks described by a damage variable. The model allows the process of fatigue initiation at the connections of the bridge-deck section to be analyzed by a CDM fatigue damage model. The service life prediction for steel bridge decks based on the online strain–time history of the bridge under the current volume of traffic could be modified by updating the representative block of the local stress history by the future online data, which will be included in the computational approach. Associated with online structural health monitoring data, Chan and Li *et al*. (2001a) further propose a methodology and strategy for fatigue damage assessment and life prediction of the bridge-deck section which has been successfully applied to the Tsing Ma Bridge. It is a valuable work since it is the first time the fatigue damage has been assessed and the service life of such a large suspension bridge with the most heavily instrumented online monitoring system in the world. It is also significant to apply the fatigue damage model based on the CDM to the fatigue damage analyses of a large suspension bridge. It will be seen that some problems have to be solved in this application, such as, counting of variable-amplitude stress cycles, statistical analysis of the representative block of cycles, the treatment of low stress cycles and so on. After solving these issues, some useful results on fatigue damage assessment and prediction of service life can be further obtained.

In addition, there is some other work dealing with fatigue evaluation of bridges.

For example, Zhao and Haldar (1996) use a linear elastic fracture mechanics-based reliability model that is updated through nondestructive inspections to evaluate the fatigue damage of steel bridges. Zheng *et al*. (1996) experimentally investigate the fatigue life of the steel section of an old bridge by using specimens cut from the chords of the old riveted steel bridge. Agerskov and Nielsen (1999) study the fatigue damage accumulation in steel highway bridges under random loading by experiments and the analysis based on fracture mechanics. Enright and Frangopol (1998) apply the time-variant reliability methods (Mori *et al*. 1993) and Monte Carlo simulation to reliably predict the service life of deteriorating highway bridges.

Fatigue design rules commonly used in practice are mainly based on the data generated from tests on either beams or small-scale specimens incorporating the weld detail of interest, subjected to unidirectional loading. Based on the above, the fatigue test can be expressed in terms of the nominal stress and the $S-N$ curve can be obtained in terms of the nominal stress approach. This approach is then adopted for fatigue design and fatigue damage calculation. BS5400 Part 10 (1982) gives guidance for steel bridge fatigue design in practice and adopts the nominal stress approach for fatigue evaluation. The classification method is used to classify the welded details according to the direction of the fluctuating stress relative to the detail, the location of the possible crack initiation of the detail and the geometrical arrangement of the detail. The corresponding coefficient of the $S-N$ relationship can then be determined from the class type and the damage

accumulation is obtained using the linear Miner's law. The fatigue behavior of welded offshore structure joints usually fails in welded joints but not the member. The nominal stress approach for fatigue design is regarded as not suitable for steel structures with complicated geometry because the stress state in such structures is complex and the definition of nominal stress is difficult.

An alternative method for the complicated welded steel joints fatigue design is the hot spot stress approach. The hot spot stress approach, which considers the structure stress concentration at the welded vicinity, has been widely used in hollow steel tubular structure fatigue design and analysis in practice. Savaidis and Vormwald (2000) use ABAQUS™ to undertake hot spot stress analyses of various welded joints of city bus floor structures. The numerical results give the correct fatigue failure location of the hot spot stress area as the experimental result shows on welded joints under cyclic constant amplitude loading. Macdonald and Haagensen (1999) perform the hot spot stress analysis for fatigue design of welded rectangular hollow section joints and identified the hot spot stress analysis for fatigue design as one of the most promising method in terms of providing a coherent and comprehensive approach to fatigue design. The influence factor of joint geometry should be considered in the calculation of stress for fatigue analysis as pointed out by BS7608 (1993), which suggests using hot spot stress analysis for such tabular nodal joints and the stress range for such joints should be in the hot spot stress range. Hot spot stress analysis, therefore, is used in fatigue resistant design and the durability estimation of welded offshore

tubular joints. However, little effort has been found on the hot spot stress approach in the application of long suspension steel bridge fatigue evaluation.

Many uncertain factors exist in the fatigue assessment of existing bridges since fatigue damage accumulation is a random variable. Some of these uncertainties, such as the random traffic loading, fatigue resistance of material, etc., are difficult to model exactly by deterministic mechanics methods. The use of deterministic evaluation of bridge fatigue mentioned above, e.g. Li *et al*. (2001a) and Chan *et al*. (2001a), can not fully consider the random character of fatigue damage accumulation. Therefore, considering that many uncertain factors exist in the process of fatigue damage accumulation in bridge structures, probability methods based on the reliability theory should be applied in bridge fatigue damage assessment. This process is more rational; however, up to now, there are few relevant studies carry out reliable evaluation attempts of the bridge fatigue damage using the data acquired from structural health monitoring systems.

2.6 MULTI-SCALE MODELING AND SIMULATION

Multi-scale modeling is a becoming a quickly evolving area of research and multi-scale simulation has been considered as a very important tool to reveal material behavior at different length and temporal scales through numerical simulations. An important motivation for this kind of modeling is to better understanding the underline physics of a phenomenon at different scales, bridging

length and time scales, of multi-scale nature in many engineer problems given the current computational capacity. There exist several review articles on multi-scale modeling and simulation (Michopoulos *et al.* 2005; Bai *et al.* 2005; Duchêne 2007; Markus 2008). Even though multi-scale problems have long been studied in mathematics and computations (Weinan *et al.* 2003; Brandt 2001), the current applications are mainly focused in the applied sciences, in particular, material science, chemistry (Li, J. *et al.* 2003), and biology (Chong 2002). Problems in these areas are often multi-physics in nature; namely, the processes at different scales are governed by physical laws of different character (Chong 2005; Michopoulos *et al.* 2005). Despite significant developments in materials simulation techniques, the goal of reliably predicting the properties and behaviors of new materials has not yet been achieved. This situation exists for several reasons that include a lack of full understanding of material behavior at different scales, absence of scaling laws, computational limitations, and difficulties associated with experimental measurements of material properties at micro and nano-scales (Ma 2006).

Scaling is the most important aspect of every physical theory. If scaling is not understood, the theory itself is not understood either (Bazant *et al.* 1997). Scaling laws governing the mechanical behavior of materials from atomistic (nano), via meso-plastic (micro), to continuum (macro) scales are very important for applications where two or multiple length scales of different orders of magnitude are involved. Appropriate scaling laws may extend the extensive knowledge

accumulated over time on material behavior at the respective length scale level. A survey of the numerical methods and physics that operate across these disparate length and time scales can be found in Liu *et al*. (2004).

The rapid development of those multiscale studies promotes the establishment of some new journals. The newly founded journal is SIAM Journal on Multiscale Modeling and Simulation (MMS). As for the nature of multiscale problems, MMS describes it as follows: "Multiscale modeling is highly interdisciplinary, with developments occurring independently across fields. A broad range of scientific and engineering problems involve multiple scales. Traditional monoscale approaches have proven to be inadequate, even with the largest supercomputers, because of the range of scales and the prohibitively large number of variables involved. Thus, there is a growing need to develop systematic modeling and simulation approaches for multiscale problems" (SIAM Journal M&M). Similarly, a number of international symposia have been held to explore the perspectives and new paradigms to cope with multiscale problems. For example, MRS Symposium on Advances in Materials Theory and Modeling-Bridging over Multiple-Length and Time Scales (Bulatov *et al.* 2001), International congress on Mesomechanics (Sih 2010, 2011), International Symposium of Multiscaling in Mechanics (Sih *et al.* 2002), etc.

The development of computational techniques for a consistent approach of multiple length and time scales probably for the analysis of multi-physics problems is a subject of intensive research in computational mechanics.

Increasing computational performance and simultaneously developed mathematical solution techniques nowadays provide a powerful platform for sophisticated modeling approach in engineering. Now the basic problems that have to be overcome are on the bridging the gap between models on the different length and time scales (Nackenhorst *et al*. 2011). An excellent description of various spatial and temporal scale bridging approaches is presented in Zohdi *et al*. (2004). Spatial multiscale approaches are grouped into categories as follows: one involves information passing between models on different length scales. The lower-level length scale is modeled first, such that its gross response as viewed on the higher-level scale is subsequently infused into that higher-level scale model. Therefore, information follows a one-way path from discrete (lower-level) to continuum (higher-level) scale models. The methods that follow this paradigm are usually called "information-passing multi-scale methods" (IPMM) or "hierarchical multi-scale methods". The other involves simultaneous modeling of both lower-level (discrete) and higher-level (continuous) length scales. The methods that follow this paradigm are usually called "concurrent multi-scale methods" in which the computational domain is divided into different regions where different simulation methods are applied. A critical issue in both methods is the correct coupling among different models in mechanical and other domains. In addition to methods aimed to extend accessible length scales, several methods have been developed to cover larger time scales. Further discussion concerning these topics is given in references (Broughton *et al.* 1999; Rudd *et al.* 2000;

Curtin *et al.* 2003; Fish 2007; Tinsley *et al.* 2005).

After the fast development of multi-scale model in material sciences for last decade, especially in nanotechnology (Chong 2007), the majority of the research findings and achievements mainly emphasize on the aspect of multi-scale materials modeling (Guo edt. 2007; Bai *et al*. 2005; Sih *et al*. 2003, 2004a, 2004b, 2005, 2006; Sih 2007, 2009; Fan 2009). As for the area of finite element analyses for structures, the studies have been preliminarily conducted and implementation has been attempted (Ladeveze *et al*. 2002; Li *et al*. 2007), and varieties of interested area had been included, for instance, concrete (Bernhard *et al*. 2011), steel frames (Khandelwal 2008), composite structures and delamination (Fish 2011; Ramm *et al*. 2011; Gosselet *et al*. 2011; Alfaro *et al*. 2011) and etc.

Lu *et al*. (2008) proposes the methodology of connecting microscopic finite element model to macro model by introducing the deformation compatibility condition at the interfaces between different-scale models. The features of spatial multi-scales involved and the related issues for multi-scale mechanics of materials and structure are reviewed in Wu *et al*. (2007). After summarizing the theories and methods in multi-scale material modeling, their research areas of interest focus on the multi-scale structural modeling and damage analyses of large civil structure with current research progresses (Li *et al*. 2007, 2009; Sun 2006; Ding *et al*. 2006, 2007, 2010; Deng *et al*. 2008; Chan *et al*. 2007, 2009; Yu *et al*. 2011; Tang 2011). Also several key issues are proposed with respect to bridging in simulation, updating and verification of the multi-scale structural model, damage

evolution in multiple temporal scales as well as the strategies of multi-scale modeling and simulation in engineering computation of large civil structure. From this point of view, the research studies that have been carried out under the leadership of Li Z.X. and Chan T.H.T (Li *et al*. 2007; Chan *et al*. 2009) are widely considered as frontier and advanced for structural multi-scale modeling and simulation and the corresponding damage analyses of large civil structures.

2.7 MIXED DIMENSIONAL COUPLING IN FINITE ELEMENT ANALYSES

After realizing the necessity of multi-scale modeling and simulation and learning about those efforts dedicated to structural analyses of large civil structures, the existing multi-scale modeling strategies and corresponding implementation methods should be firstly investigated. The most important point is to develop the most appropriate multi-scale modeling strategies and implementation methods accordingly to fulfill the requirements of damage analyses of large civil structures in combination with finite element method.

Civil infrastructure such as a long-span bridge is usually modeled in the order of magnitude of kilometers while its components are in meters. Meanwhile, it is well known that many types of defect, such as cracks and degradation of structural connections, generate locally at the material points or sectional levels which will in turn influence the entire structural behavior and contribute to global structural

damage and possibly cause structural failure. In this sense, an accurate model considering for damage degradation behavior should incorporate the physical mechanism of local damage, treated predominantly at the material point level by CDM which allows the actual fatigue behavior to be considered as a deteriorating process, into global structural analysis conducted on the structural level. The major difficulties now are the lack of a standardized framework for such nonlinear physical-based modeling in which multi-scale simulation strategy is necessary, especially for large-span structures such as long-span suspension bridges.

Accuracy and efficiency are two major concerned issues in any finite element analysis that are encouraging engineers and design analysts to seek reliable and accurate yet economical methods to determine the responses of structural components. Meanwhile, the complexity of a structure also requires the analyst to idealize the finite element model so that a solution may be obtained within a reasonable time scale. As a result, a large percentage of finite element analyses make use of reduced dimensional element types, such as beams, plates and shells in a single model. Therefore, it would be desirable to combine the reduced or lower dimensional element types with higher dimensional elements in a single finite element model to serve the various research purposes. However, these idealized models, combination of mixed dimensional elements, present mathematical difficulties at the connections between the differing element types due to the incompatibility of their nodal degrees of freedom. To achieve compatibility of displacements and stress equilibrium at the interface between the

dissimilar elements, some schemes are necessary to couple the differing element types in a way that complies with the governing equations such as those of elasticity. Coupling methods have been developed to link both sides of an interface between different types of elements. Some are for connecting similar element types while others are used to couple similar element types of dissimilar order (e.g. transitions from linear to quadratic elements).

Kinematic coupling, knows as rigid linking or linking (Adams 1999), is conventionally regarded as the most basic and widely used method of coupling both sides of a transition. It constrains the DOF of a group of slave nodes to the translation and rotation of a master node without reference to mass or force. As the constraints imposed by kinematic coupling are usually calculated as a function of the nodal coordinates, considerable stress disturbances are thus induced at the transition so that this coupling method is inappropriate in most case.

Interface elements are another class of coupling developed for many kinds of transition. The coupling terms produced by the presence of the interface element can be organized in the form of a "stiffness" matrix and assembled with other finite element stiffness matrices in the usual manner. Hence, the term "interface element" is justified and appropriate. The interface elements do not have physical stiffness associated with them as the interface stiffness matrices have non-zero entries on the off-diagonals only. Housner *et al*. (1995) and Schiermeier *et al*. (1997) develop a method for analyzing plate and shell structures composed of two or more independently modeled substructures, based on a hybrid variational

formulation with Lagrange multipliers. Since the interface elements consist only of the differences in displacement components weighted by the Lagrange multipliers, there are no conventional element of material properties.

The above coupling techniques could be applied to meshes of the same dimension, that is, dissimilar 3D meshes and dissimilar shell meshes may be coupled. Little research has been carried out on transition elements for coupling meshes of dissimilar dimension. Da´vila (1994) document an element for coupling solid to shell transitions. Gmur (1993) develop solid to shell and solid to beam transition elements for use in structural dynamic type simulations. Kim (1995) propose a transition element to connect beams to plane stress elements, which occurs frequently in the design of tall buildings (the shear walls of the elevator shaft are modeled using plane stress elements, while the remainder of the frame is usually represented as beam elements).

Constraint equations are referred as relationships among degrees of freedom that supplement the relationships represented by the basic stiffness equations. A constraint equation either prescribes the value of a degree of freedom, as in imposing a support condition, or prescribes a relationship among degrees of freedom. Multi-point constraint equation, defines a relationship between sets of displacements within a finite element model. Mathematically, there are two alternative methods used in commercial programs that apply constraints to the global or structural stiffness equations as stated as using Lagrange multipliers or using a penalty function method. Nethercott (1993) investigate the possible uses

of constraint equations for coupling dissimilar element types. The coupling of 3D continuum elements with 2D plate elements associated with 2D plate elements with 1D beam elements has been implemented by McCune (1998). On the basis of those studies, the coupling scheme is eventually proposed by McCune (1998, 2000) and Armstrong (1998a, 1998b). Monaghan (1998) further develops the coupling method that utilize an outcome of Reissner's bending theory of elastic plates (Reissner 1947) and shows that proper connections between plate and beam elements, and plate and solid elements can be achieved via multipoint constraint equations by equating the work done on either side of the dimensional interface. The solution is arrived at by introducing the assumed variation of the stresses, given by the appropriate beam, plate or shell theory, over the cross-section of the interface. This procedure is general and as long as the stress distribution due to any given loading can be determined at each interface, beam-solid (Monaghan *et al*. 1998), beam-shell (Monaghan 2000) or shell-solid (Da´vila 1994; Liao *et al*. 1988) coupling can be achieved for transitions with arbitrary shapes of cross-sections.

2.8 SUMMARY

It is acknowledged that fatigue damage is an important failure mode for large suspension bridges and welded connections are usually identified as the most vulnerable locations for accumulative fatigue damage of existing bridges. As for

the inherited disadvantage of conventional two-step analyzing method, alternatively, concurrent multi-scale modeling and simulation are considered as necessary and imperative for condition assessment of large civil infrastructure. The multi-scale strategy could be applied to build the concurrent multi-scale model on the basis of selected coupling method which can merge typical detailed joint geometry model into the global model. This model could be further updated by the online measurement data acquired by the SHM. After the verification and validation processes of updated model, the hot-spot stress of concerned locations can be directly output through a single step of analysis. Moreover, it would be able to accurately predict the stresses at the critical locations where there are no sensors installed. Furthermore, those stress information of SHM and predicted stress could be used to evaluate the health status of bridge structures.

Then key issues of the problem has become how to develop an efficient and accurate coupling method bridging different dimensional elements at respective length scales in finite element method. The proposed methodologies and implementation methods of multi-scale modeling of frame-like structure will be described in details in next chapter.

CHAPTER 3

MULTI-SCALE MODELING STRATEGY

3.1 CONCEPT OF CONCURRENT MULTI-SCALE MODELING OF CIVIL INFRASTRUCTURES

3.1.1 The Need of Concurrent Multi-Scale Modeling For Structural Deteriorating Analyses

For large civil engineering structures such as large-span bridges and tall buildings with the complicated configuration of steel truss, the service loadings are directly applied on the whole structure while the damage is prone to be occurred at the local details especially at the intersections of multiple chords and posts with inherent defects. For instance, the majority of large-span bridge three dimensional finite element models are constructed as the "fish spine" model that almost all the components of decking systems are simulated by beam elements (as shown in Figure 3.1). Although some further developed models are based on shell elements, the dimensions of these models are still at the length scale of 10^0 m and the local connection detail is still be simplified as a node which is enough for the purposes of dynamic characteristics analysis and global static responses during the design period of bridge but not for structural health monitoring and damage evaluation

instead.

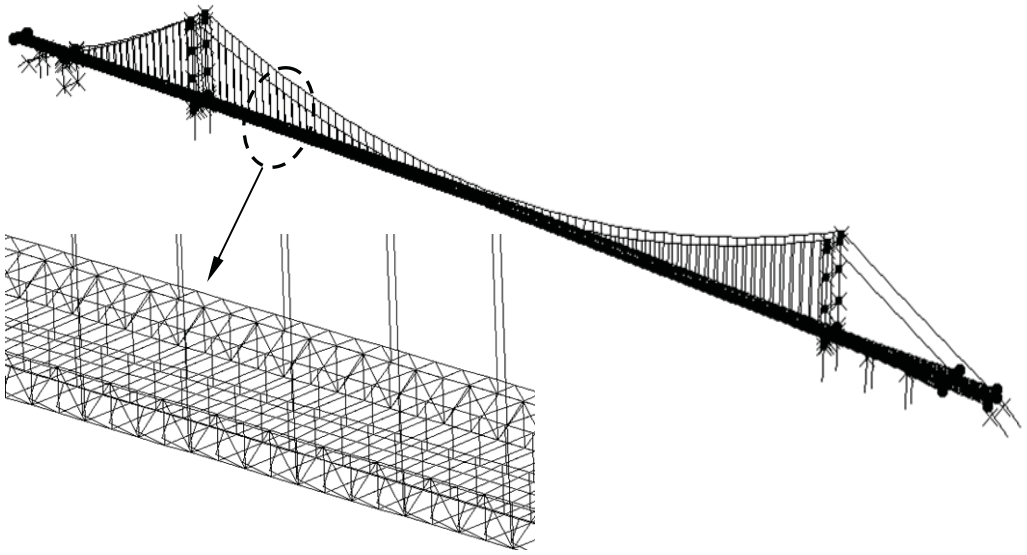

Figure 3.1 The global finite element model of a suspension bridge

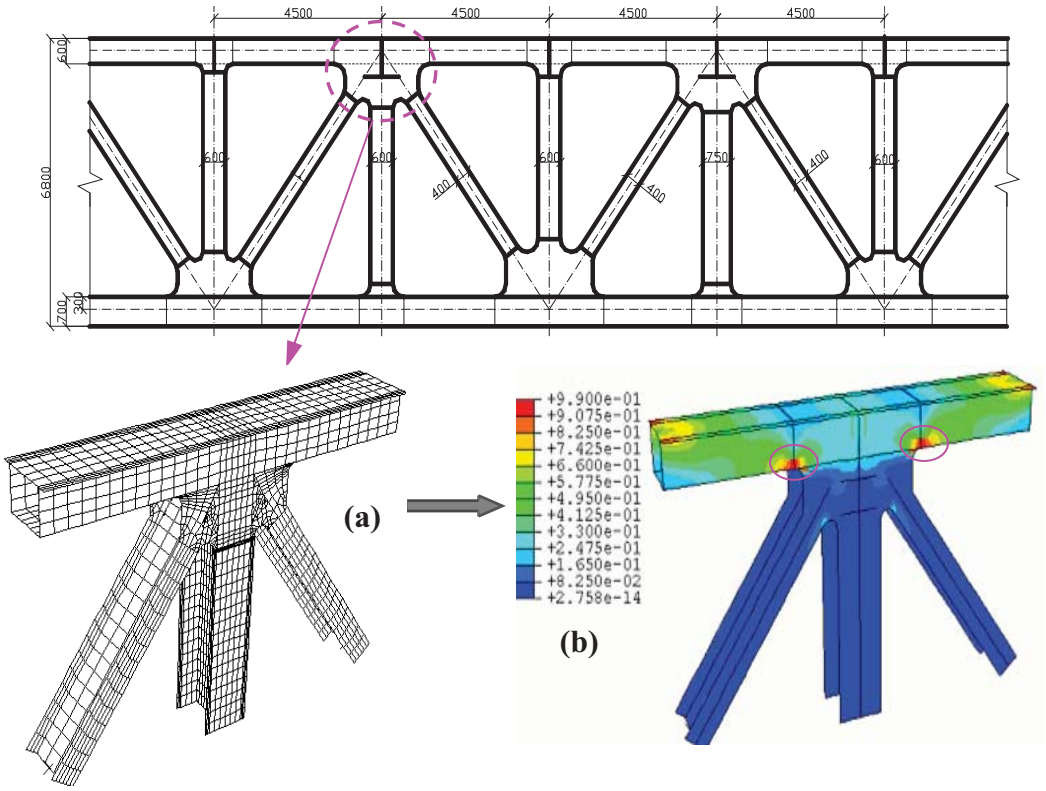

Figure 3.2 Schematic diagrams of connection region in typical steel truss: (a) local detailed FE model and (b) stress contour under certain loading case

On the contrary, the counterpart of the global scale is the local detailed model which could be constructed at the length scale of 10^{-3} m. However, it is impractical and unnecessary to model the entire structure in details with respect to computation efficiency and actual application in engineering problem. Only those regions that are commonly regarded as the areas of stress concentration and vulnerable to fatigue and fracture-related damage are focused, as shown in Figure 3.2. The welded details at these locations are usually vulnerable regions where fatigue cracks easily initiated while the global structure may be still in the elastic range, so that these locations should be paid more attentions.

The current available solution to the aforementioned problem is to use the two-step analysis method. The simplified global model and detailed local model of concerned region should be firstly developed. Then the structural analysis using the corresponding global FE model is subsequently conducted to determine the critical components and the results of concerned location would be extracted for the further purposes after applying the exterior boundary conditions on local model to perform re-analyzing process. These studies on the fatigue analysis for certain large-span bridge by the two-step method have been carried out by Li *et al*. (2001a) and Chan *et al*. (2001a, 2005) while the process can be easily implemented by submodeling technique in ANSYS™ (ANSYS Inc., 2004) and ABAQUS™ (HKS, 1998) which is a two-step analysis in nature. Obviously there are inherent difficulties of the accuracies of complicated boundary conditions which may lead to the significant errors if the extraction is not accurate enough.

In this kind of method, the lower-level length scale must be modeled first, such that its gross response as viewed on the higher level scale is subsequently infused into that higher-level scale model. Therefore, information follows a one-way path from discrete (lower-level) to continuum (higher-level) scale models. The methods that follow this paradigm are usually called “Information-Passing Multiscale Methods” (IPMM) (Michopoulos, Farhat and Fish 2005) which is the matter of time and sequence. However, the involved instantaneous material properties and damage state may vary in space and time due to their history dependence (Fish and Shek 2000) while they must be interacted concurrently in the both scale levels.

In addition, the previous study (Chan *et al*. 2003) has indicated that it may be successful for linear problem using “two-step analysis method” while unpredicted outputs resulting from accumulative errors are applied to nonlinear responses analysis. Technically speaking, the so-called multi-scale simulation by “two-step analysis method” only can be categorized as “Information-passing Multi-scale Methods” which is implemented by structural and material model construction and exchange the information at the different scales.

The key issues of multi-scale simulation based on “Information-passing Multi-scale Methods” are the accuracy of the information exchanged between different scales, especially for the highly nonlinear characteristics of structural damage analysis. However, there are inherent difficulties and inevitable obstacles if the method is adopted. When an accurate representation of the system response

is required for both length scales simultaneously, coupling of modeling on these scales is obviously necessary. Under this circumstance, the "Concurrent Multi-scale Methods" is raised and must be used, that is, the concurrent multi-scale simulation of structural behaviors based on the different models on the lower length level and higher length level. Here the term of "lower length level" refers to global scale model constructed by structural elements of beam and shell with the length scale of 10^0 m while the "higher length level" to local scale simulation of detailed connections with the length scale of 10^{-3} m.

Therefore, for the large infrastructure, the objective of structural damage analysis and simulation cannot be achieved if only implementation in single length scale level, and there is imperative need for multi-scale modeling. Moreover, as for the application in actual engineering problem, the multi-scale modeling could be incorporated with the powerful commercial programs. The proposed Concurrent Multi-Scale Modeling of (CMSM) can deal well with finite element multi-scale modeling considering global structure and local details in both length scales.

3.1.2 Physical Description on Strategy for Concurrent Multi-Scale Modeling

The structural analysis is usually carried out at the different scale levels for the different purposes. As listed in Table 3.1, for the large engineering structures, the size of beam element is usually at the magnitude of meter for global structural analysis. Meanwhile, the beam element is also adopted at the centimeter level of

Table 3.1 Physical scales and available theories for numerical analysis for long-span bridges

Scale Level	Representative Volume Element (RVE) for analyses	Objectives of analyses	Available Theory
Global Scale (Up to km)	5~10 m	Internal Forces	Theory of Structures
Component Scales (Meters)	5~10 cm	Nominal Stress	Mechanics of Materials and Theory of Elastic-Plasticity
Material Scales (Microns)	1~5 mm or less	Hot-spot Stress or Effective Stress	Meso-mechanics, Damage Mechanics

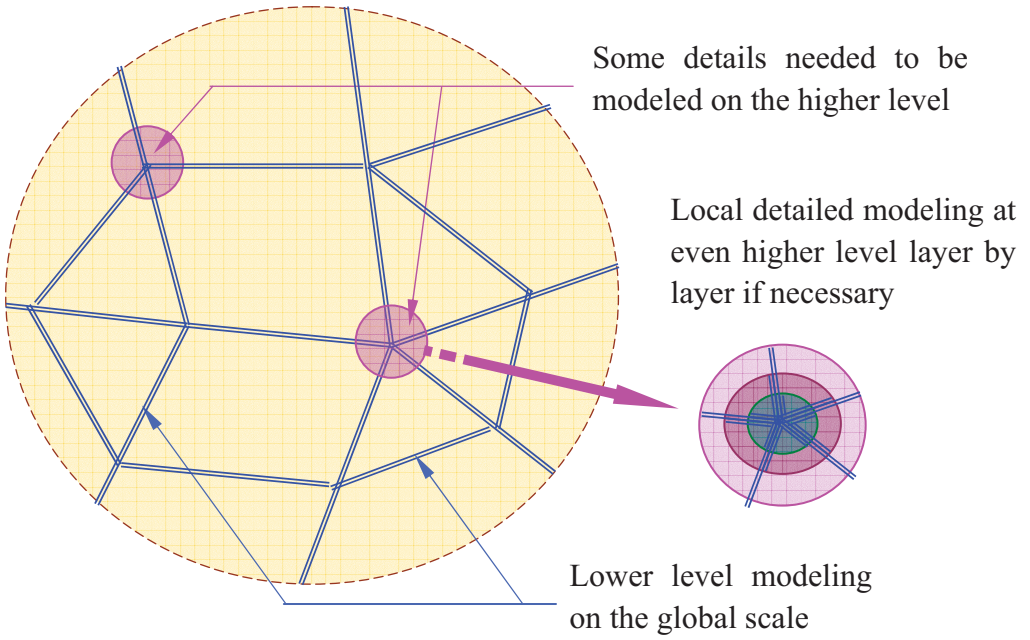

Figure 3.3 A sketch description on multi-scale modeling (Li *et al.*, 2009)

component scale for nominal stress analysis. Furthermore, the scale of material points, usually modeled with shell or solid elements, is commonly less than level of a millimeter for the local detailed hot-spot stress analysis. The major

difficulties for the existing scale modeling method are the strict limitations on structural analysis on their respective scale level instead of considering the other scales. Although some techniques such as transition element and mesh refinement has been applied in the modeling process and tried to make connections between different scale levels, they are actually still at the same scale level without real solutions to problem.

The objective of multi-scale modeling is to construct the global model at the structural level and incorporate the local concerned details models of constitutional relationships according to analyzing purposes, even the local details could be modeled layer by layer if necessary as shown as Figure 3.3. All the modeling process should be concurrent and characteristics of corresponding scale level must be taken into account at the same time. In particularly and no loss of generality, the linear analysis could be performed at the global model of structural elements and the corresponding linear responses can be obtained while nonlinear analysis must be considered to simulate the nonlinear behavior in local detailed model of lower level.

3.1.3 Modeling Strategy Based on a Commercial Computing Programs

The finite element method has been proven to be a successful and powerful tool for various kinds of structural analysis. Several general-purpose commercial computing packages such as ANSYS™, ABAQUS™, ADINA™ and SAP™ have been correspondingly developed for the analytical requirements. Almost all

the analyzing techniques adopted in FEM are easily implemented in the software. However, up to now there is no techniques provided in the existing software for concurrent simulation of global level and local detailed level, which means the implementation procedure of multi-scale modeling, needs to be further studied on the basis of FEM techniques such as substructuring and multi-point constraint equations. During the studies shown in this thesis, the general-purpose commercial software ANSYS™ and ABAQUS™ are both used to implement the modeling and analyses on the basis of the proposed method and strategies for CMSM.

3.2 MULTI-SCALE MODELING STRATEGY AND METHODS

Accuracy and efficiency are paramount in any analysis and so design analysts are often forced to use dissimilar elements in a single finite element model. The theories for beams, plates, etc., i.e., reduced dimensional forms, give accurate answers in the interior away from boundary regions near to supports and loads and from other local disturbances around geometric and material discontinuities. Therefore, reliable results can be expected when modeling such interior regions by one of the following two classes of structural elements. Beams are structural elements where two of the orthogonal dimensions are at least several times smaller than the dimension of length while plates and shells are structural elements where the thickness is at least several times smaller than the other two

dimensions. In many models, reduced dimensional element types are used in combination with higher dimensional (2D or 3D) element types in a single model. For instance, the certain structural applications of the finite element method may contain long slender regions, thin zones and complex chunky portions. Long slender regions can be represented appropriately using beam elements, thin zones can usually be modeled using shell element, and chunky portions are best represented as three-dimensional elements. However, practical models usually contain a mixture of more than one of the above regions categories. In order that each region is represented by an appropriate element type, some sort of coupling scheme is required to form a link between the meshes of different types. Appropriate coupling of these mixed dimensional models is consequently important in order to establish stress equilibrium and compatibility of strains at the interface between different types of elements.

In summary, several methods have been introduced which attempt to link both sides of the interface. Some are for connecting similar element types, others are used to couple similar element types of dissimilar order (e.g. transitions from linear to quadratic elements). Other methods have been also formulated to couple mixed dimensional transitions. Those existing methods consist of the kinematic coupling, transition elements and constraint equations, and their respective merit combined with shortcoming for accurate coupling is discussed as below.

3.2.1 The Existing Implementation Methods

Kinematic Coupling

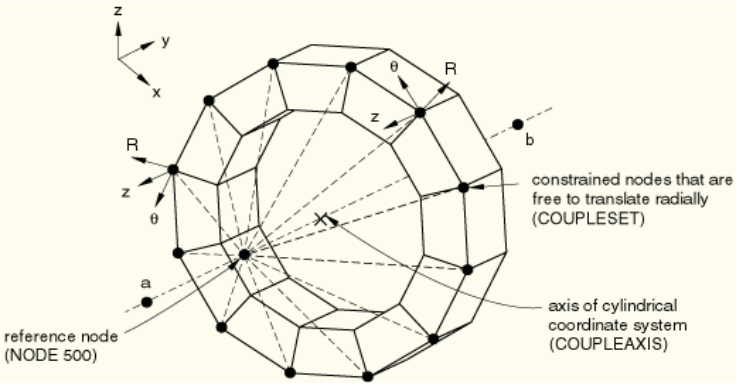

Figure 3.4 Illustration diagram of Kinematic Coupling (HKS, 1998)

Kinematic coupling is the coupling of nodes or sets of nodes without reference to mass or force. As shown in Figure 3.4, the mechanism of this method constrains the DOF of a group of slave nodes to the translation and rotation of a master node without indicating transition type, that is, master node and slave nodes form a "rigid region". No mass is introduced into the system with kinematic coupling, but it can affect the overall mode stiffness. This is particularly noticeable in regions of a model that have a shear center offset from the centroid and subject to torsional loads. As the interface is constrained from warping, the coupling method induced considerable extra torsional stiffness. Furthermore, since the constraints imposed by kinematic coupling are usually calculated as a function of the nodal coordinates, considerable stress disturbances are thus induced at the transition region, and therefore this coupling method is regarded as approximate coupling method which is not suitable for the case that requires precise connection.

Although the kinematic coupling is the easiest way of coupling, there are serious

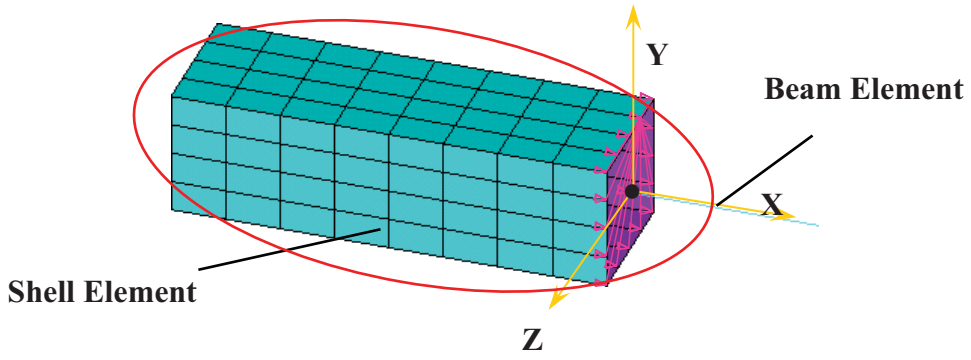

Figure 3.5 Possible influence zone by Saint-Venant's principle in the typical multi-scale model

inherited problems in it that could perhaps make all the efforts in vain for the purpose of model construction. Saint-Venant's principle suggests that the difference between the stresses caused by statically equivalent load systems is insignificant at distances greater than the largest dimension of the area over which the loads are acting. As stated as Saint-Venant's principle, in other words, geometric details causing local stress perturbation would lead to significant effect within a distance of only a few times of the detail's largest dimension. That is to say, if the coupling situation simulated at the interface between two types of elements is not the same as the one in the real case, as the above Figure 3.5 shows, the differences caused are most likely to influence the whole the model section if the model length is not large enough compared with the cross-section size. We have no idea about how big the size of the influence zone will be, but actually the real connection region is not as rigid as the kinematic coupling way would seem.

Surface-based Coupling in ABAQUS^{TM}

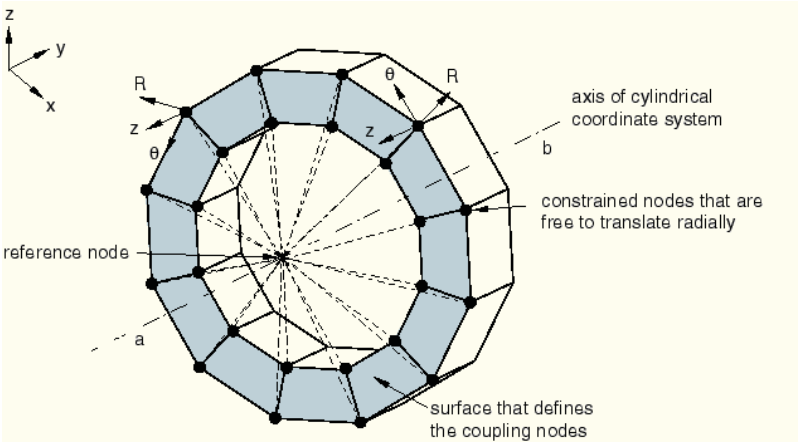

Figure 3.6 Illustration diagram of Surface-based Coupling (HKS, 1998)

As shown in Figure 3.6, HKS (1998) has documented and implemented a general transition element which couples a reference node to a group of coupling nodes defined by the surface in commercial computing program ABAQUS^{TM}. The reference node has translational and rotational DOF, while each coupling node has translational DOF active in the element. The element distributes forces and moments at the reference node as a coupling node-force distribution only. As different from the kinematic coupling, each coupling node on the surface has a weight factor assigned, which dictates the proportion of the load carried by the element that is transmitted through the coupling element. In term of use, correct coupling can only be achieved if the weight factors are accurately adopted for each node at any given interface. However, the real values of these weight factors are difficult to determine, and currently they are determined empirically by the user so that there are so many uncertainties and unpredictable factors in weight values estimation. As the rotational DOF is ignored for each coupling element,

the desired coupling situation of connecting beam element and shell elements cannot then be carried out correctly.

Mixed Dimensional Coupling Via Constraint Equations

Multi-point constraint equation, defines a relationship between sets of displacements within a finite element model. Mathematically, there are two main methods of implementing these constraints, using Lagrange multipliers or by using a penalty function method. The Lagrange multiplier method enforced constraints exactly and the penalty function method imposes constraints approximately.

The coupling method of dissimilar dimensional elements by constraint equations has been developed by McCune (1998) and Monaghan (2000) on the basis of a result from the theory of bending of elastic plates. Simple, efficient and accurate displacement coupling between regions of different dimension for both 2D-1D and 3D-2D mixed dimensional cantilevers of rectangular cross section have been demonstrated. Coupling is achieved by introducing the assumed variation of the stressed, given by the appropriate beam, plate or shell theory, over the cross-section of the interface. This solution is then arrived at by equating the work of the interface stressed in terms of the lower dimension interface rotations and transverse displacements to the work of the boundary stresses on the higher dimension side of the interface. When implemented, this method generates continuous and reliable stress contours at each transition. Since this procedure is

more general than the previous one, coupling can be achieved for arbitrary transitions, so long as the stress distribution due to any given load can be determined at each interface.

3.2.2 Mixed Dimensional Coupling of Beams with Shells

The geometry of a shell is defined by its thickness and its mid-surface, which is a curved surface in 3D space that is commonly considered as $2^1/_2$D since it is not fully 3D geometric representation. Coupling situation of beam elements with shell elements is discussed here. The procedures are performed under the premise that coupling is being applied to isoparametric shell elements, where geometry and field interpolation functions are of the same order. The proposed procedure also can be extended to elements that are less general than the shell, such as plane stress, plane strain and plate elements in applications.

The beam node at the transition has six active DOFs. Therefore, six constraint equations are required to fully couple the displacements of the shell edge to the displacements of the beam node. It is assumed that the beam axis is parallel to one of the axes of the co-ordinate system in the finite element model (if it is not parallel to one of the global co-ordinate system axes, a local co-ordinate system can be used). Under this premise, the resultant force on the beam node can be resolved into six components which coincide with DOF components of the beam node.

The derivation of the constraint equations for beam-shell coupling has been stated

by Monaghan (2000) and would be illustrated as follows for four simple loading situations, namely, axial forces, bending moment, torsion and shear forces applied at the end of the beam element. The subsequent implementation of coupling beam element and shell element with the cross-section of particular box section and corresponding FORTRAN programming code which could automatically generate the constraint equations is accordingly developed.

Axial Force

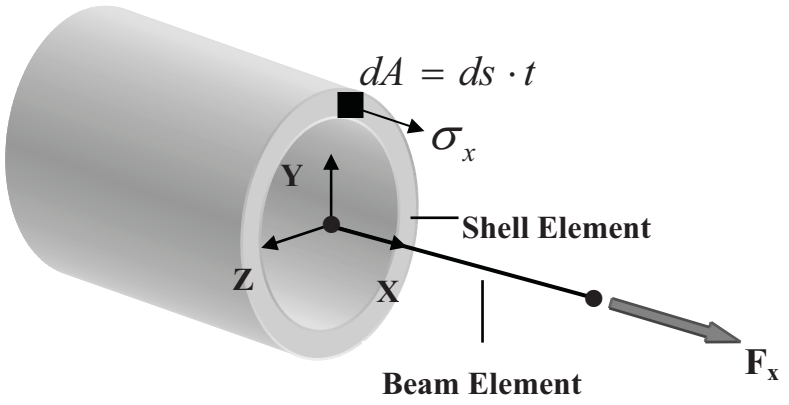

Figure 3.7 Schematic illustration of beam-shell coupling under Axial Force

The schematic description of mixed beam-shell coupling under the axial force along x-axis is illustrated as shown in Figure 3.7. The beam element is aligned with the axis of cross-section by shell elements without connecting nodes. This method aims to couple the axial displacement of the shell nodes at the interface to the axial displacements of the beam node so that the distribution of stress on the interface is similar to that given by elastic theory.

Applying the axial load alone, the only non-zero stress on the shell side is direct stress, σ_x. Equating the work done by the beam with that by the surface stress of

the shell, the following equation could be deduced:

$$F_x u = \int_A \sigma_x U dA = \int_S \sigma_x t ds \tag{3.1}$$

where F_x is the axial force along x-direction, u is the beam node displacement and U is shell node displacements, A is the cross-sectional area. Moreover, t is the shell thickness and s is the circumference of shell edge.

The axial stress could be taken as uniform over the cross-section if the shell region is slender enough and is given by

$$\sigma_x = \frac{F_x}{A} \tag{3.2}$$

In the finite element model, the axial displacement at any point is found by interpolation from nodal displacements.

$$U = [N]\{U\} \tag{3.3}$$

where $[N]$ is the shape function, and $\{U\}$ is nodal displacements.

Substituting Equation (3.2) and Equation (3.3) into Equation (3.1), we can find the following equations:

$$F_x u = \frac{F_x}{A} \sum_{i=1}^{Nelements} \int_{A_i} [N] dA \{U\} \tag{3.4}$$

The cross-section area of representative element on the edge of shell element could be expressed as follows:

$$dA = tds = \sum_{i=1}^{Nelements} t dl_i \tag{3.5}$$

then Equation (3.2) could be rewritten in the following form:

$$F_x u = \frac{F_x}{A} \sum_{i=1}^{Nelements} \int_{A_i} [N] dA \{U\} = \frac{F_x}{A} \int_s [N] t ds \{U\}$$
$$= \frac{F_x}{A} \sum_{i=1}^{Nelements} \int_{l_i} [N] t dl \{U\} \tag{3.6}$$

and Equation (3.2) can be deduced into

$$u = \frac{1}{A} \sum_{i=1}^{Nelements} \int_{l_i} t [N] dl \{U\} \tag{3.7}$$

where l is the element edge length. Since the cross-sectional area is simply the product of the edge length and shell thickness, Equation (3.7) can be written as

$$\left(\sum_{j=1}^{Nelements} t_j l_j \right) u = \sum_{i=1}^{Nelements} \int_{l_i} t [N] dl \{U\} = [B] \{U\} \tag{3.8}$$

where $[B]$ is a matrix of constants depending on the cross-sectional parameters and shape functions. Thus, we arrive at a multi-point constraint equation of beam-shell coupling for axial force of the following form:

$$-a_0 u + B_1 U_1 + B_2 U_2 + B_3 U_3 + \cdots = 0 \tag{3.9}$$

where $a_0, B_1, B_2, \cdots$. are the constants depending on the cross-section geometry and type of shape functions. u is the beam node displacement while $\{U\}$ stands for shell node displacements along x-direction in which U_1 U_2 U_3 $\cdots$ are the components.

Bending

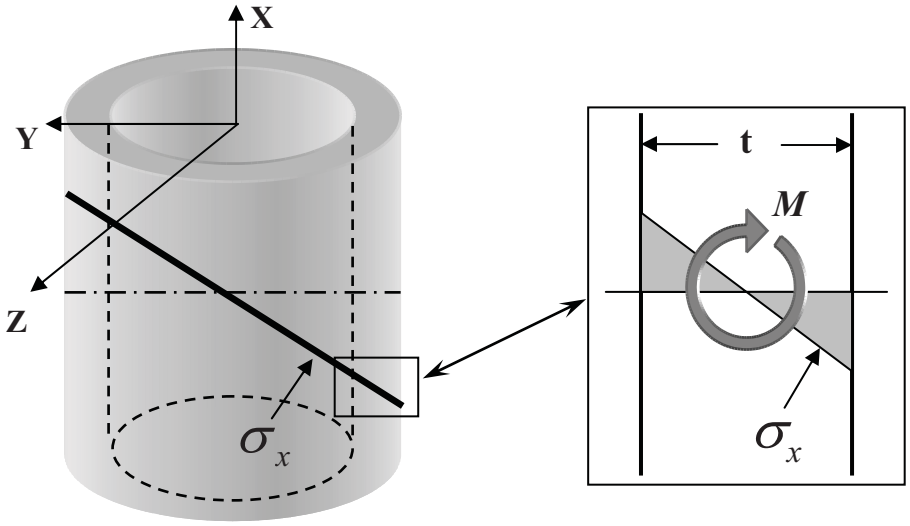

Figure 3.8 Schematic illustration of rotations produced on shell edge by bending stresses

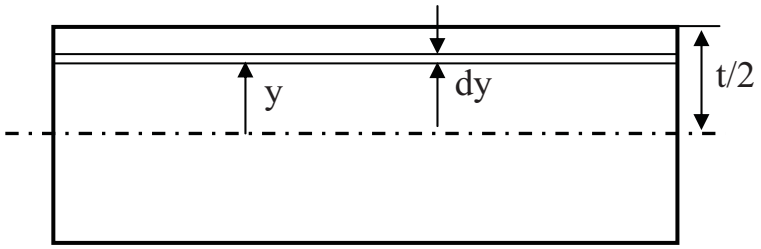

Figure 3.9 Schematic illustration of integration along the direction of shell thickness

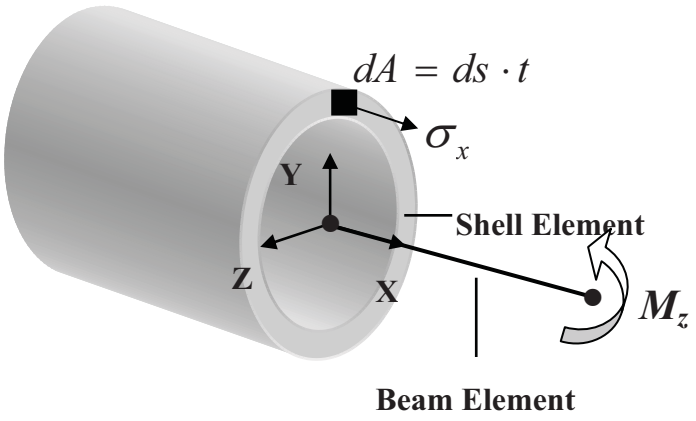

Figure 3.10 Schematic illustration of beam-shell coupling under Bending Moment

In the similar way, the loading case of bending moment is also studied to obtain the corresponding constraint equation. The only non-zero stress on the shell side of the transition is direct stress, σ_x, which varies linearly over the cross section according to the direct stress foumula subject to pure bending moment. Since this stress varies through the thickness of the shell, and then moments are produced about the shell edge. To illustrate this, bending of a thin-walled tube is investigated in this case.

Direct stress, σ_x, due to unit bending moment about the z-axis is shown in Figure 3.8. From the exaggerated portion of the tube wall, it can be seen that the stress varies linearly through the thickness.

The flexure formula of normal stress of a stragiht member under the pure bending moment can be expressed by

$$\sigma = \frac{My}{I} \tag{3.10}$$

Considering the direct stress due to the coupled bending situation subjected to moment about the y and z axes:

$$\sigma_x = M_z\left(P \cdot z + Q \cdot y\right) \tag{3.11}$$

$$P = \left[\frac{I_{yz}}{I_{yz}^{\ 2} - I_{yy}I_{zz}}\right] \quad Q = \left[\frac{I_{yy}}{I_{yy}I_{zz} - I_{yz}^{\ 2}}\right] \tag{3.12}$$

where P Q represent the reciprocals of second moment area about the x-axis and y-axis respectively. It is assumed that there is no coupling of direct stresses

induced by applying bending moments at respective axis. In relation to the mid-plane of the shell, the variation of stress through the thickness produces a moment per unit length of edge, M_s, as indicated.

The magnitude of the rotation is determined by integrating σ_x through the thickness. For a shell edge of arbitrary orientation, the moment about it may be resolved into two components

$$M_s = M_{sy}\left(\frac{dy}{ds}\right) + M_{sz}\left(\frac{dz}{ds}\right) \tag{3.13}$$

where dy/ds and dz/ds are two components of the tangential direction cosines respectively. If the shell is planar and lies on the X-Z plane, as shown in Figure 3.9, both M_{sy} and dy/ds will be zero, and so Equation (3.13) will be simplied as

$$M_s = M_{sz}\left(\frac{dz}{ds}\right) \tag{3.14}$$

For a unit moment about the z-axis of such a shell region, the rotation per unit length of edge is

$$M_s = 0 + M_{sz}\left(\frac{dz}{ds}\right) = \int_{-t/2}^{t/2} \sigma_x y dy \left(\frac{dz}{ds}\right) = 2\int_{0}^{t/2}\left[Q\left(y+\frac{h}{2}\right)\right] y dy \left(\frac{dz}{ds}\right) = R\left(\frac{dz}{ds}\right) \tag{3.15}$$

The rotation over each element is evaluated in the finite element model at the Gauss points, and subsequently further extrapolated to the nodes.

For node i, the moment is written as

$$M_{szi} = R\left[\sum_{k=1}^{2} N_i \cdot W_k \cdot \left|det\, J\right|_k \left(\frac{dz}{ds}\right)_k\right] \tag{3.16}$$

where J and W are the Jacobian and weighting factor at Gauss point, k, respectively. Two Gauss points are used here to integrate over each quadratic shell element edge.

For general (unsymmetrical) sections, a rotation will be produced about the y-axis also

$$M_{syi} = T\left[\sum_{k=1}^{2} N_i \cdot W_k \cdot \left|det\, J\right|_k \left(\frac{dy}{ds}\right)_k\right] \tag{3.17}$$

where R and T in theose two equations are integration constants.

It is obvious from the above equations that any rotation about the beam node will produce displacements in the x-direction as well as rotations about the y and z-axes of the shell edge nodes. As shown in Figure 3.10,considering the moment about the z-axis and equating the work done at the interface can be expressed as the follows:

$$M_z\theta_z = \int_A \sigma_x U dA = 2\int_0^{t/2} Q\left(y + \frac{h}{2}\right) y\left(\frac{dz}{ds}\right)\theta_z dy + 2\int_0^{t/2} P\left(z + \frac{b}{2}\right) z\left(\frac{dy}{ds}\right)\theta_y dx \tag{3.18}$$

The displacements, U, in the finite element model are described by

$$U = [N]\{U\} \tag{3.19}$$

$$\theta_y = [N']\{\theta_y\} \qquad \theta_z = [N'']\{\theta_z\} \tag{3.20}$$

On substitution, the beam rotation, θ_z, is related to shell node displacements, $\{U\}$, and rotations, $\{\theta_y\}$ $\{\theta_z\}$, by the equation

$$\begin{aligned}\theta_z &= \sum_{i=1}^{Nelements} t\left[\sum_{k=1}^{2}[N](Pz+Qy)_k \cdot W_k \cdot |det\,J|_k\right]\{U\} \\ &+ R\left[\sum_{k=1}^{2} N'' \cdot W_k \cdot |det\,J|_k \cdot \left(\frac{dz}{ds}\right)_k\right]\{\theta_z\} + T\left[\sum_{k=1}^{2} N' \cdot W_k \cdot |det\,J|_k \cdot \left(\frac{dy}{ds}\right)_k\right]\{\theta_y\} \\ &= [B]\{U\} + [C]\{\theta_z\} + [D]\{\theta_y\}\end{aligned} \tag{3.21}$$

So the multi-point constraint equations for the bending about the z-axis can be written as

$$-\theta_z + C_1U_1 + C_2U_2 + \cdots + D_1\theta_{z1} + D_2\theta_{z2} + \cdots + E_1\theta_{y1} + E_2\theta_{y2} + \cdots = 0 \tag{3.22}$$

Also considering the bending moment acting about the y-axis yields a similar equation

$$-\theta_y + G_1U_1 + G_2U_2 + \cdots + H_1\theta_{z1} + H_2\theta_{z2} + \cdots + L_1\theta_{y1} + L_2\theta_{y2} + \cdots = 0 \tag{3.23}$$

where $[C]$ $[D]$ $[E]$ $[G]$ $[H]$ $[L]$ are the matrix of constants depending on the cross-section geometry and type of shape functions.

Torsion

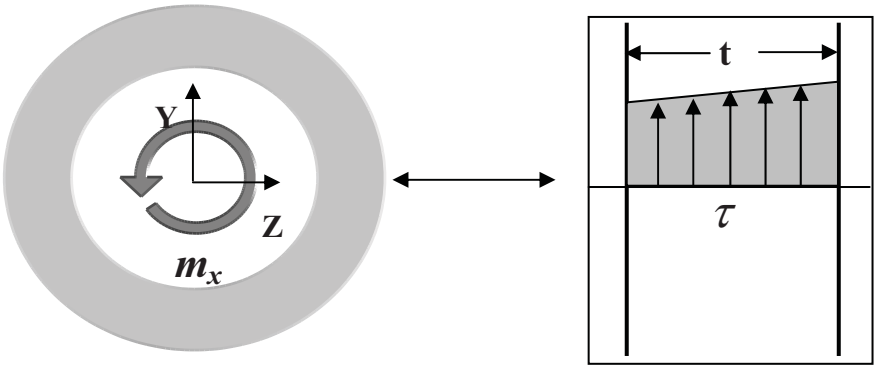

Figure 3.11 Schematic illustration of shear stress distribution of tube thickness due to torsion loading

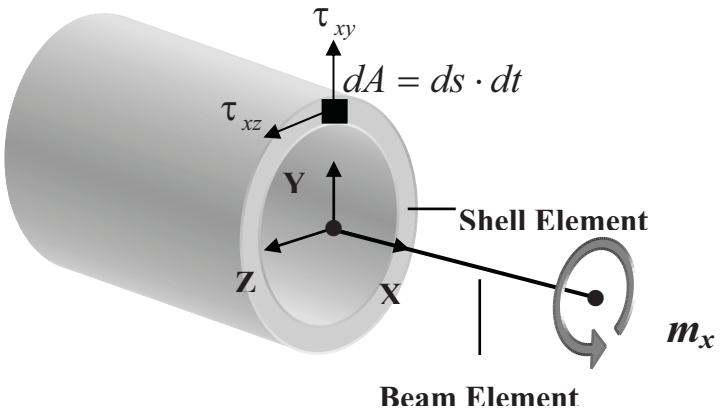

Figure 3.12 Schematic illustration of beam-shell coupling under Torsion

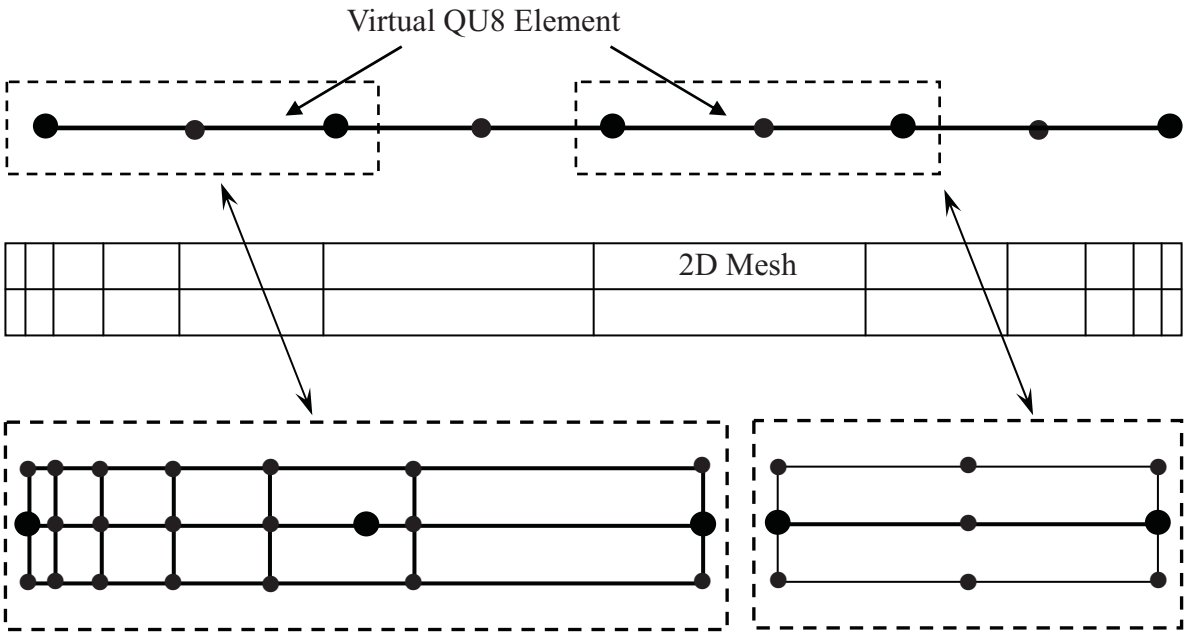

Figure 3.13 Transition shell edges swept 2D mesh and virtual 8 noded quadrilateral elements

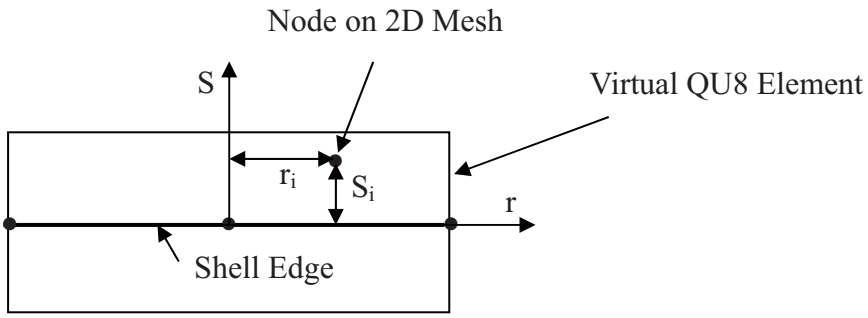

Figure 3.14 Transition from nodes on 2D mesh to nodes on shell edge

Under the action of a pure torsion, the only non-zero stresses on the shell side of the transition are shear stresses, τ_{xy} and τ_{xz}. However, these stresse components usually vary through the thickness of the shell element, and so the resulting twisting moment per unit length of edge on the shell edges must be considered.

Maximum shear stress, τ, due to a moment about the x-axis is shown in Figure 3.11. From the exaggerated portion of the tube wall, it can also be seen that the shear stress distributed over the tube's cross-sectional area varies linearly along any radial line. In relation to the midline, the variation of stress through the thickness produces a positive moment about x-axis as indicated in Figure 3.12. In the bending case, rotations occurred due to similar circumstances. However, the rotations cannot be evaluated analytically in this case. They can be obtained from a particular node by summing up the contributions from equivalent nodes on the 2D mesh. The issue of relevant nodes must be considered before contributions from nodes on the 2D mesh can be discussed.

As mentioned before, each shell edge is swept through a distance of half the shell thickness in a direction normal to the edge, thus creating two 8 noded

quadrilaterals (one on each sideof the shell edge). This 2D mesh is subsequently graded towards local features. Figure 3.13 illustrates the 2D graded mesh generated from the shell edge. In order that forces and rotations are summed up correctly for each shell edge node, nodes on the 2D mesh have to be associated with their parent shell edges. The association can be achieved by creating a virtual (pseudo) 8 noded quadrilateral for each shell edge. Two virtual elements are shown in Figure 3.13. If a node on the 2D mesh is inside this vritual element, then it contributes to the forces on the shell edge. These associations are achieved via inverse maps of the virtual 8 noded quadrilateral elements. This position is given in the logical co-ordinate system, (r, s) as shown in Figure 3.14.

By carrying out a torsion analysis on the 2D cross-section, shear stress components, τ_{xy} and τ_{xz}, are obtained for any given torque, and so the shear stresses are known at each node on the 2D mesh. The forces on these nodes must be determined to enable the forces and moments on the shell edge nodes to be evaluated. The forces are obtained by integrating the stress over the area of each 2D-element face and subsequently extrapolating the result at each integration point back to the 2D nodes. The forces in the y-direction, $\left[F_y\right]$, on the 2D mesh nodes are written as

$$\left[F_y\right] = \sum_{i=1}^{Nelements} \left[\int_{A_i} \tau_{xy} [N] dA \right] = \sum_{i=1}^{Nelements} \left\{ \sum_{k=1}^{4} \left(\tau_{xy}\right)_k \cdot w_k \cdot \left| det\, J \right|_k [N] \right\} \quad (3.24)$$

Similarly, forces $\left[F_z\right]$, are

$$[F_z] = \sum_{i=1}^{Nelements} \left[\int_{A_i} \tau_{xz} [N] dA \right] = \sum_{i=1}^{Nelements} \left\{ \sum_{k=1}^{4} (\tau_{xz})_k \cdot w_k \cdot |det\, J|_k [N] \right\} \quad (3.25)$$

where $[N]$ are the serendipity shape functions for these 8 noded quadrilaterals. If a 2D node lies on a boundary between n shell edge virtual elements, then the force for that node must be divided by n in $[F_z]$ and $[F_y]$ (in order to comply with finite element formulations over the complete shell edge transition). The forces on the shell edge nodes, due to an applied torque on the cross-section, are obtained by summing relevant shear forces. $[F_z]$ and $[F_y]$, of the 2D mesh across the virtual element faces it belongs to.

$$[P_y] = \sum_{i}^{Nelements} \left[\sum_{j=1}^{2Dnodes} F_{yj} [N] \right] \quad (3.26)$$

$$[P_z] = \sum_{i}^{Nelements} \left[\sum_{j=1}^{2Dnodes} F_{zj} [N] \right] \quad (3.27)$$

where P_z and P_y are the shell nodal forces, 2D nodes is the number of 2D nodes that lie inside each shell edge virtual element, and $[N]$ are the quadratic 1D shape functions at logical ordinate.

The moments on the shell edge nodes, due to an applied torque on the cross-section, are determined by summing moments produced due to the action of shear forces, F_z and F_y, across the virtual element faces it belongs to

$$[M_x] = \sum_{i}^{Nshelledges} \left[\sum_{j=1}^{2Dnodes} \left(F_{yj} \left(\frac{dy}{ds} \right) + F_{zj} \left(\frac{dz}{ds} \right) \right) \left(\frac{-st}{2} \right) [N] \right] \quad (3.28)$$

where dz/ds and dy/ds are the first and second components of the tangential

direction cosines respectively, s is the logical ordinate in the direction normal to the shell edge and $[N]$ are the 1D shape function at logical ordinate, r. Because the above expression is a function of the direction cosines and logical ordinate, the moment arm will always be correct in sign, even if the element orientation is clockwise.

The forces and moments on each shell edge node are known now, so a constraint equation can be generated. This equation relates the axial rotation of the beam node to the rotational and translational displacements of the nodes on the shell edge side of the transition. Considering the moment about the x-axis and equating the work done at the interface leads to

$$m_x \theta_x = [P_y]\{V\} + [P_z]\{W\} + [M_x]\{\theta_x\} \tag{3.29}$$

where m_x is the moment applied to the 2D analysis of the cross-section. A multi-point constraint equation can now be written in the form

$$-m_x\theta_x + C_1'V_1 + C_2'V_2 + \cdots + D_1'W_1 + D_2'W_2 + \cdots + E_1'\theta_{x1} + E_2'\theta_{x2} + \cdots = 0 \tag{3.30}$$

where $[C']$ $[D']$ $[E']$ are the matrix of constants depending on the cross-section geometry and type of shape functions.

Instead of directly using general solution given by the stress function introduced by Timoshenko (Timoshenko *et al*. 1970), the concept of shear flow enable us to get an approximate stress distribution of thin-walled sections subjected to torsion.

For the any point in the tube wall or for any shape of wall section, we could

always reach the conclusion that shear flow q is constant around the circumstance of any thin-walled member in torsion. Note that this is only applicable to closed sections. Once we have determined the value of shear flow in a wall, we can determine the stress at any point by dividing the shear flow by the wall thickness as $\tau_p = \frac{q}{t_p}$. For many practical problems relating to thin-walled torsion members, the shear flow applied to the whole section can be calculated as formula $q = \frac{T}{2A}$, where T is the torque load and A is the area inside the mid-thickness line.

In summary, based on the shear flow and for the calculation simplicity, the model structure is considered as the thin-walled section which can be assumed the shear stress is the same along the direction of the shell thickness so that the shear stress distribution is only the function of length of the shell edge.

Shear

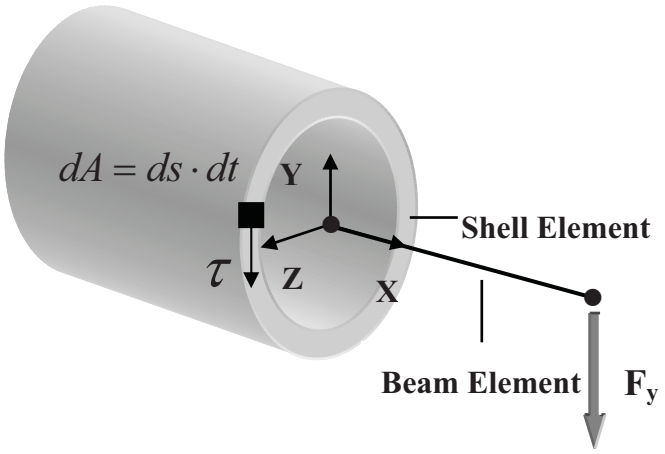

Figure 3.15 Schematic illustration of beam-shell coupling under Shear Forces

The mixed beam-shell coupling subjected to shear force is illustrated in Figure 3.15. Under the action of a pure shear force, the only non-zero stresses in the continuum are shear stress conponents, τ_{xy} and τ_{xz}. The action of a shear force on the beam node produces in plane shear resultant, N_m, twisting and bending moments per unit length, M_m and M_n, with corresponding translations and rotations of the nodes on the shell side of the interface. As with the torsion case, thin wall theory will not suffice, so a 2D analysis is required. Subsequent to the 2D analysis, forces are evaluated at the 2D mesh nodes. The forces and moment on each shell edge node are determined by implementing an inverse map.

Equating the work done at the interface due to a shear force in the y-axis leads to

$$p_y v = \lfloor P_{y1} \rfloor \{V\} + [P_{z1}]\{W\} + [M_{x1}]\{\theta_x\} \tag{3.31}$$

where p_y is the exterior shear force along y-axis applied in the cross-section. Similarly, due to a shear force in the z-axis

$$p_z w = \lfloor P_{y2} \rfloor \{V\} + [P_{z2}]\{W\} + [M_{x2}]\{\theta_x\} \tag{3.32}$$

where p_z is the shear force applied in the 2D analysis of the cross-section. $\lfloor P_{y1} \rfloor$, $\lfloor P_{y2} \rfloor$, $[P_{z1}]$, $[P_{z2}]$ are the shell nodal forces while $[M_{x1}]$, $[M_{x2}]$ the shell nodal moments of shell elements in the x-axis and y-axis respectively.

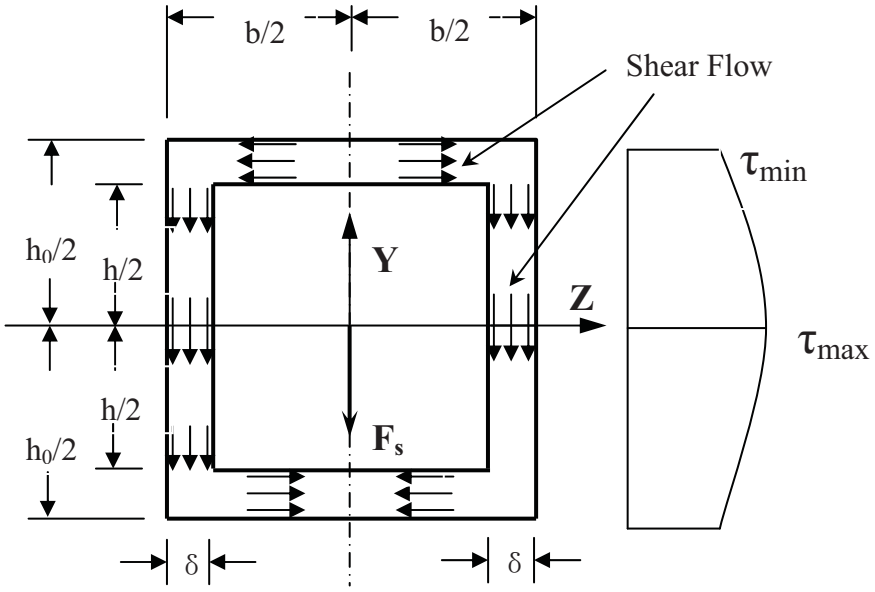

Figure 3.16 Schematic illustration of shear stress distribution of web of the thin-walled sections subjected to Shear Force

Two multipoint constraint equations can be written in the form

$$-p_y v + B_1 V_1 + B_2 V_2 + \cdots + C_1 W_1 + C_2 W_2 + \cdots + D_1 \theta_{x1} + D_2 \theta_{x2} + \cdots = 0 \qquad (3.33)$$

$$-p_z w + E_1 V_1 + E_2 V_2 + \cdots + F_1 W_1 + F_2 W_2 + \cdots + G_1 \theta_{x1} + G_2 \theta_{x2} + \cdots = 0 \qquad (3.34)$$

According to the mechanics of materials, the thin-walled section subjected to shear forces can be simulated as the "web and flange" system of the I-type cross section, in which the edges along the shear force direction can be simulated as "web" and ones normal to shear force as "flange" as shown in Figure 3.16. Under the situation of pure shear forces loading, the external shear forces are mainly resisted by the "web" and shear stresses on it could be considered as uniformly distributed about the thickness direction when the thickness of "web" is significantly less than the width of "flange". So the web shear stress of parabolic

distribution along the height could be illustrated as the following figure and expressed as the below formula:

$$\tau(y) = \frac{F_s}{16 I_z \delta}\left[b\left(h_0{}^2 - h^2\right) + 2\delta\left(h^2 - 4y^2\right)\right] \tag{3.35}$$

Although the shear stresses on "flange" is not considered in campare with those on web that they are often ignored in most cases. Furthermore, despite the shear stresses on "flange" are taken into account, their work at the shear force direction is always zero because the shear stress direction is normal to vertical of displacement. Therefore, during the derivation process of constraint equations, the shear stresses on "flange" are ignored and the web propotion is considered.

3.2.3 Implementation Methods Adopted in Multi-Scale Modeling

Modeling Method by Mixed Dimensional Coupling via Constraint Equations

A multi-point constraint equation is an equation which defines a relationship between sets of displacements within a finite element model. The adopted scheme is proposed by McCune (1998), which utilized an outcome of Reissner's bending theory of elastic plates and showed that proper connections between plate and beam elements, and plate and solid elements can be achieved via multipoint constraint equations evaluated by equating the work done on either side of the dimensional interface. This procedure is general and as long as the stress distribution due to any given loading can be determined at each interface,

beam-solid (Monaghan *et al*. 1998), beam-shell (Managhan 2000) or shell-solid (Da´vila 1994) coupling can be achieved for transitions with arbitrary shapes of cross-sections. Mixed dimensional coupling using constraint equations has been shown to give good results (Managhan 2000). In this study, only the widely used situation for coupling the beam and shell elements is presented.

Therefore, the key issue involved in multi-scale modeling is how to solve mixed dimensional coupling on the connecting interfaces at different scales. The energy equation is developed by equating the work done on the interfaces of different dimensions. It is used as the basic principle to shift between different length scales in order to derive accurate multi-point constraint equations adopted for the mixed dimensional coupling in multi-scale modeling. Furthermore, the constraint equations could be categorized as the four simple loading cases, namely, axial forces, bending moment, shear force and torsion respectively. For instance, in the axial force case, by introducing the equating work done on the either side of interfaces along the direction of axial force, the aim is to couple the axial displacements of the shell nodes at the transition to the axial displacements of the beam nodes such that the distribution of stress on the interface is similar to that given by elastic theory. Similarly, constraint equations for bending moments, shear forces, and torsion can be correspondingly derived in the same format. However, more attentions should be paid to the fact that once the type of connection elements and number of retained elements at the transition interface are determined, all the coefficients in the above constraint equations are constant

and only depend upon the cross-sectional parameters and shape functions, which makes the implementation procedure much easier and also case-special at the different choices of element types and retained nodes. The corresponding FORTRAN programming codes could be accordingly developed to obtain all the constant values on the basis of number of shell nodes retained on the interface between two types of element.

Modeling Method via Substructuring Technique

The method of substructuring in finite element method is to condense a group of finite elements into one element which represents a matrix and can be defined as a collection of elements employed to subdivide a local model into an equivalent stiffness element on the basis of linear response. In the previous finite element literatures, substructure is also referred to the single-matrix element called as super-element. The term “substructure” is used when it is needed to make clear that results are recovered within the substructure. Otherwise, both terms are used interchangeably.

The basic idea of the substructuring approach is to eliminate all but the degrees of freedom at the retained nodes needed to connect this part to the rest of the model. There are a number of good reasons to use the substructures. At the aspect of computational advantages, system matrices (stiffness, mass) are small as a result of substructuring and only the retained degrees of freedom and the associated reduced stiffness (and mass) matrix are used in the analysis until it is necessary to

recover the solution internal to the substructure. In addition, the efficiency is highly improved when the same substructure is used by multiple times. The stiffness calculation and substructure reduction are performed only once. However, the substructure itself could be used many times, which results in a significant savings in computational effort. In summary, once the stiffness calculation and substructure reduction are computed, the substructure can be used with standard elements in an analysis model, and the time and cost of analysis would be significantly reduced when the model includes the relatively large number of standard elements for structural analysis for large-scale engineering structures such as long-span bridges. This method has been considered as the popular and matured approach and it is also easily implemented in large commercial softwares like ANSYS™ and ABAQUS™.

The modeling method via substructuring technique will be adopted to incorporate the local detailed model into the global model to construct a CMSM of the structure, in which the local models of the concerned details will be treated as the substructures in the computation with the global structural model. And the local stress concentration inside the substructures, that is the local details, could be also obtained by the computation inside the substructures. It should be noticed that the modeling via substructuring technique could be more effective and beneficial when it is used in conjunction with mixed dimensional modeling by constraint equations. The detailed typical connection joint is constructed by constraint equation and substructuring as shown in Figure 3.17. The correspondingly

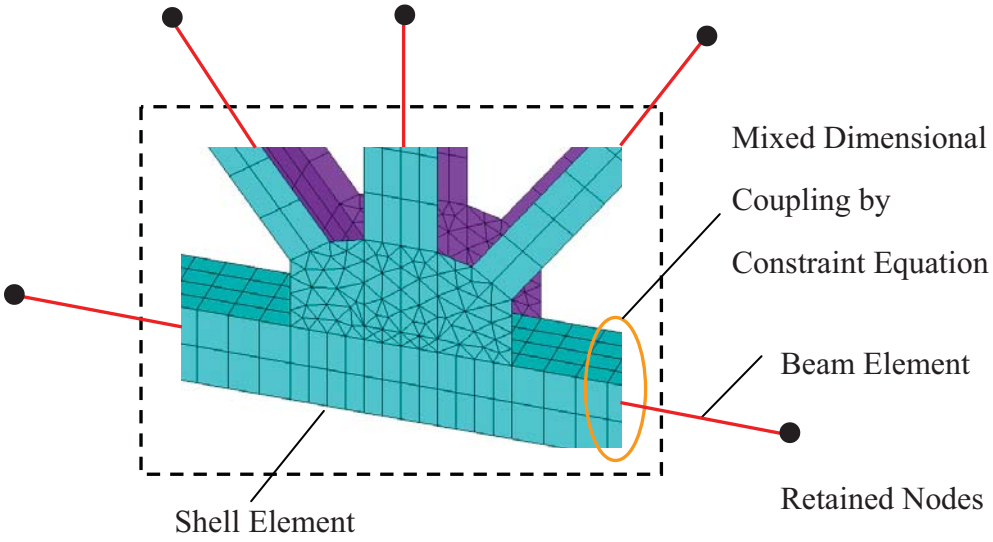

Figure 3.17 Local FE model of concerned joint by substructuring

developed constraint equations are applied at the coupling interface of beam node and shell element nodes of every component, and the whole joint is then constructed as a substructure with the retained nodes which would be incorporated into the global model to build the multi-scale model.

General Procedure for Multi-Scale Modeling

Generally speaking, for the large infrastructure, if only the structural internal forces or nominal stress are required, the global model could be constructed on "lower length level" by structural elements of beam and shell at the length scale of 10^0 m. In contrast, if the local stress distribution of critical locations for the purpose of structural health monitoring and damage evaluation needs to be evaluated, it should be modeled at "higher length level" for local scale simulation of detailed connections at the length scale of 10^{-1} m or much higher of 10^{-3} m. In order to develop an efficient model for carrying out the concurrent multi-scale

analyses of structural responses and local fatigue damage evaluation for the purpose of structural health assessment, the general procedure for developing a CMSM of a given structure can be proposed as follows:

(1) To develop the global FEM at the "lower length scale" of usual 10^0 m with structural elements such as beams and shells on the basis of design drawings of the structure. The objective of the model is to create an accurate description of the dynamic characteristics of the structure and internal forces as well as nominal stresses in the main components in order to determine the critical components in the structure.

(2) Model updating and verification by using the controlled loading tests on the structure and the data from the installed SHM system. In this step, the updating of the global structural model is based on the measured data of the modal properties by the specific tests, and then the updated model is verified by comparing the calculated results of dynamic properties and static response with the measured results or monitoring data output by the SHM system.

(3) To determine the critical locations or components of the structure by the computation and analysis on the dynamic characteristics of the structure and internal forces as well as nominal stresses in the main components.

(4) To develop the local model of the critical component in component scales of 10^{-1}m and more detailed model of critical areas such as the welded details in material scales of 10^{-3} m with multiple substructuring technique,

layer by layer if necessary. The correspondingly developed local models can be used to carry out nonlinear analysis of hot-spot stress distribution and stress concentration of the concerned locations in material scales, and also the scenarios of damage and crack initiation or growth could be introduced and simulated by damage evolution or crack propagation law.

(5) To incorporate the local detailed model into the global model to construct a CMSM of the structure. The key issues involved in coupling method between the models on their respective scales would be then investigated. Finally the concurrent multi-scale model could be used to perform the analysis on the structural deteriorating to obtain local nonlinear responses with the considered damage evolution at the material scale in the vicinity of the concerned details as well as linear response in structural components at lower stress level.

During the above modeling process, there are already so many advanced applications in both global models and local models in traditional macro-scales, but, as yet, still not in the multi-scale modeling. Therefore, the coupling relationship at the interfaces between the two scales is considered as a key issue in multi-scale modeling methodology which will be subsequently studied and discussed in details.

3.3 PRELIMINARY NUMERICAL EXAMPLE BY SIMPLE CASE STUDY

In order to illustrate the developed procedure for mixed dimensional coupling and verify its effectiveness, a case study of thin-walled cantilever beam with particular

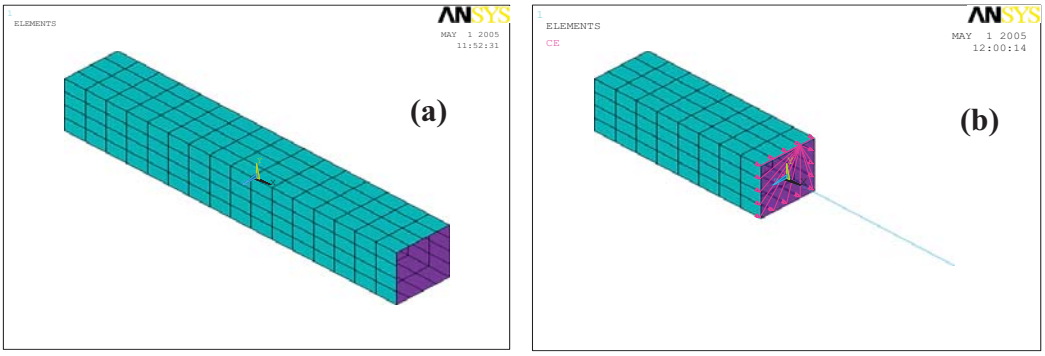

Figure 3.18 Schematic diagrams of simple model in case study: (a) full shell model (b) multi-scale model

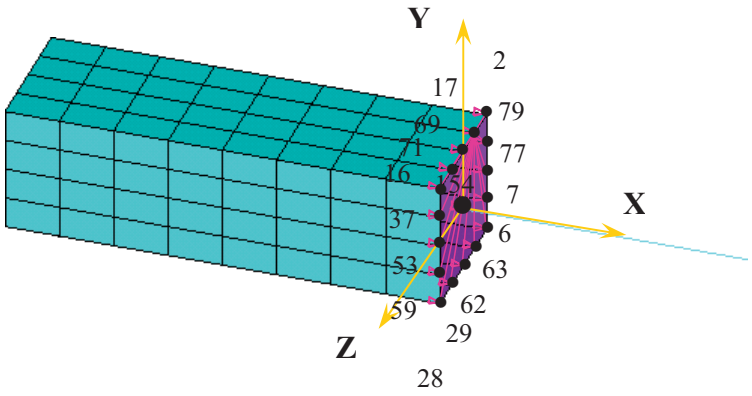

Figure 3.19 Beam-shell coupling model of box section

Table 3.2 Geometric and material data for simple case study

Overall Dimensions (mm)				Element Types	
Height	Width	Length	Thickness of plate	Beam Element (Beam 188)	Shell Element (Shell 63)
700	750	4500	30	2-noded three-dimensional elastic beam element (6 DOF)	4-noded three-dimensional elastic shell element (6 DOF)
Material Parameters					
Young's Modulus		Poisson Ratio			
200 GPa		0.3			

rectangular cross section is performed through comparison of static analysis results by full shell model and mixed-dimensional model as shown in Figure 3.18. A schematic description of beam-shell coupling with meshing and numbering of elements at the interface is illustrated in Figure 3.19. Table 3.2 lists the detailed geometric dimensions and material data adopted in this case study. It is should be noticed this case example is investigated to study mixed-dimensional coupling strategy and implementation method, and only mechanics of material is applicable.

$$
\textbf{Constraint Equations}\begin{cases}
\textbf{Axial (+X)} & -2780U_{154}+180(U_{71}+U_{69}+U_{17}+U_{29}+U_{62}+U_{63}) \\
& +167.5(U_{37}+U_{53}+U_{59}+U_{79}+U_{77}+U_{7})+173.75(U_{16}+U_{2}+U_{28}+U_{6})=0 \\
\textbf{Bending (+Y)} & -70890\ \theta_{y154}+10890\ (U_{37}+U_{53}+U_{59}-U_{79}-U_{77}-U_{7}) \\
& +17145\ (U_{28}+U_{16}-U_{6}-U_{2})+9720\ (U_{71}+U_{29}-U_{63}-U_{17}) \\
& +139.444\ (\theta_{y79}+\theta_{y77}+\theta_{y7}+\theta_{y37}+\theta_{y53}+\theta_{y59}) \\
& +69.722\ (\theta_{y2}+\theta_{y6}+\theta_{y28}+\theta_{y16})=0 \\
\textbf{Bending (+Z)} & 63640\ \theta_{z154}+10890\ (U_{17}+U_{69}+U_{71}-U_{29}-U_{62}-U_{163}) \\
& +16059.0625\ (U_{2}+U_{16}-U_{6}-U_{28})+8416.875\ (U_{37}+U_{79}-U_{59}-U_{7}) \\
& +139.725\ (\theta_{z71}+\theta_{z69}+\theta_{z17}+\theta_{z29}+\theta_{z62}+\theta_{z63}) \\
& +69.8625\ (\theta_{z2}+\theta_{z16}+\theta_{z6}+\theta_{z28})=0 \\
\textbf{Shear (-Y)} & -203648000V_{154}+28057506(V_{77}+V_{53})+25801785(V_{37}+V_{79}+V_{59}+V_{7}) \\
& +11021124(V_{2}+V_{16}+V_{6}+V_{28})=0 \\
\textbf{Shear (-Z)} & -22684800W_{154}+3159000(W_{69}+W_{62})+28790640(W_{63}+W_{29}+W_{71}+W_{17}) \\
& +12062520(W_{2}+W_{16}+W_{6}+W_{28})=0 \\
\textbf{Torque (+X)} & -9648\,\theta_{x154}+900\,(W_{2}+W_{16}-W_{28}-W_{6})+ \\
& 1800\,(W_{17}+W_{69}+W_{71}-W_{29}-W_{62}-W_{63})+837.5(V_{2}+V_{6}-V_{16}-V_{28}) \\
& +1675\,(V_{79}+V_{77}+V_{7}-V_{37}-V_{53}-V_{59})=0
\end{cases}
\tag{3.36}
$$

where U V W represent the translational displacements along x, y, z

directions respectively while θ stands for the rotational displacement of the nodes of beam element and shell elements. Meanwhile, the subscript corresponds to the node number and the axis about which the rotational angle act.

The constraint equations could be categorized as responding to four simple loading cases, namely, axial forces, bending moment, shear force and torsion respectively. Similarly, constraint equations are then deduced for axial force (along the x-direction), bending moments about the y- and z- axes (no coupling), and shear forces applied about the y and z directions (no coupling). The stress distribution due to bending moments and shear forces has been assumed in accordance with simple beam theory. In this study, the corresponding FORTRAN programming codes are accordingly developed by the author to obtain all the constant values on the basis of number of shell nodes retained on the interface between two types of element. The advantage is that only the values of several parameters implanted in programming codes should be changed if the different meshing requirements needed in terms of meshing pattern and the number of shell element nodes retained on the interface, which makes it easier to deal with the other connection patterns.

In summary, as stated in Equation (3.36), there are totally six constraint equations for one beam node at the transition interface which has six active DOFs and they could fully couple the beam node with the edge nodes on the shell elements. More attentions should be paid to the fact that once meshing pattern as well as the number of retained elements at the interface is determined, all the coefficients in

the above constraint equations are constant and they all depend upon only the cross-sectional parameters and shape functions. If the constraint equations have been determined, they are successfully incorporated in the finite element formulation by standard methods such as Lagrange multiplier or penalty function methods. All the constraint equations can be easily complemented in the large general-purpose FE software by *CE commands in ANSYS^{TM} while *EQUATION commands in the ABAQUS^{TM}.

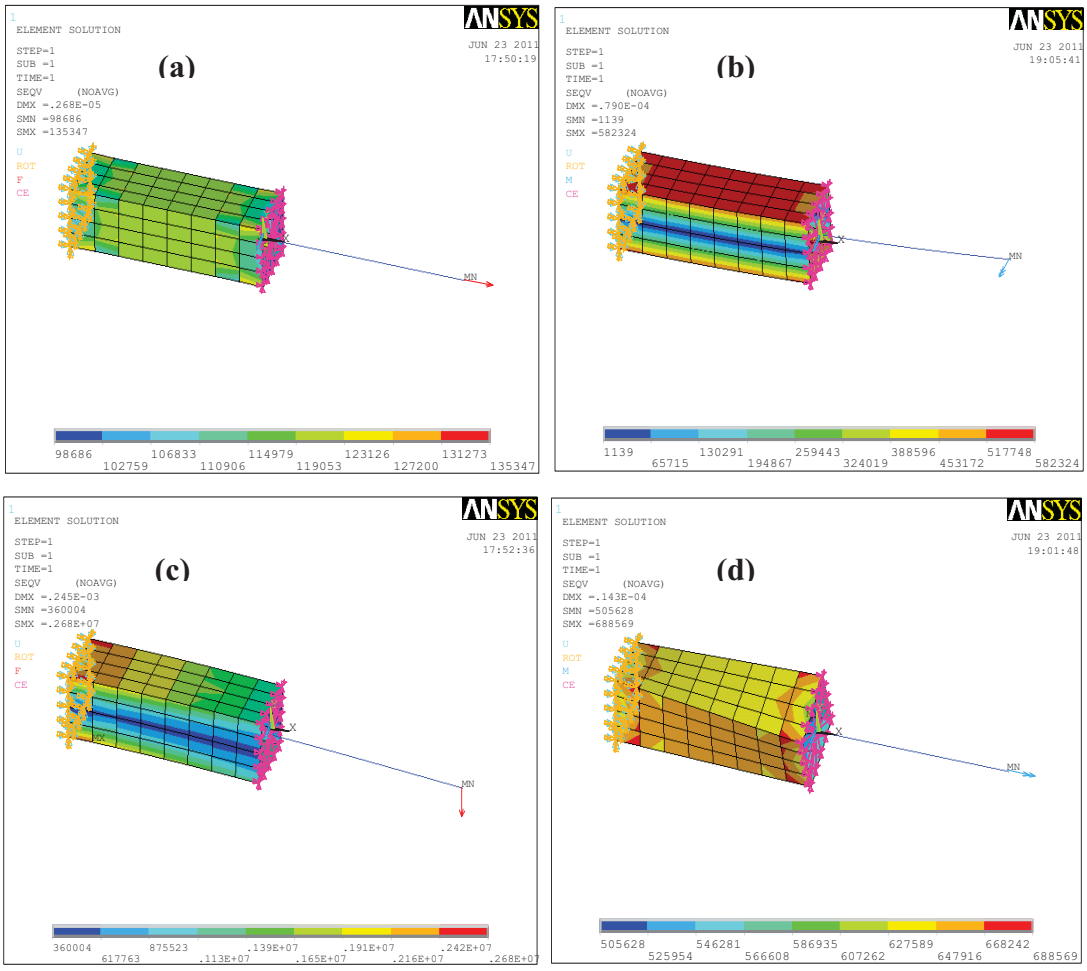

Figure 3.20 Von-Mises stress contour of multi-scale model due to:

(a) axial force (b) bending moment (c) shear force (d) torsion

There are four loading cases which have been calculated, in particular, an axial tension force of 10 kN, a bending moment of 10 kNm, a shear force of 10 kN and a torque of 10 kNm that has been applied at the free end, respectively. It should be emphasized that the constraint equations are derived based on an assumed stress distribution at the interface. Thus, they are only as good as the accuracy of the assumed stress distribution. It has been found that the derived constraint equations result in a smooth stress transition at the interface similar to that given by elastic theory. The Von-Mises stress contour figures showing the results of the coupling model under different loading cases are shown in Figure 3.20.

3.3.1 Results Comparison among Different Models

A comparison of the free end point displacements and particular point stresses among the beam model, shell model, beam-shell coupling model and theoretical value has been conducted and the results are summarized in Table 3.3. It indicates that the results of the beam model are almost identical to that of the theoretical one since the theoretical value is on the basis of the simple beam theory except that in torsion situation, there is 2% difference between them because the approximation method of shear flow is introduced into the theoretical value calculation. Moreover, the results of the shell model are slightly smaller than that of the beam model because of the type difference between the beam element and shell element, which suggests that the latter element is more rigid than the former one. The more important point is that the result of the mixed model shows a very

Table 3.3 Free end deflection and Von-Mises stress of particular location of cantilever beam using different types of model

Model Types	Deflection (m)of Free End / Error (%) due to			
	Axial Force (10 kN)	Bending Moment (10 kNm)	Shear Force (10 kN)	Torsion (10 kNm)
	longitudinal (+X)	Vertical (+Y)	Vertical (-Y)	Rotation angle (+X)
Beam model	2.6978E-6/0	7.95E-5/-0.06	2.39E-4/0.15	5.6963E-5 rad/-2.2
Multi-model (Shell Percentage 50%)	2.68E-6/-0.66	7.883E-5/-0.9	2.4334E-4/1.97	5.7229E-5 rad/-1.6
Shell model	2.68E-6/-0.66	7.9261E-5/-0.36	2.363E-4/-0.98	5.8063E-5 rad/-0.3
Theoretical Value	2.6978E-6	7.9549E-5	2.3865E-4	5.8238E-5 rad

Model Types	Von-Mises Stress (MPa) (X=0 Z=0 Upper side location) due to			
	Axial Force (10 kN)	Bending Moment (10 kNm)	Shear Force (10 kN)	Torsion (10 kNm)
Beam model	0.119904	0.549969	0.2779	—
Multi-model (Shell Percentage 50%)	0.1199/-0.003	0.5279/-4.0	0.2692/-3.1	0.36049/4.3
Shell model	0.1199/-0.003	0.5364/-2.5	0.26567/-4.4	0.37408/8.3
Theoretical Value	0.119904	0.549969	0.2779	0.34549

close agreement with that of the shell model. Despite a bit bigger difference occurs in the torque case, the maximum percentage error in other three loading

cases is found to be less than 5% with regard to both displacement and stress.

3.3.2 Different Percentage of Shell Region in Multi-scale Model

Table 3.4 Free end deflection and Von-Mises stress of particular location of cantilever multi-model constructed by different percentage of shell region

Multi-Model (Shell Region % of Beam Length)	Deflection (m) of Free End due to			
	Axial Force (10 kN)	Bending Moment (10 kNm)	Shear Force (10 kN)	Torsion (10 kNm)
	longitudinal (+X)	Vertical (+Y)	Vertical (-Y)	Rotation angle (+X)
40	2.68E-6	7.88E-5	2.2683E-4	5.707E-5 rad
60	2.68E-6	7.89E-5	2.2725E-4	5.7403 E-5 rad
80	2.68E-6	7.89E-5	2.2747 E-4	5.774 E-5 rad
Multi-Model (Shell Region % of Beam Length)	Von-Mises Stress (MPa) (X=0 Z=0 Upper side location) due to			
	Axial Force (10 kN)	Bending Moment (10 kNm)	Shear Force (10 kN)	Torsion (10 kNm)
40	0.1201	0.52833	0.25163	0.33959
60	0.11967	0.52707	0.25095	0.34212
80	0.1199	0.52740	0.25042	0.34315

Furthermore, the results of multi-models constructed by different percentage of shell region are also listed in Table 3.4. The different particular points in Table 3.3 and Table 3.4 result in the different values under the loading case of shear force. It is observed that the percentage of shell region in multi-model just has

tiny influence of less than 2% on the structural response, which could be completely neglected in structural analysis process. So from this point of view, the problem of shell percentage is not a factor should be concerned when constructing the mixed dimensional model.

3.3.3 Case Study of Indeterminate Structure

The above case study of simple beam with rectangular cross section has been investigated under the specific loading cases. Furthermore, in order to validate the developed multi-scale model, the statically indeterminate structure is needed to be studied. The propped cantilever beam with the same geometry and material information is then taken as the sample of a case study. As shown in Figure 3.21, the simple supports are added to the previous cantilever beam to make it as a statically indeterminate structure.

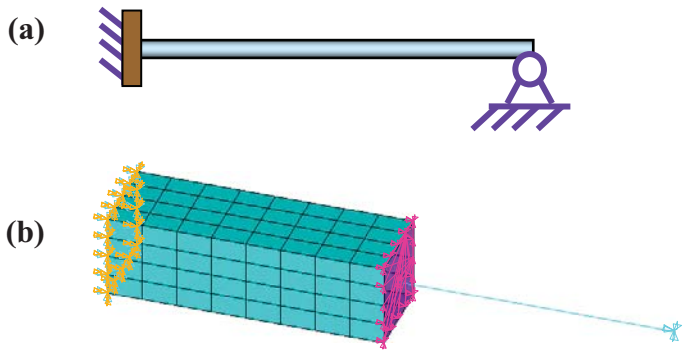

Figure 3.21 Schematic illustration of (a) typical statically indeterminate structure of propped cantilever; (b) multi-scale model of propped cantilever

Instead of comparing the results by different FE models as well as varying element percentage, the various coupling methods on the interface bridging scales

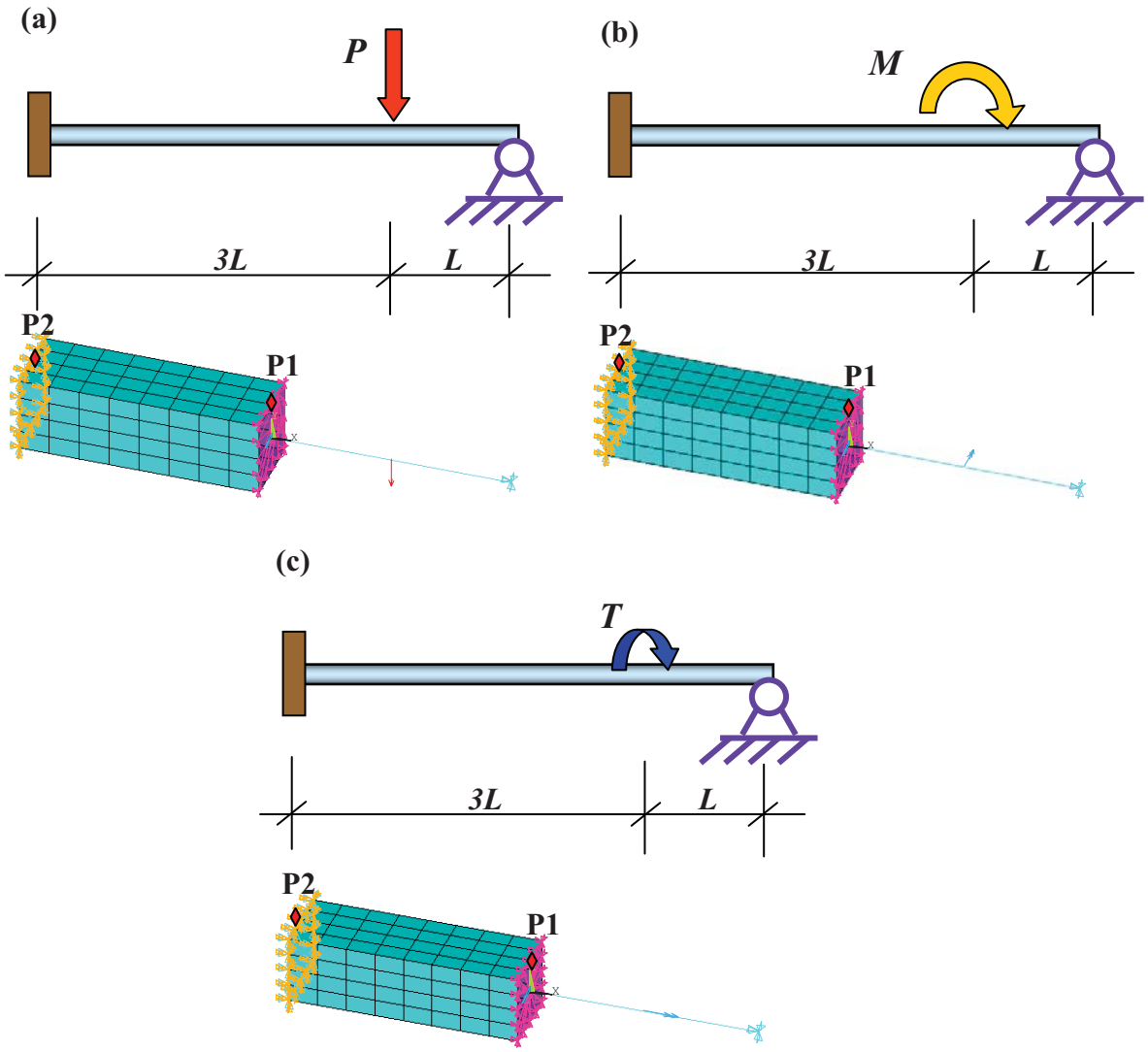

Figure 3.22 Loading cases of statically indeterminate structure of propped cantilever (a) concentrated point loading; (b) bending moment; (c)torsion

adopted by other researchers would be presented and computed under specific loading cases for verifying and validating the developed multi-scale modeling strategy and implementation methods.

In order to verify and validate the developed mixed dimensional coupling method by constraint equations through equaling the work done on the interface, as shown

Table 3.5 Comparison of deflection at load applied point and selected points Von-Mises stress by cantilever multi-scale model with ones by other different types of elements

Computed values		Model Types					
		Beam model	Shell model	Multi-model (Shell Percentage 50%)			Theoretical Value
				Coupling 1	Coupling 2	Coupling 3	
Concentrated point load (-Y) 10 kN							
Deflection at the load applied point (-Y)(m) /Error (%)		1.68E-5	1.673E-5 /-0.4	1.676E-5 /-0.24	1.663E-5 /-1.01	1.667E-5 /-0.77	1.68E-5
Von-Mises Stress (MPa) /Error (%)	P1	3.987E-2 /0.34	3.961E-2 /-0.34	3.951E-2 /-0.58	3.636E-2 /-8.5	3.934E-2 /-1.0	3.974E-2
	P2	3.27E-2 /0.4	3.264E-2 /0.21	3.245E-2 /0.37	3.224E-2 /-1.0	3.24E-2 /-0.52	3.257E-2
Bending Moment (-Z) 10 kNm							
Deflection at the load applied point (-Y)(m) /Error (%)		5.45E-6	5.385E-6 /-1.2	5.368E-6 /-1.5	5.319E-6 /-2.4	5.259E-6 /-3.5	5.45E-6
Von-Mises Stress (MPa) /Error (%)	P1	0.553 /0.78	0.544 /-0.89	0.542 /-1.23	0.495 /-9.8	0.535 /-2.6	0.549
	P2	0.224 /0.56	0.221 /-0.78	0.219 /-1.8	0.217 /-2.6	0.218 /-2.3	0.223
Torsion (+X) 10 kNm							
Rotation angle at the load applied point (+X)(rad) /Error (%)		4.703E-5	4.612E-5 /-1.9	4.634E-5 /-1.47	4.569E-5 /-2.85	4.545E-5 /-3.36	4.703E-5
Von-Mises Stress (MPa) /Error (%)	P1	0.601 /-1.48	0.582 /-4.59	0.59 /-3.28	0.556 /-8.85	0.561 /-8.03	0.61
	P2	0.601 /-1.48	0.582 /-4.59	0.59 /-3.28	0.556 /-8.85	0.561 /-8.03	0.61

Note: Coupling 1 represents constraint equations developed by author (equating work done on interface)
Coupling 2 represents constraint equations used by Lu (2008) (deformation compatibility condition)
Coupling 3 represents constraint equations used by Tang (2011) (stress compatibility condition)
P1 is the upper side point of shell element (X=0 Z=0 $+Y_{max}$) on the interface
P2 is the upper side point of shell element ($-X_{max}$ Z=0 $+Y_{max}$) on the boundary plane

in Figure 3.22, the simple loading case of the indeterminate structure of propped cantilever beam has been applied to the different models to study the efficiency and accuracy of developed multi-scale coupling method. The concentrated force load, bending moment and torsion are applied at the three-quarter length of the beam. The deflection of load applied position as well as Von-Mises stress values of two selected points (as shown in Figure 3.22) are investigated.

Table 3.5 tabulates the load applied point defection and Von-Mises stress values of selected points of the indeterminate structure of propped cantilever under the simple loading cases. The comparison of those values among the different models in terms of beam element model, shell element model and constraint equations through three coupling algorithms have been performed and the findings could be summarized as the follows:

(1) Those values by beam model are almost identical to that of the theoretical one, which is the same as the finding that those values are almost identical in determinate structure. In other words, the theoretical value is calculated on the basis of the simple beam theory in both determinate and indeterminate structures.

(2) The results of the shell model is slightly smaller than that of the beam model which suggests the characteristics that shell element is more rigid than beam element.

(3) As for the comparison of three coupling algorithms, constraint equations developed by the author is closer to the theoretical values and considered as better

than the other two coupling algorithms. However, there are relatively large difference on stress value of selected interface point by deformation compatibility development since it only accounts for deformation compatibility on the either side of interface but neglects the in-plane displacement of interface which possibly result in such errors. With the distance far from the interface and force applied location, such differences are then significantly reduced according to the Saint-Venant's principle.

In conclusion, on the basis of the above development of multi-scale modeling strategy and implementation methods as well as the simple case studies of applying it to the determinate cantilever beam and propped cantilever structure, it is easily found that during the process of multi-scale modeling at spatial levels, the essential part is universally acknowledged that how to develop an efficient and accurate coupling method connecting different dimensional elements at respective length scales in finite element method. Among those various bridging scales methods, many researchers have recognized constraint equation method as the more convenient and efficient way. For instance, Lu *et al*. (2008) proposes the methodology of connecting microscopic finite element model to macro model by introducing the deformation compatibility condition at the interfaces between different-scale models. Sun (2006) combines Lu's method and substructuring technique to construct multi-scale model. Tang (2011) also develops constraint equations by fulfilling the requirements of stress compatibility condition at the interfaces. All of their works aim to develop their own coupling method, but they

are all constraint equations in nature but they are developed through different coupling algorithms. From this point of view, constraint equations have been introduced to deal with multi-scale modeling problem for years but the development of constraint equations using the coupling algorithm of equating the work done on the interface between the different scales is rarely found so that it could be considered as innovative and original. Moreover, the results comparison validates that the developed coupling method in this project is found to be more efficient and accurate than the others in application for multi-scale modeling.

It should be noticed that coupling algorithm is considered to be the most challenging task to form a link between different types of elements in multi-scale modeling. The existing coupling methods impose limitations on practical application for their inherited defects and case-specific usage. The energy equation, as a fundamental principle, is used to shift between edges of interfaces connecting different length scales. The crucial part is how to derive the proper compatibility conditions on the basis of energy equation. The deformation and stress compatibility equations are just the expression formats of compatibility conditions. In this thesis, the complicated loading situations has been decomposed into four simple loading cases, each of which introduces the assumed variation of the stresses, given by the appropriate beam, plate and shell theory, over the cross-section of the interface. This method is a general procedure for arbitrary transitions and could generate continuous and reliable stress contours. Moreover, the corresponding constraint equations have been successfully derived and easily

implemented in the case study. The multi-scale model result shows a good agreement with those by traditional full element models in both determinate and indeterminate structures. Therefore, the developed coupling method has been verified to be accurate and efficient. From this point of view, the energy equation is regarded as the necessary and sufficient condition at the aspect of mechanical mechanism for multi-scale modeling.

3.4 SUMMARY

The concurrent multi-scale modeling of engineering structures is considered as absolutely necessary and imperative for a damage-oriented model that is able to simulate damage behaviors considering local deterioration processes as well as the structural global response in both scale levels for the purpose of evaluating their health statuses.

The multi-scale modeling strategy and methodology is firstly investigated. A mixed dimensional coupling method using multi-point constraint equations is introduced that is deduced by equating the work done on either side of the mixed dimensional interface. In this study, attention is paid on the multi-scale model that is widely used and constructed by coupling shell element with beam element. The constraint coefficients in terms of displacement compatibility equations on four loading cases are successfully derived by the specifically developed FORTRAN programming codes and implemented on case-specific condition at the definite

choice of element types and retained nodes. Combined with substructuring technique, the application of mixed dimensional modeling can be more beneficial. The multi-scale modeling strategy and methodology for a long-span bridge is further proposed as a general procedure.

A simple numerical case study is then preliminarily investigated that the results of multi-scale model response is in good agreement with those by full beam or shell elements. Moreover, the percentage of shell elements constructed in multi-scale model has hardly any influence on structural response. The similar conclusion could also be drawn in indeterminate structure of propped cantilever beam. The coupling method has been verified to be an accurate and efficient analysis method at the aspect of analytical simulation.

CHAPTER 4

EXPERIMENTAL AND ANALYTICAL CASE STUDY ON THE DEVELOPMENT OF CMSM

4.1 INTRODUCTION

The research group under the leadership of Prof. LI, Zhaoxia of Department of Mechanics in Southeast University (SEU) has performed the research studies focusing on topics of multi-scale modeling strategy and corresponding implementation methods for years. In order to provide the measurement data as the experimental basis to serve the various study purpose of group members, the laboratory tests on a typical scaled down steel truss section have been carried out in SEU 2005. This laboratory test is performed for the purpose of validating the proposed CMSM in term of simulation results and calculation efficiency to fulfill the multi-scale implementation procedure.

The critical locations of Tsing Ma Bridge due to fatigue damage under train loading and truck loading have been identified as the outmost part of the upper chord in steel deck where stands the longitudinal truss section along the bridge (Chan *et al*. 2003). The scaled down specimen of steel truss (as shown in Figure

4.1(c)) is thus designed and manufactured on the basis of drawings of longitudinal truss section (as shown in Figure 4.1(b)) extracted from that suspension bridge decking system (as shown in Figure 4.1(a)). It is believed that the results obtained from the experimental and numerical study on the scaled down truss specimen would be also applied to the real full scale bridge structure according to the similarity principle.

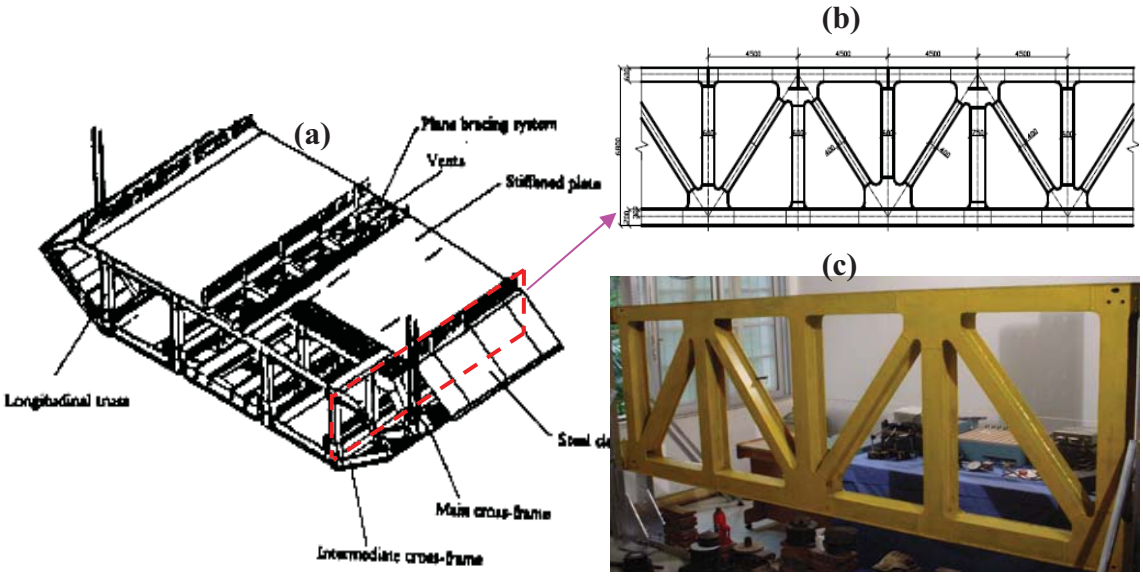

Figure 4.1 Illustration figures of steel truss specimen manufacturing (a) Configuration of TMB decking system (b) Typical longitudinal truss section (c) Reduced-scale specimen of longitudinal truss in laboratory

The experimental studies on the static responses of the bridge longitudinal truss with typical welded details is carried out to obtain corresponding results on the concerned regions for comparison with those of simulations by different modeling methods, namely global models of full beam element, full plate element and multi-scale models by substructuring and constraint equations techniques, respectively. The involved issues about model updating and validation are also

briefly discussed.

4.2 EXPERIMENTAL STUDY ON STATIC RESPONSES OF STEEL TRUSS

The test on static response of typical steel longitudinal truss specimen has been performed in laboratory of Department of Mechanics of SEU in January 2005. Throughout the measurements on the scale down steel truss specimen including the connection and welding details under the circumstance of simple designated loading, the experimental study aims to investigate the structural nominal stress and hot-spot stress distribution of local detailed region subjected to service loading, in order to provide a solid basis for the subsequent procedures of structural parameters identification and model updating and validation.

4.2.1 Laboratory Test Set-up and Procedure

Figure 4.2 Overview of laboratory test set-up:
(a) steel truss specimen (b) test instruments

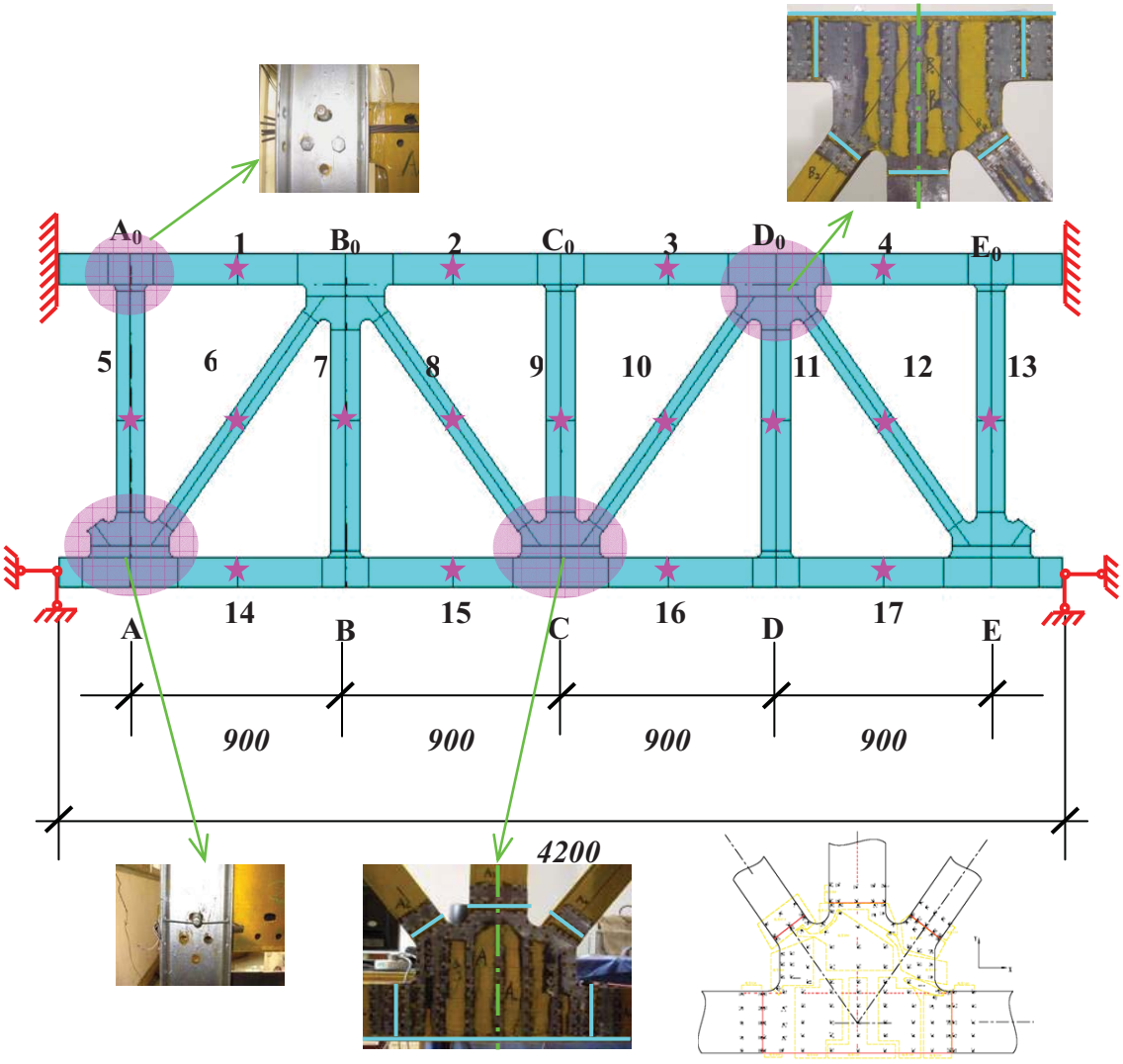

Figure 4.3 Schematic illustration of strain gauges mapping for nominal stress (stars) and local concerned region (shade areas) combined with boundary condition simulation (in mm)

The test setup of steel truss specimen and the corresponding test instruments are briefly illustrated as Figure 4.2. As shown in Figure 4.3, the boundary conditions are ideally simulated as the fixed supports at both ends of up-chords and simply supported bottom chords which have been implemented by steel connecting bolts in laboratory condition. The mapping locations of the installed two types of strain gauges are illustrated. The single-element strain gauges are installed at the

mid-point of each brace or chord of the specimen where those points are assumed to provide the nominal stress information. Meanwhile, the three-element rosette gauges as shown in shade areas are regarded as located at a specific joint "hot-spot" where the local stress distribution situation is more concerned. There are 350 strain gauges in total installed at the concerned regions.

The material property parameters are determined by a preliminary test through pure bending method, and the Young's modulus of steel is adopted as 206.0 GPa and Poisson ratio as 0.259 for subsequent analysis.

The specimen is subjected to specific loadings to obtain the static responses of nominal stress and hot spot stress distribution situation for subsequent result comparison. The important aspects involved in the experiments have been briefly introduced, and test procedure in more details could be found in Yin (2006) who devoted his study to the specimen manufacturing and experimental test in laboratory.

4.2.2 Dynamic Characteristics Test

Because of the relatively simple small structure, the modal test is conducted by impulse excitation method of SIMO (Single Input Multiple Output) using hammering to determine the dynamic properties in terms of mode shape and frequencies under the simulated boundary conditions.

The boundary conditions are the important issues that should be carefully

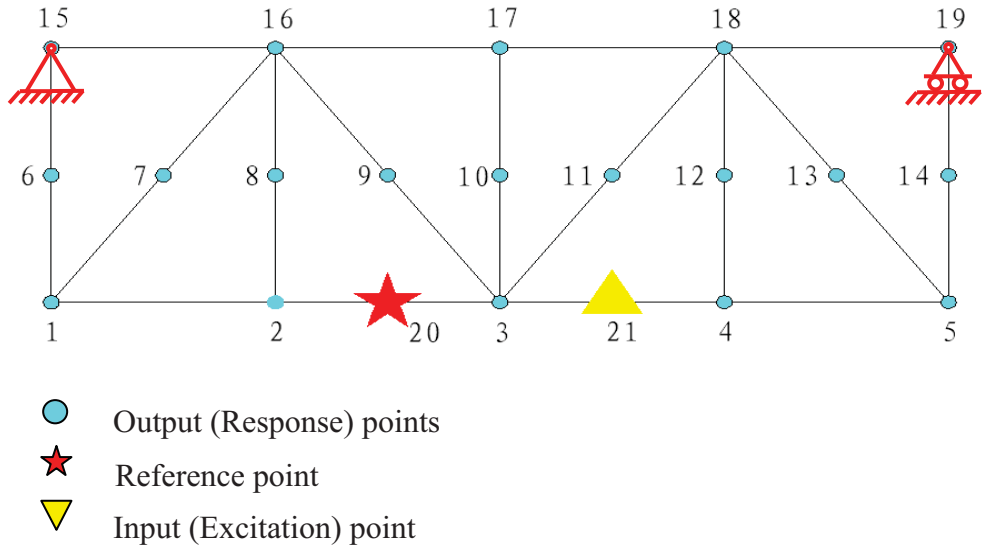

Figure 4.4 Schematic diagram of excitation point and measurement points and reference point locations in modal test

considered in the modal analysis. The idealized way is regarded as free suspension or rigid fixing while it is difficult for either of them to implement in laboratory condition. Because of the limitation of the laboratory equipment and trying to reduce the influence of boundary conditions on modal parameter result as much as possible, the boundary conditions are eventually selected as suspending the entire structure on the either node of top chord (Node No. 15 & 19 as shown in Figure 4.4) and setting free at the bottom.

Meanwhile, in order to compare the experimental result with that of the numerical analysis, the three-dimensional FE model of steel truss is developed using ANSYS^{TM} by shell elements of SHELL 63. The actual constraint conditions in laboratory test are eventually selected that there are three bolts and one separate bolt at the either end of the upper chord and bottom chord respectively to simulate the fixed end support and pin support in the real situation as much as possible.

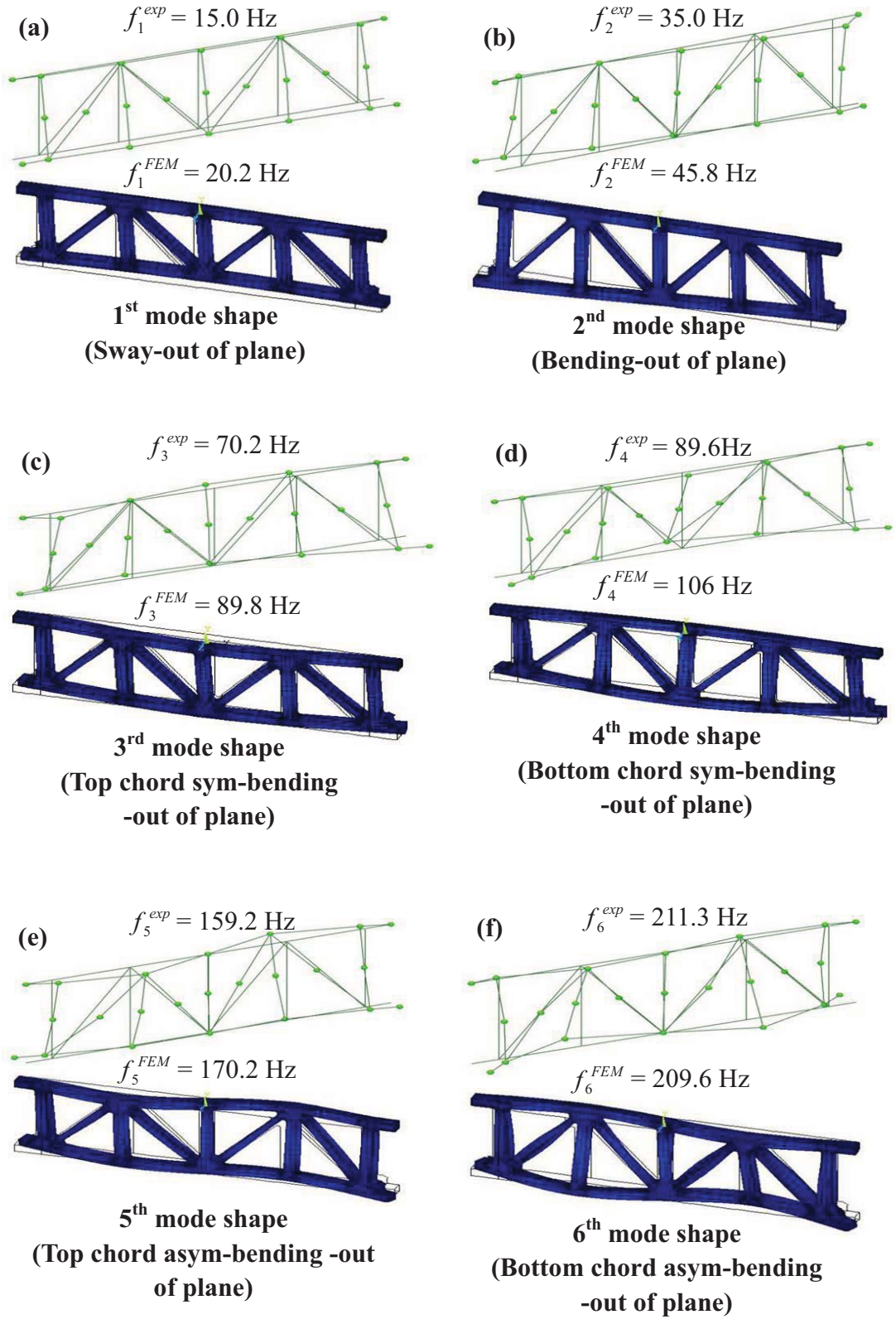

Figure 4.5 First 6 mode shapes obtained from FE analysis (f^{FEM}) and experimental test (f^{exp})

Table 4.1 The comparison of test values and calculated ones of first six order mode shapes and corresponding MAC values

Mode No.	Nature of modes	FE analysis (Hz)	Laboratory Test		Differences (%)	MAC values
			Frequency (Hz)	Damping ratio (%)		
1	Sway-out of plane	20.2	15.0	0.869	34.89	0.950
2	Bending-out of plane	45.8	35.0	2.207	30.9	0.711
3	Top chord sym-bending (out of plane)	89.8	70.2	0.676	27.92	0.722
4	Bottom chord sym-bending (out of plane)	106.0	89.6	1.417	18.27	0.952
5	Top chord asym-bending (out of plane)	170.2	159.2	0.451	6.9	0.973
6	Bottom chord asym-bending (out of plane)	209.6	211.3	0.783	-0.8	0.925

The first six selected mode shapes out of the plane have been identified by experimental modal analysis and correlated the respective order of numerical results as shown in Figure 4.5. The corresponding frequency values and damping ratios are also listed in Table 4.1. The correlation between modal parameters identified from the test and those calculated numerically can be evaluated by comparing the values of the natural frequencies and corresponding mode shapes. Table 4.1 shows the comparison of the numerically calculated frequencies from the three-dimensional finite element analysis and experimentally identified frequencies from the laboratory tests.

To evaluate the correlation of all calculated mode shapes and measured mode

pairs, the Modal Assurance Criterion (MAC) index (Friswell and Mottershead 1995) is then applied. The MAC value between the *i*th mode of the measurement and the *j*th mode of the computation is calculated using the formulae

$$\mathrm{MAC}(\phi_{ei}, \phi_{aj}) = \frac{(\{\phi_e\}_i^T \{\phi_a\}_j)^2}{(\{\phi_e\}_i^T \{\phi_e\}_i)(\{\phi_a\}_j^T \{\phi_a\}_j)}$$

where $\{\phi_e\}_i$ is the *i*th modal vector identified from ambient vibration field test, $\{\phi_a\}_j$ is the *j*th modal vector obtained from the finite element model analysis. MAC is a scalar quantity ranging from 0 to 1, representing the degree of correlation between two sets of modal vectors, 1 for perfectly correlated and 0 for perfectly uncorrelated.

From the given MAC values in Table 4.1, it can been seen that higher values are found for the most significant modes, which demonstrates a good correlation between the identified and calculated mode shapes either the symmetric bending modes or asymmetrical ones. However, there are some discrepancies. The possible reasons for those differences are mainly due to the following factors: (1) The idealized boundary conditions are assumed and simulated in computed frequency calculation. (2) It is relatively difficult to accurately simulate the desired boundary condition in laboratory test which will greatly influence the dynamic characteristics results. (3) It is found that the reaction frame used in laboratory test is not stiffened enough to provide the rigid supports during the test process described in Yin (2006).

4.2.3 Nominal Stress

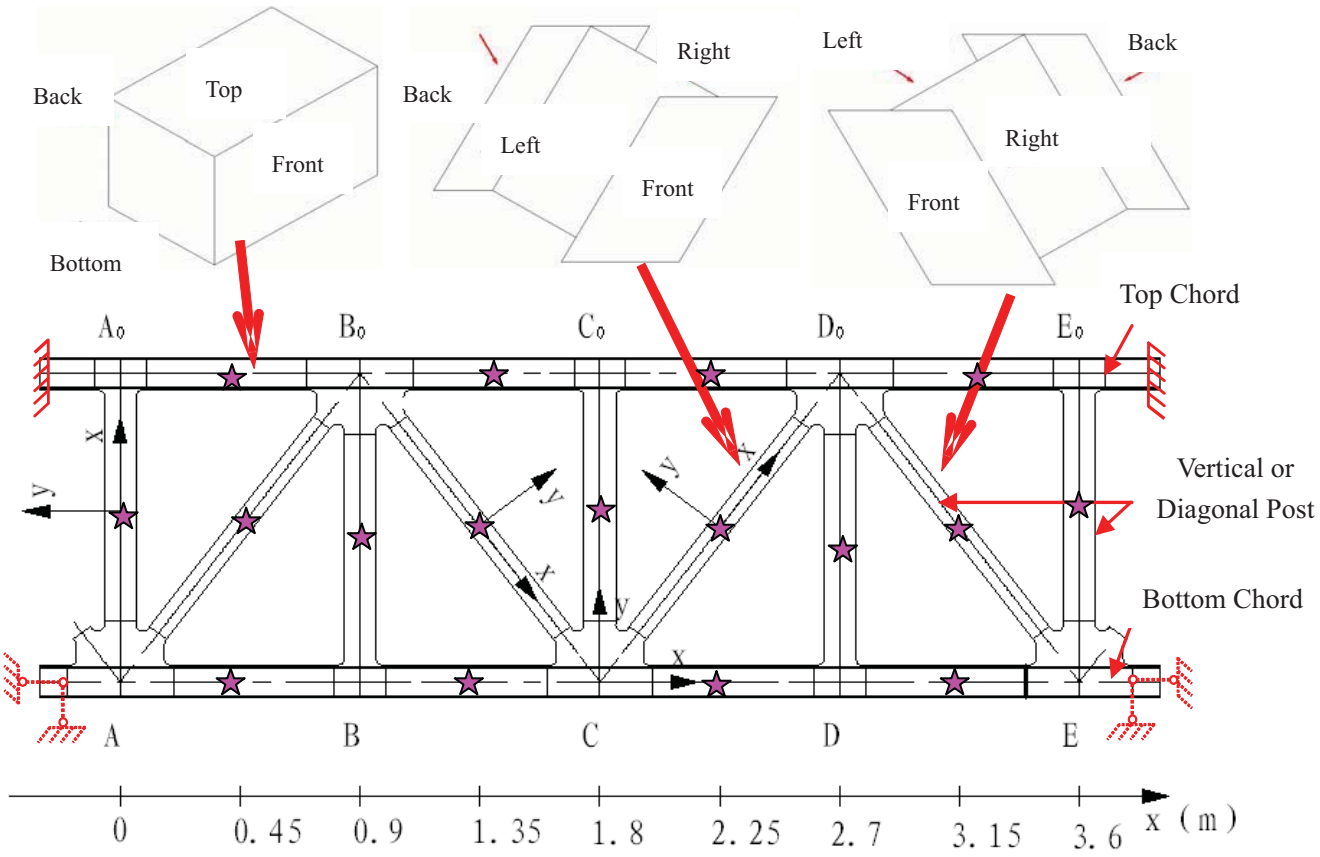

Figure 4.6 Schematic diagram of strain gauges installation locations and boundary conditions for component nominal stress

In order to investigate the situation of nominal stress distribution of steel truss structure under the specific loadings, the strain gauge measurements installed at the mid-point locations of each component as shown in Figure 4.6. It is assumed that the stress value of mid-point location accurately reflect the nominal stress of the component. For the purpose of reducing the effects of asymmetry of boundary conditions and loading cases that is inevitably occurred in laboratory test as well as unpredicted uncertainties and factors, strain gauges have been installed on four sides of component in terms of front, back, left and right sides. The corresponding boundary conditions associated with different loading case scenarios in terms of

concentrated loading and uniformly distributed loading in static response laboratory test are listed in Table 4.2. Before the static response test for nominal stress, a preliminary test has been performed to check the faulty sensors and measurement data under stepped loadings for its repeatability to ensure reliable results. Also, the proper data processing method of simple arithmetic averaging method has been adopted for the strain values from the four side gauges.

Table 4.2 Boundary condition and loading cases scenarios in laboratory test

Boundary Conditions No.			Loading types	Loading Applied Position	Loading Steps
BC1	1	BC2 5	Concentrated Point load	B	10、20、25、30 (kN)
	2	6		C	10、15、20 (kN)
	3	7		D	10、20、25、30 (kN)
	4	8		B&D	10、20、25、30 (kN)
BC1		9	Uniformly-Distributed load	Bottom chord	0.08、0.06、0.04、0.02（MPa）
BC2		10			

* Boundary Condition (BC)1: Three bolts at the either end of top chord with bottom chord free
Boundary Condition (BC)2: BC1 plus one bolt at the either end of bottom chord

Table 4.3 shows the maximum principal stress on truss component nominal locations by 3D bar under the stepped-loading case with two kinds of boundary conditions. Each column represents the maximum principal stress of component subjected to each stepped loading.

Table 4.3 3D bar graphs of stepped-loading maximum principal stress on truss component nominal locations under various loading cases

Loading cases	Boundary Conditions BC1	BC2
	Concentrated loading	
B	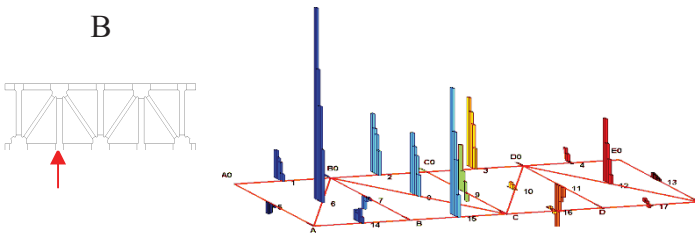	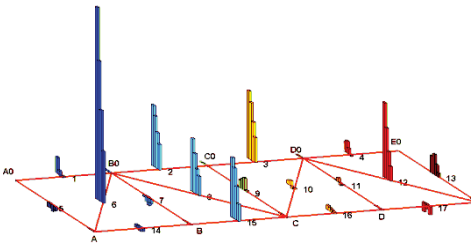
C	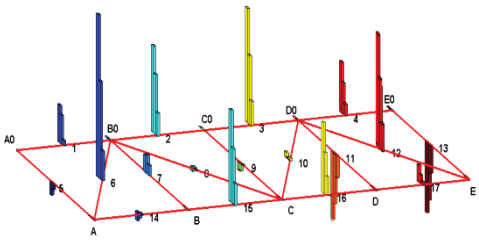	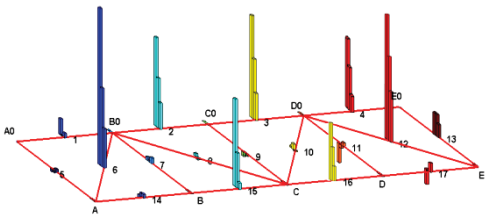
D	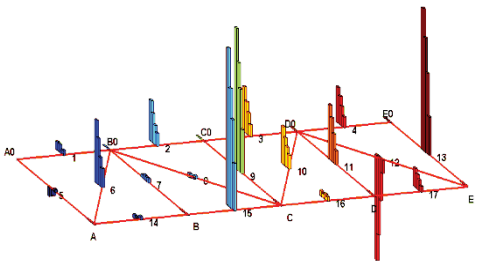	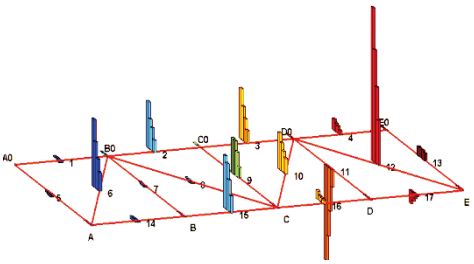
B&D	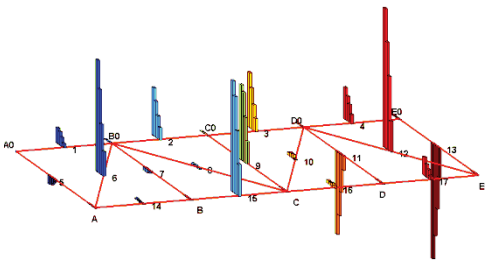	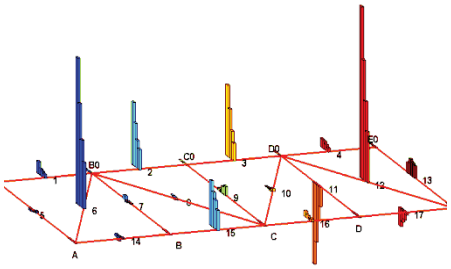
	Uniform-distributed loading	
	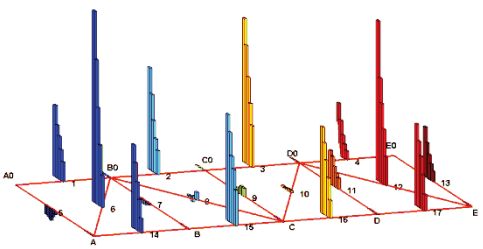	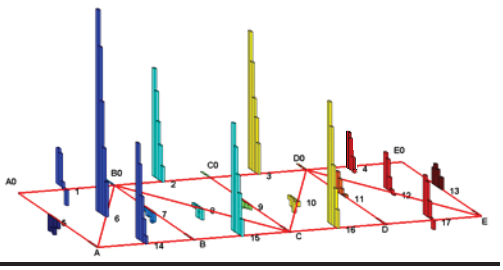

From the above bar graphs of component maximum principal stress, it can be seen that under the same boundary condition, the absolute value of component nominal stress near the loading positions are relatively larger than others. Under the concentrated loading situations, as for the symmetric loading cases of C and B&D, stress conditions are not strictly symmetric due to the possible test errors as well as the factors of test instruments and environment, in which the better symmetry is found in loading case of C than in B&D. Meanwhile, the results from asymmetric loading cases of B and D show the eccentric phenomenon that the bigger nominal stress values are obtained at the points close to the loading applied locations. Moreover, it is obvious that the different amplitude and distribution situation is observed under the same loading step with different boundary conditions, which suggests that the stress results are greatly influenced by the constraint condition. In addition, the top chord gives the bigger nominal stress values combined with the corresponding locations at bottom chord. With respect to the different loading conditions, it is obvious that the stress results under the uniformly-distributed loading cases are better than those under concentrated loadings at the aspects of regularity and symmetry.

4.2.4 Hot-spot Stress

The local concerned detail for hot-spot stress study is selected as C (as shown in Figure 4.3), and the connecting joint region of bottom chord close to location C is illustrated in Table 4.4. Three stepped concentrated loadings are applied at the

Table 4.4 Colorful contour graphs of stepped-loading hot-spot stress of maximum principal at concerned locations under various loading cases

Loading cases	Loading steps of Concentrated loading (KN)		
	10	20	30
B	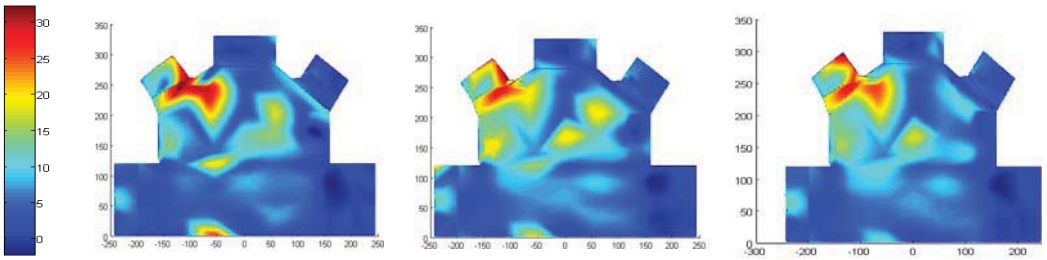		
C	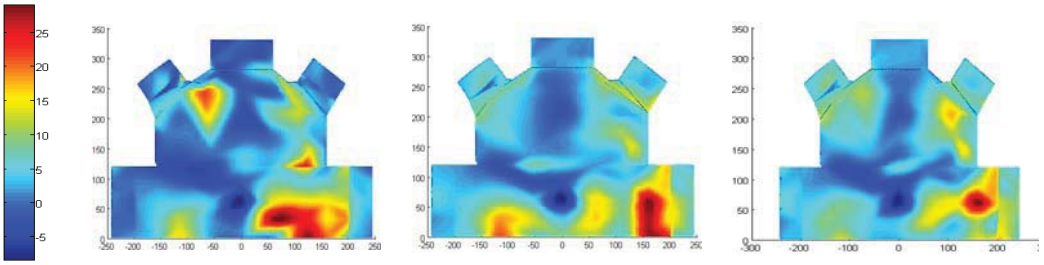		
D	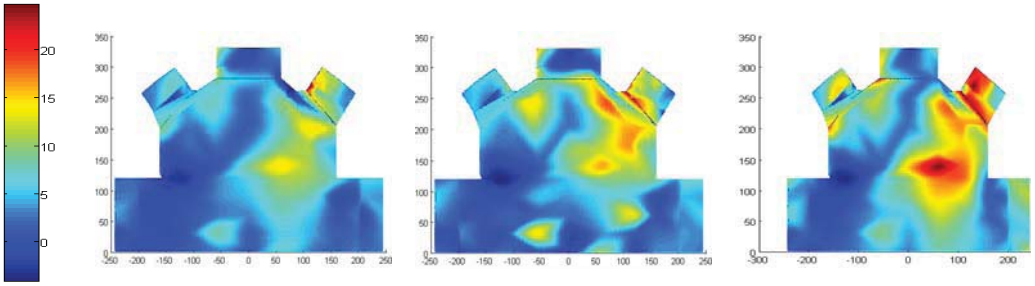		

Loading steps of Uniformly-distributed loading（MPa）				
0.019	0.039	0.058	0.077	0.097
BC1				
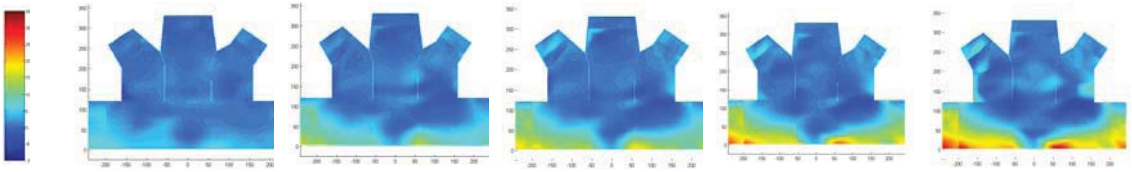				
BC2				
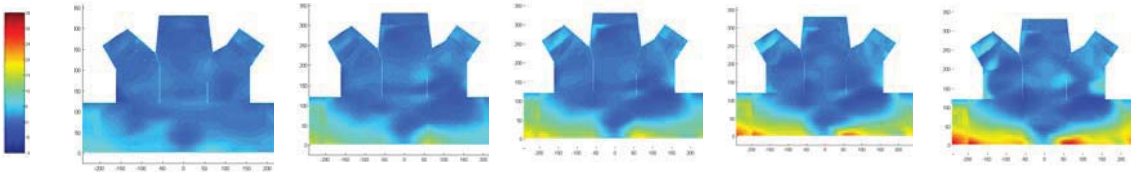				

point C and five stepped uniformly-distributed loading are directly applied at the bottom chord and the hot-spot stress distribution of this concerned region has been investigated. For the effective study of the hot-spot stress at the concerned location, it would be better to graphically visualize the stress data from the limited amount of strain gauges. The visualization procedure is performed on the platform of MATLAB. The coordinates along X and Y axis represents the actual location of amounted strain gauge while the shade of stress contour for the stress amplitude. Since the limited number of strain gauges is involved in this laboratory test leading to the sparse data point and can not be used for continuous graphing, the algorithm of "bicubic" polynomial interpolation with finer precision and smoothness is introduced then. It could be found that, from the contour graphs of hot-spot stress distribution on concerned location as shown in Table 4.4, the larger amplitude near the loading point showing the strong localization effect under the circumstance of concentrated loadings while symmetric distribution under uniform-distributed loadings. The possible reason may be responsible for the unsymmetrical stress results is steel ground frame is found not to be stiffened enough to provide the rigid supports. Moreover, the localization effect and out-of-plane bending caused by concentrated point load may also contribute to the unsymmetrical results. The same findings of pattern as in nominal stress situation could be discovered that the hot-spot stress distribution under the uniformly-distributed loading case is better that the one under concentrated loading case, and relatively large stress value are located at the region of the

flanges of bottom chord. The principal stress value is becoming larger and larger gradually from middle to both ends and the obvious irregularity occurred at the welding region.

4.3 DEVELOPMENT OF DIFFERENT FE MODELS

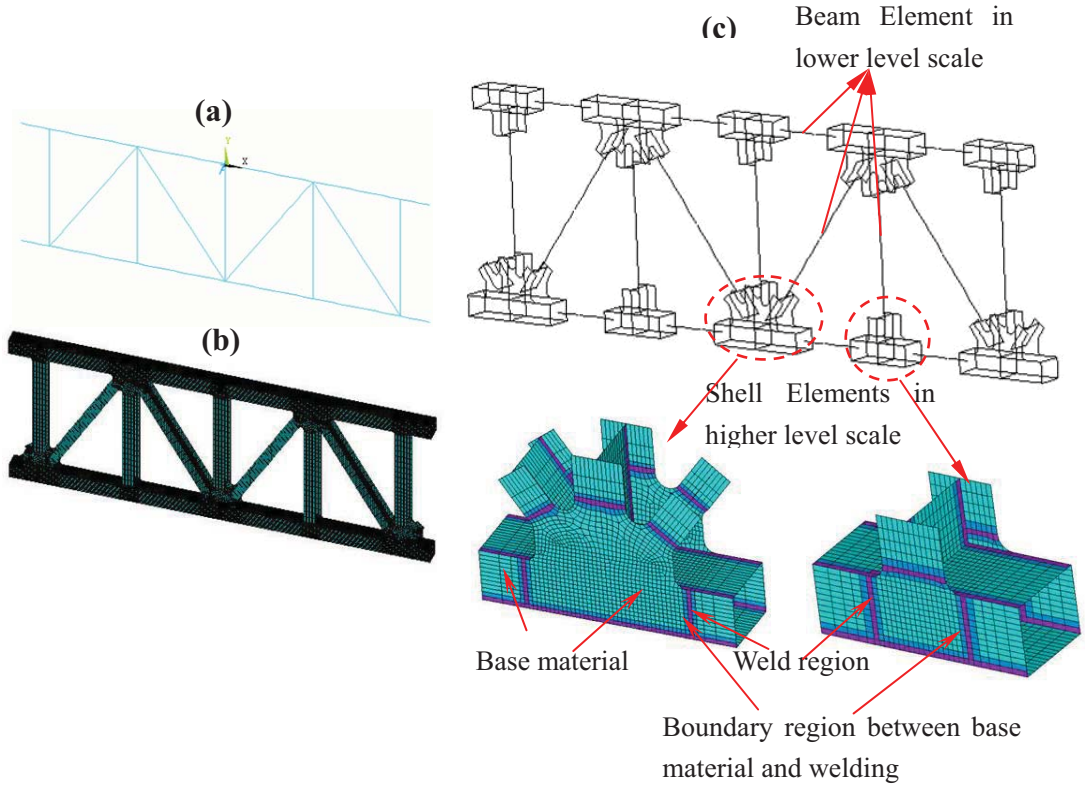

Figure 4.7 Three models developed by different modeling methods: (a) global model with full beam elements; (b) global model with full shell elements; (c) multi-scale model with substructuring and constraint equations respectively

Based on the proposed procedure for developing the concurrent multi-scale model and the adopted implementation methods, the multi-scale models of the steel truss section are constructed by using the substructuring and constraint equations

respectively as shown in Figure 4.7(c). Different parameters of materials are considered in the different areas of the structure, such as the base material of steel, solder at welds and transition areas between steel and weld. In order to compare the efficiency and accuracy of the developed multi-scale model, models using the traditional beam and shell elements are also built as shown in Figure 4.7(a) and Figure 4.7(b) where the same parameters of materials aforementioned as Figure 4.7(c) are considered in the full shell model for comparison.

In order to verify and validate the developed multi-scale model of steel truss section, an investigation on comparing the dynamic characteristics, static response of nominal stress and hot-spot stress distribution and computation efficiencies among the different finite element models are then carried out.

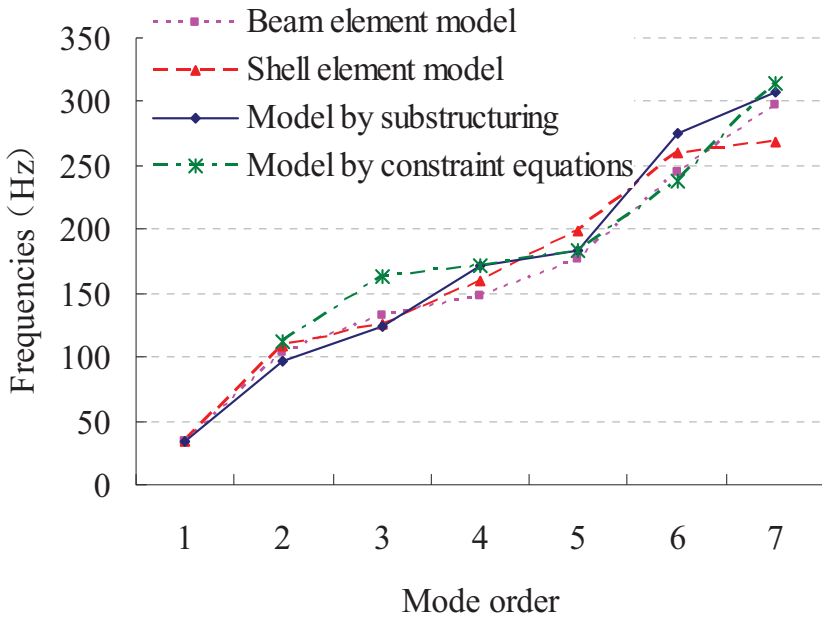

Figure 4.8 The first seven order frequencies value by four different analytical models

The dynamic characteristics of different models are investigated by performing single input multiple output method with hammer punching excitation under the same boundary conditions as shown in Figure 4.3, i.e. fixed supports at both ends of the upper chord while pin supports at the bottom chord. The corresponding results of frequencies on the first seven orders are compared, as seen in Figure 4.8. It can be clearly seen that the frequencies of the four models agree well with each other except that the differences among them are not even at each order.

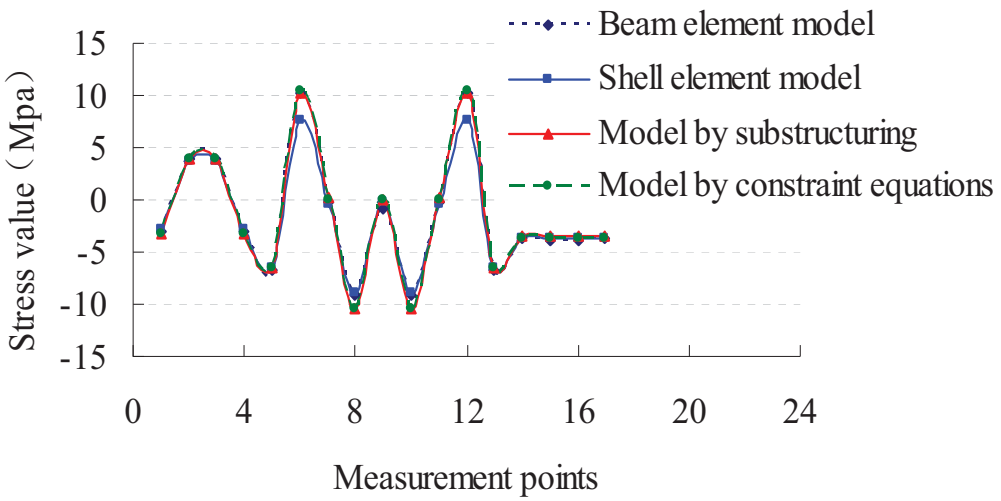

Figure 4.9 The nominal stress at the measurement points by four modeling methods under the specific loading at point C

The static responses of the models are calculated at the specific concentrated loading of 10kN applied at point C under the same boundary conditions. As shown in Figure 4.9, the comparison of calibrated nominal stress is performed at the measurement points which indicates good agreement with those from the analytical models. The hot-spot stress distributions of (a)(a'), (b)(b') and (c)(c'), corresponding to the marked focused area around the points of A_0, B_0, A (see

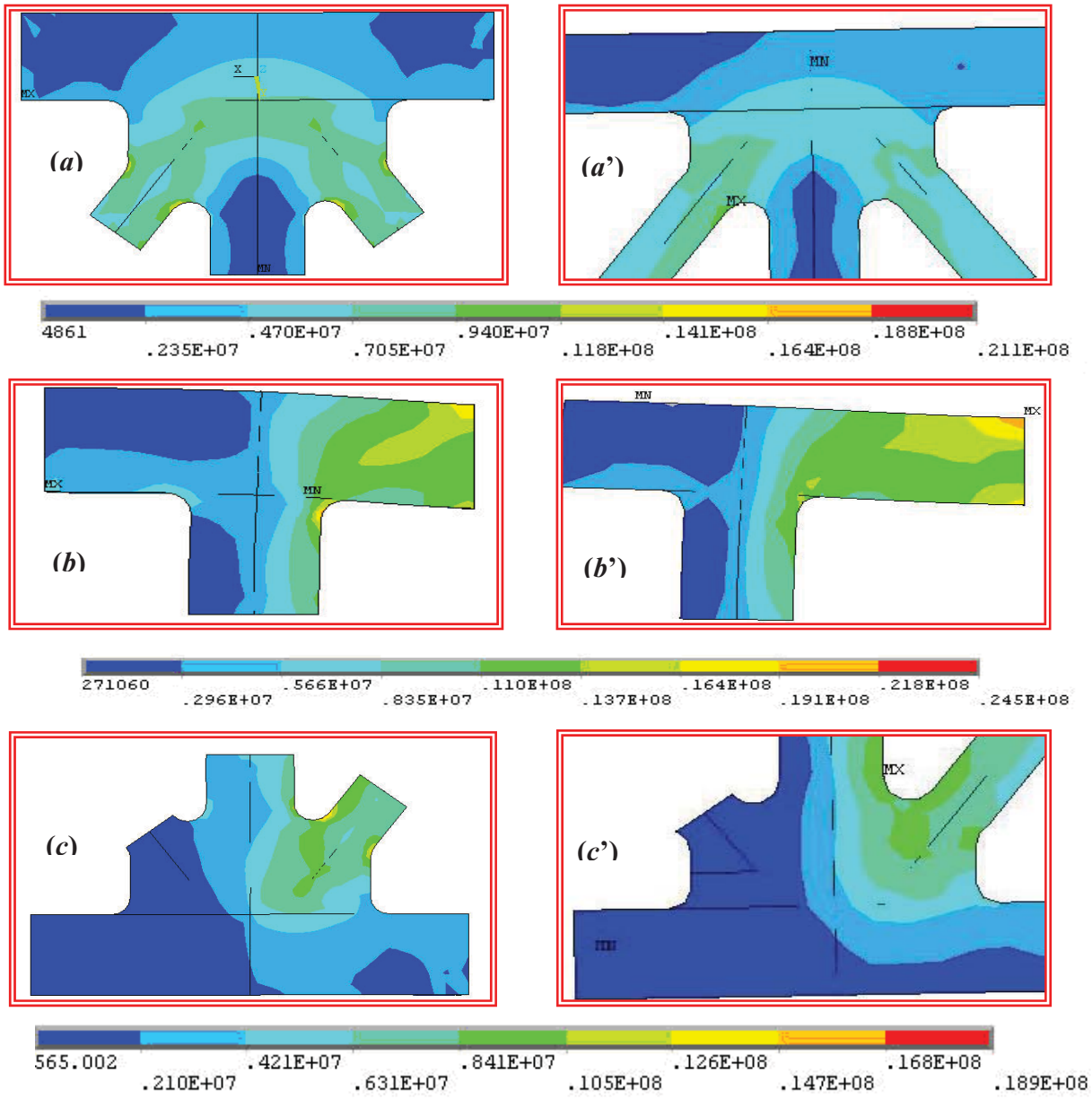

Figure 4.10 The hot-spot stress distribution at the concerned area of multi-scale model by constraint equations (a)(b)(c) and shell model (a')(b')(c')

Figure 4.3) respectively, also give almost the similar contour figures at the focused area between results from the shell element model and by multi-scale model as shown in Figure 4.10. The tiny difference lies on the location of interface area in substructure, which suggests that interface selection should be

relatively far away from the welding or stress concentration area that the resulting error hardly has any influence on the hot-spot stress distribution situation.

Table 4.5 Comparison on computation efficiencies between three models on static responses and dynamic characteristics

Modeling Methods		Beam Element	Shell Element	Multi-scale Model	
				Substructure	Constraint Equations
Number of Elements		220	34946	216	21366
Computation Duration Time (seconds)	Static Response	1	402	6	133
	Dynamic Characteristics	2	2493	21	181

Considering the involved computing costs, comparison of computation efficiencies of the three different analytical models in terms of computation time on static responses and dynamic characteristics are tabulated in Table 4.5. This suggests that multi-scale model by both substructure and constraint equations can be significantly more efficient than other models in responses calculation, especially the model by substructure in dynamic responses.

Therefore, on the basis of comparison between the first seven order frequencies, nominal stress and concerned area hot spot stress distribution and calculation efficiencies, the proposed different models served respective purpose and possessed corresponding advantages and drawbacks. All the models could be used to obtain dynamic characteristics, and model by beam element can easily

output the nominal stress at the global level without local information while the full shell element model could further get the local stress situation of concerned area by increasing the number of elements number but such enormous number of elements is impractical in modeling of large infrastructure. Moreover, comparing with the full shell element (3D) model, the developed multi-scale model could reduce the element number and satisfy all the needs of instantaneously obtaining the global information and local stress situations. The aforementioned comparison result indicates that the analytical simulation results by multi-scale model agree well with those by full shell element model within engineering error range. In addition, the high calculation efficiency by multi-scale model on relatively small structure suggests that it would be much more efficient, especially when combined with substructuring technique, if the multi-scale model is used in simulation case with high computation cost, for instance, highly nonlinear dynamic responses considering the complicated situations of traffic loading and earthquake loading, etc.

In conclusion, the developed multi-scale model has been validated and verified to be accurate and efficient by analytical and experimental studies. Furthermore, it also has been proven to be close to a full shell element model but better with its high calculation efficiency. It can be further applied to a large-span full-scale bridge structure for evaluating its structural health status with the help of structural health monitoring data.

4.4 MODEL UPDATING AND MODEL VERIFICATION

From Table 4.1, there have relatively huge discrepancies of natural frequencies between the analytical and experimental values. Other than the factor that boundary conditions of the steel truss specimen which could not accurately simulated in calculation, the steel ground frame (shown in Figure 4.2) is found not to be stiffened enough to provide the rigid supports in Yin (2006). In this sense, in order to accurately simulate the experimental environment and provide the solid basis for model updating, the whole truss system consisting of steel truss specimen and ground supporting frame should be modeled and computed for dynamic characteristics test instead of mere steel truss part.

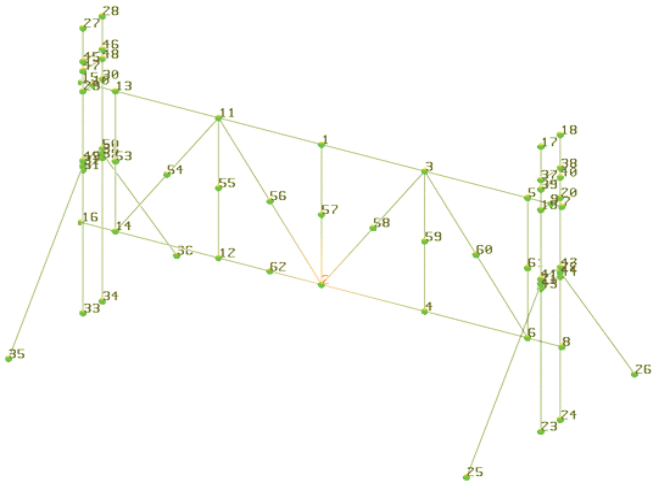

Figure 4.11 The truss system model in MACRAS

MACRAS (2009) is an integrated experimental modal analysis system that has been widely used for mechanical and structural modal analysis. As shown in Figure 4.11, the experimental model of the truss system has been constructed by discretising the structure into 61 nodes and connecting all nodes by members to

(a) $f_1^{exp} = 13.75$ Hz

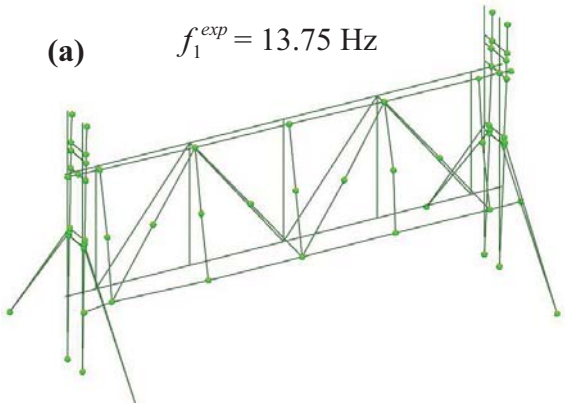

(b) $f_2^{exp} = 38.76$

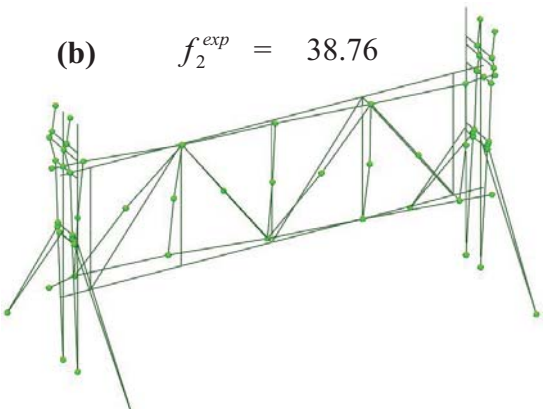

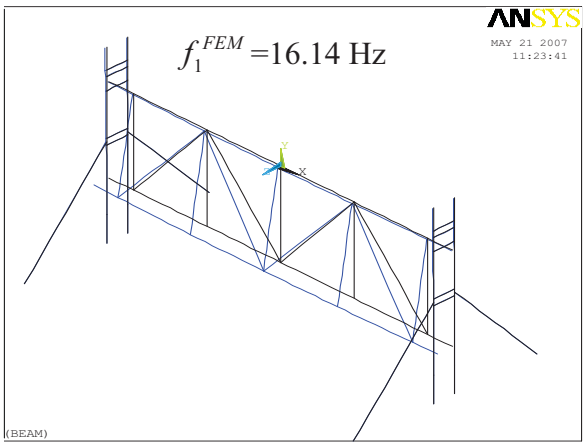

1st mode shape
(Sway-out of plane)

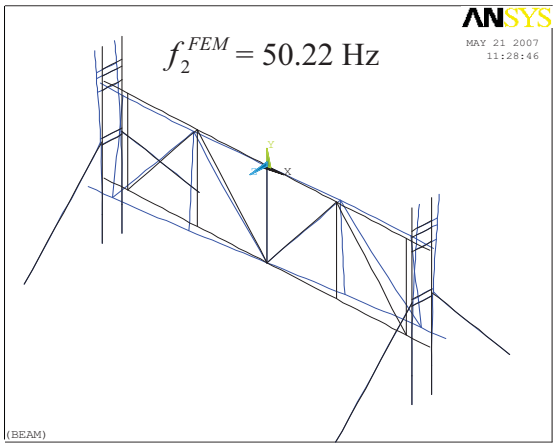

2"u mode shape
(Bending-out of plane)

(c) $f_3^{exp} = 75$ Hz

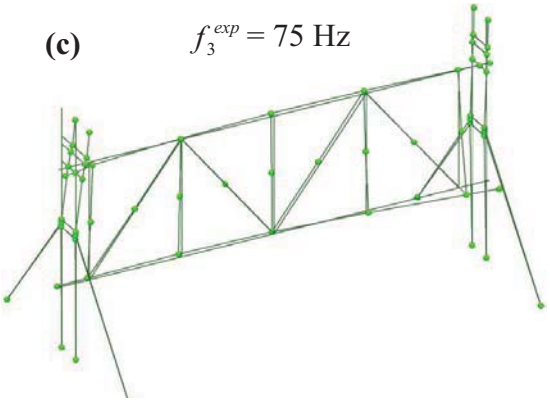

(d) $f_4^{exp} = 93.75$ Hz

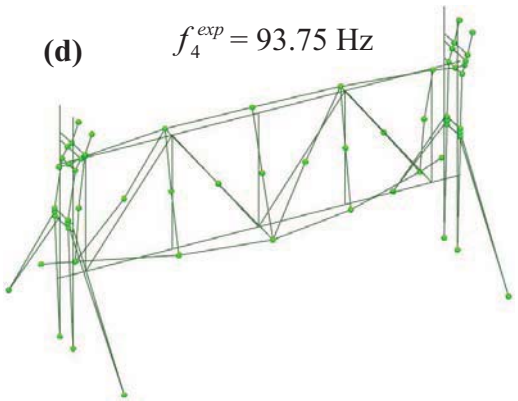

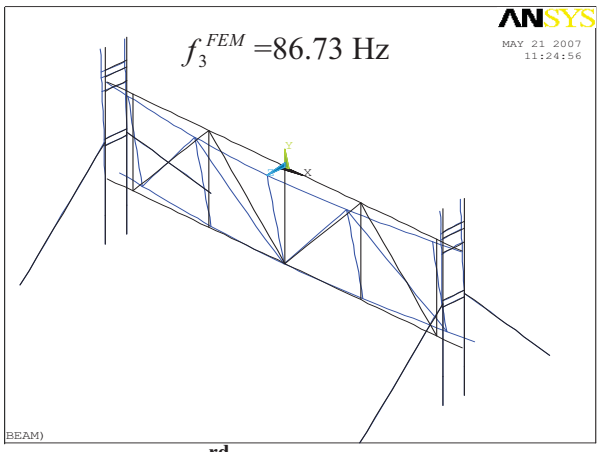

3rd mode shape
(Top chord sym-bending -out of plane)

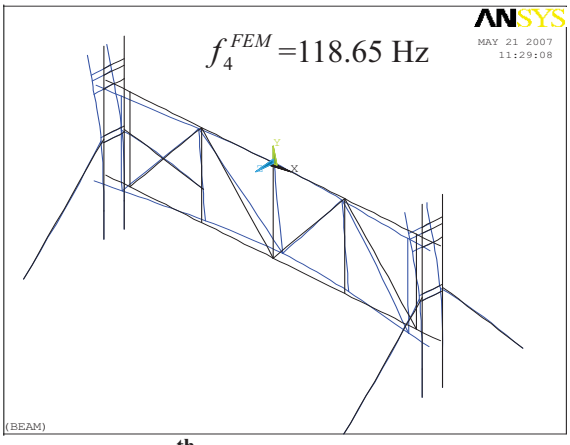

4th mode shape
(Bottom chord sym-bending -out of plane)

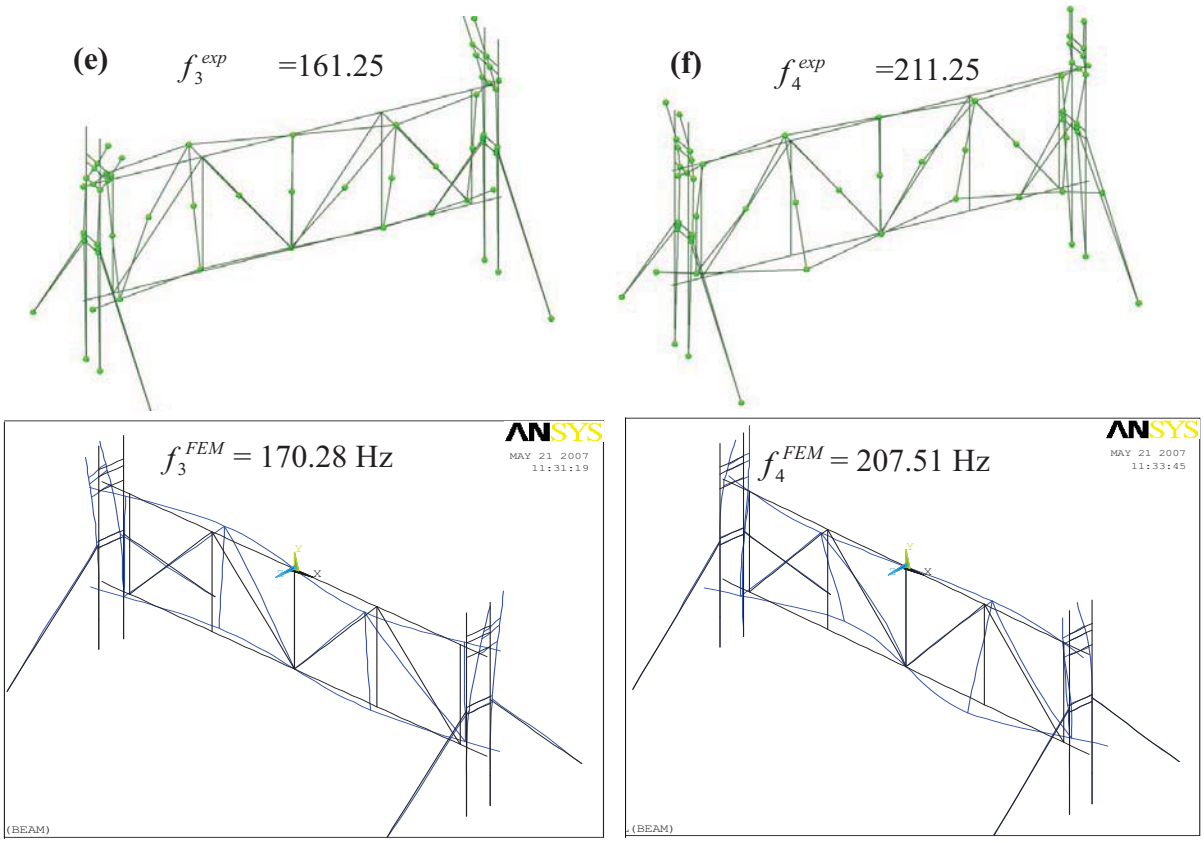

5th mode shape
(Top chord asym-bending -out of plane)

6th mode shape
(Bottom chord asym-bending -out of plane)

Figure 4.12 First 6 mode shapes comparison of the truss system between measurement and computation

reflect the structural configuration. The same excitation method of SIMO and measurement points and reference point involved in modal test as shown in Figure 4.4 have been adopted. At the same time, the analytical model of truss system is also built by beam element in ANSYS for comparison. Form the modal test results from MACRAS, there are a lot of mode shapes have been identified. However, only the truss specimen dominant mode shapes are of our interests. The first 6 order mode shapes comparison of truss system has been carried out between measured values and computed ones as shown in Figure 4.12. It should be noticed that Figure 4.4 shows mode shapes of only truss specimen while

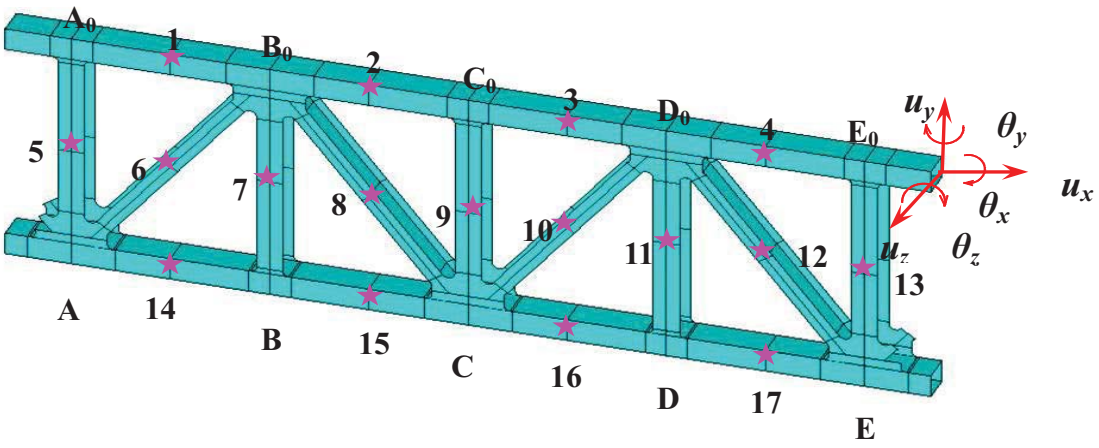

Figure 4.13 The decomposed boundary condition in laboratory test simulation

Table 4.6 Natural frequency comparison between analytical (initial FEM) and experimental values

Mode No.	Mode Shape Description (truss specimen dominant)	Truss system structure				
		Initial FEM			Updated FEM	
		Measured Frequency f_{exp} (Hz)	Computed Frequency f^{i}_{FEM} (Hz)	Difference (%)	Computed Frequency f^{u}_{FEM} (Hz)	Difference (%)
1	Sway-out of plane	13.75	16.14	17.38	15.08	9.67
2	Bending-out of plane	38.76	50.22	22.78	38.042	1.94
3	Top chord sym-bending (out of plane)	75.0	86.73	13.95	78.591	5.04
4	Bottom chord sym-bending (out of plane)	93.75	118.65	21.01	102.72	8.76
5	Top chord asym-bending (out of plane)	161.75	170.28	5.39	160.84	0.16
6	Bottom chord asym-bending (out of plane)	211.25	207.51	1.76	203.36	0.25

Figure 4.12 shows truss system with the same mode shapes of corresponding orders.

All the above computed results from truss system model are based on the assumption that there are rigid connections between truss specimen and ground supporting frame. Since the ground supporting frame has been modeled in the truss system structure, the connecting rigidity between truss specimen and ground supporting frame is then considered as the most important factor that would greatly influence those values.

Sun (2006) constructs the truss specimen model by shell elements and performs the model updating process on the basis of results from modal test. As shown in Figure 4.13, she decomposes each of boundary connection on the upper chord into six DOFs. Then three translational (u_x, u_y, u_z) and rotational (θ_x, θ_y, θ_z) DOFs are represented by different manual tuning values of spring stiffness to study the effect of spring stiffness at every direction on the final frequency value.

The same method of decomposing the connections into six spring stiffness has been then adopted. The spring stiffness values have been updated on the basis of the eigenvalue sensitivity study. The comparison of first 6 order natural frequency values between measurement and computation before and after updating with corresponding differences is tabulated in Table 4.6. It is easily noticed that frequency values of the truss system structure are different from ones of only truss specimen in Table 4.1. Also smaller differences between measured values and

computed ones by initial FE model in truss system are found than those in truss specimen. Moreover, the modeling of whole truss system has taken the influences of ground supporting frame on the frequency values into account which is considered to be closer to the real situation in laboratory. The boundary constraint parameter in term of spring stiffness values suggests that the differences between measured frequencies with calculated ones before and after updating significantly reduced from average error from 13.71% to 4.3%, especially the first 4 order mode shapes, which is regarded as in excellent agreement with measurement within engineering error range.

Table 4.7 Initial and updated values of selected parameters for experimental model updating

Structural Part	Parameters	Initial Estimates	Updated values	Differences (%)
Parent material of steel	Modulus of Elasticity	206 GPa	213 GPa	3.4
Welding region	Modulus of Elasticity	214.3 GPa	228.5 GPa	6.6
	Thickness of welding	6 mm	6.8 mm	13.3

As for the updating process of experimental multi-scale model, the sensitivity-based updating method is adopted in this study. The structural parameters that need to be updated are selected on the basis of corresponding sensitivity analysis result. During the preliminary test before the laboratory formal experiment, the parameters of material properties such as the Young's modulus of

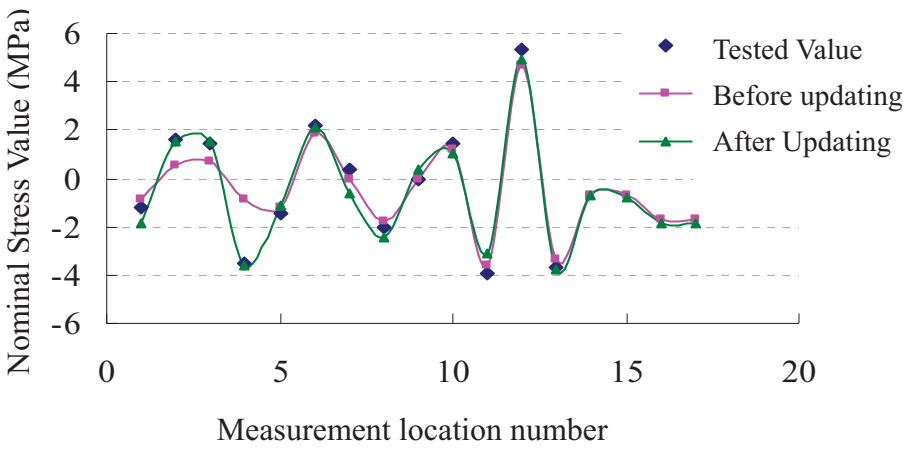

Figure 4.14 Comparison of the calculated results of nominal stress by the initial and updated parameters respectively with those measured ones at measurement points

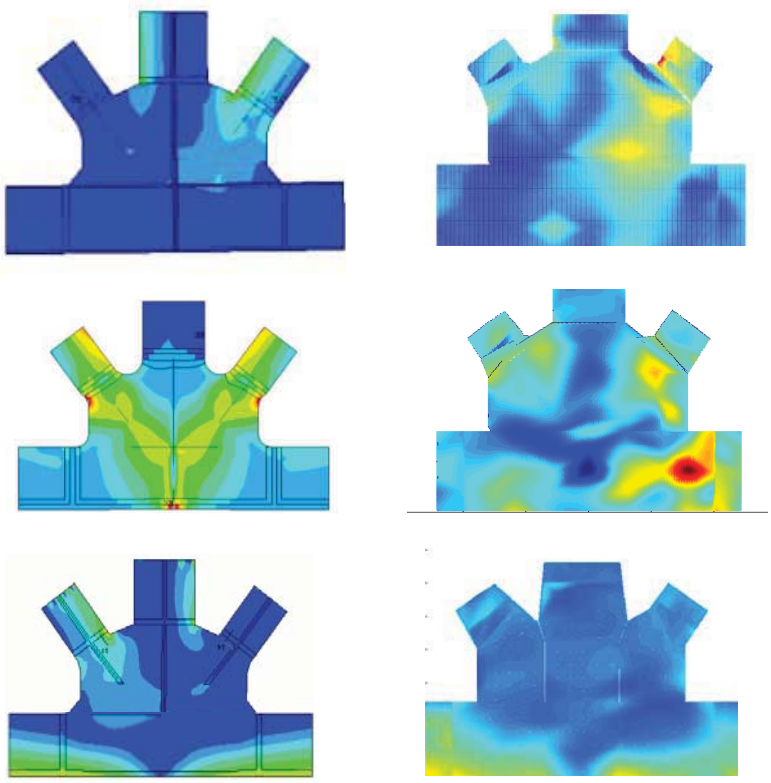

Figure 4.15 Hot-spot stress distribution comparison of region C between updated values and measured ones subjected to loading case of (a) Point load at D; (b) Point load at C (c)Uniformly-distributed load on bottom chord

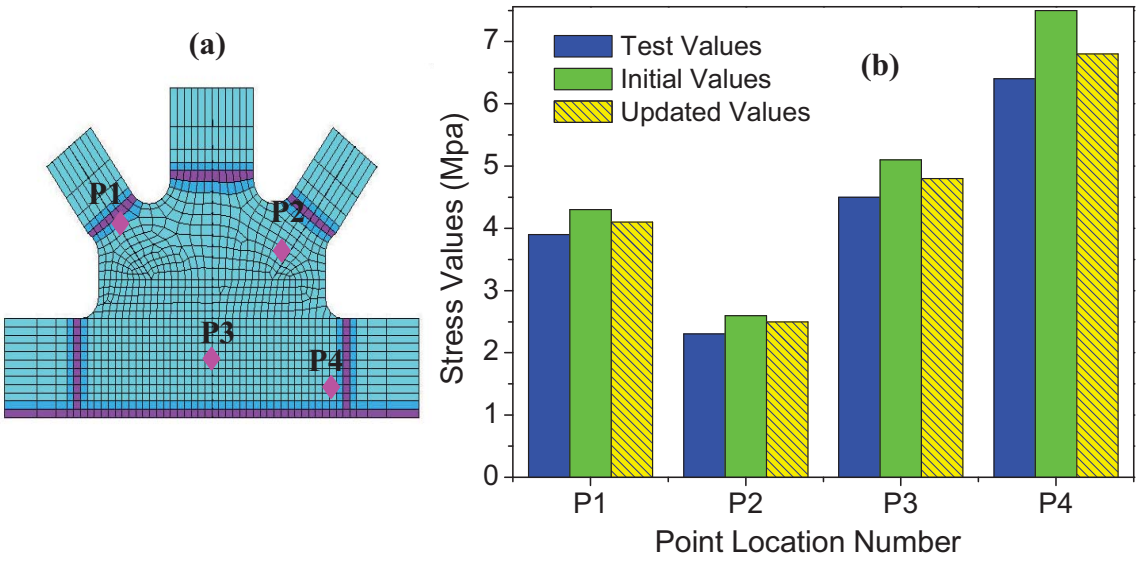

Figure 4.16 Stress comparison of computed values of updated model with test ones on selected points of local concerned area

parent material of steel truss as well as the Young's modulus of the welding have been determined. There exist uncertainties and disunities on these parameter values, so the material properties around the concerned area of vicinity of welding toe with respect to elasticity modulus of parent material of steel and welding as well as the thickness of welding are eventually selected as the parameters for updating.

The tested values of nominal stress of measured point at the locations as shown in Figure 4.3 are adopted as the objective function for the model updating process. The sensitivity-based model updating procedure is thus carried out and the selected parameter values are updated and tabulated in Table 4.7. From the Figure 4.14 of nominal stress comparison on measurement points, the updated values are obviously found to be closer to the test ones than the results from initial parameter value. Moreover, the updated values are also used for hot-spot stress distribution

computation and the comparison by updated parameter values with measurement is shown in Figure 4.15. In addition, as illustrated in Figure 4.16, stress values of some representative points in analytical model with updated values are output and compared with the initial ones as well as the measurement data.

4.5 PROCEDURES OF MULTI-SCALE MODEL UPDATING AND VERIFICATION FOR CIVIL INFRASTRUCTURES

The strategies and methods of model updating and verification have been investigated and the most popular sensitivity-based model parameter updating method is employed on the multi-scale model of scaled specimen of truss section which has been constructed based on the developed modeling strategy and method mentioned before. The multi-scale model has been updated and validated to be used as the most accurate baseline model close to the real situation of structure for the subsequent numerical simulation, and it can be served as a reference or even a guideline for modeling of similar structures. Therefore, the updating and verification procedures could be outlined as follows.

4.5.1 The Procedure of Model Updating

The multi-scale model updating procedure is generally summarized in three aspects.

(1) Selection of response data as reference which are customarily the measured

data, such as measured frequencies and mode shapes from the ambient vibration test mainly for dynamic property oriented model updating. As for the large civil infrastructure, the static or dynamic response data directly obtained from structural field test can also be used for static response oriented model updating.

(2) Selection of proper model updating method. In this study, the sensitivity-based parameter updating method is eventually selected because of its clear physical meaning of the selected parameters and successful application to the civil structure.

(3) Selection of parameters to update, and the corresponding responses should be sufficiently sensitive. The number of parameters should be kept small and it would be most effective in producing a genuine improvement in structural modeling. Sensitivity analysis is thus conducted for choosing the structural parameter with the consistent large values. The other important factors such as selected modes, initial estimation and bound limitations of parameters and convergence criteria for iteration combined with objective function should be also carefully considered during updating process.

Model updating is a model tuning process by iteration steps to modify the selected parameters based on the reference data than before so that the closer-to-real model can be achieved.

4.5.2 The Procedure of Model Verification (from SHM Data)

The verification procedure serves the purpose of measuring how many discrepancies left between the FE model predictions and reference data after the model updating. The generalized form of model verification procedures could be described as follows.

First of all, the dynamic characteristics predicted by the updated model with respect to natural frequencies and mode shapes would be closer to the measured data from ambient vibration test or structural health monitoring data directly obtained from the installed sensors than those before updating.

Secondly, the updated model could be further verified at the global scale level, in particular, at the aspect of component nominal stress by comparison of static response between the predicted results by updated model and the monitoring data or test data available at the selected points.

Verification would be finally carried out to focus on the local scale level if the monitoring data or experimental data are available at the concerned hot-spot area for comparison.

4.6 SUMMARY

In order to validate the proposed multi-scale modeling strategy, a typical steel truss section from an existing large-span bridge is selected as the reduced-scale

steel truss specimen for the laboratory tests and the study of multi-scale implementation procedure. The comparison of dynamic and static responses between the calculated results by different analytical finite element models indicates that the proposed multi-scale model is found to be the most efficient and accurate. The verification of the model with results from the tested truss under the specific loading shows that, responses at the material scale in the vicinity of local details as well as structural global behaviors could be obtained and fit well with the measured results. The model updating procedures on the multi-scale model are then performed based on the sensitivity-based updating method of the selected model parameters. The updated multi-scale model is further verified to act as the baseline model which is assumed to be the finite element model closest to the real situation of the structure available for the subsequent numerical simulations. The developed multi-scale model has been validated and verified to be accurate and efficient by experimental and analytical studies. Furthermore, the comparison result has proven that the multi-scale model is close to full 3D model but better with its high calculation efficiency, so it can be further applied for engineering multi-scale simulation. The general procedures of multi-scale modeling strategy associated with model updating and verification are eventually proposed for nonlinear modeling of large civil engineering structures.

CHAPTER 5

DEVELOPMENT OF MULTI-SCALE MODEL OF A LONG-SPAN BRIDGE

5.1 INTRODUCTION OF WASHMS AND TMB

5.1.1 Wind and Structural Health Monitoring System (WASHMS)

Figure 5.1 The overview of three bridges in WASHMS

Real-time Structural Health Monitoring Systems (SHMS) which integrates the techniques of sensing and instrumentation, modeling and simulation, data

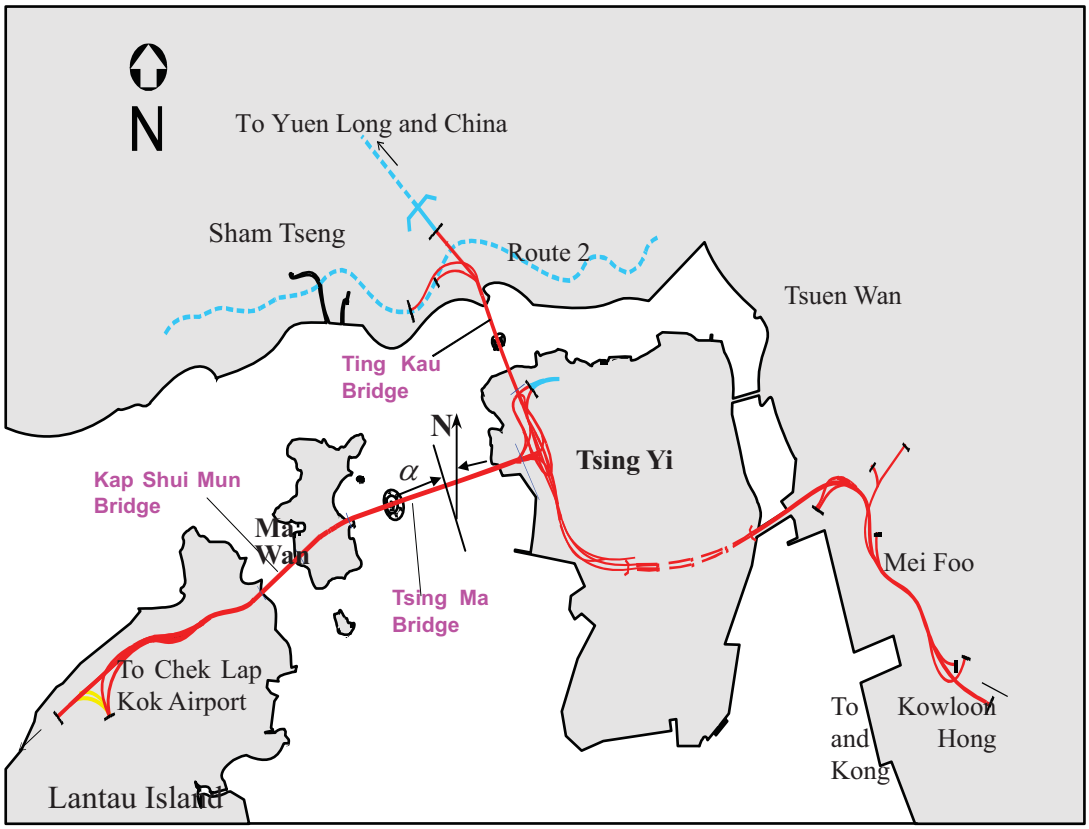

Figure 5.2 Location plan of three bridges

interrogation and management and design and analysis of long-span bridges, have been designed, installed and operated over the past decade to monitor the structural health conditions of long-span bridges under in-service condition. In Hong Kong, a structural monitoring system called "Wind and Structural Health Monitoring System (WASHMS)" (Lau *et al*. 2000; Wong *et al*. 2000a, 2000b, 2000c) has been devised by the Highway Department of the Hong Kong Special Administrative Region (SAR) Government in Tsing Ma Control Area (TMCA) to monitor structural health and performance of the three cable-supported bridges built for the development of the new airport of Hong Kong, namely, Tsing Ma (Suspension) Bridge (TMB), the Kap Shui Mun (Cable-stayed) Bridge (KSMB) and the Ting Kau (Cable-stayed) Bridge (TKB) as shown in Figure 5.1. Figure 5.2

shows the layout of the transportation network system in TCMA and respective locations of TMB, KSMB and TKB in TMCA. A SHMS is currently becoming a standard monitoring system in the design and construction of large-scale and multi-disciplinary bridge projects such as the Shenzhen Western Corridor (SWC) (Highways Department 2002a; Wong 2004), Stonecutters Bridge (SCB) (Highways Department 2002b; Wong 2004), and SuTong Bridge (STB).

This WASHMS is composed of six modules, namely, the sensory system, the data acquisition and transmission system, the data processing and control system, the bridge health evaluation system, the portable data acquisition system and the portable inspection and maintenance system. The monitoring items are generally classified into three categories, namely, the loading sources (or input parameters) which include wind, temperature, traffic (highway and railway) and seismic loadings; system characteristics (or system parameters) which include static influence coefficients and global dynamic characteristics; and bridge responses (or output parameters) which include variation in geometric configuration (or displacements of the bridges), stress/strain distribution, cable forces and fatigue stress estimation. The system also comprises various kinds of sensors such as accelerometers, strain gauges, displacement transducers, level sensors, anemometers, temperature sensors and weigh-in-motion sensors for monitoring and evaluating the structural health of these bridges to ensure bridge safety under operation and further to facilitate inspections and maintenance activities on the bridges.

5.1.2 Tsing Ma Bridge (TMB)

Figure 5.3 The Tsing Ma Bridge (Li *et al*. 2001b)

The Tsing Ma Bridge, as shown in Figure 5.3, 2.2 km total in length with a main span of 1377m, commissioned on May 22, 1997, is the longest suspension bridge in the world that carries both highway and railway traffic. The location of the bridge is shown in Figure 5.2 from which it can be seen that the bridge serves as a main section of the Lantau Link supporting highway and railway transport between Tsing Yi Island and Lantau Island and it conducts the essential part of the transport network between the new facilities and existing commercial centers of Hong Kong Island and Kowloon.

The Tsing Ma Bridge, stretching from Tsing Yi Island to Ma Wan Island, carrying a dual three-lane highway on the upper level of the bridge deck and two railway tracks and two carriage ways on the lower level within the deck, cross

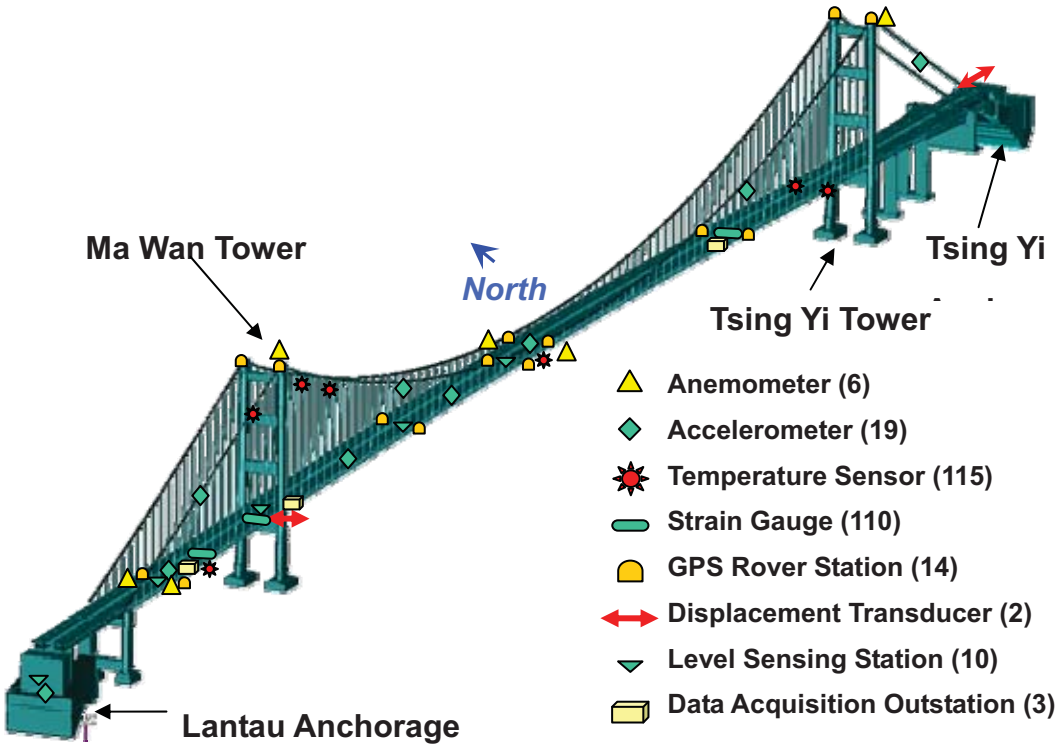

Figure 5.4 Layout of sensory systems of TMB (Wong, K.Y. 2007)

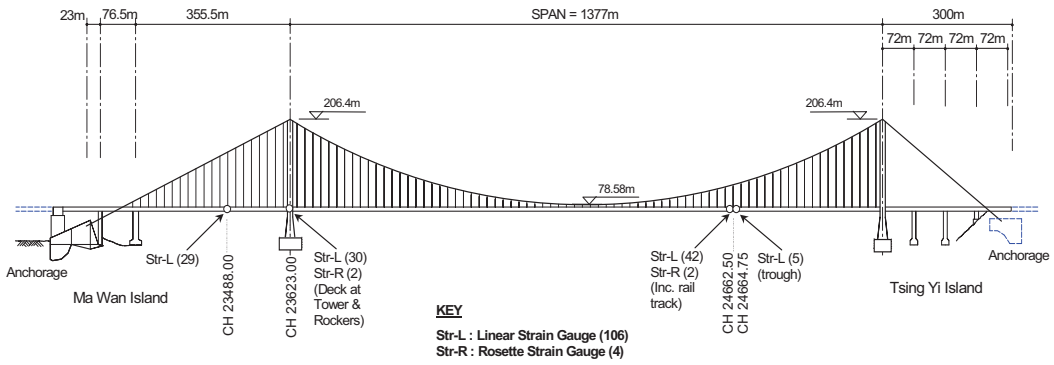

Figure 5.5 Configuration and strain gauges layout of the Tsing Ma Bridge (Li *et al.* 2001a)

the main span of 1377m between the Tsing Yi tower in the east and Ma Wan tower in the west (as shown in Figure 5.5). The height of tower is 206m from the base level to the top of tower saddle. The two towers are reinforced concrete structures built on massive reinforced concrete slabs found on competent rock.

The two main cables of 36m apart in the north and south are accommodated by the four saddles located at the top of the tower legs in the main span. On the Tsing Yi side, the main cables are extended from the tower saddles to the main anchorage through the splay saddles to constitute a 300m Tsing Yi side span. In the counterpart of the Ma Wan side, the main cables extended from the Ma Wan tower are held first by the saddles on Pier M2 at a horizontal distance of 355.5 m from the Ma Wan tower and then by the main anchorage through splay saddles at the Ma Wan abutment. The bridge deck is a hybrid steel structure continuing between the two main anchorages. It is suspended by suspenders in the main span and the Ma Wan side span. On the Tsing Yi side the deck is supported by three piers rather than suspenders. This arrangement and the difference of span between the Ma Wan side and the Tsing Yi side introduce some asymmetry with respect to the mid-span of the bridge.

The WASHMS for the Tsing Ma Bridge totally comprises of approximate 350 sensors which could be divided into several groups according to the sensor types including accelerometers, strain gauges, displacement transducers, level sensors, anemometers, temperature sensors and weigh-in-motion sensors as shown in Figure 5.4. These different kinds of data from corresponding sensors serve various research purposes. Since the subsequent analysis would be mostly conducted on the basis of strain data, we are specifically more concerned about the strain gauges installed locations and the corresponding data from them for fatigue analysis. The strain gauges are installed at the bridge-deck sections as

shown in Figure 5.5. The strain gauge locations are at the rail track sections (Chainage (CH) 24662.5), bridge-deck trough section (CH 24664.75) and deck at tower and rocker bearing links (CH 23623.00). The most critical parts of the cross-frames for fatigue damage have been identified during the design structural health monitoring system by the Flint and Neill Partnership (1998). Therefore, all these strain gauges are supposed to be installed at critical parts of the bridge-deck sections.

5.2 THE MACRO-MODEL OF TMB

5.2.1 Bridge Configuration Description

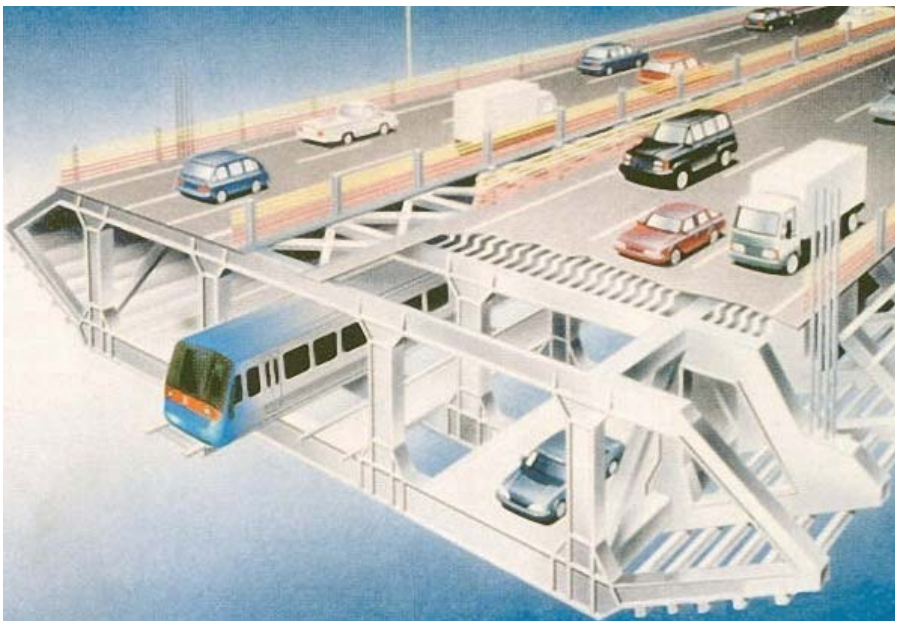

Figure 5.6 Schematic configuration of Tsing Ma Bridge decking system (Wong, K.Y. 2007)

A 3D finite element global structural model of TMB embodying the properties of

almost all the structural elements is developed, including longitudinal trusses, cross-frames, deck plates, tower beams, main cables, hangers, etc. As shown in Figure 5.6, Tsing Ma Bridge is a double-deck suspension bridge. The bridge deck is a hybrid steel structure consisting of vierendeel cross-frames supported on two longitudinal trusses acting compositely with stiffened steel plate that carry the upper and lower carriageways. The stiffened plates acting with two longitudinal braced trusses provide the vertical bending stiffness of the bridge deck. Transverse shear forces are carried by the steel plates together with the plane bracing systems that join the plates at both upper and lower flanges and span vent openings. The mixed plane bracing-plate systems enable the longitudinal truss to provide lateral bending stiffness. At the main span and the Ma Wan side span, the deck is suspended from the main at an 18m interval. Near the Ma Wan and Tsing Yi bridge towers, the bridge deck changes to incorporated two additional inner longitudinal trusses to share forces with the main trusses, and the deck plates extend over the center to cover the full width of the bridge without vent openings. The cross section of the bridge deck also changes in the Tsing Yi side span and in the area near the Ma Wan abutment where the deck is supported by piers.

5.2.2 Finite Element Modeling of Deck System

The bridge deck at the main span is a suspended deck and the structural configuration is typical for every 18m segment, which including one main cross

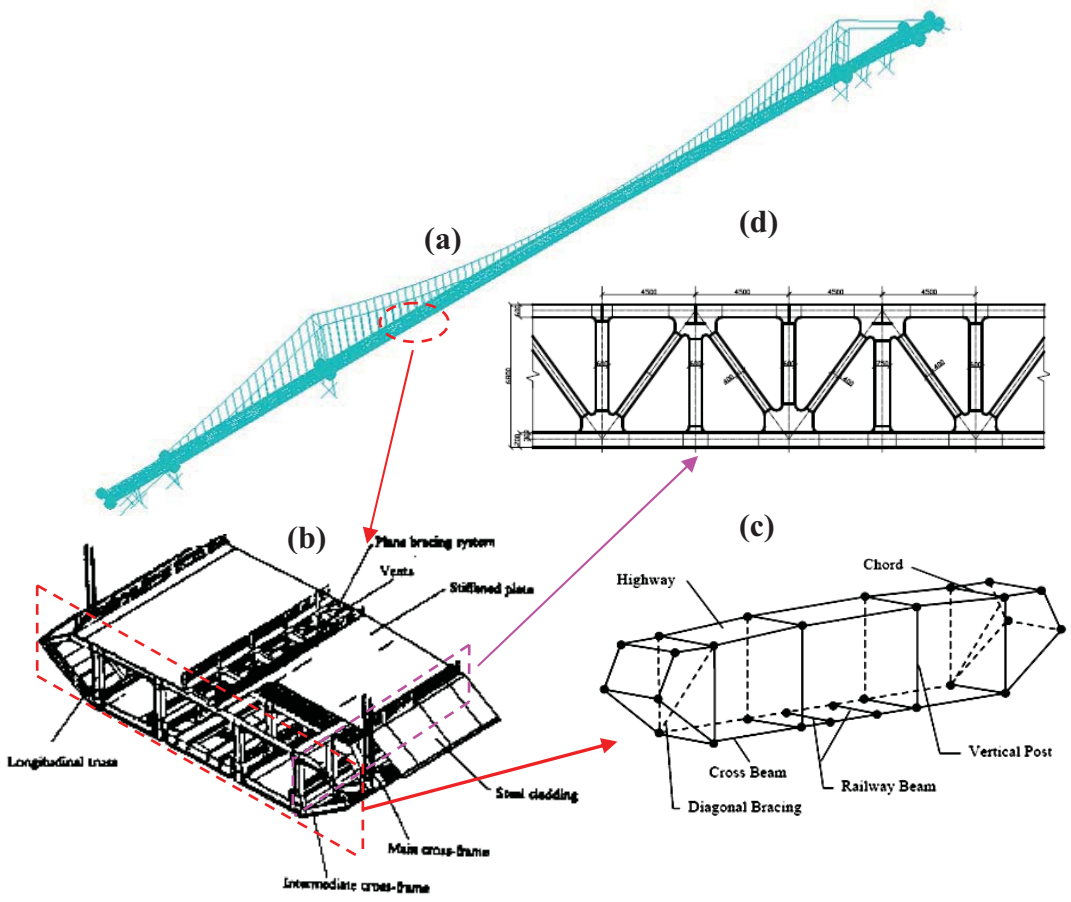

Figure 5.7 Three dimensional FE model of TMB deck section (a) global model; (b) configuration schematic; (c) cross-section FE model; (d) longitudinal truss

frame and four neighboring intermediate cross frames while two of them are on each side of the main cross frame in 4.5m apart from each other connected by two outer longitudinal trusses. Figure 5.7(b) illustrates a typical 18m suspended deck section consisting of main longitudinal trusses, cross frames, highway decks, railway tracks, and bracing. Two longitudinal trusses link up the cross frames along the bridge longitudinal axis to act as the main girder of the bridge. Each longitudinal truss (Figure 5.7(c)), comprising of upper and lower chords and vertical and diagonal members, are modeled as 3D, two-node iso-parameteric

beam elements (B31) having six DOFs at each node.

Bending, torsion and axial force effects are all considered in each space beam element. The section details are also embodied in the corresponding elements. The top and bottom chords are modeled as space beam elements with box sections while vertical posts and diagonal bracings are represented by I-beam elements. Meanwhile, each cross frame is comprised of upper and lower chords, inner struts, outer struts, and upper and lower inclined edge members. The deck section is suspended to the main cable by connecting to the intersections of edge members of the main cross frame through suspender units. Two pairs of sway bracings are connected from the suspension points at the main cross frame to the outer ends of the upper chords of the two adjacent intermediate cross frames to strengthen the structural stability. Two symmetrical bays of top highway deck plates are supported by the upper chords of cross frames and longitudinal trusses. As for the bottom deck, there are two railway tracks that they are laid on the central bay with one row of central bracing and two rows of outer cross bracings added to brace the bottom chords of cross frames. The two railway tracks are made up of two inverted T-beams welded to flange plates and each of them is represented by continuous beam elements (B31) with I-section.

Deck plates and deck troughs comprise the orthotropic deck, which is considered as one of the important issues in the cable-supported bridge modeling. The trough along the transverse direction of the deck plate makes deck behave in orthotropic manner and it is ideally required that the modeling should be as close to real

configuration as possible. However, it is impractical and unnecessary to model the every configuration in detail to make the huge model consume the significantly increasing computation costs. To solve the modeling problems properly, this kind of "geometric orthotropic plate" could be converted to "physical orthotropic plate" according to the equivalence principle and the 4-node quadrilateral membrane element (M3D4) is then employed to model the stiffened deck plates. The equivalent section properties of the elements are estimated by calculation in advance. The deck plates are meshed by every two adjacent cross frames in the longitude direction while span cross the longitudinal trusses along the transverse direction.

5.2.3 Finite Element Modeling of Towers, Cables, Piers and Boundary Conditions

The Tsing Yi and Ma Wan towers are reinforced concrete structures, and each tower consists of two reinforced concrete legs that are linked by four reinforced concrete portal beams fixed at the base. Since the stress or strain in the towers is not what we concerned about in the subsequent analysis and there are no sensors installed, the towers could be represented by the multilevel frame in modeling. For the modeling simplicity, the legs are modeled by three-dimensional Timoshenko beam elements with six DOFs at each end (B31). Since the dimensions of the cross section varies from its bottom to its top, the tower legs are classified as 17 beam sections with the different dimensions and assume that the

geometric properties of the beam element are constant along its axis with an average value on every beam section based on the design drawings. The four portal beams are also modeled by B31 but with the different cross section dimensions. The tower saddles are very stiff and their stress distributions are not considered in the global bridge model, so the saddles are constructed with the 2-node rigid beam element RB3D2. The cable system consists of two main cables and 95 pairs of suspender units. The cable between the adjacent suspender units is modeled by one spatial beam element (B31) of circular cross section while each suspender unit is modeled by one single two-node beam element. The cable elements are considered to be capable of resisting tensile force only and geometric nonlinear due to cable tension are taken into account. Moreover, the initial conditions of main cables and suspender units could be defined in term of initial stress.

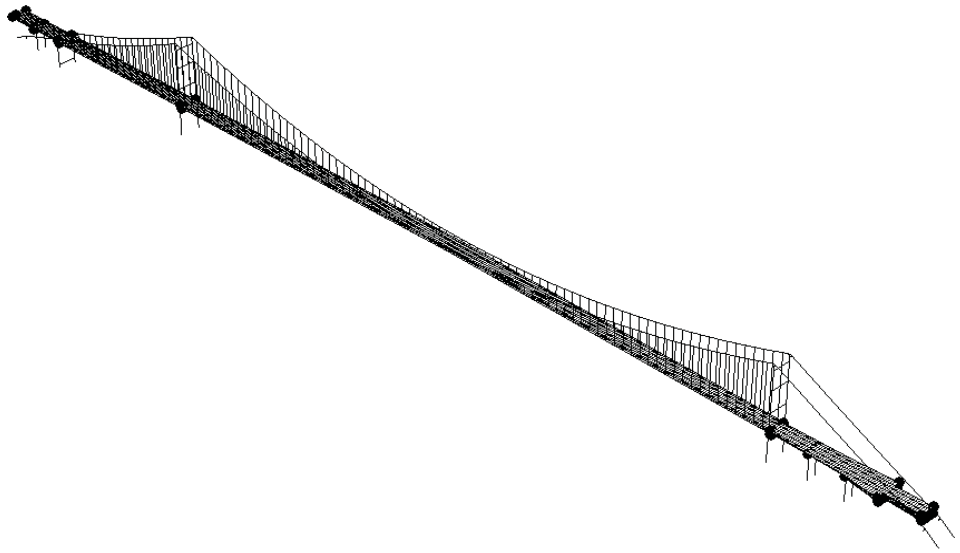

Figure 5.8 Full three dimensional finite element model of TMB

The two side spans on the Ma Wan side and Tsing Yi side are supported by two

and three piers, respectively. These piers are similarly modeled using beam element B31 and considered about the connections between the piers and the bridge deck. The boundary conditions of the global bridge model are simulated using different supports. Since the tower legs and piers are settled on the rock, the foundations for all the piers and towers are simulated as fixed supports, and at the both ends of main cables as well. The connection relationships between the tower and bridge deck, and bridge deck and piers are so complicated that the sole fixed supports or simple supports can't completely simulate the real condition. A special-purpose flexible joint element (JOINTC), made up of three translational springs and three rotational springs, is then introduced to model joint interaction in linear or nonlinear manner. The constraints on the translational directions without on rotations are adopted at the deck on the Ma Wan side. The movement of deck along the longitudinal direction is allowed on the deck end of the Tsing Yi side. In addition, the concentrated mass element (MASS) are used to include the mass of rigid areas of towers that are nonstructural members. The entire three dimensional finite element model of TMB with more than 7300 nodes and 19000 elements is constructed as shown in Figure 5.8. All of the aforementioned corresponding geometric and material properties could be found in detail in Xu *et al*. (1997).

5.2.4 Ambient Vibration Test

Experimental modal analysis is used to obtain an experimental model of a

structure which describes its dynamic behavior through a set of natural frequencies, mode shapes, and damping ratios. This information is obtained from a modal test of the structure during which the structure is excited and the responses of the structure are captured by a set of sensors. Field dynamic testing of a bridge provides a direct way to estimate its dynamic characteristics. There are three main types of dynamic tests for bridge structure: (1) forced vibration tests; (2) free vibration tests; and (3) ambient vibration tests. In the forced vibration method, the bridge is excited by artificial way and correlated input-output measurements are performed. In the case of large scale flexible bridges, like cable-supported bridges, it often requires very heavy equipment and involves significant resources to provide controlled excitation at sufficiently high levels (Okauchi *et al*. 1997), which becomes difficult and costly. Free vibration tests of bridges are carried out by a sudden release of a heavy load or mass appropriately connected to the bridge deck (Cunha *et al*. 2001). Both forced and free vibration tests, however, need an artificial way to excite the bridge. Moreover, traffic has to be shut down during the tests, which could be a serious problem for intensively used bridges. During the past few years, operational modal testing has been proven to be a valuable alternative for the use of classic forced vibration testing. Instead of using one or more artificial excitation devices, in-operation modal testing makes use of the freely available ambient excitation caused by natural excitation sources on or near the test structure. Especially in the case of civil engineering structures, the latter can be considered as an important advantage,

since the use of artificial excitation devices (large shakers, drop weights) can be considered expensive and impractical. Another advantage is that the test structure remains in its operating condition during the test, which can differ significantly from laboratory conditions.

In summary, ambient vibration tests have an advantage of being inexpensive since no extra equipment is needed to excite the bridge. It corresponds to the real operating condition of the bridge. The service state does not have to be interrupted to use this technique and it can be continuously executed while the bridge is under its normal serving condition. Therefore, ambient vibration tests outwitted forced vibration measurement in those aspects and have been successfully applied to several large scale cable-supported bridges, like the Golden Gate Bridge (Abdel-Ghaffer and Scanlan 1985), the Roebling Suspension Bridge (Ren *et al*. 2004a), the Kap Shui Mun cable-stayed bridge (Chang *et al*. 2001). In case of ambient vibration tests, only response data are measured while actual loading conditions are not measured. A modal parameter identification procedure will therefore be needed to base itself on output-only data. However, many challenges exist in the experimental modal analysis of real bridges using ambient vibration measurements. There have been several modal parameter identification techniques available that are developed by different investigators for different purposes. The mathematical background for many of these methods is often very similar, differing only from implementation aspects (data reduction, type of equation solvers, sequence of matrix operations, etc.). The benchmark study has

been carried out for evaluating the dynamic characteristics from ambient vibration data (Ren *et al*. 2004b). Nevertheless, relatively long records of response measurements are required and the signal levels are considerably low in ambient vibration testing.

Table 5.1 Few free-vibration frequencies of TMB by laboratory tests and computation, unit (Hz) (Chan *et al*. 2003)

Mode Description	Experimental Results			Computed Results		Mean value
	HK PolyU	THU	HK HD	MMHK	FNP	
Lateral						
First	0.069	0.069	0.070	0.065	0.064	0.0674
Second	0.164	0.161	0.170	0.164	0.149	0.1616
Vertical						
First	0.113	0.114	0.114	0.112	0.112	0.113
Second	0.139	0.137	0.133	0.141	0.133	0.1366
Torsion						
First	0.267	0.265	0.270	0.259	0.253	0.2592
Second	0.320	0.320	0.324	0.276	0.268	0.3016

The ambient vibration field test of Tsing Ma Bridge, after the completion of bridge deck, is carried out by The Hong Kong Polytechnic University (PolyU) under the auspices of the Hong Kong Highways Department from July 1st to August 1st 1996. Due to the complexity of the mode shapes, the responses along more than one direction at some measurement points have to be recorded. Considering the complicated bridge configuration, the availability of instruments

and the site as well as time constraints for the measurement, it is decided to divide the main span of bridge into 48 measurement sections that are conducted in a sequential pattern. There are also two reference points at each section selected for accelerometers recording the response signal for normalization. After the normalization of the acceleration responses, the Power Spectral Density (PSD) functions of those responses are obtained using Fast Fourier Transform (FFT) to identify the natural frequencies while the corresponding mode shapes extracted by evaluating the cross spectra and coherence functions. The more details about the test setup and corresponding methodology combined with identification procedures could be found in Zhan *et al*. (1999).

Meanwhile, some free vibration frequencies have been also separately measured by other agencies such as Tsing Hua University (THU) in China, and the Hong Kong Highways Department (HKHD). The designer Mott MacDonald Hong Kong Ltd. (MMHK) and the checker Flint & Neill Partnership of UN (FNP) of TMB also theoretically analyze and give the first few frequencies results (Lau *et al*. 1999). Comparison of the first few order frequencies by laboratory test results and analytical ones, also combined with the arithmetical mean values are tabulated in Table 5.1.

5.2.5 Preliminary Study on Dynamic Characteristics

The analytical macro model of TMB can be validated by the corresponding modal parameters identified from the field ambient vibration test. Typical first few order

computed mode shapes of TMB are listed in Figure 5.9. The validation process could be assessed by comparing graphical representation of corresponding computed and measured mode shapes of first few orders as shown in Figure 5.10. It indicates that there is a good correlation between the computed and identified mode shapes of the specific vibration modes.

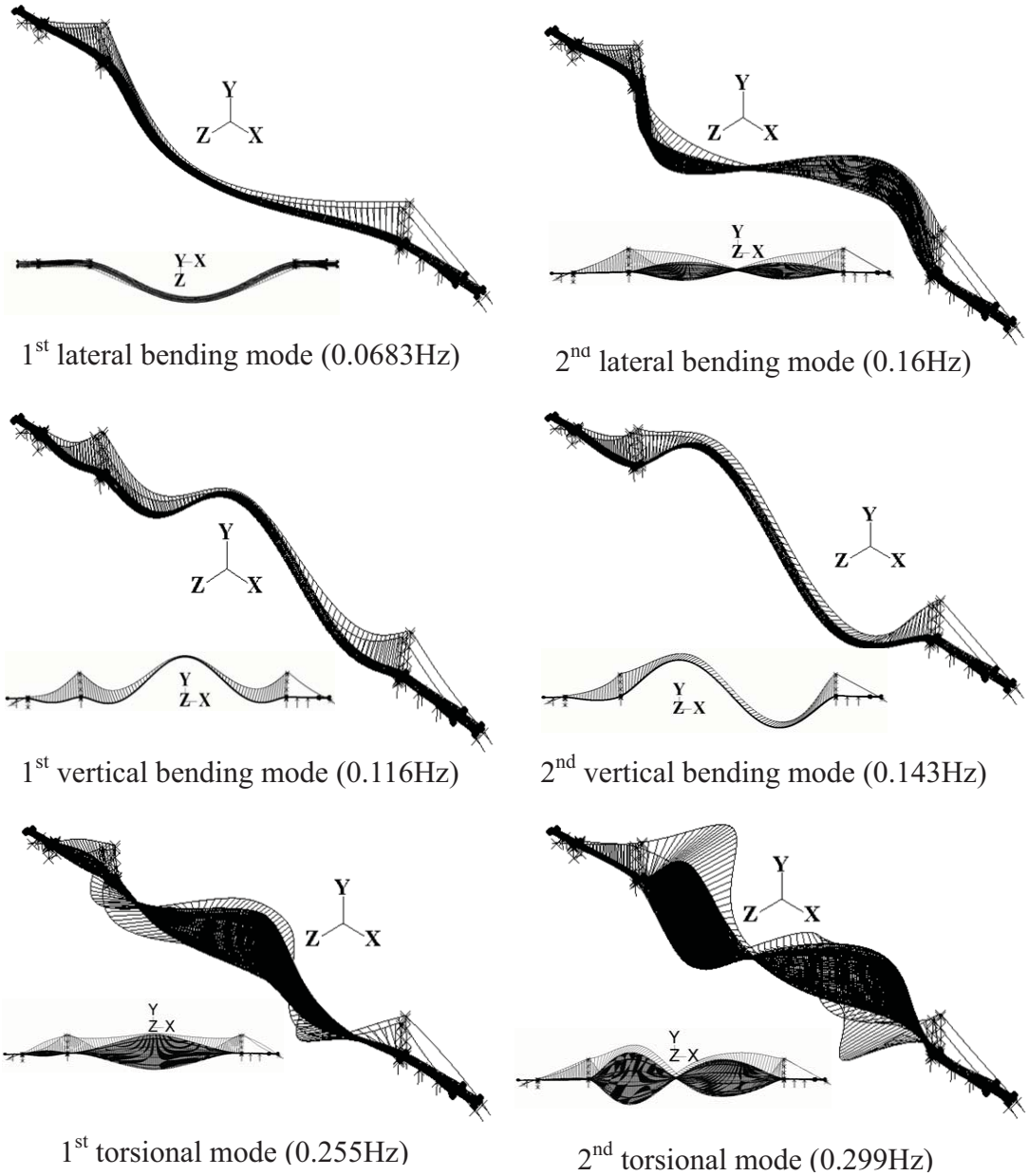

1st lateral bending mode (0.0683Hz)

2nd lateral bending mode (0.16Hz)

1st vertical bending mode (0.116Hz)

2nd vertical bending mode (0.143Hz)

1st torsional mode (0.255Hz)

2nd torsional mode (0.299Hz)

Figure 5.9 Typical first few order computed mode shapes of TMB

Table 5.2 Comparison of measured and calculated modal parameters of first 17 modes (CS stands for Central Span and MW for Ma Wan)

Mode Number (Notation)	Nature of Mode shape	Measured Frequency f_{exp} (Hz)	Computed Frequency f_{FEM} (Hz)	Differences (%)	MAC
1 (L1)	CS deck lateral bending (0.5-wave)	0.069	0.0683	-1.0	0.997
2 (V1)	CS deck vertical bending (1-wave)	0.113	0.1157	2.4	0.997
3 (V2)	CS deck vertical bending (0.5-wave)	0.139	0.1426	2.6	0.972
4 (L2)	CS deck lateral bending (1-wave) coupled with torsion (1-wave)	0.164	0.16	-2.4	0.992
5 (V3)	CS + MW deck vertical bending (2-wave)	0.184	0.1846	0.33	0.822
6 (L3)	CS cable local sway: in phase (0.5-wave)	0.214	0.217	1.4	0.8
7 (L4)	CS cable local sway: in phase (1-wave)	0.226	0.2179	-3.58	0.917
8 (L5)	CS cable local sway: in phase (0.5-wave); CS deck lateral bending	0.236	0.2194	-7.0	0.917
9 (L6)	CS deck torsion + lateral bending	0.24	0.2203	-8.2	0.954
10 (V4)	CS + MW deck vertical bending (2.5-wave)	0.241	0.2355	-2.3	0.973
11 (T1)	CS deck torsion	0.267	0.2547	-4.6	0.986
12 (V5)	MW deck vertical bending (0.5-wave)	0.284	0.2941	3.6	0.912
13 (L7)	CS deck lateral bending	0.297	0.2992	0.74	0.955
14 (T2)	CS deck torsion	0.320	0.2819	-11.9	0.938
15 (V6)	CS + MW deck vertical bending (3-wave)	0.327	0.3289	0.58	0.744
16 (L8)	MW cable local sway: in phase (0.5-wave)	0.336	0.3446	2.6	0.994
17 (L9)	MW cable local sway: out of phase (0.5-wave)	0.352	0.3553	0.94	0.99

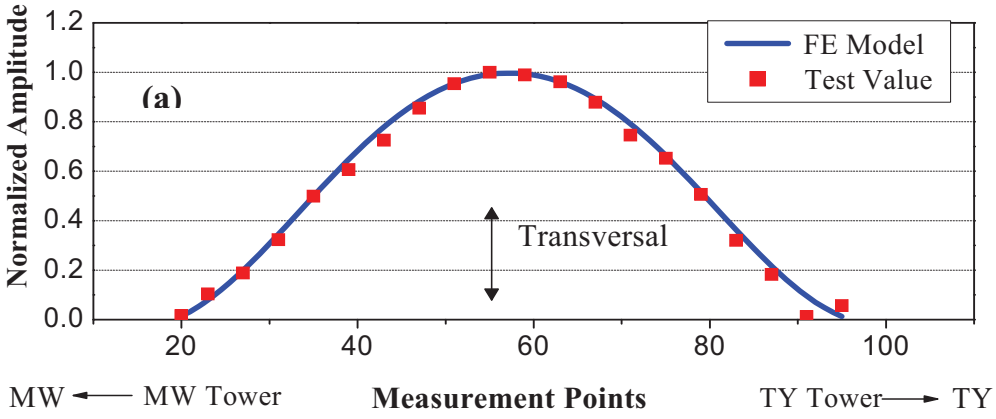
Normalized Amplitude
1.2
1.0
0.8
0.6
0.4
0.2
0.0
(a)
FE Model
Test Value
Transversal
20
40
60
80
100
MW
MW Tower
Measurement Points
TY Tower
TY

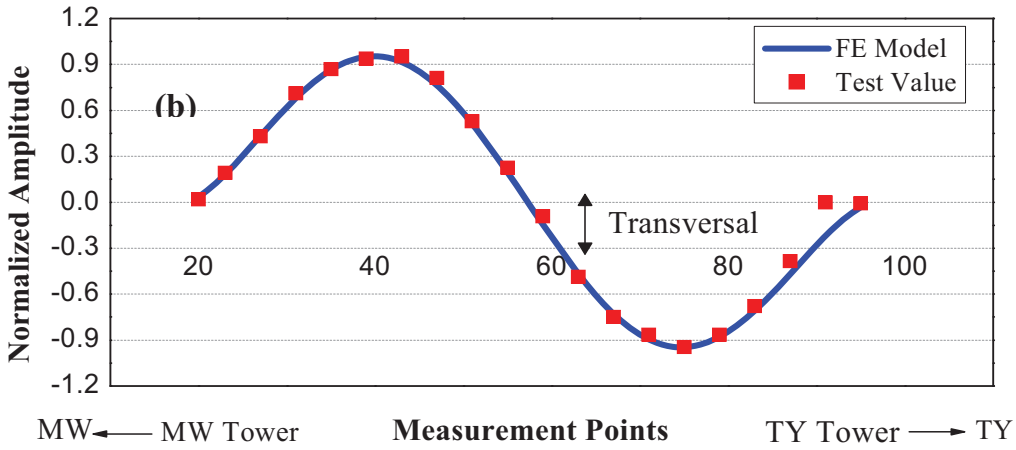
Normalized Amplitude
1.2
0.9
0.6
0.3
0.0
-0.3
-0.6
-0.9
-1.2
(b)
FE Model
Test Value
Transversal
20
40
60
80
100
MW
MW Tower
Measurement Points
TY Tower
TY

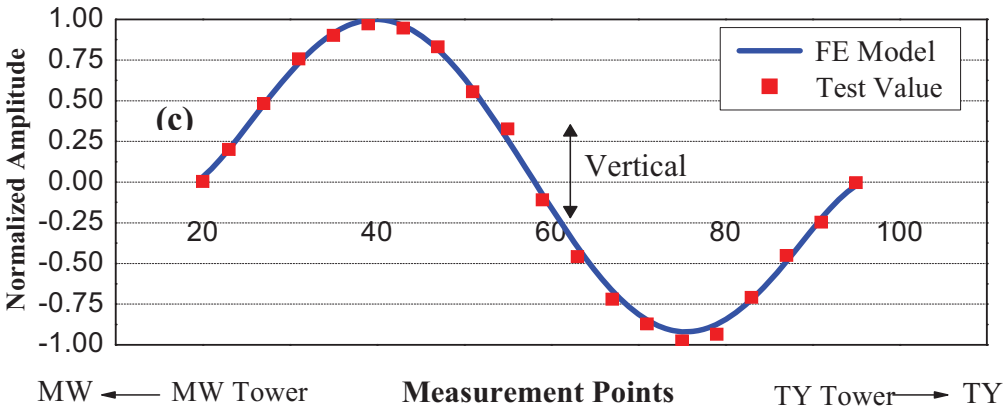
Normalized Amplitude
1.00
0.75
0.50
0.25
0.00
-0.25
-0.50
-0.75
-1.00
(c)
FE Model
Test Value
Vertical
20
40
60
80
100
MW
MW Tower
Measurement Points
TY Tower
TY

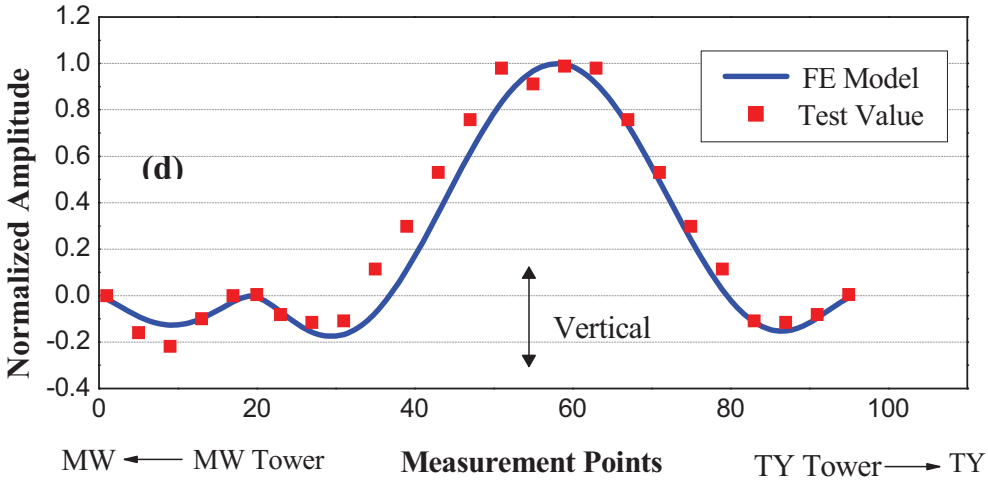
Normalized Amplitude
1.2
1.0
0.8
0.6
0.4
0.2
0.0
-0.2
-0.4
(d)
FE Model
Test Value
Vertical
0
20
40
60
80
100
MW
MW Tower
Measurement Points
TY Tower
TY

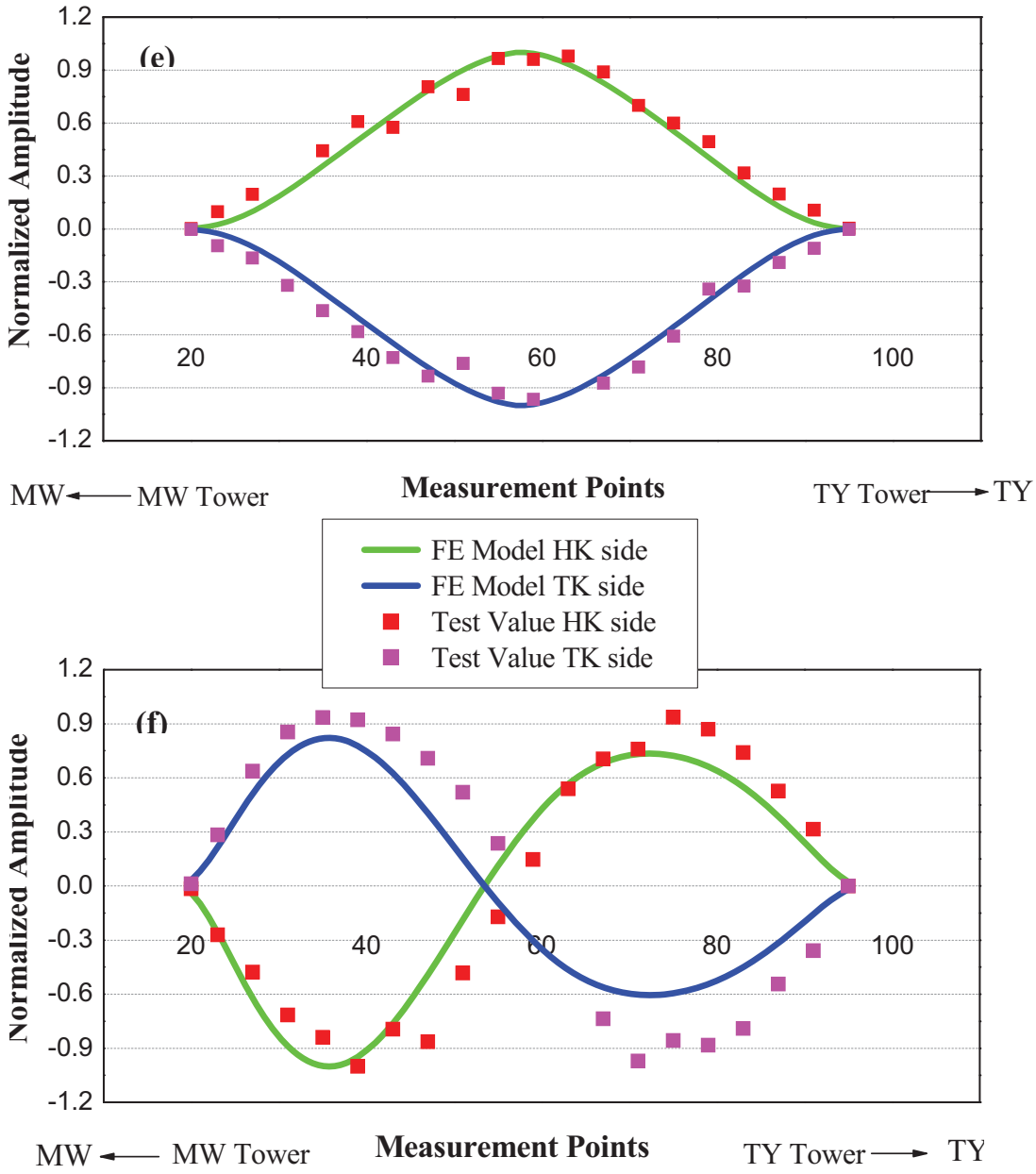

Figure 5.10 Graphical comparison of calculated first few mode shapes and experimental values: (a)1st lateral bending (b)2nd lateral bending (c)1st vertical bending (d)2nd vertical bending (e)1st torsional mode (f)2nd torsional mode

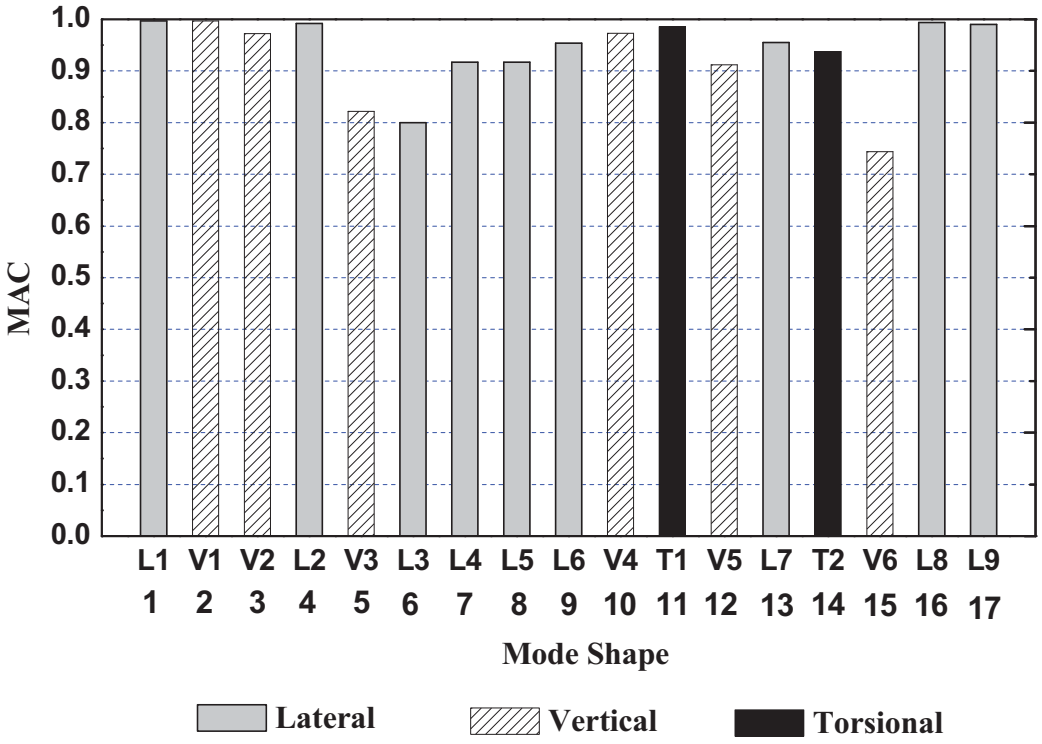

Figure 5.11 Modal Assurance Criterion (MAC) values of first 17 mode shapes

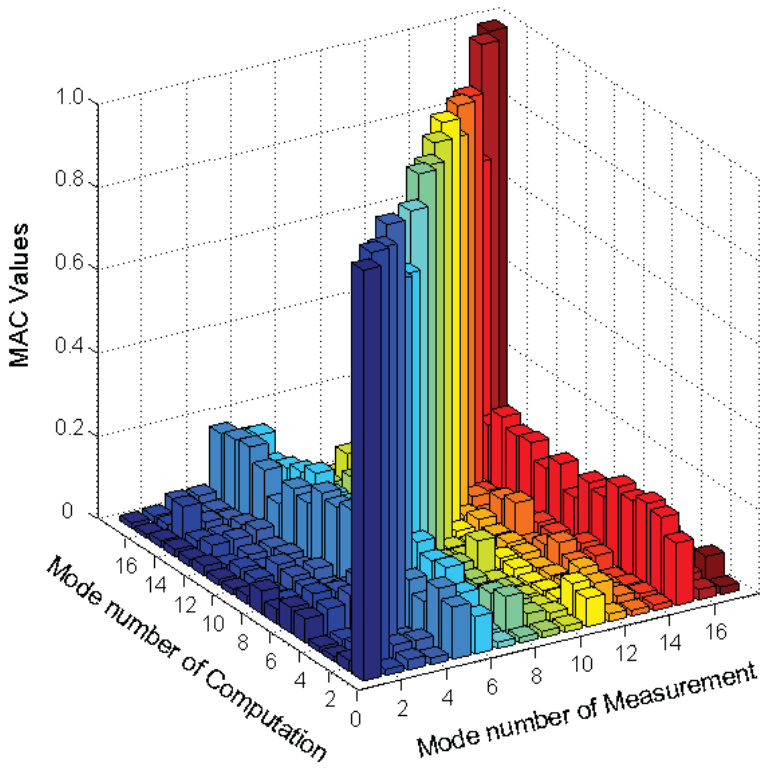

Figure 5.12 3D figure of corresponding MAC values

The computed natural frequencies and mode shapes which correspond to the first 17 order frequency values and mode shapes of measurement are listed in Table 5.2. It can be seen that the differences between the calculated and measured natural frequencies are smaller than 10% except that the largest values is -11.9% in the second torsional mode of vibration. Moreover, the corresponding MAC values are tabulated and graphically shown in Figure 5.11 and also the 3D MAC matrix in Figure 5.12. The two axes on the plane stand for the mode number of measurement and calculation respectively while the height of columns represents the MAC values in 3D figure. It is also demonstrated that the corresponding high MAC values for some significant modes are found which indicates a good correlation between the identified and computed mode shapes on the diagonal. However, values of off-diagonal elements are not as good as diagonal ones, especially related to the modes No. 5, 6 and 15 which also have the relatively poor diagonal result, maybe attribute to the following: (1) The limited number of sensors is used in the ambient vibration test and normalization at reference point probably lead to the accumulated error in identification. (2) The specific order of mode shape is considered to be dominant at certain direction within some parts of structures with respect to vertical, lateral in terms of bending, torsion and sway in plane and out-of-plane in mode shape identification from measurement while in the actual case every mode shape is the complicated coupling of aforementioned situations, which possibly result in the discrepancies. (3) The large differences may exist in the situations of dominant of central span combined with side span as

well as the local cable sway.

5.3 MACRO MODEL MODIFICATION ON SENSITIVITY-BASED METHOD

As mentioned before, a comprehensive survey on the model updating techniques can be found in Mottershead and Friswell (1993) and Natke *et al*. (1994). A literature review on the finite-element model updating techniques and their applications to damage detection and structural health monitoring can also be found in Doebling *et al*. (1998). As for the parametric updating method, it typically involves using the sensitivity of the parameters to find their changes (Farhat and Hemez 1993; Friswell and Mottershead 1995; Fritzen *et al*. 1998). This sensitivity-based parametric updating approach has an advantage of identifying parameters that can directly affect the dynamic characteristics of a structure. Also, by employing this method, one may acquire an immediate physical interpretation of the updated results. In this study, an improved sensitivity-based parameter updating method is employed for the model updating of TMB. This method is based on the eigenvalue sensitivity to some selected structural parameters that are assumed to be bounded within some prescribed regions according to the degrees of uncertainty and variation existing in the parameters, together with engineering judgments. The changes of these parameters are found by solving a quadratic programming problem.

5.3.1 Sensitivity-based Model Updating Method

Sensitivity-based Parameter Updating Formulation with Constraints

An improved sensitivity-based updating algorithm described in Zhang *et al*. (2000) is employed in this study. The formulation and the main features of the updating procedure are reviewed as follows.

By discretizing an undamped continuous system into a n degrees of freedom FE model, the ith eigenvalue λ_i and the corresponding eigenvector (mode shape) ϕ_i can be obtained by solving the following eigenequation

$$K_i\phi_i = \lambda_i M\phi_i \tag{5.1}$$

where K and M ($n \times n$) are the structural stiffness and mass matrices, respectively. Typically, the stiffness and mass matrices are functions of structural parameters, including geometrical and material properties as well as boundary conditions. If a set of structural parameters ($p_{i,a}, i = 1,\ldots,n_p$) can be estimated for design and represented by a vector P_a

$$P_a = \left\{ p_{i,a} \middle| i = 1,2,\ldots,n_p \right\}^T \tag{5.2}$$

where n_p is the total number of structural parameters, then a set of eigenvalues (Λ_a) can be obtained from the model and is expressed as

$$\Lambda_a = \left\{ \lambda_{i,a} \middle| i = 1,2,\ldots,n_a \right\}^T \tag{5.3}$$

where n_a is the total number of the computed modes. The subscript a in

Equations (5.2) and (5.3) is used to indicate that the corresponding properties are related to the "prediction" by the finite element analysis.

Also, the modal characteristics of the structure can be obtained from experiments as

$$\Lambda_e = \left\{ \lambda_{i,e} \middle| i = 1,2,\ldots,n_e \right\}^T \tag{5.4}$$

where Λ_e is the vector of the measured eigenvalues; and n_e the total number of the measured modes. The subscript e in Equation (5.4) is used to indicate that the corresponding properties are obtained from the measurements.

In general, the experimental (Λ_e) and the predicted modal properties (Λ_a) do not necessarily correlate well due to inaccuracy in both the FE modeling and the measurements. In the present FE model updating procedure, it is intended to modify the FE model (but not the measured data) so that the predictions can be in better agreement with the experimental data. As mentioned before, any inaccuracy in connection with a finite-element model may come from three possible sources, namely, model structural errors, model order errors, and model parameter errors. If it is assumed that the measured modal properties are very close to the actual behavior of the structure and that the model parameter errors are the main contributor to the inaccuracy of the finite element model, then the model errors could be reduced or corrected through the model updating procedure.

Let P represents the vector of structural parameters after updating

$$P = \left\{ p_i \middle| i = 1,2,\ldots,n_p \right\}^T \tag{5.5}$$

It may be assumed that the total number of measured modes is the same as the total number of predicted (or calculated) modes ($n_e = n_a$). The functional relationship between the measured and the initial predicted eigenproperties can be approximated by a first-order Taylor-series expansion with respect to the structural parameters as follows (Friswell and Mottershead, 1995):

$$\delta\Lambda = S\delta P \tag{5.6}$$

where $\delta\Lambda$ is the eigenvalue residual vector and δP the perturbation vector of structural parameters defined respectively as

$$\delta\Lambda = \Lambda_e - \Lambda_a \tag{5.7}$$

$$\delta P = P - P_a = \left\{ \delta p_i \middle| i = 1,2,\ldots,n_p \right\}^T \tag{5.8}$$

where S is sensitivity matrix, containing the first derivative of the eigenvalues with respect to the structural parameters evaluated at the initial estimate P_a or, in the following iterative scheme, at the current parameter estimate. The higher order terms in the Taylor-series expansion are neglected under the assumption that the changes in the structural parameters between successive iterations are small. The perturbation of structural parameters can be obtained by solving Equation (5.6).

Many approaches have been proposed to solve this inverse problem and basically can be classified according to whether there are more structural parameters than

measured modal properties or vice versa. When there are more measured modal properties than structural parameters ($n_e > n_p$), an optimal solution may be derived in a sense that it minimizes a least-squared error function as the form (Friswell *et al*. 1995).

$$J_1 = (S\delta P - \delta\Lambda)^T W_E (S\delta P - \delta\Lambda) \tag{5.9}$$

where W_E is the positive-definite weighting matrix, reflecting the relative confidence in the accuracy of various measured modes.

On the other hand, when there are more structural parameters than measured modal properties ($n_p > n_e$), the problem may be restated as a constrained optimization problem as the form:

$$\begin{array}{ll} \text{minimize} & J_2 = \delta P^T W_P \delta P \\ \text{subject to} & S\delta P = \delta\Lambda \end{array} \tag{5.10}$$

where W_P is the positive-definite weighting matrix.

By adding the above two objective functions,

$$J_3 = \delta P^T W_P \delta P + (S\delta P - \delta\Lambda)^T W_E (S\delta P - \delta\Lambda) \tag{5.11}$$

the new objective function then has the advantages of both J_1 and J_2 if the two weighting matrices are properly chosen. The first term on the right-hand side of Equation (5.11) acts both as a regulator that eliminates the possible ill-conditioned problem associated with the second term and as a perturbation monitor that provides proper constraints to the updated structural parameters. It is

thus decided to use the objective function J_3 in this study.

However, it is quite possible that the use of parameter perturbation to minimize the objective function can result in relatively large variations. These extreme values not only violate the assumption of the first-order Taylor-series approximation, but also produce an updated result that may be physically meaningless. In order to guarantee the physical significance of updated parameters and avoid physically impossible updated parameter values, inequality constraints for the structural parameters are introduced by Zhang *et al*. (2000) as follows:

$$B_l \le P \le B_u \tag{5.12}$$

where B_l and B_u are the vectors of lower and upper bounds for the structural parameters P, respectively. Subsequently, the structural parameter perturbations are bounded by

$$b_l \le \delta p \le b_u \tag{5.13}$$

where b_l and b_u are lower and upper bounds of the perturbation, respectively. Thereby, the parameter updating can be achieved by minimizing the objective function subjected to the constraints in the form of Equation (5.13).

The iterative procedure starts with the selection of a proper set of parameters for adjustment together with the upper and lower bounds of each parameter. The parameter used in the initial finite-element model is taken as the starting point for

the iteration. In each iteration step, an eigenvalue sensitivity analysis is performed using the parameters updated in the previous iteration. The eigenvalue sensitivities can be approximated by

$$S_{ij} = \frac{\Delta\lambda_i}{\lambda_i}\frac{p_j}{\Delta p_j} \tag{5.14}$$

where S_{ij} is the dimensionless (normalized) sensitivity of the ith eigenvalue λ_i with respect to the jth parameter p_j, Δp_j is the perturbation of parameter p_j and $\Delta\lambda_i$ is the change of eigenvalue λ_i due to Δp_j.

The convergence criteria for the iteration are set as

$$\left| f_a^{(k)} - f_{exp} \right| \le tolerance \tag{5.15}$$

$$\left| \frac{\Lambda_a^{(k+1)} - \Lambda_a^{(k)}}{\Lambda_a^{(k)}} \right| \le tolerance \tag{5.16}$$

where $f_{\exp}$ is the vector of the measured natural frequencies and $f_a^{(k)}$ and $\Lambda_a^{(k)}$ are the vector of the analytical natural frequencies and eigenvalues of the kth iteration, respectively. The fast criterion (5.15) relates the global convergence of the analytical natural frequencies to the measured natural frequencies while the second criterion (5.16) represents the convergence during iterations. The iteration would be terminated if either one of these two criteria is satisfied.

Then the constrained optimization may be further stated as the following quadratic programming problem:

$$\text{minimize} \quad J(x) = \frac{1}{2} x^T W x \quad \text{subjected to}$$

$$A_i x = d_i \quad (i = 1, \ldots, n_e) \quad \text{and} \quad A_i x \le d_i \quad (i = n_e + 1, \ldots n_e + 2n_p) \tag{5.17}$$

where

$$x = \begin{Bmatrix} \delta P \\ S\delta P - \delta\Lambda \end{Bmatrix} \tag{5.18}$$

$$d = \begin{Bmatrix} \delta\Lambda \\ b_u \\ -b_l \end{Bmatrix} \tag{5.19}$$

$$A = \begin{bmatrix} S & -I \\ I & 0 \\ -I & 0 \end{bmatrix} \tag{5.20}$$

$$W = \begin{bmatrix} W_P & \\ & W_E \end{bmatrix} \tag{5.21}$$

where A_i and d_i represent the i th row of matrix A and vector d respectively.

The solution of this updating approach is affected by the selection of the weighting matrix W_P. It may be reasonable to determine the matrix W_P in such a way that those parameters estimated with greater confidence do not deviate too much during each iteration step. Also, the weighting matrix W_P can be chosen to restrain those parameters that may affect eigenvalues in a nonlinear manner from drastic changes in each iteration step. On the other hand, the other weighting matrix W_E should be chosen to ensure the agreement between the finite-element analysis and the measured results. Therefore, the constraint optimization solution is outline as Equations (5.17)-(5.21) and the whole updating procedure could be

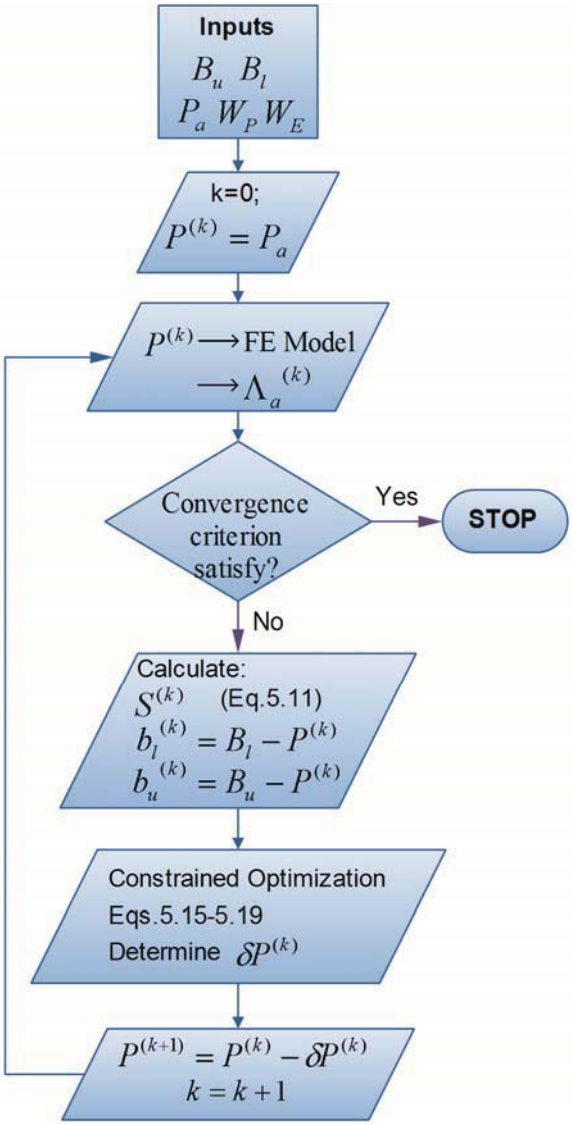

Figure 5.13 Flowchart for the sensitivity-based model updating with parameter constraints

carried out as the flowchart shown in Figure 5.13. This eigenvalue sensitivity-based updating method has been successfully applied to complex of structures of long-span cable-stayed bridge (Zhang *et al*. 2001) and suspension bridge (Zhang *et al*. 2000).

Selection of Parameters and Modes

As we all known, the model order errors resulting from the linear discretization

are usually insignificant for eigenvalue predictions. It may say that the differences between the predicted and the measured natural frequencies largely result from the inaccurate estimation of structural parameters such as material properties, geometric parameters, and boundary conditions. Theoretically speaking, all possible structural parameters can be selected for adjustment in the updating procedure. However, it would take computational costs if too many parameters are included. Therefore, the set of parameters to be updated should be carefully selected. As for the scaled specimen model, some geometric parameters such as the lengths of the components and cross-sectional dimensions can be measured quite accurately which should not be the candidate parameters for updating. On the contrast, the boundary condition is complicated in laboratory simulation and there exist uncertainties and disunities because of either material itself or the processing technology, the material properties around the concerned area of vicinity of welding toe with respect to welding thickness and elasticity modulus are eventually selected as updating parameters.

Ideally, it would be better if we can match as many modes as possible between the measurement and the FE prediction. However, the request is not always true when applied in the practical engineering. In the area of health monitoring and damage detection of complex structures, it is found that the global mode is usually at the low order while the higher modes are more sensitive to local damage. Therefore, it is not practical and also unnecessary to include modes (especially those higher modes) when the emphasis is focused on the dynamic properties at the global

level.

5.3.2 Macro Model Modification

Actual dynamic properties of the bridge are now known through ambient field vibration testing as investigated in previous study. Moreover, the structural or material parameters that may significantly affect the modal properties of the bridge, so this initial FE model now could be calibrated by adjusting the structural model parameters to match the frequencies and mode shapes obtained through ambient testing.

Theoretically speaking, all possible parameters relating to the geometric, elastic, and inertial properties as well as the boundary conditions should be considered for adjustment in the updating procedure. However, from the comparison result of free vibration frequencies and mode shapes of computed values by initial FE macro model with that by measurement as tabulated in Table 5.2, it clearly shows the maximum difference between the calculated values and mean experimental ones is -11.9%, which is considered to be acceptable within the allowable engineering error range. However, the model modification on the basis of sensitivity-based method is still to be performed anyway and intended to reduce the engineering error as much as possible.

Three main kinds of structural parameters at the aspects of cable, decking beam elements and decking membrane elements in terms of mass density and modulus

Table 5.3 Parameters selected for updating

Structural Part	Parameters	Notation	Initial Estimates	Bounds
Cable	Mass density	M_c	7935 kg/m^3	±20%
Beam	Mass Density	M_b	7800 kg/m^3	±20%
Elements in decking	Modulus of Elasticity	E_b	2×10^{11} Pa	±20%
Membrane	Mass Density	M_m	11500 kg/m^3	±20%
Elements in decking	Modulus of Elasticity	E_m	2×10^{11} Pa	±20%

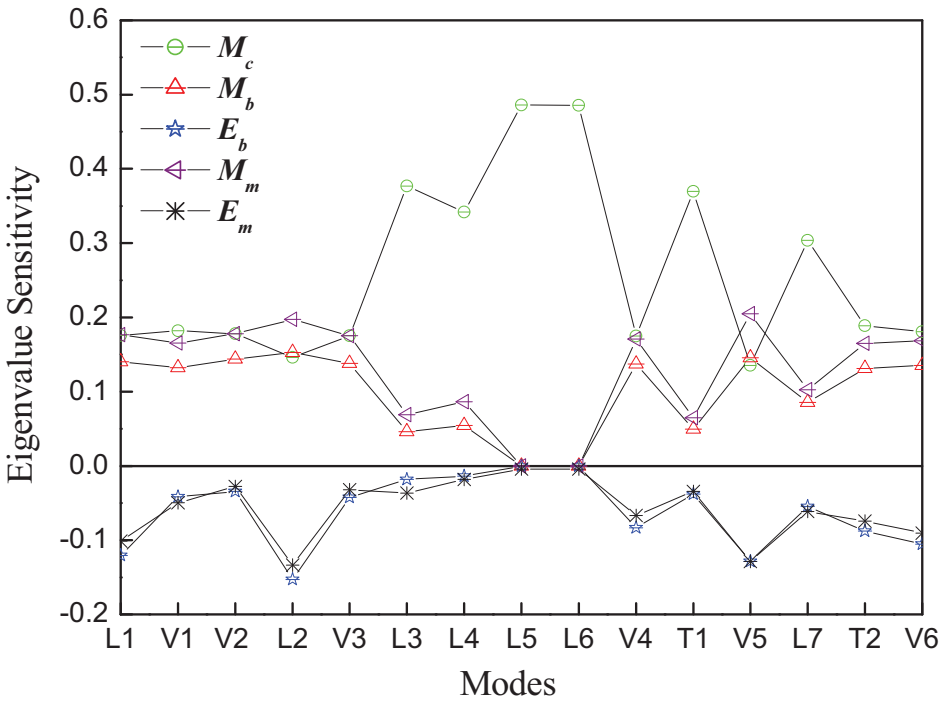

Figure 5.14 Sensitivity of eigenvalues to selected updating parameters

of elasticity are selected as parameters for updating. The initial estimate values of those parameters are summarized in Table 5.3 together with the upper and lower bounds of 20%. The lowest 15 order modes with frequencies ranging between 0 and 0.327 Hz would be matched between the updating finite element analysis and

the measured results. The eigenvalue sensitivities of the 15 selected modes with the corresponding dimensionless sensitivity of selected modes to the parameters are illustrated in Figure 5.14.

Table 5.4 Parameters for initial and updated models

Structural Part	Parameters	Initial Estimates	Updated values	Differences (%)
Cable	Mass density	7935	8325	4.9
Beam Elements in decking	Mass Density	7800	8563	9.8
	Modulus of Elasticity	2×10^{11}	1.98×10^{11}	-1
Deck plate	Mass Density	11500	10800	-4.2
	Modulus of Elasticity	2×10^{11}	1.95×10^{11}	-2.5

The sensitivities normally ranged between -0.2 and 0.5 and the trends of these curves are irregular so that the conclusions are relatively difficult to make. Roughly, we can see that eignevalue of each mode are affected by the properties of that component. For instance, parameter of cable mass density greatly influences eigenvalues, especially in the few middle orders of modes list while the other four parameters have the smaller effects on the eigenvalues in positively or negatively.

The sensitivity-based model modification procedure is then carried out as described in the flowchart. Table 5.4 shows the updated values of structural parameters as compared to the initial estimates. It is seen that mass density of

Table 5.5 Frequency comparison for initial and updated models

Mode No.	Measured Frequencies $f_{\exp}$ (Hz)	Computed Frequencies from Finite Element Model by		MAC
		Initial Model $f_{FEM}{}^{i}$ Hz / (Error in percentage compared with $f_{\exp}$)	Updated Model $f_{FEM}{}^{u}$ Hz / (Error in percentage compared with $f_{\exp}$)	
1 (L1)	0.069	0.0683(-1.0)	0.0685(-0.72)	0.997
2 (V1)	0.113	0.116(2.7)	0.115(1.77)	0.997
3 (V2)	0.139	0.143(2.9)	0.142(2.16)	0.972
4 (L2)	0.164	0.16(-2.4)	0.165(0.61)	0.992
5 (V3)	0.184	0.185(0.54)	0.186(1.1)	0.822
6 (L3)	0.214	0.217(1.4)	0.22(2.8)	0.8
7 (L4)	0.226	0.218(-3.54)	0.223(-1.32)	0.917
8 (L5)	0.236	0.219 (-7.2)	0.225(-4.6)	0.917
9 (L6)	0.24	0.220 (-8.3)	0.23(-4.2)	0.954
10 (V4)	0.241	0.236(-2.1)	0.238(-1.24)	0.973
11 (T1)	0.267	0.255(-4.5)	0.27(1.12)	0.986
12 (V5)	0.284	0.294 (3.5)	0.29(2.11)	0.912
13 (L7)	0.297	0.299 (0.67)	0.295(-0.67)	0.955
14 (T2)	0.320	0.282(-11)	0.299(-6.6)	0.938
15 (V6)	0.327	0.329(0.6)	0.32(-2.14)	0.744

decking beam element has been largely modified, with the change of approaching 10%. The mass densities of cable and decking membrane elements are modified moderately and modulus-related parameters are pretty much slightly changed.

The frequency comparison giving the measured results together with those of the initial and final updated model is summarized in Table 5.5 and the corresponding frequency differences are plotted as shown in Figure 5.15. It is easily seen that, in

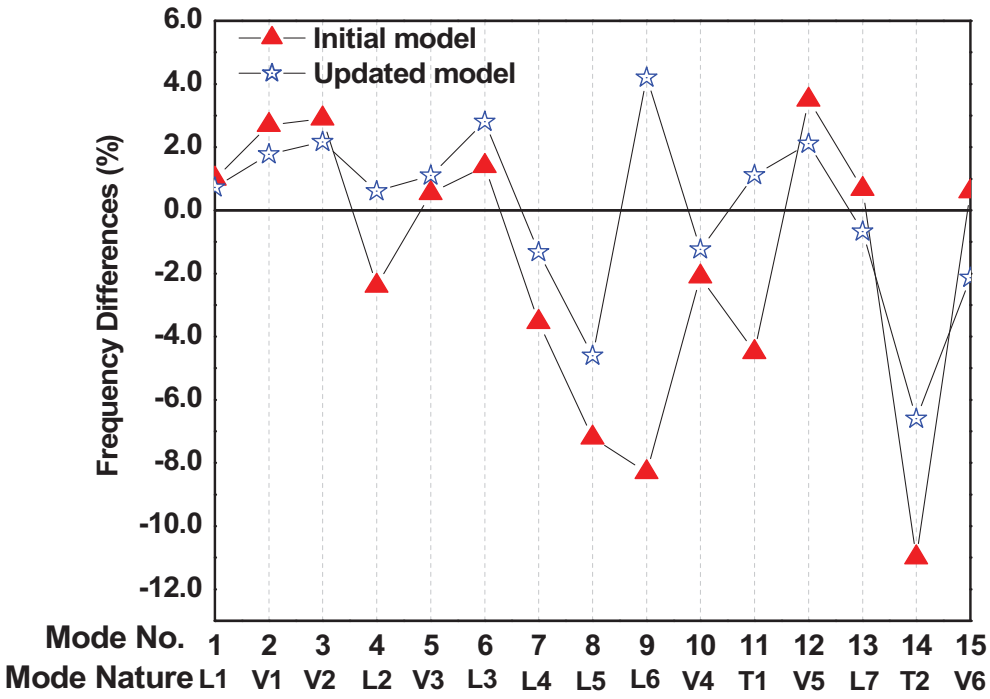

Figure 5.15 Frequency differences between the measured and the calculated results before and after modification

general, the large differences between majority of the measured and the initial results can be reduced while on certain order mode shape small increase are also observed.

After the model modification on the basis of sensitivity-related method, the modified macro model is considered as "better" than the initial one, in some sense, closer to the ambient vibration measurements.

5.4 GLOBAL MODEL VERIFICATION

5.4.1 Model Verification Methods and Procedure

During the establishment of initial global model of TMB, the coordinates of the

structure are based on drawings and the initial configuration constitute accordingly. The real configuration of the whole bridge is usually achieved by the field test after the completion of bridge construction, which is often slightly different from the initial configuration. So the initial deformed configuration of the finite element model should be identical to completed initial geometry alignment of the bridge deck. The process for finding the target configuration of the bridge in initial equilibrium state under dead loads is referred to as "configuration-finding". Therefore, the initial equilibrium configuration is so important that it is the basis of preceding modal analysis and the subsequent analysis steps. It should be determined under the combination of dead loads and initial stress of cables and suspenders before the live load and succeeding dynamic analysis is carried out.

The modal analysis then should include the following two steps:

(1) The static analysis should be conducted firstly to obtain the initial equilibrium configuration under the dead loads and main cable pre-tensions.

(2) The modal analysis (free vibration) is then carried out on the basis of deformed equilibrium positions.

The modal analysis is carried out on the basis of initial equilibrium configuration of developed global structural model of TMB which is obtained from aforementioned "configuration-finding" process implemented by the static analysis of initial bridge model under the dead loads and initial stress of main

cables and suspenders. The implementation process will not be discussed in detail in this study.

After the “configuration-find” process is completed on the basis of the developed global model of TMB on the structural scale, the macro-model should be verified before any analyzing procedure carried out on it. Model verification strategy serves the modeling objectives. Since the macro-model and subsequent developed concurrent multi-scale model are constructed for the fatigue damage analysis and condition assessment procedure, the model verification procedure should be performed to meet the needs of calculation accuracies of dynamic characteristics, static responses and dynamic responses respectively.

5.4.2 Simulation of Typical Train Loading

The TMB carries both loadings of highway and trains. Theoretically speaking, its dynamic response is caused by the combination of the aforementioned both loadings. However, the truck loading is relatively complicated since it varied with traffic flow, vehicle types and road roughness as well as the vehicle’s lateral positions. Moreover, there are so many uncertainties in formulating the equivalent truck-loading model. As the counterpart, the Airport Express train has the fixed axle spacing and known axle loadings, and particularly it runs on a fixed schedule of across the bridge every 12 minutes from 05:50 a.m. to 01:15 a.m. everyday. In this sense, the train-loading model is therefore relatively more reliable than the truck-loading model.

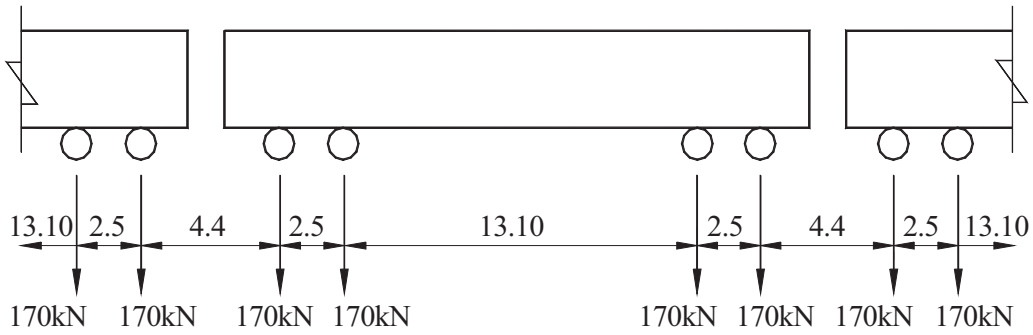

Figure 5.16 Schematic configuration of train model (in m)

The accurate train-bridge model is constructed by Xia *et al*. (2000) to investigate the dynamic interaction between the train and long-span suspension bridge. Their results suggest that the dynamic interaction between them is insignificant so that the running train could be simply simulated as moving loads without considering the interaction. When the speed of the moving load is slow, the crawling speed load could be considered as static load and the corresponding response could be taken as the influence line of the response.

A typical train model (Xia *et al*. 2000), as shown in Figure 5.16, is used to simulate the actual MTR train running on the TMB with approximate 170KN each axle loading and 10 cars full of passengers while the train is fully loaded.

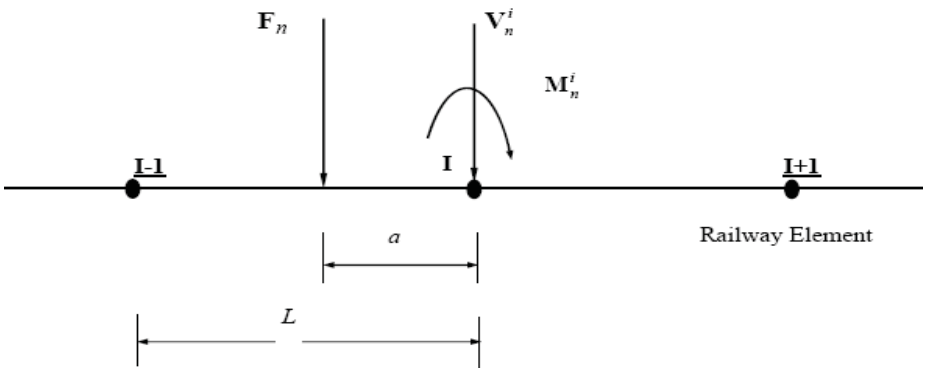

Figure 5.17 Schematic illustration of railway living loading and nodal forces

Considering a random ith node in railway elements (I-1, I) and (I, I+1), the nodal force V_n^i and moment M_n^i caused by nth live axle load F_n (as shown in Figure 5.17), is a function of ith node space location X_i and the axle load F_n local position ξ:

$$\mathbf{V}_n^i = \mathbf{V}_n^i(\xi_n, \mathbf{x_i}), \quad \mathbf{M}_n^i = \mathbf{M}_n^i(\xi_n, \mathbf{x_i}) \qquad (-1 \le \xi_n \le 1) \tag{5.22}$$

where $\xi_n = \pm a / L$, L is the longitudinal dimension of a railway element, and a is the distance between F_n position and *i*th node along train running direction. When $|\xi_n| \ge 1$, the nth axle force F_n is out of the elements (I-1, I) and (I, I+1), and will not affect the *i*th nodal forces.

In thinking of axle load F_n as a live load, its position varies with time t and the train speed V_0:

$$\xi_n = \xi_n(t, V_0) \tag{5.23}$$

While a train is running on the bridge, the nodal forces at *i*th node are the total equivalent forces caused by all axle forces of a train, i.e.:

$$\begin{aligned} \mathbf{V}^i &= \sum \mathbf{V}_n^i(F_n, V_{0,} t) \\ \mathbf{M}^i &= \sum \mathbf{M}_n^i(F_n, V_{0,} t) \end{aligned} \tag{5.24}$$

Once the axle loading and train constant speed is determined, the equivalent force and equivalent moment could be then computed in terms of time histories and applied on the nodes of train track elements as the simulation of real train loading.

5.4.3 On Static Responses

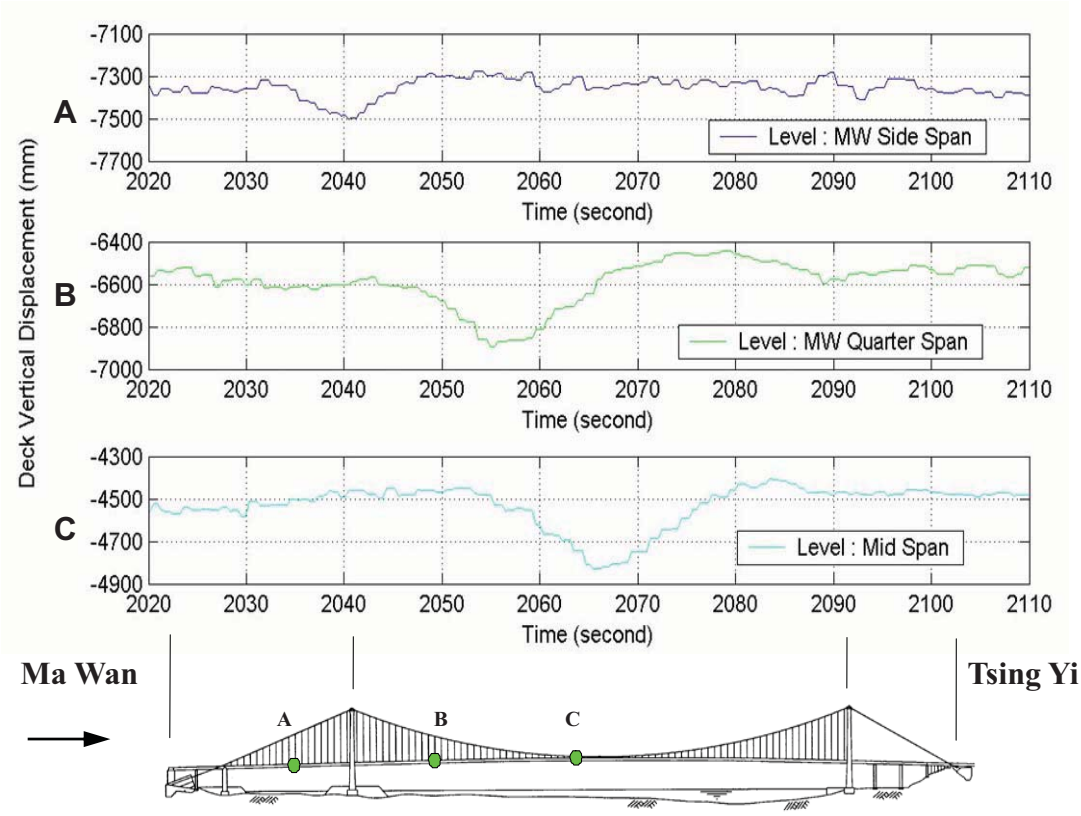

Figure 5.18 Selected vertical displacement influence line in Tsing Ma bridge deck (North Edge) (Guo 2005)

Apart from the dynamic characteristics with respect to natural frequencies, the developed macro model should be further verified with respect to static and dynamic responses. The data of vertical displacement influence line at the locations of A, B and C (see in Figure 5.18) where GPS level stations are installed in the bridge deck is collected from the field test performed under a typical train loading by Guo (2005). As for the numerical analysis, the simulated train loading has been properly calculated by aforementioned introduced method and then applied to the global model to obtain the responses at those sensor-installed locations. There are relatively large differences between the measurement data

and predicted ones as shown in Figure 5.19.

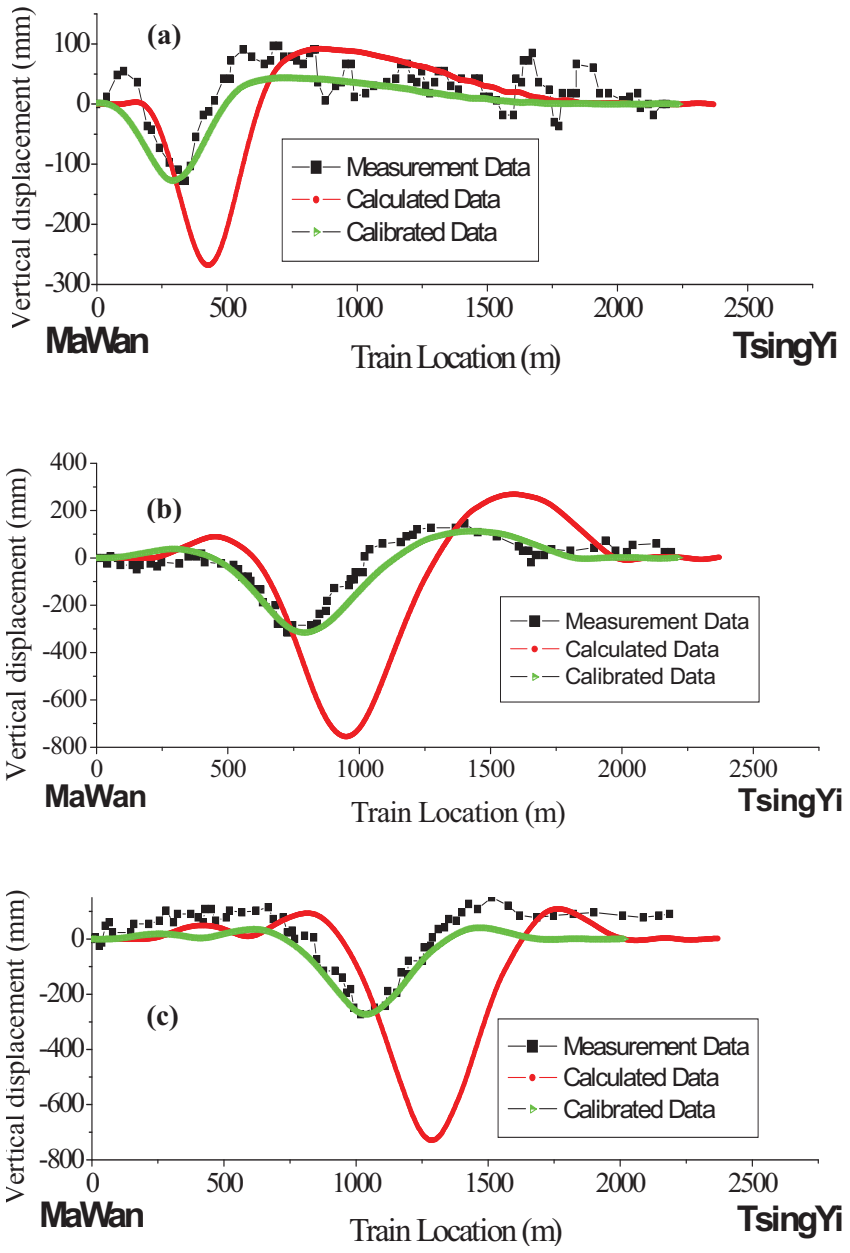

Figure 5.19 Comparison of calibrated values with calculation and measurement at GPS locations corresponds to: (a) location A; (b) location B; (c) location C

The large discrepancies could be mainly due to three reasons as follows:

(1) Amplitude of train loading. The simulated typical train loading is estimated

on the basis of the situation of full loading that is larger than the real experimental value, which results in the larger vertical displacement.

(2) The possible time-shift. During the simulation analysis, the time zero is assumed when the train begins to pass through the bridge. However, the selected measurement data is just a segment of the whole time-history record without clearly knowing when the starting time is.

(3) The X-axis scale. The standard train is assumed to be traveling across the bridge at a constant speed of 30 m/s while in practice it may not be so. The differences of train speed between the simulation and real train result in the different scales along the X-axis.

In order to compare the calculated values at these locations with the measurement data with respect to the vertical influence line, three factors considering each of the above mentioned three reasons are calculated for attempting to tune the factored values to fit the configuration of measurement data as the dash triangular line in Figure 5.19(a) that corresponds to GPS location A. Once the three factors are determined, the coefficients are then multiplied to all three cases and the original calculated data is calibrated as shown in Figure 5.19 (b) and (c). It can be easily seen that all the calibrated data are now in better agreement with the measurement than the original prediction values, indicating that the developed macro model is reliable and accurate in static response analysis of bridge (Chan *et al*. 2007).

5.4.4 On Dynamic Responses

Furthermore, besides the validation with respect to the dynamic characteristics, the developed global model also needs to be validated at aspects of dynamic responses for the purpose of subsequent fatigue analysis emphasizing on structural dynamic behavior.

The question that is turned to transient linear dynamic response under the moving load could be solved by applying modal superposition method. The effective modal mass is a modal dynamic property associated with the modal characteristics, and it is also a measure to classify the importance of a mode shape when a structure is excited by enforced acceleration. Effective modal mass has been used successfully in determining the necessary number of vibration modes required in Response Spectrum Method (RSM) for high-rise buildings. When the total effective modal mass exceeds 90 percent of the total mass of the structure, the accuracy of RSM can be ensured for high-rise buildings, while here all modes with effective modal masses greater than 5% of the total mass are taken into account. In this case, first 80 order modes are then selected to meet the requirements of the effective modal masses and the modal damping is adopted as 0.5%. The linear bridge response under the simulated train loading could be eventually calculated.

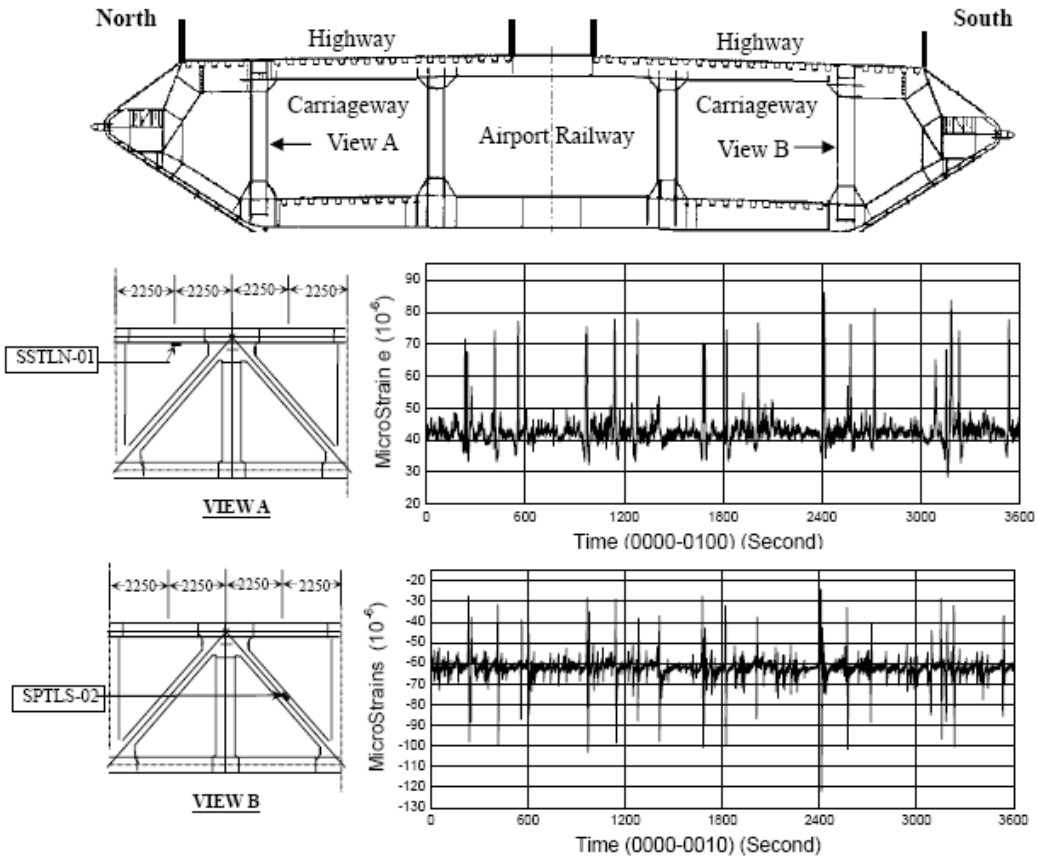

Figure 5.20 Typical locations of strain gauges in bridge deck and corresponding one-hour strain-time history

The comparison of the computed results with monitoring data with respect to the dynamic responses should be performed to validate the developed finite element. The verification method has been proposed by Chan *et al*. (2003).

The online monitoring data have been collected from the strain gauges of WASHMS permanently installed in the bridge. Typical cross-sections of bridge deck of Chainage (CH) 24662.5 (as shown in Figure 5.5), which is adjacent to the three-fourth main-span of Tsing Yi Tower, is selected since these stain-gauges installed locations are assumed to be the most vulnerable zones (comparatively speaking) for the fatigue damage during the design stage. In addition, the fatigue

critical locations are also identified as the outmost part of the upper chord on bridge deck by applying the simulated train loading and traffic loading on the aforementioned developed TMB FE model separately for the simulation calculation. In this sense, the longitudinal truss has been considered as the most critical parts along the bridge and two typical strain gauges at the both sides of bridge deck section are shown in Figure 5.20. The strain gauges “SSTLN-01” locates on the top chord of the north outer longitudinal truss while “SPTLS-02” on the left diagonal bracing of the south outer longitudinal truss.

As mentioned before, the measured strain-time data should be the bridge dynamic response under both the train loading and highway loadings. However, the computed results are only obtained under the circumstances of simulated train loadings and it is not easy to separate the train responses from those under the loading combination. Therefore, the monitoring data should be extracted and calibrated in some way accordingly and some simplifications be made for the purpose of comparison of calculation values and measurement ones on the basis of following issues.

The monitoring data during the period of midnight from 12:00p.m to 1:00 am of Nov.3, 1999 of two above strain gauges have been selected and plotted in Figure 5.20. At this period of time, the running cars and trucks in the bridge are in small amount in comparison with the numbers in whole day while the railway is still on service regularly.

Moreover, the previous study indicates that the dynamic response induced by highway loading is relatively smaller than those by train loading. Based on the above two factors, the one-hour strain-time history at the specific time could be assumed as the monitoring data under the mere train loading and represent the characteristics of dynamic responses of the bridge.

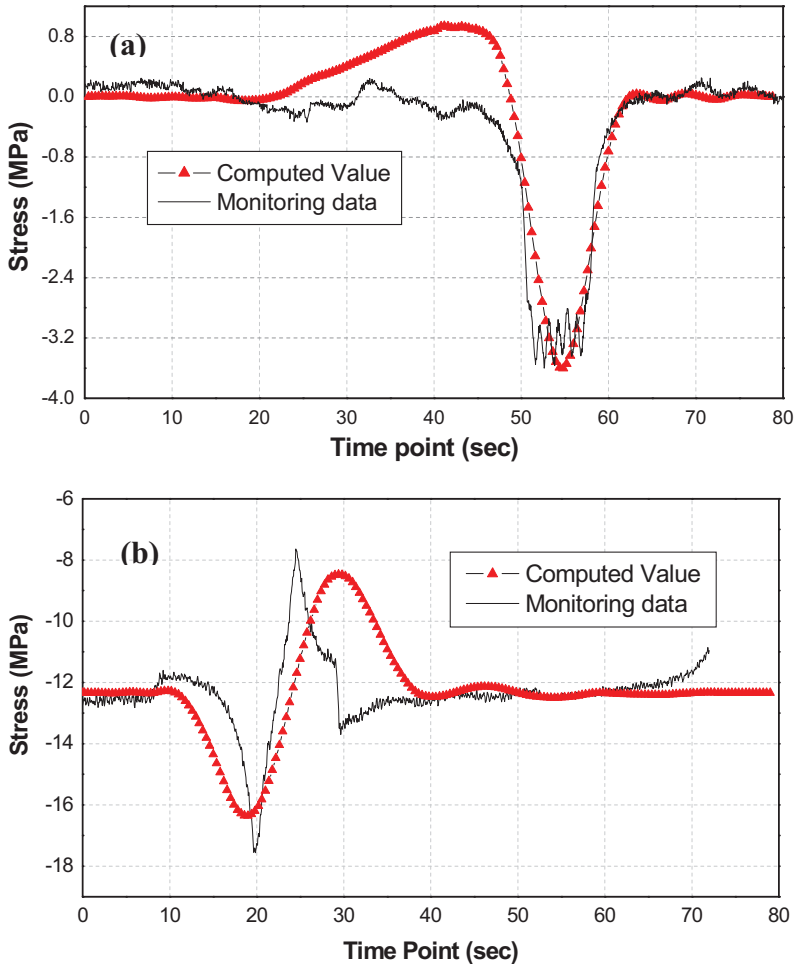

Figure 5.21 Dynamic response comparison of computed values with monitoring data at sensor-installed locations: (a) SSTLN01; (b) SPTLS02

Some features of the selected strain history curve could be studied by observing the plotted figures. The strain-time history curve in one hour can be considered to be composed of many small pulses of strain and higher pulses at the rate of

approximately one high pulse per three minutes. Each high pulse in term of sudden change of strain-time curve corresponds to the passage of one train. The small pulses are mainly caused by the environmental factors such as wind, temperature and etc., which is significantly less than those induced by train loading in amplitude.

As shown in Figure 5.21, only dynamic responses in term of one stress cycle within the train passage that are extracted from the monitoring data of aforementioned two strain gauges installed locations are used to be compared with the corresponding computed values. For the purpose of implementation of comparison, the recorded original strain data should be processed by transferring to stress and also calibrated for comparison with the computed values, for instance, the selected stress curve should be moved to locate at the same time as the computed data, and the measured stress value ought to be equal to the computed ones at zero time point. The stress values are easily obtained by using Hook's Law of taking Young's modulus as 200GPa with the assumption that all the dynamic responses behave merely in linear manner. The X-axis is the time period that the standard train passes through the whole bridge with the constant speed of 30m/s.

The comparison indicates that the computed values are relatively in good agreement with the monitoring data in some extent. The possible reasons maybe responsible for the discrepancies are listed as follows:

(1) The curve of computed value is ideally smooth and just a stress cycle within the passage of a train. However, with the measured data, it is relatively rough consisting of a main stress block cycle with some small cycles that reflect local dynamic interaction between the running train and bridge structure, especially oscillation and localization effect which is not considered in computation

(2) The assumption has been made that the extracted monitoring data are the real response of bridge under mere train loading while they are the responses under the loading combinations of train, truck and other unpredicted environmental factors.

(3) The train loading is simulated on the basis of the situation of full loading that is considered as the maximum value on computation. The assumption has been made so that the real loading situation is unlikely to be larger than this value, which explains the stress differences between computed values and measured ones.

(4) During the simulation analysis, the time point zero is appointed when the train begins to pass through the bridge. However, the selected measurement data is just a segment of the whole time-history record without clearly knowing when the starting time is.

(5) The train is assumed to be traveling through the bridge at a constant speed of 30 m/s while in real situation it may not be so. The differences

of train speed between the simulation and real train lead to the different scales along the X-axis.

Generally speaking, apart from the possible factors which could lead to those differences between the computed values and measurement data, the developed structural global finite element model of bridge is validated at the aspect of dynamic responses. The same comparison result to verify the global model could be obtained from Chan *et al*. (2003) except for a little difference of fitting extent.

Moreover, from the viewpoint of dynamic characteristics, because the differences between the computed natural frequencies and measured ones mentioned before are mostly smaller than 10% so that finite element modeling error is assumed to be within the allowable engineering error range, and associated with the relatively high MAC value indication of good correlation between computation and measurement, the constructed global finite element model of TMB is regarded as the reliable and effective model which could be used to study the static and dynamic responses on the global length scale level under various loading situations and no need for the further model updating process in this study.

5.5 LOCAL MICRO-MODEL OF HOT-SPOT AREA

5.5.1 Critical Cross-section and Locations Identification

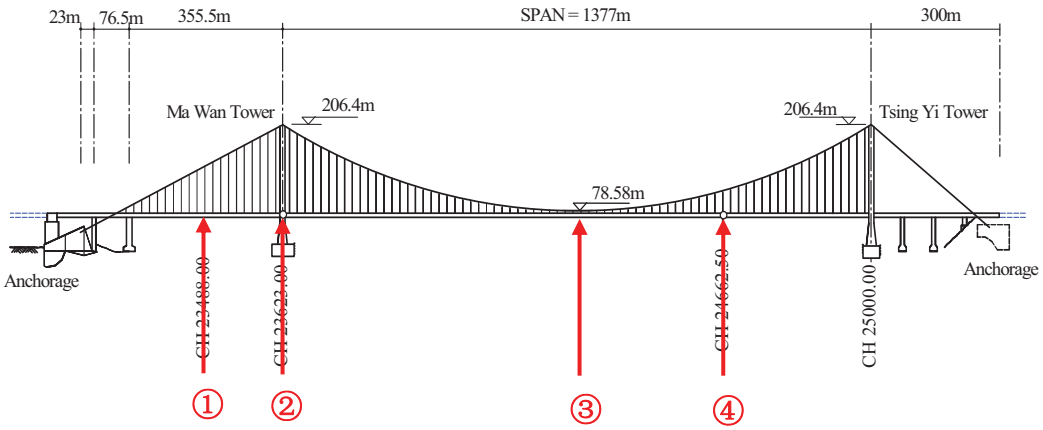

Figure 5.22 Selected critical cross-sections under investigation along the bridge

During the design stage and following verification process of the long-span suspension bridge, we usually concern about the control parameters such as the mid-span deflection, maximum internal forces in control cross-section, horizontal displacement on the top of tower, maximum tension forces in main cable and etc. The typical cross-sections of the decking system are investigated to determine the critical fatigue locations, as shown in Figure 5.22, the four critical investigated cross-sections are selected as ① approximate middle of MW side-span (CH23460), ② MW tower (CH23623), ③ Mid-span, ④ approximate quarter of main-span (CH24662.5), in which the strain gauges are designed to be permanently installed in these fatigue vulnerable cross-sections.

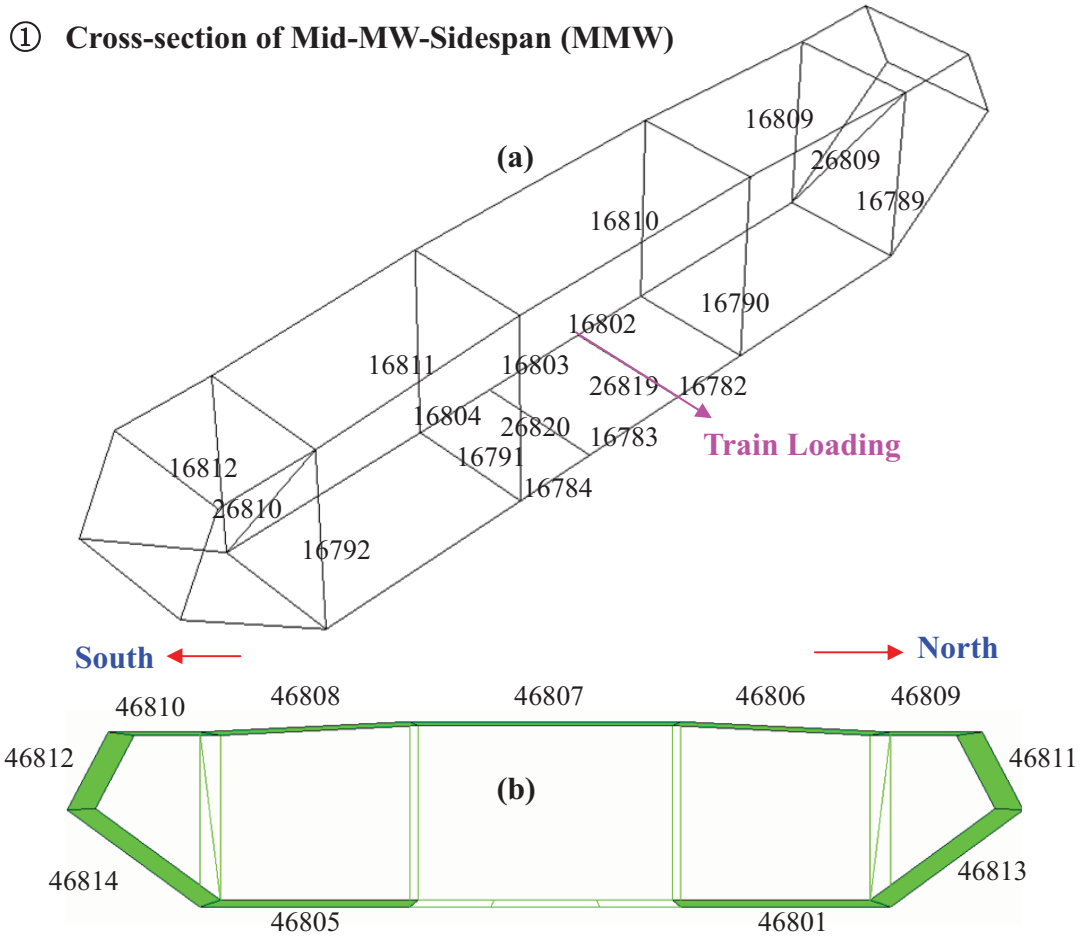

Figure 5.23 Element numberings at MMW cross-section (a) beam elements numbering; (b) shell and membrane elements numbering

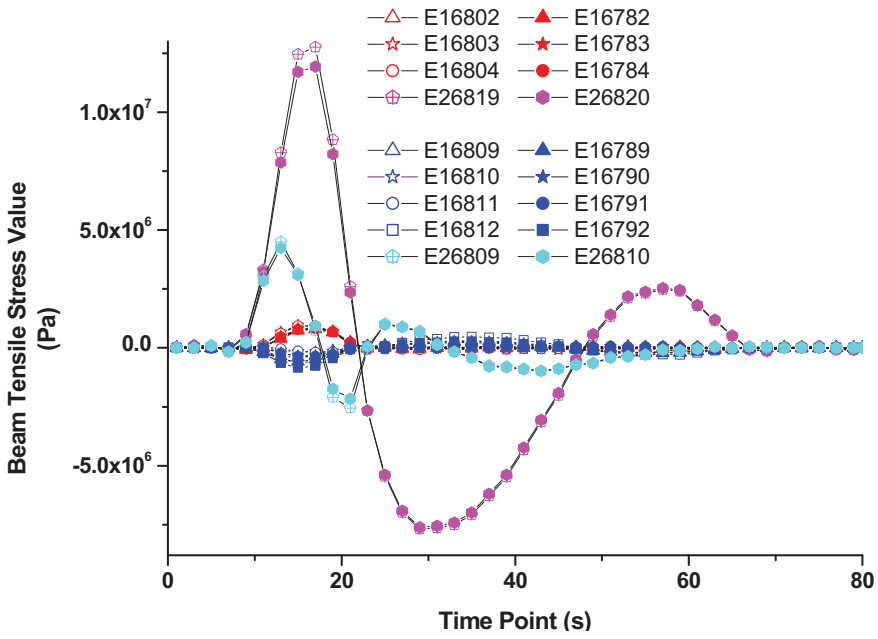

Figure 5.24 Tensile stress-time history of beam elements at MMW under the specific train loading

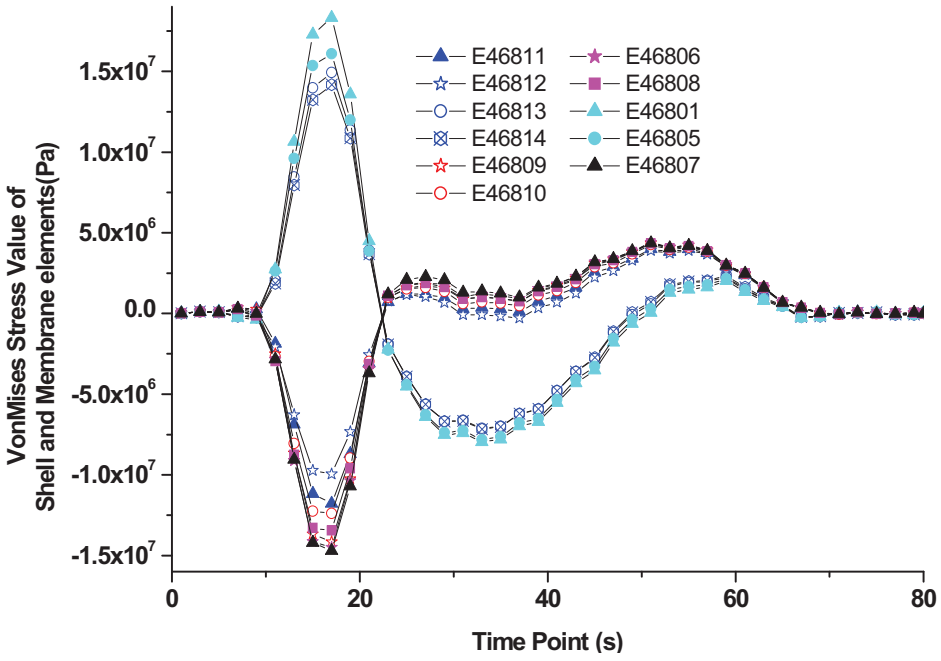

Figure 5.25 Von-Mises stress-time history of shell and membrane elements at MMW under the specific train loading

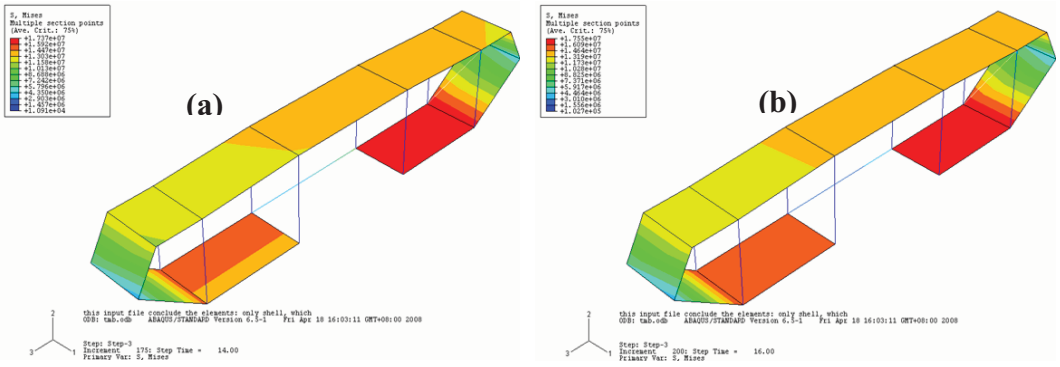

Figure 5.26 Contour plot of shell and membrane elements at MMW at the time points of (a) t=14s; (b) t=16s

② **Cross-section of MW Tower (MWT)**

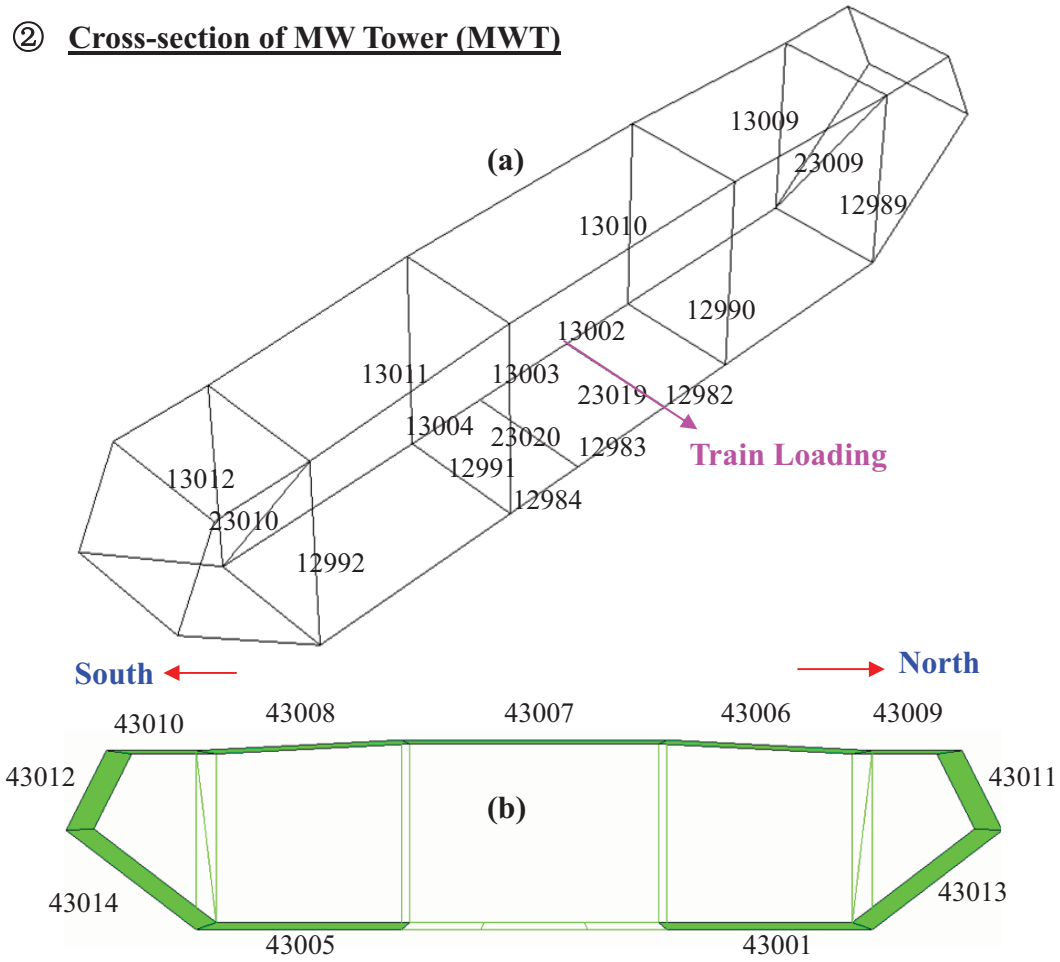

Figure 5.27 Element numberings at MWT cross-section (a) beam elements numbering; (b) shell and membrane elements numbering

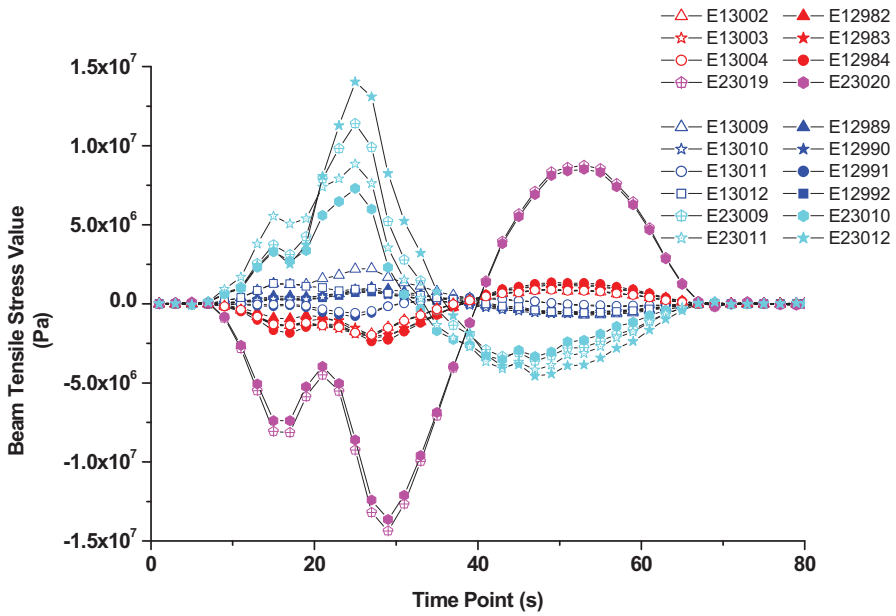

Figure 5.28 Tensile stress-time history of beam elements at MWT under the specific train loading

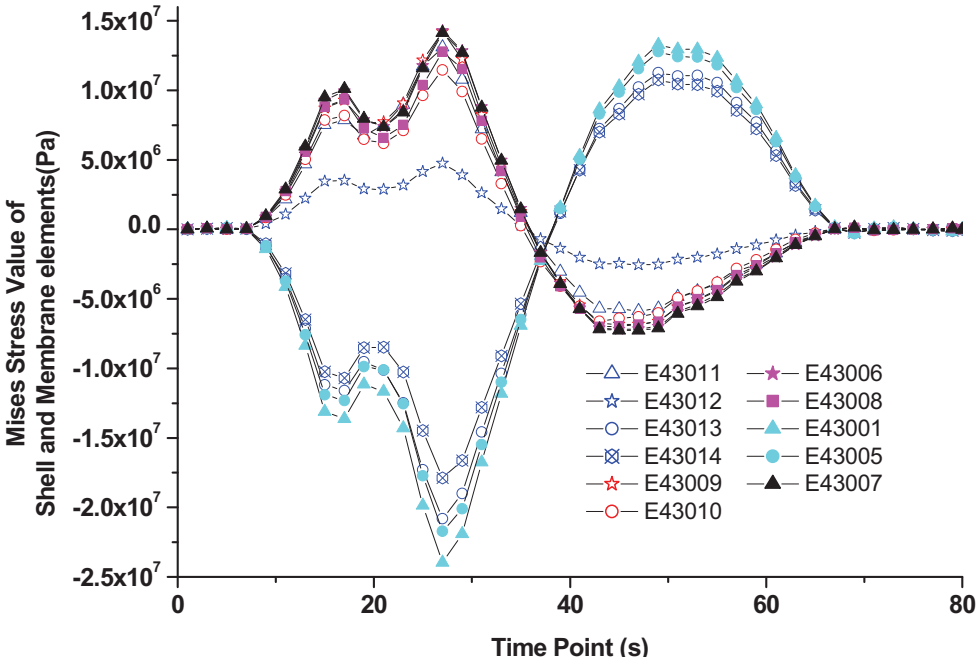

Figure 5.29 Von-Mises stress-time history of shell and membrane elements at MWT under the specific train loading

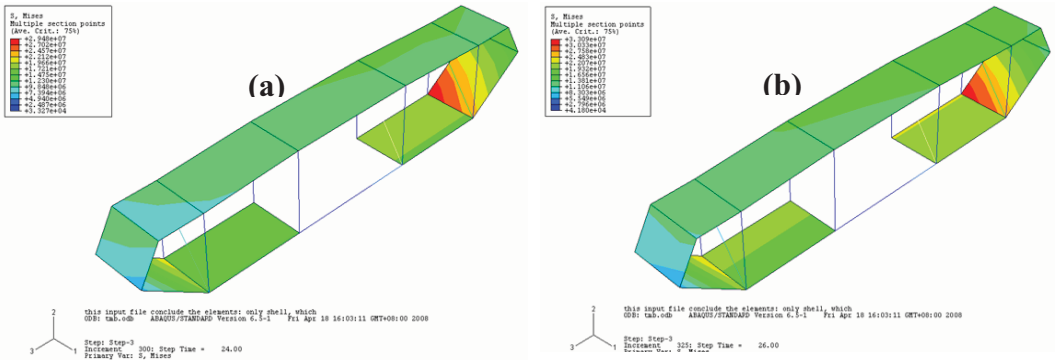

Figure 5.30 Contour plot of shell and membrane elements at MWT at the time points of (a) t=24s; (b) t=26s

③ **Cross-section of Mid-span (MS)**

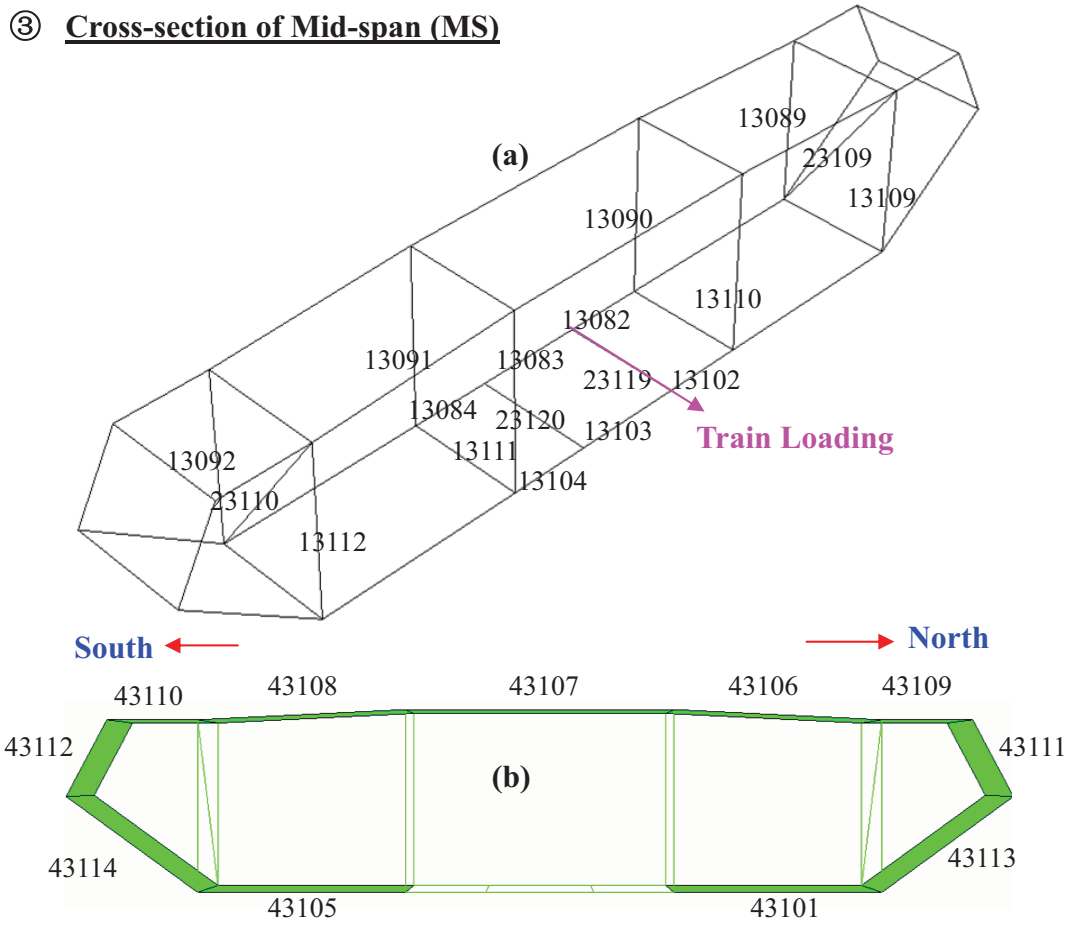

Figure 5.31 Element numberings at MS Cross-section (a) beam elements numbering; (b) shell and membrane elements numbering

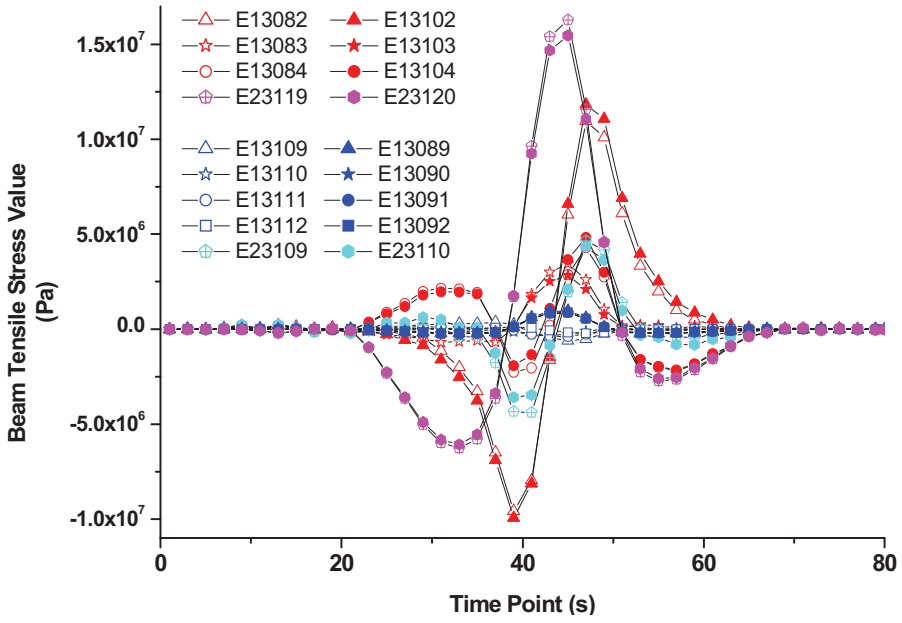

Figure 5.32 Tensile stress-time history of beam elements at MS under the specific train loading

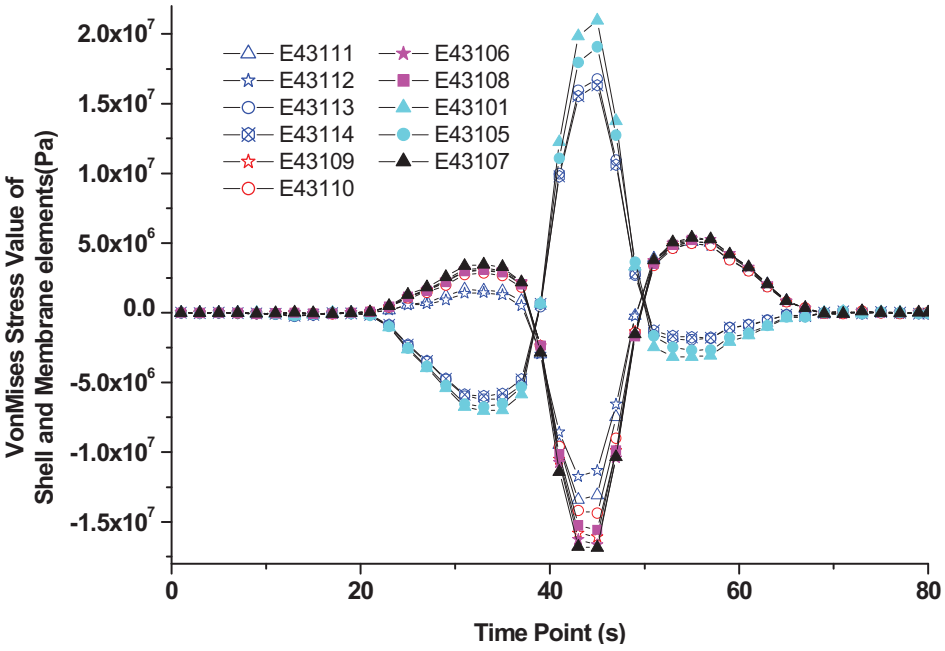

Figure 5.33 Von-Mises stress-time history of shell and membrane elements at MS under the specific train loading

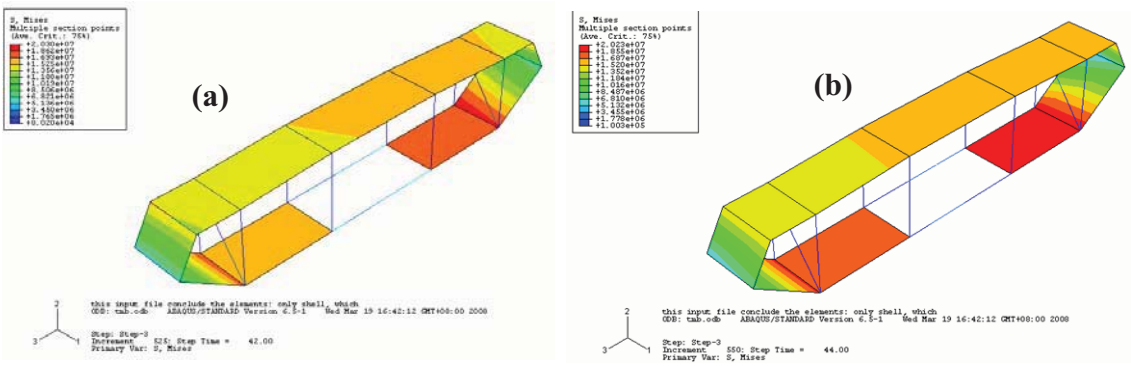

Figure 5.34 Contour plot of shell and membrane elements at MS at the time points of (a) t=24s; (b) t=26s

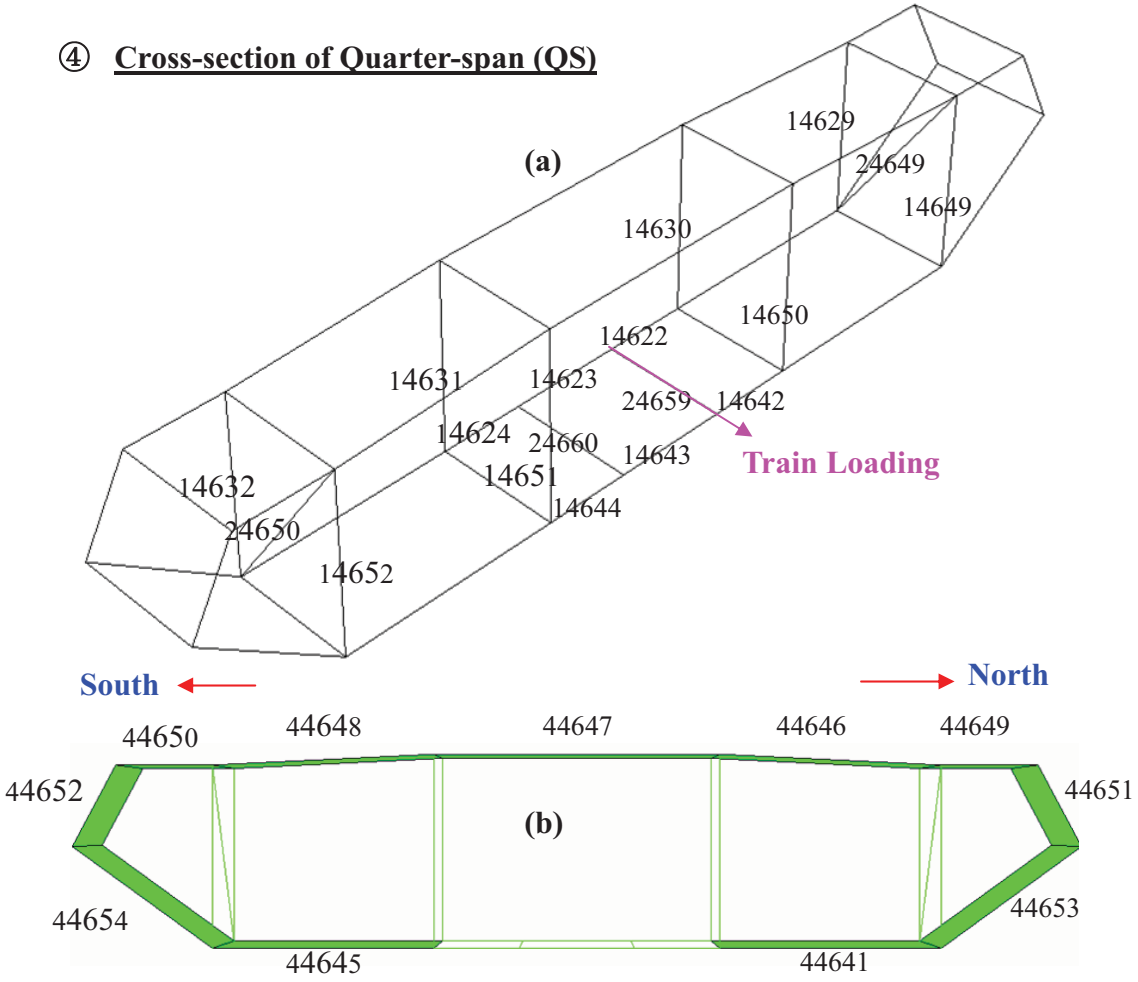

Figure 5.35 Element numberings at QS Cross-section (a) beam elements numbering; (b) shell and membrane elements numbering

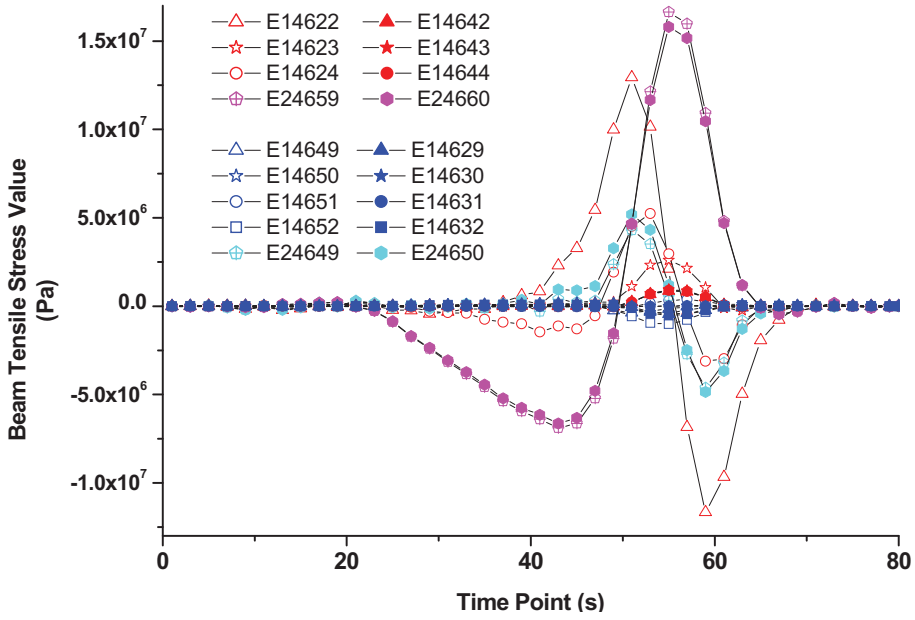

Figure 5.36 Tensile stress-time history of beam elements at QS under the specific train loading

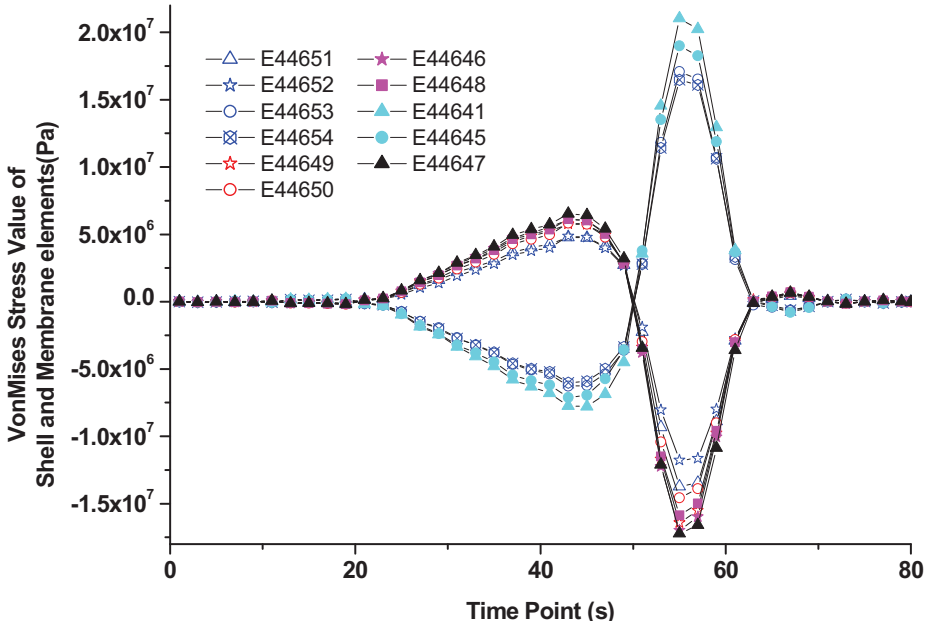

Figure 5.37 Von-Mises stress-time history of shell and membrane elements at QS under the specific train loading

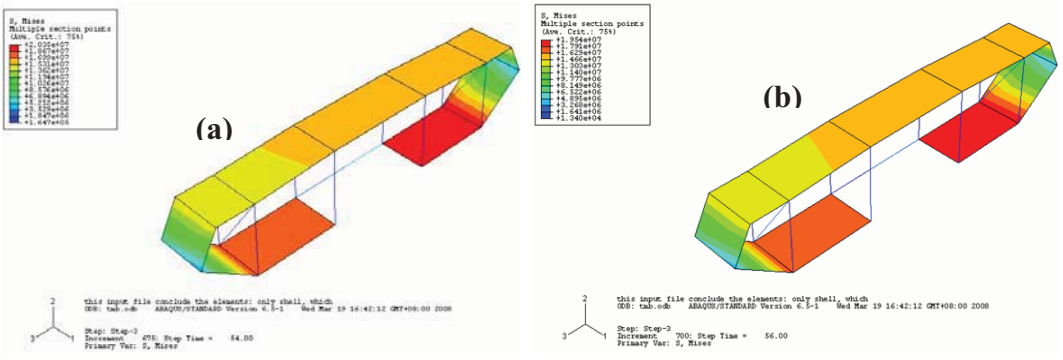

Figure 5.38 Contour plot of shell and membrane elements at QS at the time points of (a) t=24s; (b) t=26s

Since all the simulation analyses are carried out under the circumstance of subjected to specific train loading, the aforementioned developed train loading is chosen as the simulated loading case and then applied on the train track of the north side with traveling from Ma Wan Tower to Tsing Yi Tower as shown in Figure 5.23(a), Figure 5.27(a), Figure 5.31(a) and Figure 5.35(a). The four selected fatigue vulnerable cross-sections are assumed to be critical under the

loading case of typical train passage. Then the responses of four selected critical cross-sections under the simulated train loading is then obtained and the corresponding stress-time history of beam, shell and membrane elements within the period of train passing through the bridge are plotted as shown from Figure 5.23 to Figure 5.38, and some findings can be stated as follows:

(1) The duration of a train passing through the whole bridge is about 80 seconds at the simulated constant speed of 30 m/s. The members at critical cross-sections of MMW and MWT are only affected at the time period from 9 to 65 seconds while ones of MS and QS from 21 to 65 seconds.

(2) The time point of maximum stress value occurring at the certain cross-section is almost equal to the time point when the train arriving at that location.

(3) The locations of the largest stress values locations of shell and membrane elements are at the outmost part of bottom side while the big ones of beam elements are adjacent to the train loading applying position or diagonal post in outmost longitudinal truss. The critical location of the selected cross-section subjected to simulated train loading is then determined as the shell element at outmost part of bottom side.

(4) Apart from the localization effect of train loading, it could be seen within the steel girder that the intermediate vertical posts is of small stress value while the components of longitudinal truss standing at the outer-side of steel girder are of relatively larger values, especially the diagonal chord would draw more

attentions.

(5) Since the simulated train loading is directly applied on the north side train track, the stress values of elements adjacent to those locations are distinctly higher than those of other locations, which indicated the phenomenon of localization effect. Moreover, the membrane element stress values of bottom side are larger than ones of top side inside steel girder cross-section. Also the feature of asymmetry is noticed that the stress result of the elements at north side is bigger than those at south side because of the asymmetric train loadings.

5.5.2 Local Detailed Model

Other than the standard train loading, the computed bridge response under the single lane, double lane and triple lane truck loading are also studied by Chan *et al*. (2003). The result suggests that the stress distribution in typical deck has the same distribution trend, where the largest value of stress is near the outmost part of the upper chord and the bottom cross-frame between the rail tracks. The critical locations due to fatigue damage are then identified as at the outmost part of upper chord and the bottom cross-frame between the rail tracks, which agrees well with the result obtained from the aforementioned critical cross-section identification.

No loss of generality, the CH24662.5 is chosen as the critical cross-section, the near quarter-span cross-section close to Tsing Yi side as shown in Figure 5.5. As for along the longitudinal direction, the outmost part is represented by the

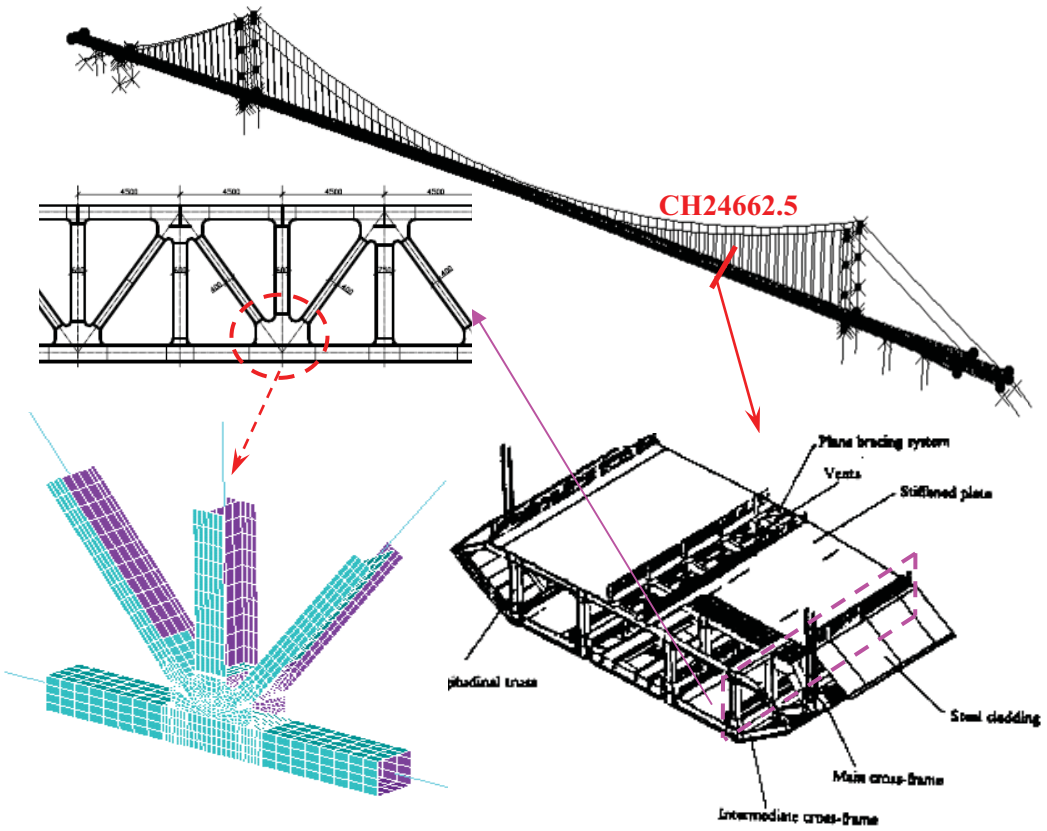

Figure 5.39 Local detailed model of welded connection of longitudinal truss

longitudinal steel truss. Since the welded regions are vulnerable to fatigue damage, an efficient FE model for fatigue analysis should be used to output the real stress values at these locations. The local detailed model is then proposed to calculate the hot-spot stress in the welded region for fatigue damage and the subsequent remaining fatigue life analysis. There are several kinds of welding connections in decking system of TMB. As shown in Figure 5.39, the local detailed model is chosen at the bottom intersection of the longitudinal beam and vertical post with the connection of fillet welds to investigate a typical welded region for multi-scale modeling strategy. Around the local detailed welding region, the fine-mesh shell

elements are adopted while the beam elements connected with global structural model at the distant end. At the interface between those two kinds of elements, the developed multi-scale modeling strategy and corresponding procedure could be then applied. Moreover, the higher dimensional shell element could be further utilized to express the real configuration of the actual structure and considering the deteriorating process by simulating the damage-related structural mechanical behavior during the analyzing procedure.

5.6 CONCURRENT MULTI-SCALE MODEL DEVELOPMENT

As mentioned before, in order to perform the nonlinear analyses on instantaneous response of materials in the vicinity of local details as well as on structural behavior due to local damage, model shift between the local material model of critical details and the components as well as global models is necessary. Alternatively, the multi-scale model strategy is proposed by integrating different levels of structural elements to meet the needs of various research purposes. In this study, the structural components represented by structural elements at the global level are involved in the multi-scale modeling process. As the counterparts, the critical components and local details are considered as necessary for accurately evaluating the possible damage in material level. Therefore, apart from the global model developed in the previous steps, the critical components and local details should be also further identified by structural analyzing procedure.

5.6.1 Multi-scale Modeling

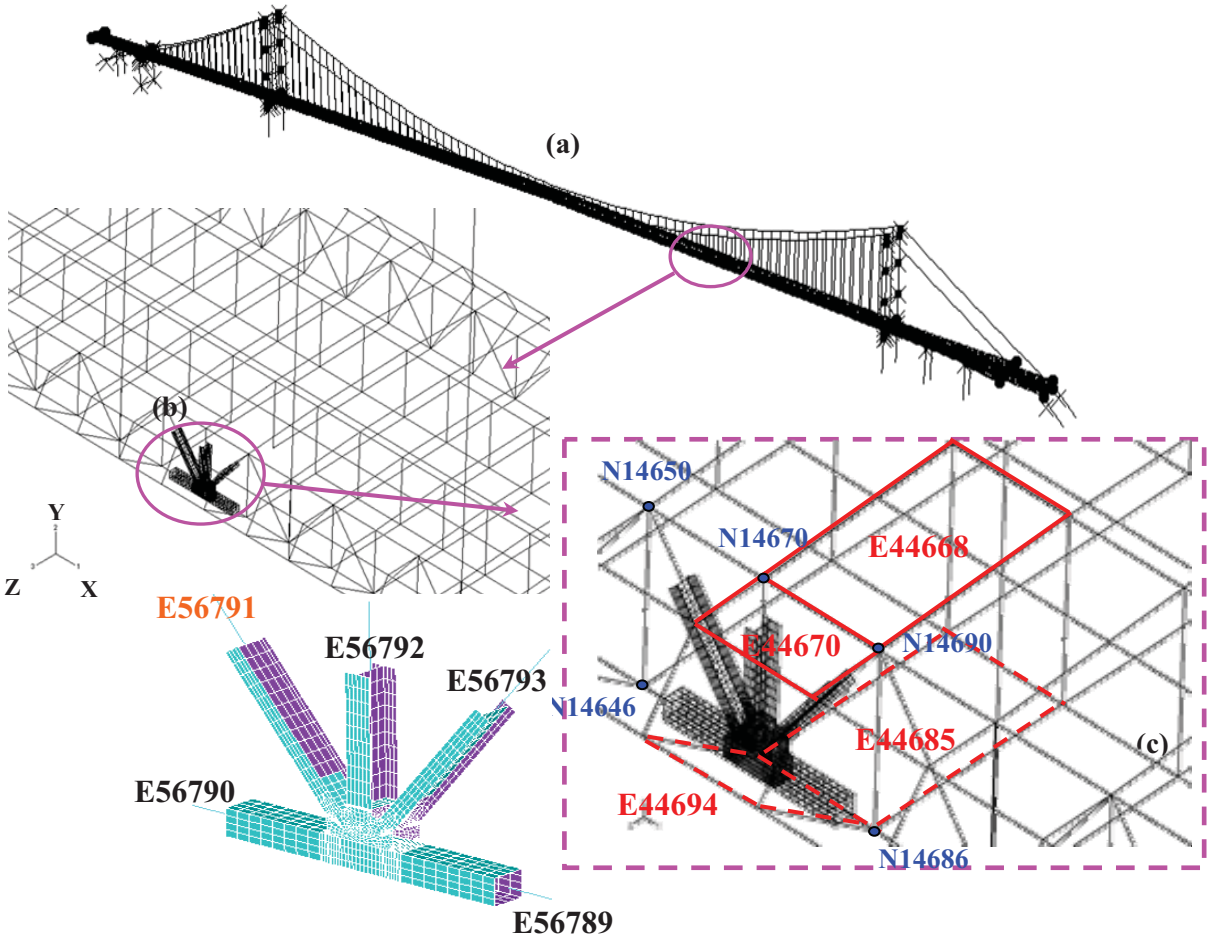

Figure 5.40 Multi-scale model of TMB: (a) conventional model with beam and shell elements; (b) multi-scale model; (c) local detailed model

On the basis of the above developed TMB global model, the concerned details of joints should be considered and merged into the global model to construct the multi-scale model. In the global model (Figure 5.40(a)), the component is modeled as space beam element while the shell element would be required to simulate the joint details for the deteriorating process. There are six standard elements identified and modeled in the typical longitudinal truss section of TMB and the joints are repeated along the longitudinal direction of the bridge. Based on the mixed dimensional method by constraint equations and substructuring

technique, any concerned detailed joint (Figure 5.40(c)), which has been identified as the vulnerable regions to fatigue damage, could be modeled as substructure and incorporated into the global model to obtain the multi-scale model (Figure 5.40(b)). In the concerned local detailed model, the components such as the upper and lower orthotropic steel decks, the pavement structures and the aerodynamic stainless steel sheets have been considered as equivalent simpler models in the global model. It is understood that if these components are not modeled properly, such bridge model would be much more flexible than real structure and the computed results due to train-induced displacements will be larger than that of the measured results. Therefore these components could have to be modeled on the basis of real structure in details if necessary. The multi-scale FE model of TMB is eventually developed and it could be updated using the online monitoring data and field test results. Furthermore, the local damage evolution and its influence on the structural response can be considered and simulated in the modeling. The developed model, as a discrete physical and mathematical representation of the bridge, will be served as a baseline FE model for multi-scale analysis to provide the global structural stress distribution and local damage evaluation accounting for deterioration at critical locations. Meanwhile, within the developed multi-scale model of TMB, different sets of theories are applied to serve various objectives. For example, on the global length scale of meters, mechanics of structures is sufficiently applied to the overall model to obtain internal forces of members of structure. For the purpose of

nominal stress of component at the length scale of centimeters, mechanics of materials and theory of elastic-plasticity are required. In order to obtain the effective stress or hot-spot stress of concern region at the length scale of material point of millimeter or less, mesomechanics and continuum damage mechanics are considered as essential.

5.6.2 Simplified Multi-scale Model Verification

Before applying the multi-scale model for condition assessment, the modal properties of developed model under free vibration and static response would be verified in advance. Meanwhile, the comparison of the computed results with those of original global model and online output data would also be carried out to verify the efficiency and accuracy of the developed multi-scale model.

Dynamic characteristics

The first few free vibration frequencies of developed multi-scale TMB model incorporating one local detailed connection region is analyzed and compared with that by conventional global model. The first two dominant mode shapes at the aspects of lateral, vertical and torsional is tabulated in Table 5.6 in comparison with those computed values by global model and field test results by the Hong Kong Polytechnic University (HK PolyuU) and the Hong Kong Highways Department (HK HyD) (Chan *et al*. 2003). The calculated values are used to compare with the mean experimental values to obtain the maximum relative

Table 5.6 Few free vibration frequencies comparison of TMB original model and multi-scale model

Mode Description	Experimental Results			Calculated Results by FEM				
	HK PolyU	HK HyD	Mean	Original Global Model		Multi-scale Model		Modal Mass Participation Factors
				Value	Difference (%)	Value	Difference (%)	
Lateral								Z-component
First	0.069	0.068	0.0685	0.0683	-0.292	0.0683	-0.292	1.3324
Second	0.164	0.158	0.161	0.160	-0.621	0.160	-0.621	-0.0296
Vertical								Y-component
First	0.113	0.113	0.113	0.116	+2.65	0.116	+2.65	-0.035
Second	0.139	0.138	0.1385	0.143	+3.25	0.143	+3.25	0.989
Torsion								X-rotation
First	0.267	0.244	0.2555	0.255	-0.196	0.255	-0.196	52.2
Second	0.320	0.266	0.293	0.299	-2.05	0.299	-2.05	32.5

difference is 3.25%, which indicates that the frequencies calculated by the multi-scale model agree well with the measured and the analyzed ones. Furthermore, it is easily found that the free vibration frequencies computed by multi-scale model are identical to those by structural global model, which is explained that by theoretically speaking, the local subtle change only influences the local mode shape that usually occurs at high order while it won't change the dynamic characteristics that represents global mode shapes in low order.

Nodal displacements and component nominal stress

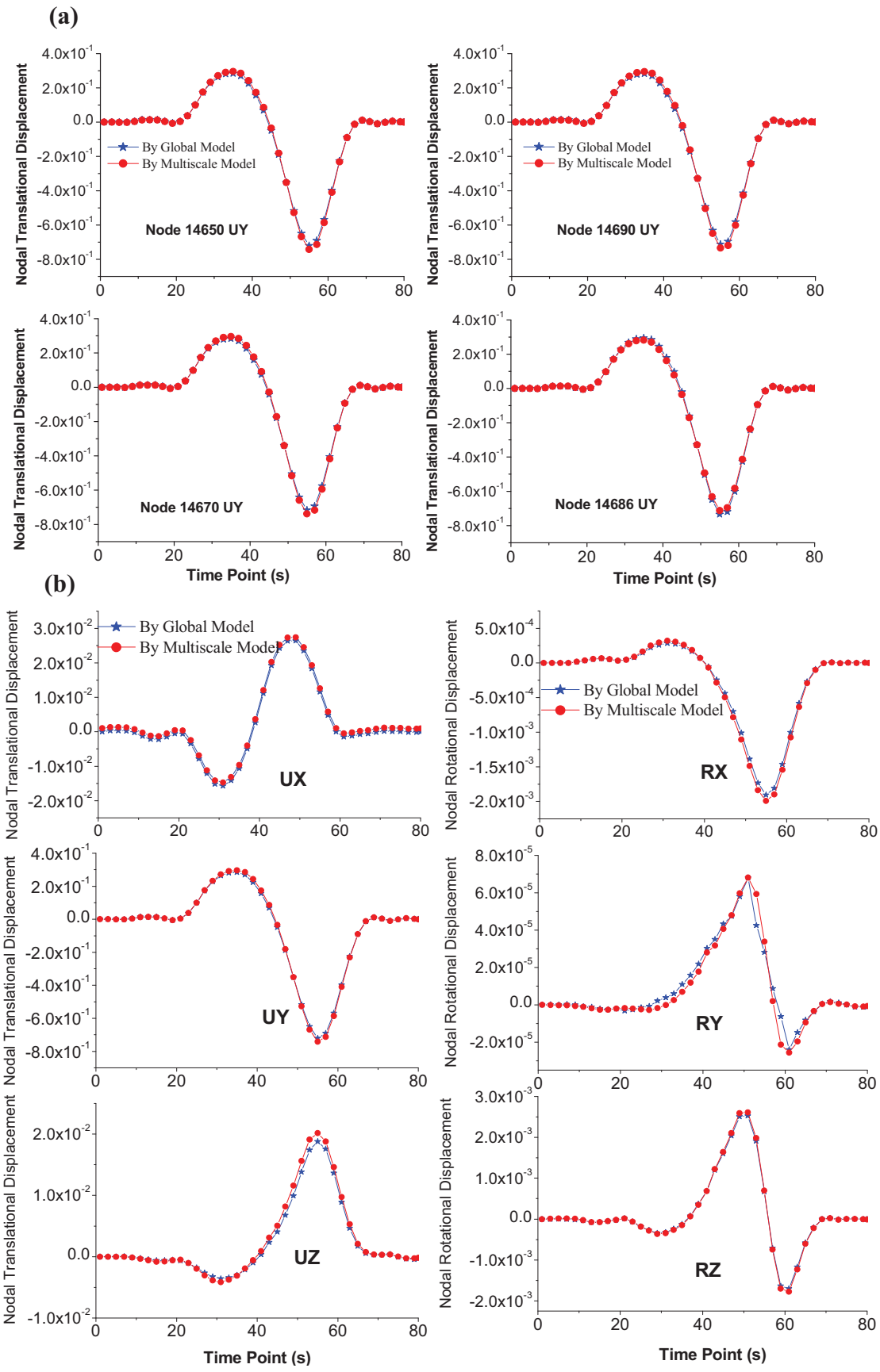

Figure 5.41 Nodal displacement comparison around multi-scale coupling: (a) translational displacement of few adjacent nodes (b) six components of 14690 nodal displacement

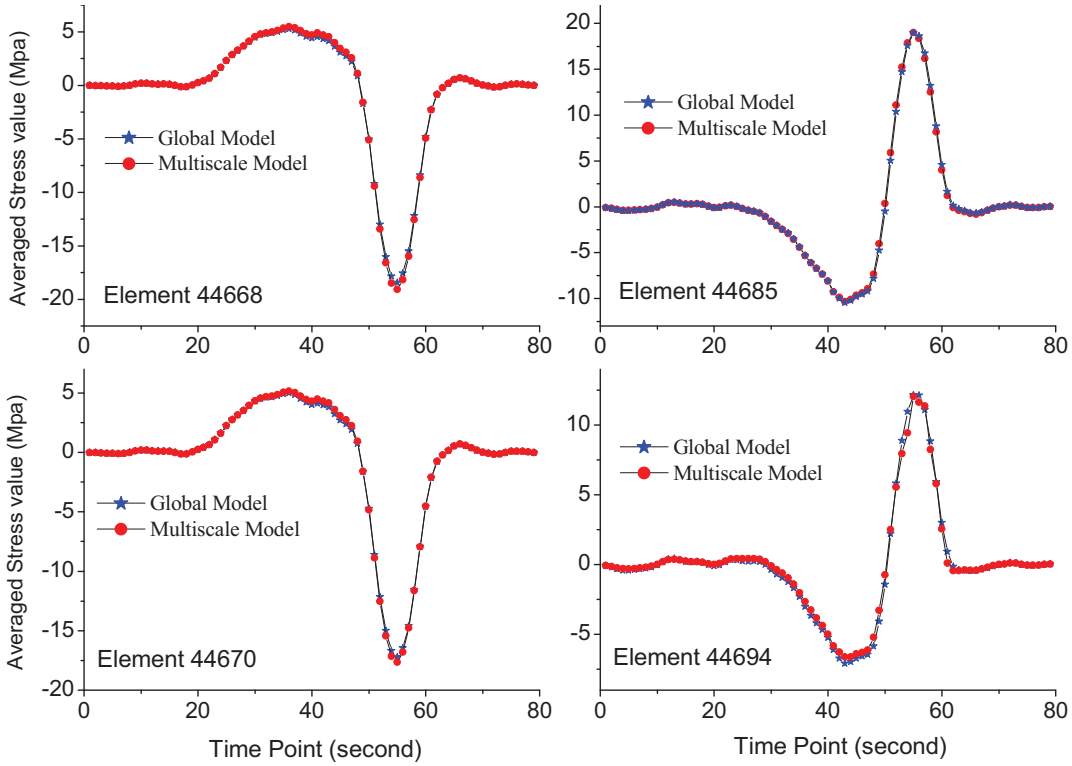

Figure 5.42 Averaged stress value comparison around multi-scale connection interface

The loading case of typical train loading that is simulated on the above assumption moving across the bridge is then applied to the developed multi-scale model and nodal displacements as well as component nominal stresses of the elements around the connecting interface are investigated. The numbering of corresponding nodes and elements are illustrated in Figure 5.40. Several nodal translational displacements along y-axis and six components of specific nodal displacements have been compared by global model with those by multi-scale model in Figure 5.41. It can be easily observed that, at the aspects of dominant vertical translational displacements of few adjacent nodes or selected connection node of 14690, the nodal displacement results by two kind of models are in excellent agreement with each other. The similar conclusion could be drawn on

the basis of following comparison of averaged nominal stress value around the multi-scale connection interface as shown in Figure 5.42.

5.6.3 Comparison of Multi-scale Model with Two-step Analysis

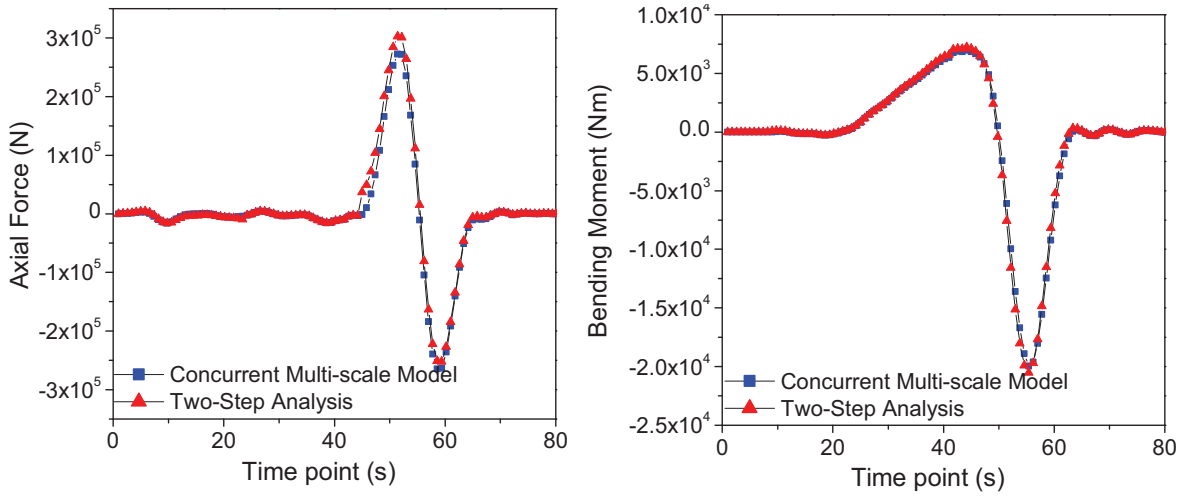

Figure 5.43 Axial force and bending moment comparison of element No. 56791 in multi-scale model with those by corresponding element in global model

In order to investigate the superiority of multi-scale model as compared to the traditional two-step analysis, the loading case of a typical train passing through the bridge has been applied on both the global model and the developed multi-scale model of TMB. As shown in Figure 5.40(b), within the multi-scale model, element No. 56791 is the diagonal post which is built by beam element and it is connected with shell elements using the developed coupling method. The corresponding beam element of that diagonal post is easily located in the global model. Then the axial force and bending moment subjected to the aforementioned loading case of two elements in their respective model has been extracted and compared as shown in Figure 5.43. Theoretically speaking, those values should be

identical because the multi-scale modeling method is developed on the basis of two-step analysis method. Nevertheless, the tiny discrepancies could be found which is definitely due to the modeling differences of the concerned location. Combined with the above facts that nodal displacements and average stress values of elements around the connecting interface in multi-scale model are in good agreement with the ones by global model, it is reasonable to believe that the developed multi-scale model could be used for accurately output the internal force and nominal stress of the components.

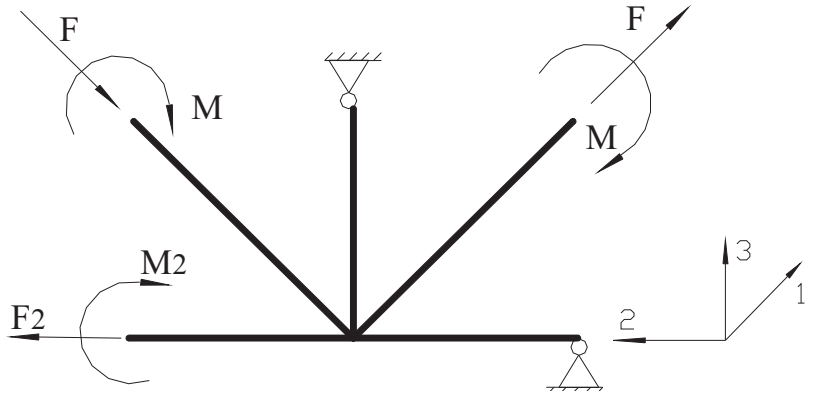

Figure 5.44 Schematic diagrams of boundary conditions around concerned region during extracting from the global analysis result in two-step analysis

However, other than the component nominal stress of the bridge structure, the comparison of hot-spot stress distribution of critical locations by multi-scale model and the two-step analysis are more concerned. As shown in Figure 5.44, the boundary conditions are simulated when extracted from the global structural analysis result in the two-step analysis. In the similar way, the same typical train loading that is moving across the bridge from TY side to MW side is still used as the loading case and three specific time points (as shown in Figure 5.45) have

been selected for hot-spot stress distributions.

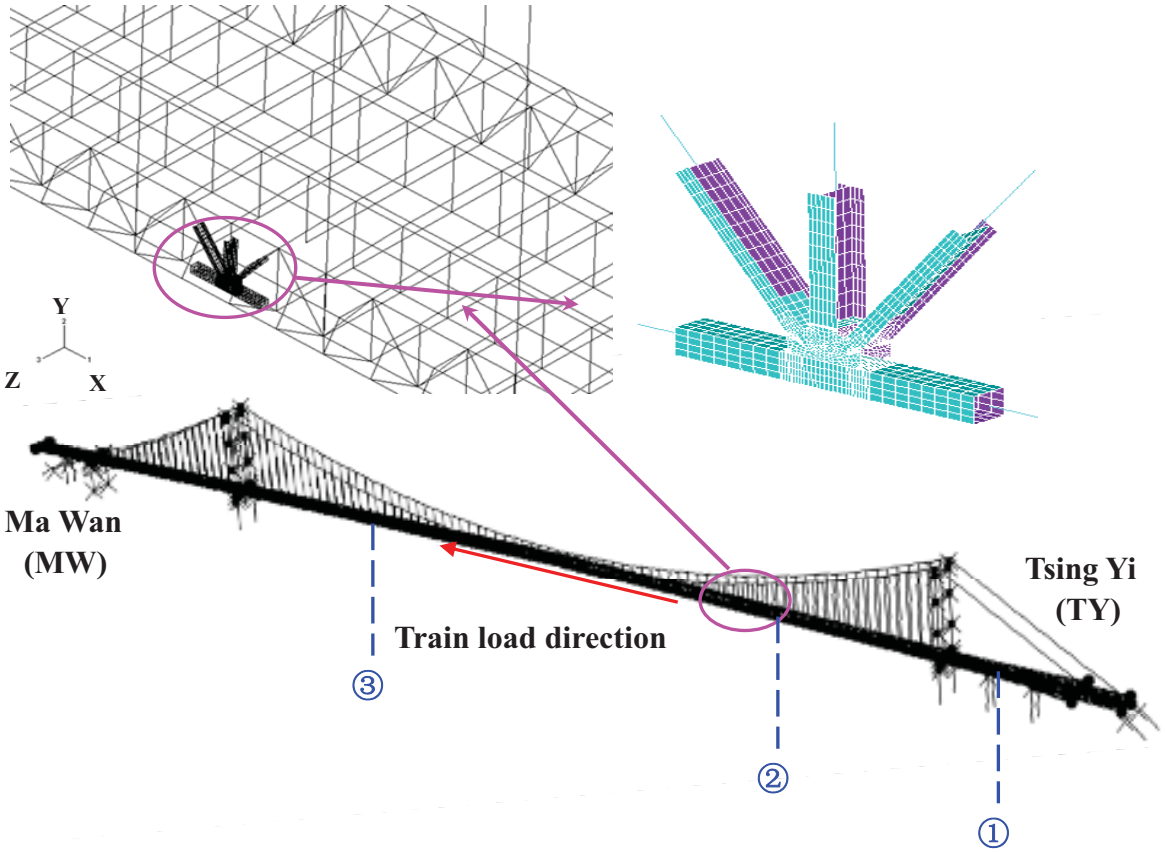

Figure 5.45 Schematic diagrams of selected time points of typical train loading passing through the bridge structure (1) 10s (2) 25s (3) 52s

The duration time of the typical train load passing through the whole bridge is 79 seconds. The critical location on the longitudinal truss section at the quarter span close to TY side has been selected as concerned region and corresponding hot-spot stress contour by multi-scale model and by traditional two-step analysis on selected time points are plotted in Figure 5.46. The small differences between the two methods are most likely to result from imprecise extracting the boundary conditions from the global analysis result in two-step analysis. However, this step of effort could be achieved on the coupling interface with more accuracy and reliability by coupling algorithm.

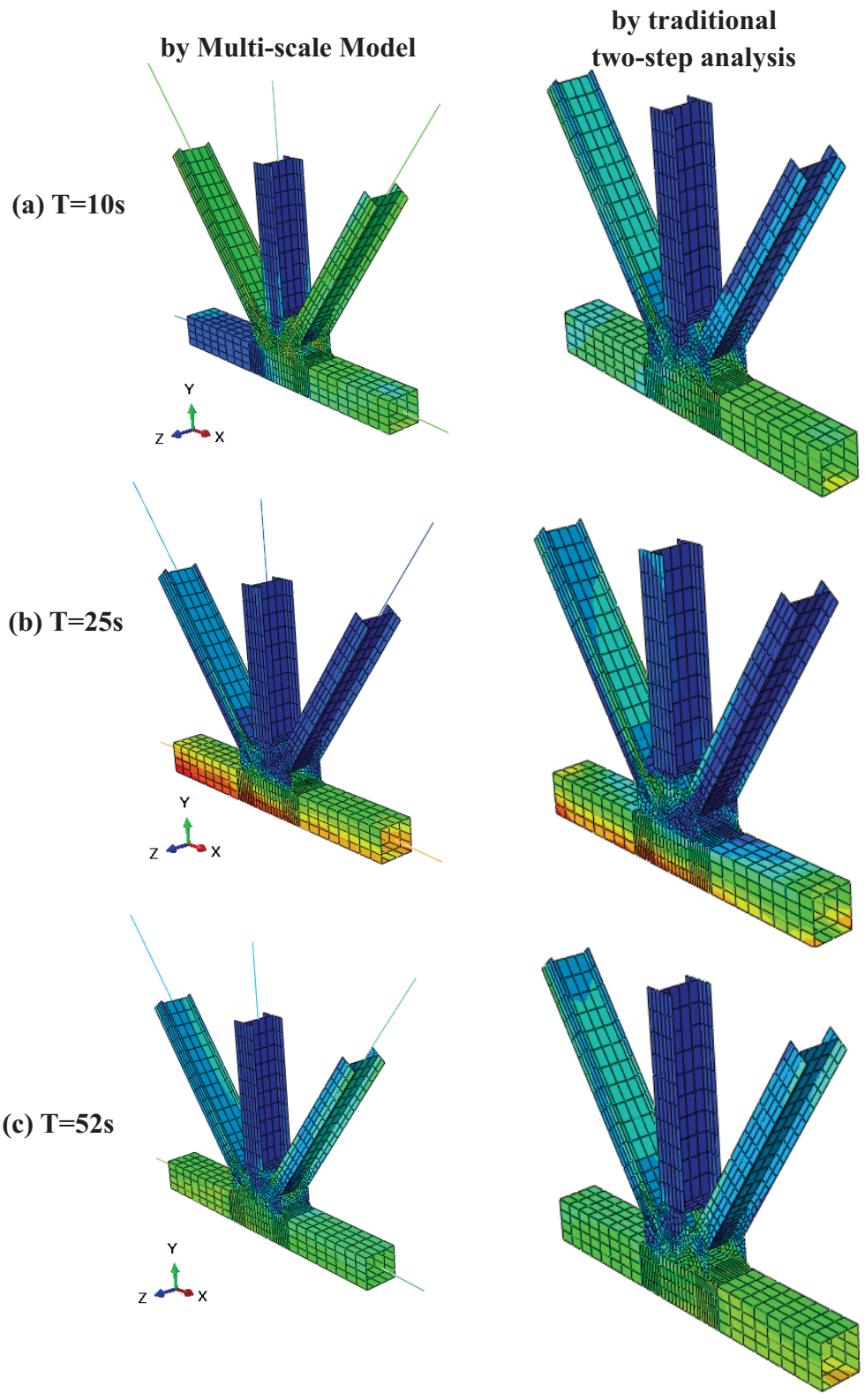

Figure 5.46 Hot-spot stress contour comparison of concerned region by multi-scale model with one by traditional two-step analysis at time points of (a)T=10s; (b)T=25s; (c)T=52s

As compared with two-step analysis method, the advantages of multi-scale modeling method can then be summarized as follows:

(1) As for the internal forces and nominal stress of the component of a structure, the proposed multi-scale model could provide as accurate and reliable results as ones by two-step analysis.

(2) The inherited disadvantages of extracting boundary conditions from global analysis result by two-step analyzing method make the multi-scale model method superior to provide more accurate and reliable results of hot-spot stress values of concerned region.

(3) The multi-scale model could simultaneously output the nominal stress and hot-spot stress distribution while either of those values are only obtained separately in each step in two-step analysis process.

(4) With respect to computing efficiency, it would take almost the same period of time to build the multi-scale model as constructing global and local models involved in two-step analysis. However, the developed multi-scale model can then be used for multiple loading cases to obtain the desired parameter values by a single step while the two-step analyzing procedure must be carried out for each loading case.

(5) When combining with the substructuring technique of multiple concerned regions with the same configuration, the computation costs can be significantly reduced since the substructure could be used many times as the standard element,

particularly when the model includes a great number of standard elements for structural dynamic analysis of large-scale complicated engineering structures such as long-span bridges.

In conclusion, the proposed multi-scale model is proven to be able to output more accurate and reliable nominal stress and hot-spot stress distribution as well as significantly high efficiency in computation costs as compared to the traditional two-step analysis.

5.7 SUMMARY

As a practical engineering application case study, a multi-scale model of long-span bridge of Tsing Ma Bridge is constructed according to the aforementioned multi-scale modeling strategy. The identified critical components at the longitudinal truss with connection details are locally modeled and incorporated into the structural global model to obtain the corresponding multi-scale model. Without loss of generality, the developed multi-scale model with only one local detailed connection is investigated for the purpose of strategy study. The procedures of model verification and sensitivity-based model updating are further carried out. The comparison results under the standard train loading suggests that the output of updated multi-scale model agrees well with those of the global model and the monitoring data within the acceptable engineering range, which indicates that, at the same engineering level, the developed multi-scale

model is more convenient and appropriate for subsequent fatigue damage analyses.

CHAPTER 6

FURTHER DEVELOPMENT OF MULTI-SCALE MODELING OF TMB FOR NONLINEAR NUMERICAL ANALYSIS

6.1 NONLINEAR PHYSICAL-BASED MODEL

The multi-scale modeling strategy and implementation methods has been successfully proposed, on the basis of which the corresponding multi-scale model of TMB is then developed by incorporating the local detailed model of critical regions into structural global model at respective length scale level. Then structural overall responses at the component scale and hot-spot stress distribution at the local scale could be obtained simultaneously. However, nowadays the major problems maybe due to the fact that most of the fundamental theories and approaches of SHM use linear structural model before and after damage when the high nonlinear manners are expected. In this chapter, the developed multi-scale model is tried to be extended for nonlinear situation. Both linear and nonlinear seismic responses under the El-Centro earthquake wave are investigated as case study. Finally the damage-induced nonlinear computing algorithm on the basis of

multi-scale model is intended to be proposed for future research.

6.1.1 Necessity of Nonlinear Physical-based Modeling

Over the past decades, rapid development has been made on modern long-span cable-supported bridges. The suspension bridge and cable-stayed bridges are the main categories of cable-supported bridge and distinguished from each other not only in aesthetical configuration but also in their respective mechanical features. Long-span cable-supported bridges, due to their large dimensions and high flexibility, usually have extremely long fundamental periods. This feature distinguishes them from most of other structures and strongly affects their dynamic behavior. The length of central span ranges from 400 to 1000 m or even longer. With the increasing central span length of modern cable-stayed bridges, the trend of the bridge is to use more shallow and slender stiffening girders to meet the requirements of aerodynamics. In this case, bridge safety (strength, stiffness, and stability) under service loadings and environmental dynamic loadings (such as impacts, winds, and earthquakes) presents increasingly important concerns in both design and construction.

Although many advances have been made, many problems remain unknown or unsolved, in turn it would lead to serious limitations on the practical use of installed structural health monitoring system. The major problem may be due to the fact that the fundamental theory and approach of SHM mostly use linear structural models before and after the damage. The way forward is to develop a

damage-oriented model that is able to account for the major effects of damage, locally deteriorating processes and nonlinear influences on structural response.

The finite element model of a long-span bridge is usually constructed by the order of magnitude of kilometers while its components are modeled in meters. In practical simulation analysis of such a large structure on the global level, the FE model is often composed of treating one component as one element, which is enough for the purpose of structural global analysis. However, in some cases such as fatigue analysis and damage detection, since the damage is typically a local phenomenon, more attentions should be placed on the local detailed characteristics which are not represented in the aforementioned global model. At most they are considered to be in virgin state while the deteriorated condition of structures and its influences on structural stress and strain response are neglected in the calculation of structural stress. It is well known that many types of defect, such as cracks and degradation of structural connections, generate locally at the material points or sectional levels which will in turn influence the entire structural behavior and contribute to global structural damage and possibly cause structural failure. In this sense, an accurate model for analyzing such degradation behavior should incorporate the physical mechanism of local damage, treated predominantly at the material point by continuum damage mechanics, into global structural analysis and the corresponding FE analysis would become further complicated if these factors are taken into account. The major difficulty is the lack of a generalized framework for such nonlinear physical-based modeling in which

multi-scale simulation strategy is necessary, especially for long-span bridges. The local damage on the scale of the material point, usually less than a millimeter for steel, should be modeled based on the theory of continuum damage mechanics for hot-spot stress analysis and then inserted into the global model on the theory of structural dynamics.

Therefore it is essential to develop multiple spatial scales for the damage analysis of civil infrastructure considering structural deteriorating.

6.1.2 Nonlinearity in Long-Span Cable-Supported Bridge

It is well known that the increase in the center span length of cable-supported bridges made nonlinear analysis inevitable. For this special type of flexible, long-span cable-supported bridge, nonlinear analysis is essential for evaluating the stresses and deformations that are induced not only by static loads but also by dynamic loads, such as vehicular traffic, wind, and earthquakes.

A long-span cable-supported bridge exhibits nonlinear characteristics under various loadings. The nonlinearity that consists of geometrical and material nonlinearities may come from the following sources:

- The sag effect of inclined cable stays which is a nonlinear axial force-elongation behavior for the inclined cable stays under different tension load levels due to the sag initiated by their own weight.
- The combined interaction axial load and bending moment acting on the cable

in cable-stayed bridge.

- The large displacement effect produced by the geometry changes of the structure (known as $P-$delta effect) which is usually considered in bridge tower.
- The nonlinear stress-strain behavior of materials (material nonlinearity).

Many researchers have studied the dynamic behavior and seismic response of this kind of highly nonlinear structure. Some investigators disregard all sources of nonlinearities (e.g., Krishna *et al*. 1985) while others include one or more of these sources. Most nonlinear analyses of cable-stayed bridges have focused on plane (Fleming 1979) or space (Kanok-Nukulchai and Guan 1993; Boonyapinyo *et al*. 1994) geometric nonlinear behavior. But some analyses (Nakai *et al*. 1985; Seif and Dilger 1990) involve both geometric and material nonlinearities and reveal that the material nonlinearity is dominant in the nonlinear static behavior of long-span cable-stayed bridges. It is particularly true for long-span segmental concrete cable-stayed bridges. Dumanoglu and Stevern (1989) analyze the earthquake response of modern suspension bridges subjected to asynchronous longitudinal and lateral ground motion with the plane and linear finite-element model. Wilson and Gravelle (1991b) study the dynamic behavior of cable-stayed bridges through a linear elastic 3D finite-element model. In their studies the modal behavior has been predicted by the finite element model which is compared to measured ambient vibrations of the full-scale cable-stayed bridge.

A cable-supported bridge is usually composed of three main structural parts (or

bridge elements); namely, cable, girder (deck), and tower. These structural parts may be made of different materials. Therefore, a long-span cable-supported bridge is often a complex system composed of different materials. The material nonlinear analysis of a long-span cable-supported bridge depends on the nonlinear stress-strain behavior of individual materials for individual structural element. As a matter of fact, large member stresses may be induced under strong ground motions. However, as for the same material, when some points (integration points) of an element exceed the yielding limit of individual material, the stiffness matrix of the element should be revised to form the elastic-plastic stiffness matrix.

6.1.3 Nonlinear Considerations and Algorithms

A popular approach to consider the sagging of inclined cables is to introduce the concept of equivalent modulus of elasticity, which is firstly suggested by Ernst (1965) as follows:

$$E_{eq} = \frac{E}{1 + \frac{(L_0 \gamma)^2}{12\sigma^3} E} \tag{6.1}$$

where E_{eq} is the equivalent elastic modulus of inclined cable, E is cable material effective elastic modulus, L_0 is horizontal projected length of the cable, and γ stands for weight per unit volume of the cable and σ represents cable tensile stress. For a longer span, even the effective Young's modulus should be computed by iteration according to the cable stress in any particular stage.

Like all nonlinear structural analysis problems, the nonlinear analysis of a long-span cable-stayed bridge finally reduces to form the nonlinear incremental equilibrium equations of the system and to solve these equations. Nonlinear finite element methods (NFEM) have been a popular way to study the nonlinear behavior of long-span cable-stayed bridges. Based on the characteristics of the geometric nonlinear sources described above, some NFEM formulations have been proposed. In the formulation presented by Fleming (1979) or Nazmy and Abdel-Ghaffar (1990a) for example, the sag effect of cables is accounted for by the Ernst's equivalent elastic modulus concept, the structural geometric change due to large displacement is included in updating each set of node coordinates, whereas the axial force-bending moment interaction effect is considered by the stability beam functions.

It is commonly assumed that the geometrical deformations of structural members in a long-span bridge are characterized by large displacements and large rotations but small strains. With the developments of the finite-deformation theory and nonlinear FEM techniques with computers, researchers are more likely to use the finite deformation theory to study the nonlinear behavior of long-span cable-stayed bridges. There are several rigorous NFEM formulations available such as total Lagrangian formulation, updated Lagrangian formulation, and co-rotational formulation. In this study, the updated Lagrangian NFEM Formulation (UL) is used.

Based on the large deformation but small strain assumption, the global

equilibrium equation can be established together with the consideration of the initial stress effects. In addition to the linear stiffness, the tangential stiffness of a geometric nonlinear structure will include the geometric stiffness and the large deformation stiffness. In practice, for the geometric nonlinear analysis, the modified Newton-Raphson method is used to solve the nonlinear equations, in which the loads are applied incrementally on the structure and the Newton-Raphson iterations are performed in each load step. For the material nonlinear analysis, when stresses on some Gauss integration points of an element exceed the limit stress of individual materials, the stiffness matrix of the element is revised to form the elastic-plastic stiffness matrix. In the seismic response analysis, the nonlinear differential equations of motion are directly integrated by the Newmark-β method. The integration constants $a = 1/4$ and $b = 1/2$ are chosen, which corresponds to an unconditionally stable scheme. In each time step, the Newton-Raphson iteration technique is used to obtain the solution that satisfies both equilibrium equations and material constitutive relationships.

Another important feature of long-span bridges is the effects of the dead loads. The dead loads of a long-span cable-stayed bridge always contribute approximately 80-90% to total bridge loads. After the bridge is completed, and before the live loads are applied, the bridge has sustained large dead loads so that the large deformations and initial stresses that already exist in each member should be considered. Therefore, dead loads are applied before the earthquake so that nonlinear seismic analysis should start from the deformed equilibrium

configuration due to dead loads. In other words, to consider the effect of dead loads, the seismic response analysis should involve two steps: (1) The static analysis under dead loads to form the deformed equilibrium configuration; and (2) the seismic response analysis starting from the deformed configuration due to dead loads. Ren (1997) performs the comparison between seismic response starting from the un-deformed initial configuration and that from deformed equilibrium configuration due to dead loads, which shows that the initial equilibrium configuration is essential to start the seismic response analysis. Both linear and nonlinear seismic response analyses of long-span cable-supported bridges should start from the deformed equilibrium configuration due to dead loads.

6.2 SEISMIC RESPONSE OF MULTI-SCALE MODEL OF LONG-SPAN BRIDGE

For the special type of flexible structure with long period such as long-span cable-supported bridges, nonlinear analysis is essential for evaluating the stress and deformations induced by not only the static loads but also the dynamic loads such as daily traffic, wind or even ultimate event of earthquake and typhoon. When the span length increases, a pronounced nonlinearity in the response may be expected, which will result in a considerable increase in the displacement and deformation of bridge unexpectedly. From this point of view, it is particularly

essential to perform the study on the nonlinear seismic response of long-span bridges to understand the seismic behaviors.

6.2.1 Linear Seismic Response Analysis of Large-span Bridge

Usually, most anti-seismic design codes for bridge engineering around the world are only feasible for moderate span brides, not for large span ones. The native anti-seismic code for road engineering only lists the items for the arch and beam bridges with the span shorter than 150m. The seismic responses of large span bridges, usually with the span of over a thousand meters, should be studied further to understand their characteristics under the earthquake excitations, with complex geological conditions at different pier bases, and also some basic problems related to the large span bridges, like traveling wave effect, nonlinear effect, soil-structure interaction, should also be further analyzed carefully.

6.2.2 Seismic Response Analysis under Consistent and Non-consistent Ground Motion

Motion equations under consistent excitation

When bridge structure is subjected to the consistent seismic excitation, the motions at different pier bases are the same because of the base rigidity hypothesis, and structural internal force is caused by its dynamic response. The movement equation of bridge structure could be written as follows:

$$[M]\{\ddot{U}^d\}+[C]\{\dot{U}^d\}+[K]\{U^d\}=-[M]\{\ddot{U}_{g0}\} \tag{6.2}$$

where $[M]$, $[C]$, $[K]$ are mass, damping and stiffness matrices respectively, $\{U^d\}$ is dynamic relative displacement of structural node and $\{\ddot{U}_{g0}\}$ is acceleration at coordinate original point.

Motion equations under non-consistent excitation

Supposing the vibration differential equation of bridge structure in coordinate system is:

$$[M]\{\ddot{U}\}+[C]\{\dot{U}\}+[K]\{U\}=\{P\}-[M]\{\ddot{U}_{g0}\} \tag{6.3}$$

where $[M]$, $[C]$, $[K]$ stands for mass, damping and stiffness matrices of bridge structure respectively, $\{U\}$ is dynamic relative displacement of structural node and $\{\ddot{U}_{g0}\}$ is accelerogram at coordinate origin and $\{P\}$ is external load.

It is known that every supporting point of the structure moves in the same way as base does, structure doesn't suffer from the external dynamic loads during earthquake, so the Equation (6.3) may be rewritten as:

$$\begin{bmatrix} M^{aa} & M^{ab} \\ M^{ba} & M^{bb} \end{bmatrix}\begin{Bmatrix} \ddot{U}^a \\ \ddot{U}^b \end{Bmatrix}+\begin{bmatrix} C^{aa} & C^{ab} \\ C^{ba} & C^{bb} \end{bmatrix}\begin{Bmatrix} \dot{U}^a \\ \dot{U}^b \end{Bmatrix}+\begin{bmatrix} K^{aa} & K^{ab} \\ K^{ba} & K^{bb} \end{bmatrix}\begin{Bmatrix} U^a \\ U^b \end{Bmatrix}=\begin{Bmatrix} P^a \\ P^b \end{Bmatrix}-\begin{bmatrix} M^{aa} & M^{ab} \\ M^{ba} & M^{bb} \end{bmatrix}\begin{Bmatrix} \ddot{U}_{g0} \\ \ddot{U}_{g0} \end{Bmatrix} \tag{6.4}$$

in which, superscript a represents the node parameters without suffering from external load, and superscript b stands for the parameters related to supporting points, and the load at no supporting point $\{P^a\}=\{0\}$.

The supporting movement could cause the displacement at all nodes of structure.

It is assumed that the supporting point vibrates together with base, in which U^{bs} is relative displacement to coordinate origin, U^{as} is pseudo static relative displacement at other nodes caused by supporting displacement to movable coordinate system. The total relative displacements to movable coordinate at each node are equal to the sum of pseudo static relative displacement and dynamic relative displacement.

$$\begin{Bmatrix} U^{a} \\ U^{b} \end{Bmatrix} = \begin{Bmatrix} U^{as} \\ U^{bs} \end{Bmatrix} + \begin{Bmatrix} U^{ad} \\ U^{bd} \end{Bmatrix} \tag{6.5}$$

where, U^{ad} represents the dynamic displacement at non-supporting points, U^{bd} stands for the dynamic relative displacement at supporting points.

At any moment, $\{U^{bd}\} = \{0\}$ is fixed. So substitute Equation (6.5) into Equation (6.4), then

$$\begin{bmatrix} M^{aa} & M^{ab} \\ M^{ba} & M^{bb} \end{bmatrix} \begin{Bmatrix} \ddot{U}^{ad} \\ \ddot{U}^{bd} \end{Bmatrix} + \begin{bmatrix} C^{aa} & C^{ab} \\ C^{ba} & C^{bb} \end{bmatrix} \begin{Bmatrix} \dot{U}^{ad} \\ \dot{U}^{bd} \end{Bmatrix} + \begin{bmatrix} K^{aa} & K^{ab} \\ K^{ba} & K^{bb} \end{bmatrix} \begin{Bmatrix} U^{ad} \\ U^{bd} \end{Bmatrix} =$$
$$- \begin{bmatrix} M^{aa} & M^{ab} \\ M^{ba} & M^{bb} \end{bmatrix} \begin{Bmatrix} \ddot{U}^{as} \\ \ddot{U}^{bs} \end{Bmatrix} - \begin{bmatrix} C^{aa} & C^{ab} \\ C^{ba} & C^{bb} \end{bmatrix} \begin{Bmatrix} \dot{U}^{as} \\ \dot{U}^{bs} \end{Bmatrix} - \begin{bmatrix} M^{aa} & M^{ab} \\ M^{ba} & M^{bb} \end{bmatrix} \begin{Bmatrix} \ddot{U}_{g0} \\ \ddot{U}_{g0} \end{Bmatrix} + \begin{Bmatrix} 0 \\ P^{b} \end{Bmatrix} - \begin{bmatrix} K^{aa} & K^{ab} \\ K^{ba} & K^{bb} \end{bmatrix} \begin{Bmatrix} U^{as} \\ U^{bs} \end{Bmatrix} \tag{6.6}$$

The second term in Equation (6.6) could be ignored in small damping structure, and the sum of last two terms should be equal to zero, namely,

$$\begin{Bmatrix} 0 \\ P^{b} \end{Bmatrix} - \begin{bmatrix} K^{aa} & K^{ab} \\ K^{ba} & K^{bb} \end{bmatrix} \begin{Bmatrix} U^{as} \\ U^{bs} \end{Bmatrix} = \begin{Bmatrix} 0 \\ 0 \end{Bmatrix} \tag{6.7}$$

thus the following expression could be obtained:

$$\left[K^{aa}\right]\left\{U^{as}\right\}+\left[K^{ab}\right]\left\{U^{bs}\right\}=\left\{0\right\} \tag{6.8}$$

Differentiating above equation twice and then substituting it into Equation (6.6), so it can be further rewritten as

$$\begin{bmatrix} M^{aa} & M^{ab} \\ M^{ba} & M^{bb} \end{bmatrix}\begin{Bmatrix} \ddot{U}^{ad} \\ \ddot{U}^{bd} \end{Bmatrix}+\begin{bmatrix} C^{aa} & C^{ab} \\ C^{ba} & C^{bb} \end{bmatrix}\begin{Bmatrix} \dot{U}^{ad} \\ \dot{U}^{bd} \end{Bmatrix}+\begin{bmatrix} K^{aa} & K^{ab} \\ K^{ba} & K^{bb} \end{bmatrix}\begin{Bmatrix} U^{ad} \\ U^{bd} \end{Bmatrix}= -\begin{bmatrix} M^{aa} & M^{ab} \\ M^{ba} & M^{bb} \end{bmatrix}\begin{Bmatrix} -\left[K^{aa}\right]^{-1}\left[K^{ab}\right]\ddot{U}^{bs} \\ \ddot{U}^{bs} \end{Bmatrix}-\begin{bmatrix} M^{aa} & M^{ab} \\ M^{ba} & M^{bb} \end{bmatrix}\begin{Bmatrix} \ddot{U}_{g0} \\ \ddot{U}_{g0} \end{Bmatrix} \tag{6.9}$$

Let

$$\left\{\ddot{U}_{bg}\right\}=\begin{Bmatrix} -\left[K^{aa}\right]^{-1}\left[K^{ab}\right]\ddot{U}^{bs} \\ \ddot{U}^{bs} \end{Bmatrix}$$

$$\left\{\ddot{U}_{bg}+\ddot{U}_{g}\right\}=[R]\left\{\ddot{U}_{g0}\right\} \tag{6.10}$$

then Equation (6.9) could be simplified as

$$[M]\left\{\ddot{U}^{d}\right\}+[C]\left\{\dot{U}^{d}\right\}+[K]\left\{U^{d}\right\}=-[M][R]\left\{\ddot{U}_{g0}\right\} \tag{6.11}$$

Equation (6.11) is eventually the differential motion equation for bridge seismic response, where $[R]$ is the seismic affecting matrix considering traveling wave effect and multi-excitation. When considering traveling wave effect and multiple excitations, different supporting freedom has different U^{bs} values at the same moment, the seismic inputs at different supporting points may be different. Otherwise, the ground motion at different supporting points in same direction should be the same and the relative displacement at supporting points is zero, i.e., $\left\{U^{as}\right\}=\left\{U^{bs}\right\}=\left\{0\right\}$, and the affecting matrix $[R]$ equals to unit matrix $[I]$ at this moment. Then the differential motion equation would be changed into

$$[M]\{\ddot{U}^d\}+[C]\{\dot{U}^d\}+[K]\{U^d\}=-[M][I]\{\ddot{U}_{g0}\}=-[M]\{\ddot{U}_{g0}\} \qquad (6.12)$$

Equation (6.12) is the differential equation without considering traveling wave effect and multiple excitations.

6.2.3 Input Ground Motions

Table 6.1 Maximum allowable horizontal acceleration of ground motion at different fortification intensity region

Regions with different Seismic fortification intensity	7	8	9
Ground motion maximum horizontal acceleration	0.125g	0.25g	0.5g

Table 6.2 PGA adjustment scalar of original ground acceleration

Components	PGA (cm/s^2)	Seismic fortification intensity	Adjustment scalar
N-S Component (transversal direction)	341.7	7 (0.125g)	$0.125g / 3.417 = 0.3585$
W-E Component (longitudinal direction)	210.1		$0.125g / 2.101 = 0.583$
Vertical direction	206.3		$0.125g / 2 / 2.063 = 0.2969$

In order to evaluate the effect of strong ground motion on the seismic response behavior of long-span suspension bridge, the El-Centro 1940 earthquake record is used in this study. Because of its large peak ground acceleration and wider frequency range in practical engineering application, a ground motion recorded at

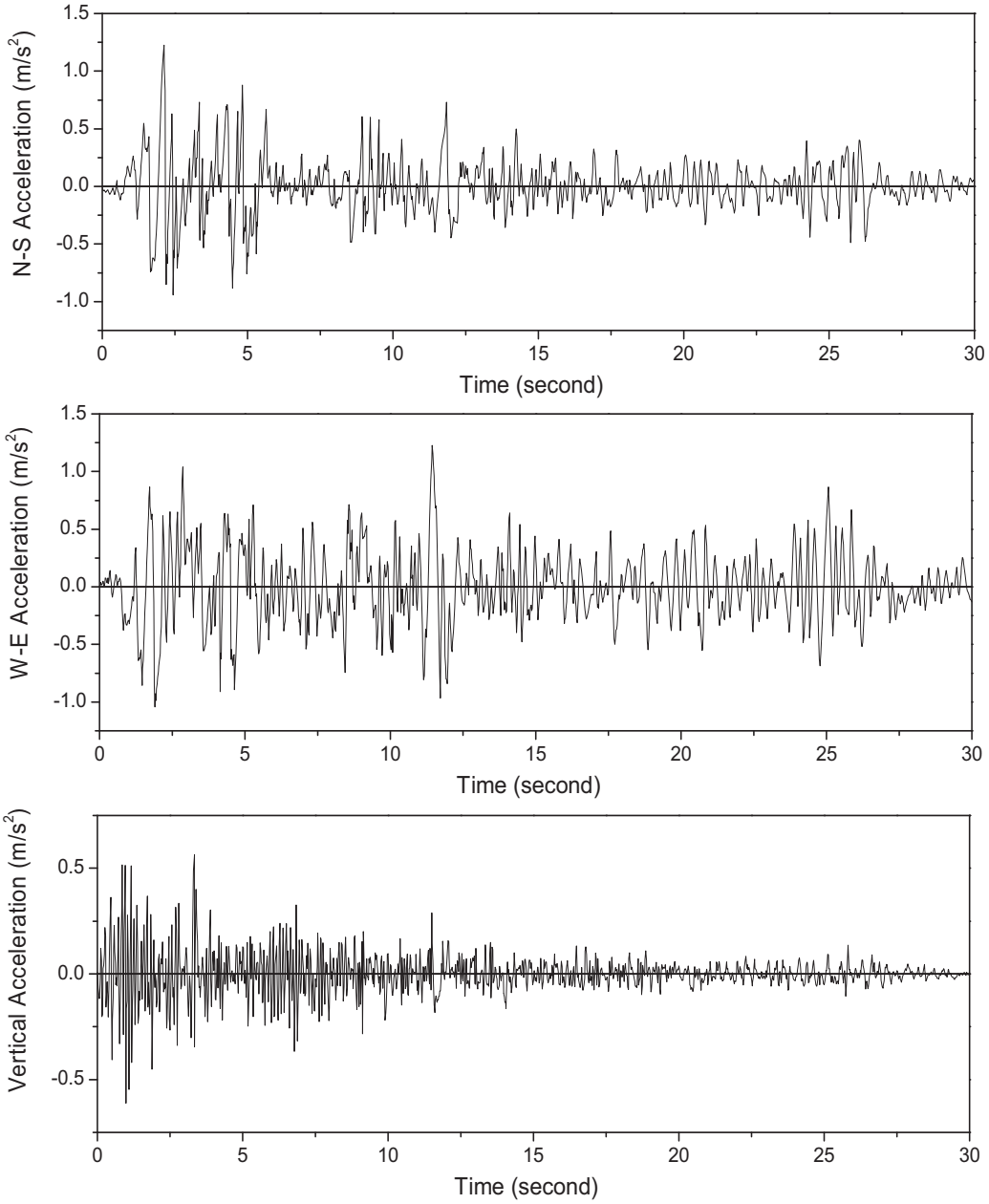

Figure 6.1 The amplitude-adjusted El-Centro ground acceleration

a site in El-Centro, California, during the Imperial Valley, California, earthquake of May 18, 1940, known as the El-Centro 1940 earthquake record, is considered as the typical example of large earthquake among the existing earthquake records and more appropriate for design basis in comparison with the other ground motion waves. It is chosen as the sample ground motion acceleration input with

the components at the directions of N-S, W-E and vertical corresponding to the bridge transversal, longitudinal and vertical direction, respectively.

As tabulated in Table 6.1, according to the China scale of seismic intensity and code of seismic design for highway bridge (JTJ004-2005), the Tsing Ma bridge locates at Tsing Yi Region on the II site and in the region of Seismic fortification intensity 7. Therefore, the original ground motion record data is needed to be proportionally adjusted through multiplying by a scalar to fit peak ground motion acceleration with the corresponding seismic fortification intensity. In simple word, the original ground motion record is scaled to 0.125g which is the design seismic level for actual bridge to remain linear under this earthquake intensity. The peak ground accelerations (PGA) of each component are then listed in Table 6.2. The three components of amplitude-adjusted El-Centro ground acceleration are plotted in Figure 6.1. In the numerical computations of the seismic responses, a total time duration of 30 seconds of the record and time interval of 0.02 second are used. It is found that those time steps are appropriate during the seismic response analysis.

6.2.4 Linear Seismic Response by Global Model under Consistent Excitation

To perform the linear seismic response time history analysis for the long-span suspension bridge, the conventional way is to consider for modification of cable elastic modulus and the gravity stiffness at static equilibrium state subjected to dead loads, on the basis of which the modal superposition method or direct

integration method is then applied. As for the general procedure of seismic response analysis, researchers more concerned about the qualitative results. The modal superposition method is then adopted to study the linear dynamic response.

The modal superposition method used in modal dynamic time history analysis is regarded as being computationally inexpensive and can provide insight into the dynamic behavior of a structure. With modern eigenvalue/eigenvector extraction techniques, the cost of obtaining a sufficient basis of eigensolution is not excessive, and the subsequent computational effort involved in obtaining the dynamic response by modal superposition method is relatively small. The basic concept of modal superposition is that the response of the structure is expressed in terms of a relatively small number of eigenmodes of the system. The orthogonality of the eigenmodes uncouples this system. Furthermore, only eigenmodes that are close to the frequencies of interest are usually needed. The modal superposition is treated as linear perturbation analyzing method and the linear response is obtained from perturbation step. However, the nonlinearity could be accounted for at the preceding general step which leads to the current modulus (tangent modulus) is taken as the linear stiffness for perturbation program.

It is unnecessary and even impossible to use all the mode shapes for most practical problems. Theoretically speaking, the contributions of all the modes must be included in order to obtain the exact value of the response. Relatively few modes can, however, usually provide the sufficiently accurate results and the

modal summation can be truncated to include only the first few modes. For the small span beam bridge or arch bridge, good approximate solutions could be obtained via superposition by mode shapes of only first few orders. However, as for the large-span suspension bridge, high order modes contributed to the structural response that lead to more modes should be considered for the satisfactory result. Several building codes required that at least 90% of the modal participating mass should be included in the calculation of response for each principal horizontal direction. This requirement is based on a unit base acceleration in a particular direction and calculating the base shear force due to that load.

As long-span bridges bear global deformation at very low frequency and local deformation at relatively high frequency, assuming the bridge local deformation to be included in the response, the first 200 modes are eventually selected in the linear seismic response analysis using modal superposition method. The effective masses are more than 95% of the total masses when the first 200 modes are used in the dynamic analysis, therefore the number of modes is considered as being enough for dynamic response. In addition, considering that long-suspension bridges are lightly damped structures, the modal damping is chosen as 0.5%. Here only internal forces and displacements are desirable, so theory of structures is applied then.

The elastic seismic time-history response of the long-span suspension bridge under the amplitude-adjusted earthquake record is studied. The first analysis step

is the static computation under dead loads, as mentioned earlier. In this static analysis step, the geometric nonlinear analysis is performed where the equilibrium iterations are needed. The second analysis step is the seismic response analysis.

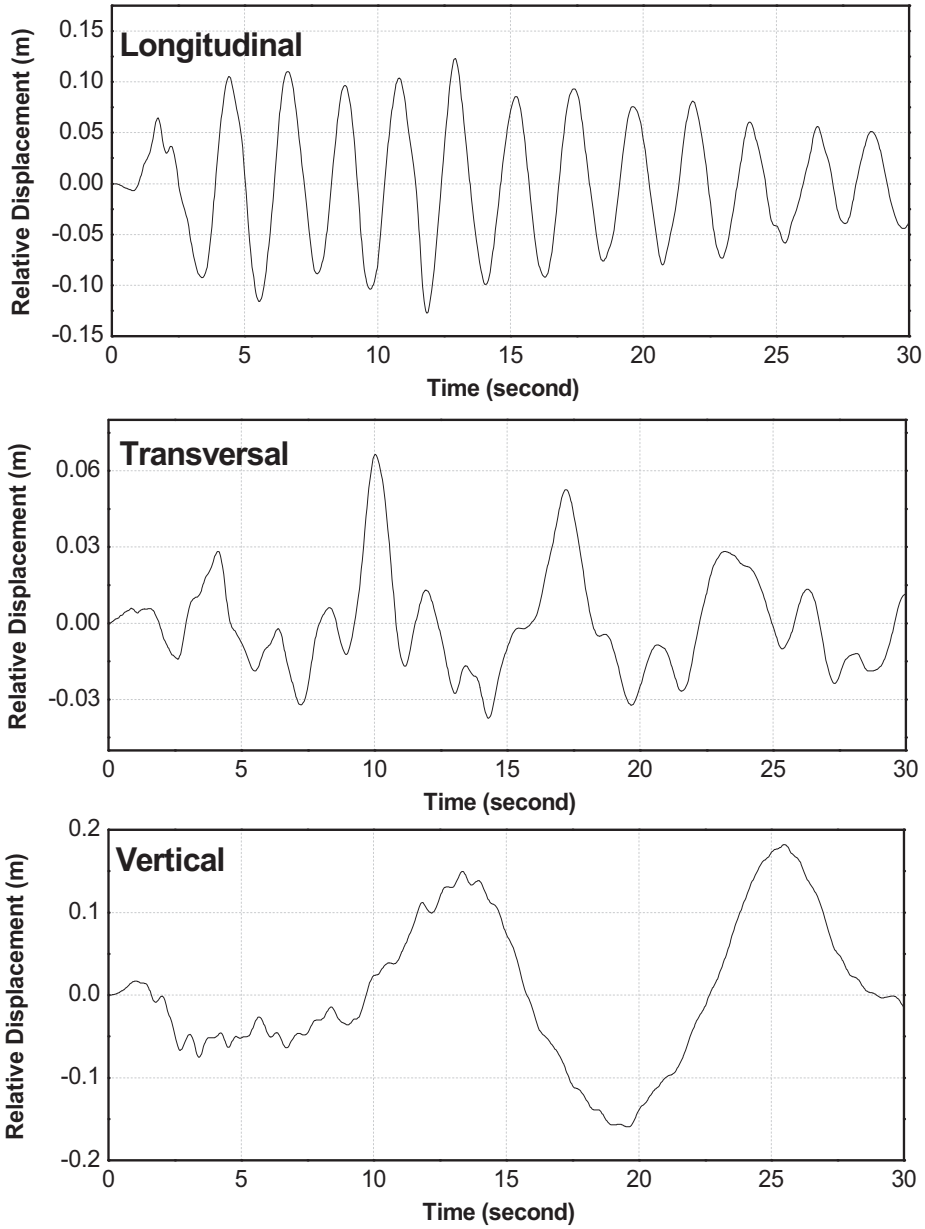

Figure 6.2 Relative displacement-time history of mid-span cross-section

The strong ground motion record as introduced and amplitude-adjusted El-Centro wave are input along the combined longitudinal, transversal and vertical directions. Furthermore, the seismic response is computed starting from the

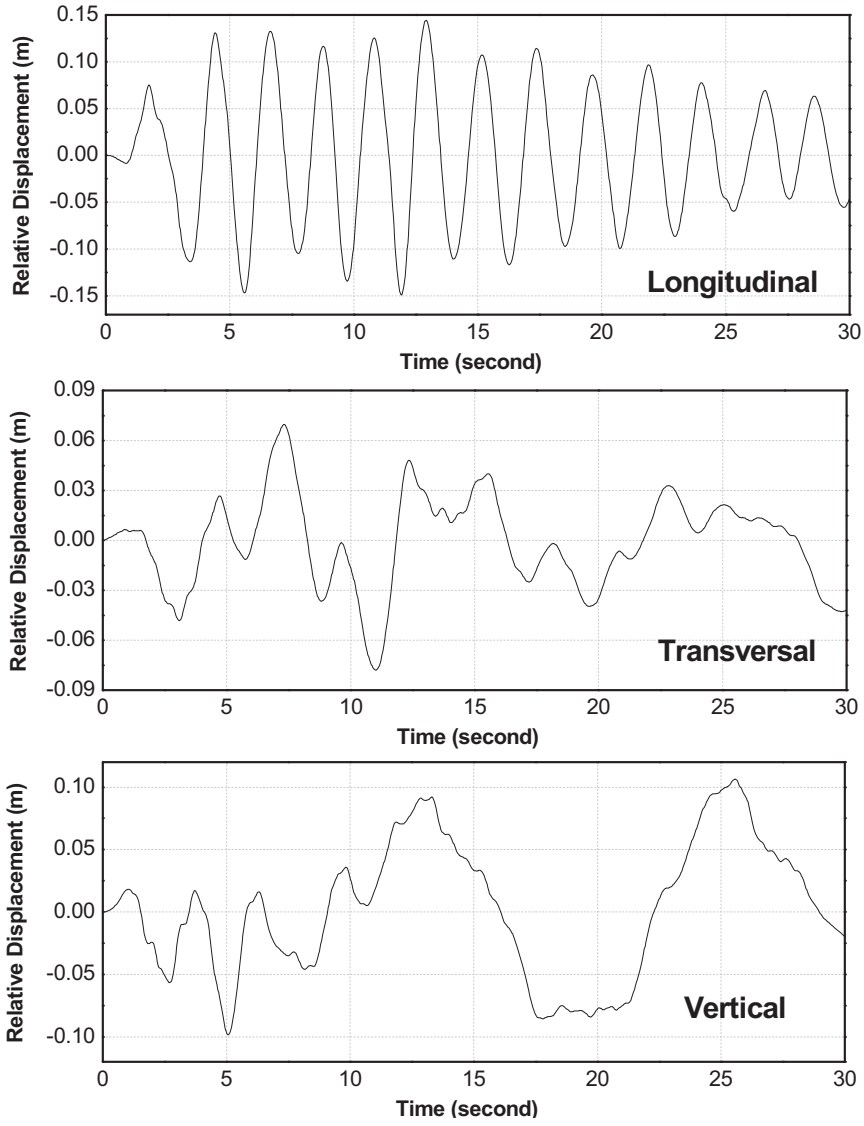

Figure 6.3 Relative displacement-time history of quarter-span cross-section

Table 6.3 Maximum reaction responses at the bottom of towers

Towers	Q (MN)		N (MN)	M (MN•m)	
	direction at			direction at	
	local 1	local 2		local 1	local 2
Ma Wan side	29.9	21.8	-176	-2430	420
Tsing Yi side	-32.3	19.8	-182	2270	355

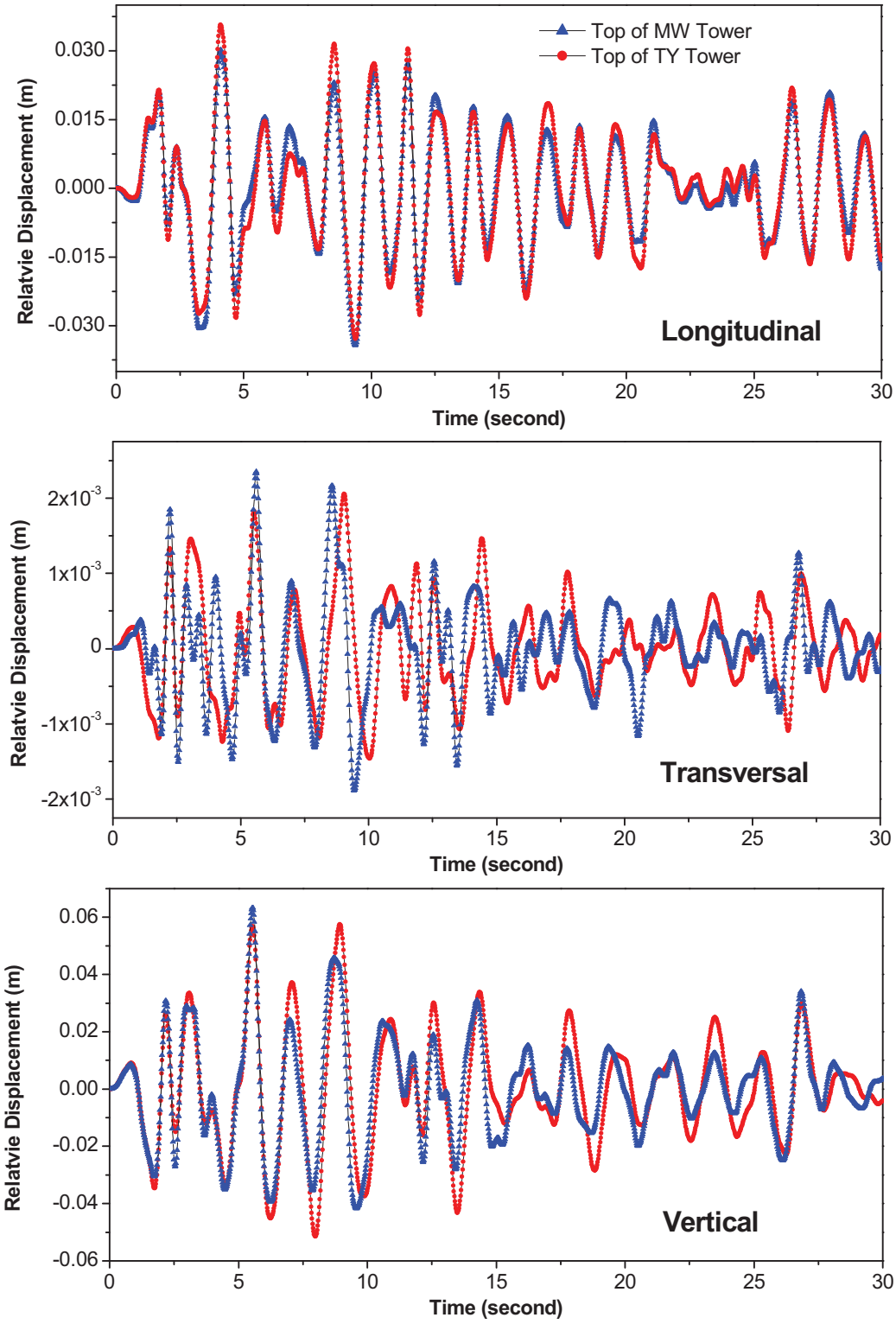

Figure 6.4 Relative displacement-time history response of top of towers

deformed equilibrium configuration due to dead loads.

During the seismic calculation case, the following time-history seismic responses

are recorded:

- Relative displacement time-history response at the directions of longitudinal, transversal and vertical at the mid-span and quarter-span as well as the top of two towers.
- Reaction time-history responses at the bottom of the two towers-the shear force, axial force, and bending moment.

In the process of subsequent analyses, the abbreviation of MW stands for Ma Wan side while TY for Tsing Yi side as convenience.

Only parts of results are listed in this study. The three-directional relative displacement time-history response under the combined three directional ground acceleration of mid-span, quarter-span and top of two towers are shown in Figure 6.2-Figure 6.4, respectively. Table 6.3 tabulates the maximum reaction responses at the bottoms of towers subjected to the aforementioned combined three directional ground acceleration.

From the results of relative displacements response of mid-span and quarter-span, the similar trend of displacement curves are observed with only small differences in amplitude. However, the comparison between top of tower displacements indicated that the relatively large differences resulted from the asymmetry of bridge configuration, particularly at the transversal direction.

As for the reaction time-history response at the bottom of two towers, Figure 6.5 shows the asynchronous response at the aspects of axial force, shear force and

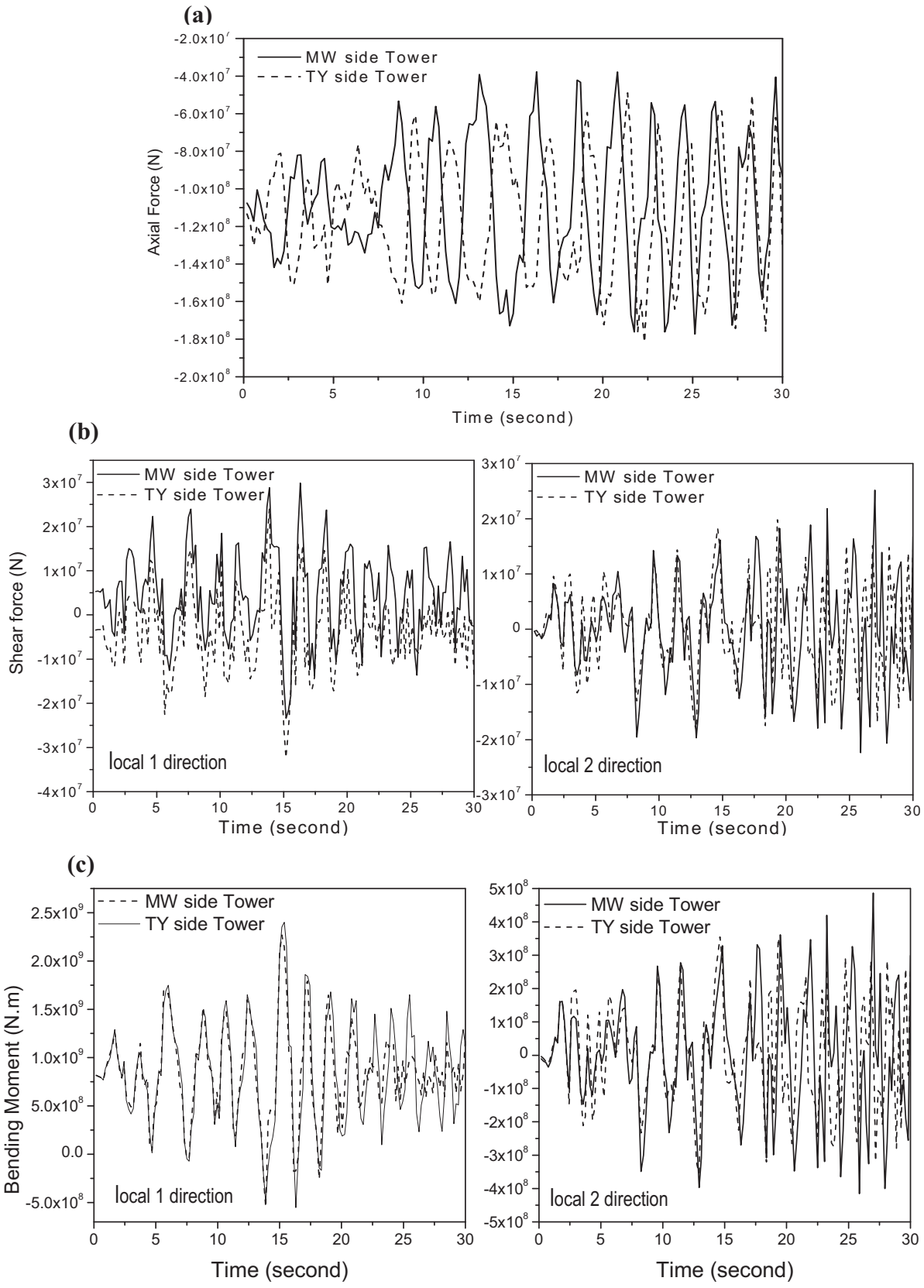

Figure 6.5 Internal force comparison between MW side tower and TY side tower (a) axial force (b) shear force (c) bending moment at the bottom of towers

bending moment and the maximum reaction response values are given in Table 6.3. The seismic responses show high dependence on the characteristics of earthquake records and the dynamic properties of the bridge. Nevertheless, the seismic responses results suggest that the earthquake record with the largest PGA value does not necessarily induce the greatest maximum responses.

6.2.5 Evaluation of Nonlinear Seismic Responses of Long-span Bridge

As mentioned before, although there are many researchers have studied the dynamic behavior and seismic response of this kind of high nonlinear structure, some investigators disregard all sources of nonlinearities while other including one or more sources. Nevertheless, the elastic-plastic seismic responses of long-span suspension bridge have been seldom conducted before. As a matter of fact, relatively large member stresses are usually induced by strong ground motion.

Generalized motion equations for nonlinear analysis

Replacing the relative parameter expression with absolute ones, the equations of motion Equation (6.2) for an n degrees of freedom bridge system expressing dynamic equilibrium at time point t could be rewritten as follows:

$$M\ddot{u}_t + C_t\dot{u}_t + K_t u_t = R(t) \tag{6.13}$$

where M C_t and K_t are the mass, damping and stiffness matrices, respectively, and where $R(t)$ is the applied dynamic load vectors. Vectors $\ddot{u}_t$

$\ddot{u}_t$ and u_t are the absolute acceleration, absolute velocity and absolute displacement respectively.

While the structural system is nonlinear, the coupled equations of motion, Equation (6.13), must be solved using step-by-step integration method. Considering a time interval Δt starting at time point t and assuming that the stiffness and damping matrices at time point t, i.e., K_t and C_t, can be applied over the full time interval, one obtains the equations of motion in the incremental form as

$$M\Delta\ddot{u}(t) + C_t\Delta\dot{u}(t) + K_t\Delta u(t) = \Delta R(t) + MB\Delta\ddot{u}_g(t) \tag{6.14}$$

where

$$\begin{aligned} \Delta\ddot{u}(t) &= \ddot{u}(t+\Delta t) - \ddot{u}(t) \\ \Delta\dot{u}(t) &= \dot{u}(t+\Delta t) - \dot{u}(t) \\ \Delta u(t) &= u(t+\Delta t) - u(t) \end{aligned} \tag{6.15}$$

and

$$\begin{aligned} \Delta R(t) &= R(t+\Delta t) - R(t) \\ \Delta\ddot{u}_g(t) &= \ddot{u}_g(t+\Delta t) - \ddot{u}_g(t) \end{aligned} \tag{6.16}$$

Modified input ground motion

In the previous part of studying the linear seismic response of long-span bridges, amplitude-adjusted El-Centro ground acceleration components have been adopted. However, when those input ground acceleration components are used in nonlinear seismic response analysis, the relatively small component stresses are observed

which indicates that all the structural components' stresses are below the yielding stress value so that they still remain elastic instead of stepping into plastic range. Therefore, in order to enlarge the component stress to yield for plasticity, the original El-Centro earthquake records are used in the subsequent analysis. The study on elastic-plastic seismic response is then carried out by inputting these earthquake records in the longitudinal direction (East-West (E-W) component), vertical direction and combined longitudinal and vertical directions.

Material data

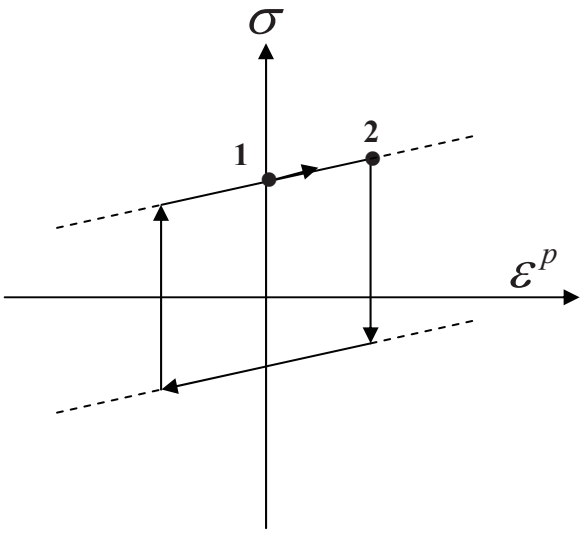

Figure 6.6 Schematic diagram of constitutive relationship of bilinear hysteretic model for steel girder

Although the suspension bridge mainly consists of three components, namely steel stiffened girder, main cable and towers with different material properties, only the elastic-plastic behavior of steel girder is considered in this study. In other words, the main cable and towers are assumed to remain elastic throughout the seismic duration time.

The elastic-plastic constitutive model of steel girder under the cyclic loading taken in this analysis is the widely-used bilinear hysteric model for structural steel Q235 as shown in Figure 6.6, where the parameter values are taken as $\sigma_1 = 235$ MPa, $\varepsilon_1 = 0$; $\sigma_2 = 300$ MPa, $\varepsilon_2 = 0.0313$.

Nonlinear seismic response evaluation

Therefore, the nonlinear seismic time-history responses of long-span suspension bridge under the selected ground acceleration are studied with the developed multi-scale model of TMB. As for the comparison study, the linear seismic response analysis is also carried out. Geometric nonlinearity and material nonlinearity can be accounted for during elastic-plastic seismic response analysis. The computation procedures could be divided into two steps. The first analysis step is the static calculation under dead loads as the "initial configuration" for seismic response analyzing procedure. In this static analysis step two cases are considered. One case is the linear analysis under dead load where there is no equilibrium iterations while the other is geometric nonlinear analysis where equilibrium iterations are needed. That is, the deformed equilibrium configuration due to dead loads is the starting point for the subsequent analyzing process. The second analysis step is seismic response analysis. The original El-Centro wave data is taken as input ground motion along longitudinal direction (E-W component), vertical direction (vertical component) and combined longitudinal and vertical directions, respectively.

On the basis of analyzing results from the elastic and elastic-plastic overall seismic response analyses of long-span suspension bridge on structural global scale under the strong ground motion, the following qualitative findings could be made.

- The effect of the dead loads must be considered in the seismic response analysis of long-span suspension bridges. Both linear and nonlinear seismic analyses should start from the deformed equilibrium configuration due to dead loads.

- Compared with seismic time-history response results under the longitudinal direction inputs, vertical direction inputs, and combined longitudinal and vertical inputs, it is found that the superposition principle is not suitable to the seismic response of long-span bridges even in the linear seismic response case. Seismic responses under combined longitudinal and vertical inputs are not the simple sum of the individual longitudinal and vertical component inputs due to the coupling effect that exists between longitudinal and vertical seismic responses. This is probably caused by the complicated structural dynamic characteristics of such long-span cable-supported structures.

On the basis of the above finds obtained from the numerical computation, the nonlinear seismic response focusing on the critical location by multi-scale model has been attempted to be performed with considering geometric nonlinearity on structural global scale while material nonlinearity on the local detailed model. The

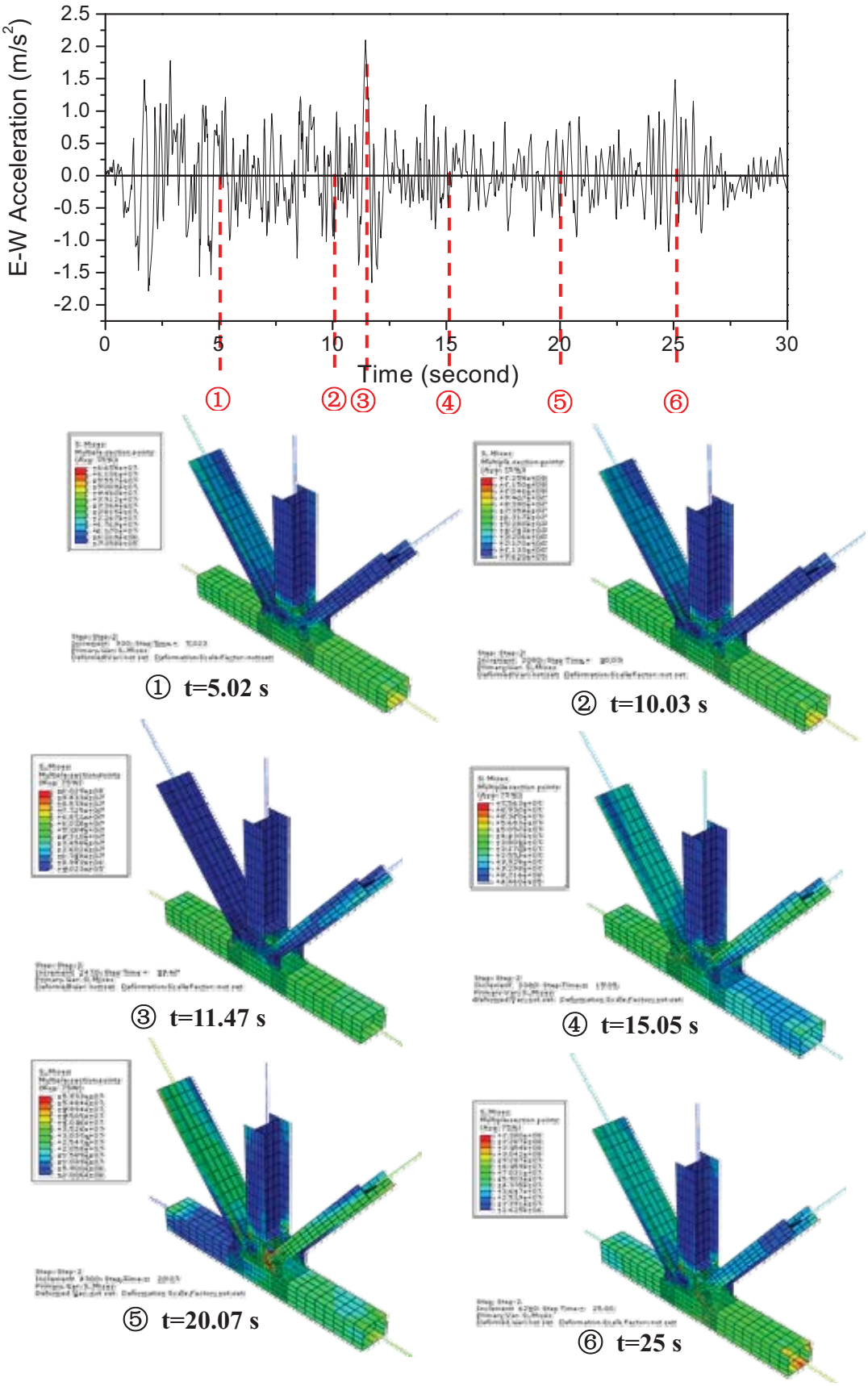

Figure 6.7 Hot-spot stress distribution of critical region by multi-scale model subjected to seismic loading

hot-spot stress distribution of local detailed model at different time point of the duration of El-Centro earthquake wave is graphically displayed in Figure 6.7. The local detailed model of critical region is constructed by coupling of beam element with shell elements using aforementioned multi-scale modeling strategy. And the theory of mechanics of structures is applied to global length scale while mechanics of materials on local detailed model. Although the material nonlinearity and corresponding nonlinear computing algorithm have been introduced in nonlinear numerical analysis, the Von-Mises stress values indicate that all of the elements are in low stress level and still in the elastic range. The reason which could be explained about the attempt failure on the nonlinear seismic response calculation maybe due to the following factors: (1) The applied earthquake loading is not strong enough to make the element of critical region step into plasticity; (2) It is more likely that another location other than the identified critical region has yield under the seismic loading. It is also obvious that the earthquake record with the largest PGA value does not necessarily induce the greatest maximum responses and vice versa.

6.2.6 Seismic Response Analysis Considering Wave Passage Effect

Extended structures such as long bridges can be subjected to very differing motions along their length due to the spatial variability of the input seismic motion. The effect of the spatial variation of the seismic ground motions on the response of bridge structures has been concerned for decades. The spatial

variation of seismic ground motion may be regarded as the result of the combination of three different phenomena: (1) the so-called wave-passage effect, which is the difference in the arrival times of seismic waves at different locations along the bridge; (2) the incoherence effect, resulting from reflections and refraction of waves through the soil during their propagation, as well as the difference in the manner of superposition of waves arriving from an extended source at various locations; and (3) the local effect, due to the difference in local soil conditions at each location. Because of insufficient knowledge of the mechanisms underlying the spatial variability of the motion, it is often assumed that the spatial variability is attributed only to the wave passage effect.

Traveling wave (also referred to wave passage) effect is a special type (the same wave but arriving at different times) of earthquake ground motion variation. The influences of the wave-passage effect on the responses of bridges have been investigated by several researchers. Most researchers come to the conclusion that for standard highway bridges with relatively short fundamental periods ($T<2s$), the traveling wave effect does not need to be considered. Monti *et al*. (1996) study the nonlinear responses of symmetric bridges with symmetric boundary conditions. They have found that the traveling wave effect on the response consists essentially in a reduction of the dynamic part due to the incomplete synchronization of the excitation for the range of apparent velocities in excess of 500 m/s. Harichandran (1999) investigates the influence of spatial variations of earthquake ground motions on long-span bridges, and concludes that identical

excitations severely underestimate the axial forces in all arch members and overestimate axial forces in the deck and bracings. For a long-span arch bridge subjected to site specific ground motions, traveling wave effect is shown to be important and distinct (Xu, Y. *et al*. 2003).

The phenomena of non-consistent ground motion do exist and have been verified by the observation results of ground motion. However, the consistent excitation assumes that seismic ground motions at structural supports are entirely identical without phase differences, which is reasonable and acceptable to the small planar size structure. While for the large scale infrastructures, such as long-span cable-stayed bridge, suspension bridge, multi-span steel girder bridge, many researchers replace synchronous input with the multi-point excitation method in practice.

Nowadays traveling wave method has been popularly adopted in seismic response investigation of a bridge subjected to non-consistent excitation. This method is based on the following assumptions: (1) soil condition is identical (2) seismic wave travels at certain speed and waveform remains unchanged at structural supports with phase differences and decayed amplitude. Although the assumptions impose limitations on the practical application of traveling wave method, it still express the characteristics of seismic wave traveling to some extent, and also the seismic response features of long-span bridges.

The following assumptions in seismic response analysis considering traveling

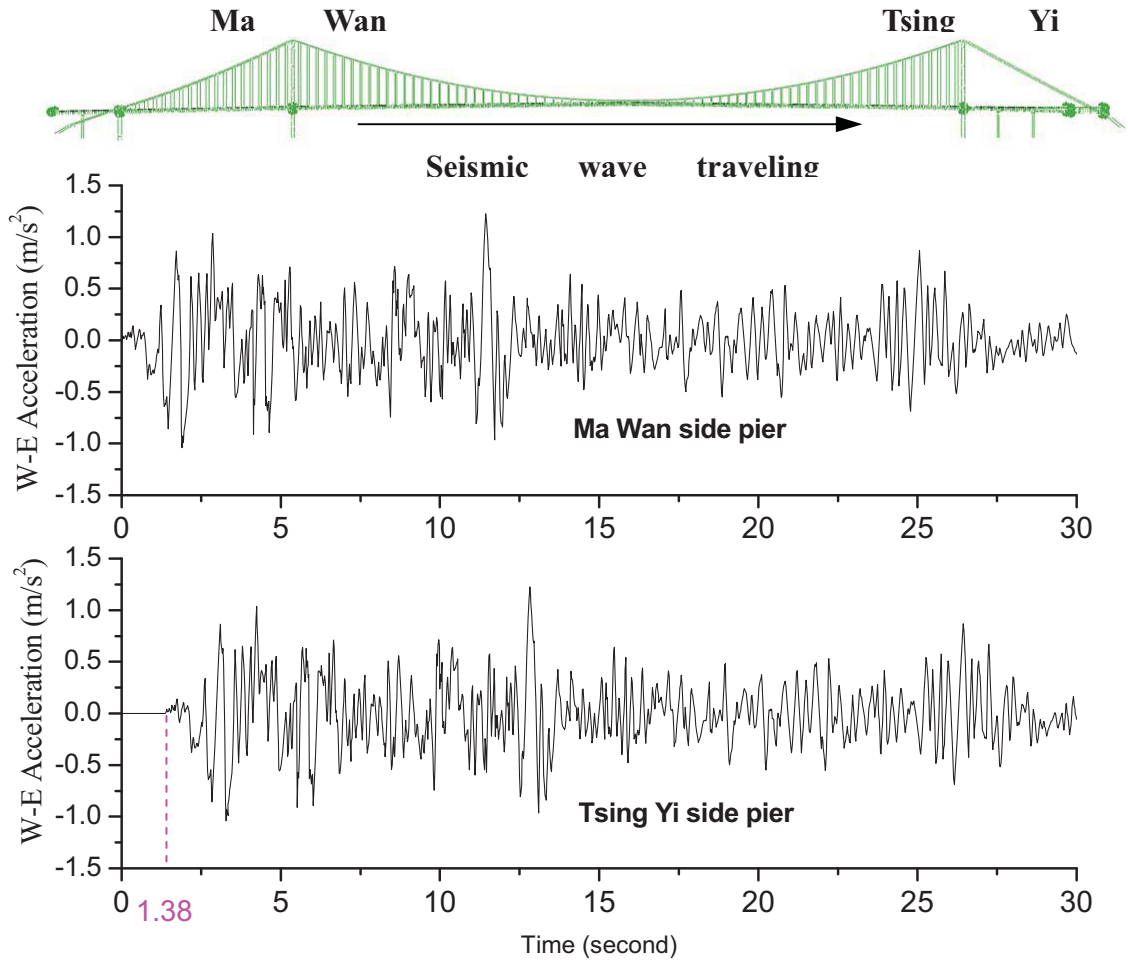

Figure 6.8 Schematic illustration of processing original data considering traveling wave effect

wave effect have been made as follows:

(1) Seismic wave travels from Ma Wan side to Tsing Yi side at the velocity of 1000 m/s.

(2) Traveling wave effect in this study is only used to illustrate the influence of phase differences of seismic wave on the pier supports, without taking the wave dissipation, amplitude decay and waveform change into account.

(3) Only the traveling wave effect on the longitudinal direction at the two

towers, namely, Ma Wan Tower and Tsing Yi Tower, are investigated in this study, regardless of traversal and vertical components and combination effect and other piers.

(4) The large mass method (LMM) (Leger *et al*. 1990) is adopted for regarding multi-support excitation and implemented by supplementing zero values to seismic wave before it reaches the other towers.

(5) The amplitude adjusted El-Centro wave is chosen as the ground motion input and duration period is 30 seconds with time step of 0.02s.

Table 6.4 Comparison of maximum internal forces at concerned locations between consistent excitation and traveling wave effect

Concerned locations			Loading cases			
			consistent excitation		non-consistent excitation (traveling wave effect with apparent velocity of 1000 m/s)	
			N (kN)	M (kNm)	N (kN)	M (kNm)
Steel girder of decking system	Mid-span		1.69E6	-86E3	-9.11E5	41.5E3
	Quarter-span		1.64E6	-26.5E3	1.64E6	-22.6E3
Bottom of towers	Ma Wan Side		-1.25E8	-2.42E9	-1.15E8	-1.48E9
	Tsing Yi Side		-1.34E8	2.06E9	-1.3E8	3.75E9
Lowest frame beam of towers	Ma Wan Side	M2	-	3.5E7	-	7.93E7
		M3	-	4.81E7	-	-6.79E7
	Tsing Yi Side	M2		4.68E7	-	4.55E7
		M3		6.02E7	-	-4.22E7

In this study, for the purpose of investigating the traveling wave effect on the seismic response of long-span bridge, the bridge is only longitudinally excited by adjusted El-Centro record. For the site specific ground motion, the apparent velocity of wave is taken as 1000 m/s, thus the time lag between two tower supports is 1.38s as shown in Figure 6.8. It is generally believed that when the apparent velocity increases, especially when it exceeds 2 to 3 km/s, the traveling effect decreases and finally reaches the situation of consistent excitation.

The maximum internal forces comparison at the concerned locations along the bridge between the consistent excitation and non-consistent excitation considering traveling wave with apparent velocity of 1000 m/s is carried out to evaluate the traveling wave effects on the seismic response of long-span bridge. As listed in Table 6.4, the comparison result shows that the internal forces of deck system at the mid-span and quarter-span are lower under the traveling wave situation than that by consistent excitation. The same result could be obtained at MW Tower while bending moment of TY Tower shows the opposite finding.

It can be seen from the preceding results that traveling wave has the very complex effects on different components of the bridge. Traveling wave effects make the dynamic responses increase at the certain locations while decrease at the others, so that there is no universal pattern or conclusion on determining how the traveling wave influence the seismic responses of bridge. The same result could be obtained for the traveling wave effect on the hot-spot stress distribution. Therefore, in this sense, the traveling wave effect is considered as case-specific

and should be particularly investigated for target bridge structure.

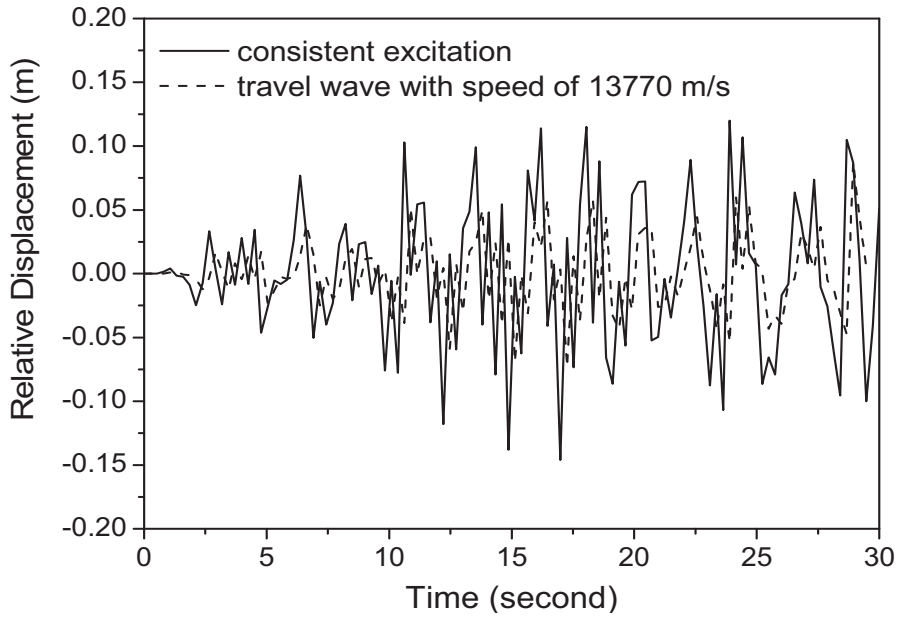

Figure 6.9 Relative vertical displacement-time history of mid-span under the consistent excitation and traveling wave

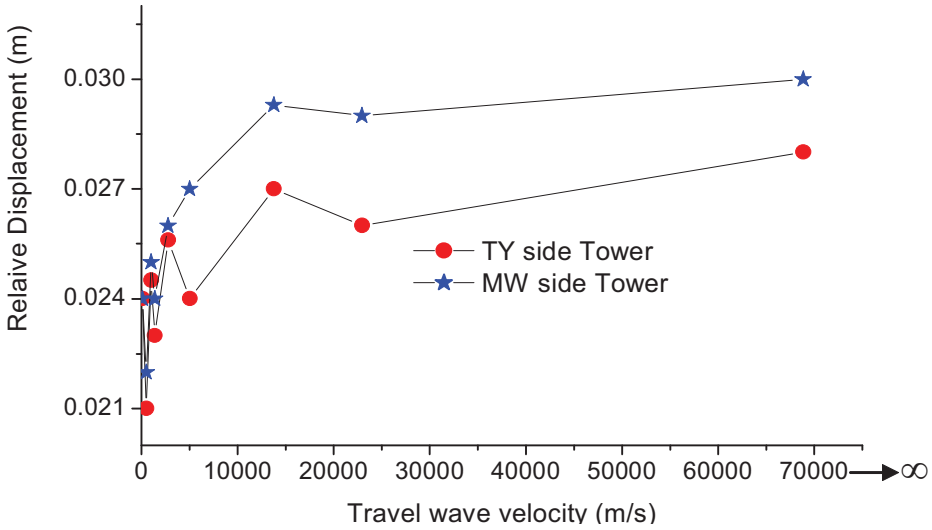

Figure 6.10 Relative longitudinal displacement of top of two towers with varying traveling wave

In order to study the seismic response of bridge with the varying velocity of traveling wave, the maximum relative displacement of tops of two towers and mid-span are tabulated in Table 6.5. The seismic wave velocity may significantly

Table 6.5 Relative displacement of key positions of TMB under traveling wave excitation with different apparent velocities

Apparent velocity of traveling wave (m/s)	Time lag (s)	Maximum longitudinal relative displacement of top of towers (mm)		Maximum relative displacement of mid-span at direction of (mm)	
		MW	TY	Longitudinal	Vertical
100	13.77	24.4	24.2	18.1	162
500	2.75	22.8	21.9	18.5	158
1000	1.38	25.4	24.5	18.7	155
1380	1.0	24.7	23.9	19.2	153
2750	0.5	26.5	25.6	19.8	148
5000	0.275	27.6	24.3	20.5	141
13770	0.1	29.3	27.2	20.8	139
22950	0.06	29.2	26.9	20.7	138
68850	0.02	30.1	28.1	21.1	136
Consistent excitation (∞)	0	29.8	27.8	20.9	135

vary with different circumstances, which would lead to the response changed accordingly. Figure 6.9 shows relative vertical displacement comparison of mid-span under the consistent excitation and traveling wave with 13370 m/s speed. It is also noted that the relative displacement is not monotonously increased with traveling wave speed growth as illustrated in Figure 6.10.

In summary, on the basis of aforementioned seismic response comparison under

the consistent excitation, the traveling wave effect is proven to be significant and considerably influences the seismic response of long-span bridges with respect to the structural global responses and local hot-spot stress distribution in some way. Moreover, the apparent velocity of traveling wave also affects the result to some extent. Therefore, the traveling wave effect should be further studied in details on the target long-span bridge specifically. In this case, the traveling wave effect must not be ignored. Furthermore, the apparent velocity of traveling wave highly depended on the ground site and may be changed with different circumstances. Unless the relatively precise data is available, it may be advisable for designers to select a range of possible velocities and to base their design on the most conservative result thus obtained.

6.3 NONLINEAR COMPUTING ALGORITHM WITH MULTI-SCALE MODEL

After the nonlinear dynamic response analysis has been performed with introducing simple constitutive equations, the relative complicated constitutive relationship could be also easily incorporated into the nonlinear computing algorithm. Moreover, the nonlinear computing algorithm on the basis of damage-induced constitutive formulation is further investigated and eventually proposed for future research.

6.3.1 Constitutive Formulation of Isotropic Unified Damage Law

Before the nonlinear seismic response analysis is fully carried out, the constitutive model of steel material should be selected as the basis of computation algorithm for nonlinear iteration procedure. Within the scope of continuum damage mechanics and irreversible thermodynamics, various forms of damage evolution laws are developed for the description of damage evolution behavior and deterioration process occurred in steel plastic deformation. The previous investigations agree that the ductile damage occurs at the steel structure when subjected to seismic loading without accounting for strain rate effect. Moreover, the isotropic damage constitutive model proposed by Lemaitre (1996) is commonly considered as being appropriate to describe the damage evolution procedure so that it has been widely used for its high computation accuracy and convenient expression combined with simple application. Lemaitre's constitutive model is composed of two elements, namely, strain-damage coupled constitutive equations and damage evolution laws. In this study, these formulas are rewritten in incremental forms in the framework of continuum damage mechanics and plasticity.

On the basis of description of the damage mechanics and the strain equivalent principles, the uni-axial laws of elasticity and plasticity of a damaged material have been derived, and four main relations which comprise the basis of damage mechanics could be written as follows (Lemaitre, 2005)

$$\begin{cases} \varepsilon_e = \dfrac{\sigma}{E(1-D)} & \text{for elasticity} \\ \left| \dfrac{\sigma}{(1-D)} - X \right| - R - \sigma_y = 0 & \text{as the plastic yield criterion} \\ \varepsilon_p < \varepsilon_{pD} \rightarrow \quad D = 0 & \text{as the damage threshold} \\ D = D_c \quad \rightarrow & \text{crack initiation} \end{cases}$$

where ε_e is elastic strain, E is elastic modulus of undamaged material, D is damage variable, σ_y is yield stress, R is stress due to isotropic hardening, X is the back stress ε_p is plastic strain, ε_{pD} is threshold value of plastic strain before microcrack initiation and D_c critical value of the damage at mesocrack initiation, respectively.

An important problem in the mechanics of material is the determining of an analytical expression for the state potential and potential of dissipation. The thermodynamics provides the general framework and some restrictions to ensure that the main variable governing the damage evolution or the damage rate ($\dot{D}$) is its associate variable (Y), the energy density release rate. Then the dissipative damage potential function (F_D) is primarily a function of Y. Many observations and experiments show that the damage is also governed by the plastic strain which is introduced through the plastic multiplier ($\dot{\lambda}$) as

$$\dot{D} = \dot{\lambda} \frac{\partial F_D}{\partial Y} \qquad \text{if} \quad p > p_D \quad \text{or} \quad max\omega_s > \omega_D \tag{6.17}$$

where p is the accumulated plastic strain, and Y is the elastic strain energy per

volume unit released at constant stress (due to damage increments in the form of the stiffness loss):

$$Y = \frac{(3/2)\sigma_{ij}{}^{D}\sigma_{ij}{}^{D}}{2E(1-D)^2} \cdot \left[\frac{2}{3}(1+\nu) + 3(1-2\nu)\left(\frac{\sigma_H}{\sigma_{eq}} \right)^2 \right] = \frac{\sigma_{eq}{}^{2}}{2E(1-D)^2} R_v = \frac{\tilde{\sigma}_{eq}^2}{2E} R_v \quad (6.18)$$

Given $\tilde{\sigma}_{eq} = \frac{\sigma_{eq}}{(1-D)}$ is the effective stress (corresponding to the effective resisting area $A(1-D)$, σ_{eq} is the Von-Mises equivalent nominal stress (corresponding to the nominal resisting area A). σ_{ij}^{D} is the deviatoric component of stress tensor, X_{ij}^{D} is the component of back stress tensor.

with $\dot{\lambda}$ calculated from the constitutive equations of (visco-) plasticity coupled with the damage deduced from the dissipative potential function (F)

$$F = f + F_X + F_D \quad (6.19)$$

Lemaitre's damage potential function can be expressed as:

$$F_D = \frac{Y^2}{2S(1-D)} \quad (6.20)$$

where S is damage energy strength, and Y is the elastic strain energy per volume unit released at constant stress.

The (visco-) plasticity loading function f is determined by the von Mises criterion

$$f = \left(\frac{\sigma}{1-D} - X \right)_{eq} - R - \sigma_y = \sigma_v \quad (6.21)$$

where

$$\left(\frac{\sigma}{1-D}-X\right)_{eq}=\sqrt{\frac{3}{2}\left(\frac{\sigma_{ij}^{D}}{1-D}-X_{ij}\right)\left(\frac{\sigma_{ij}^{D}}{1-D}-X_{ij}\right)}$$

σ_v is the viscous stress for viscoplasticity, $\sigma_v=0$ for plasticity

In the form of the normality rule as

$$\dot{\varepsilon}_{ij}^{p}=\dot{\lambda}\frac{\partial F}{\partial\sigma_{ij}}=\dot{\lambda}\frac{\partial f}{\partial\sigma_{ij}}=\frac{3}{2}\frac{\frac{\sigma_{ij}^{D}}{1-D}-X_{ij}}{\left(\frac{\sigma}{1-D}-X\right)_{eq}}\frac{\dot{\lambda}}{1-D} \tag{6.22}$$

coupled with the definition of the accumulated plastic strain rate, $\dot{p}=\sqrt{\frac{2}{3}\dot{\varepsilon}_{ij}^{P}\dot{\varepsilon}_{ij}^{P}}$

and of the evolution law for the variable r,

$$\dot{r}=-\ddot{\lambda}\frac{\partial F}{\partial R}=-\dot{\lambda}\frac{\partial f}{\partial R}=\dot{\lambda} \tag{6.23}$$

leads to $\dot{p}=\frac{\dot{\lambda}}{1-D}$

Therefore, the full damage constitutive equation is (Krajcinovic and Lemaitre 1987)

$$\begin{aligned}&\dot{D}=\left(\frac{Y}{S}\right)^{s}\dot{p}\quad if\quad max\,\omega_s>\omega_D\quad or\quad p>p_D\\&\dot{D}=0\quad if\quad not\\&D=D_c\rightarrow\quad mesocrack\quad ininiation\end{aligned} \tag{6.24}$$

where s is the material parameter that is function of the temperature.

$$\begin{cases} Y = \dfrac{\tilde{\sigma}_{eq}^2 R_v}{2E} \\ R_v = \dfrac{2}{3}(1+\nu) + 3(1-2\nu)\left(\dfrac{\sigma_H}{\sigma_{eq}}\right)^2 \end{cases} \quad \text{in the simplest case}$$

The complete analytical expression of the potential of dissipation is comprised of the damage potential defined by Equation (6.20) the plastic potential defined by Equation (6.21). Based on those formulas, Lemaitre constitutive model of isotropic ductile damage for steel material can be summarized as follow:

(1) Damage constitutive equations:

- Components of stress and strain tensors:

$$\sigma_{ij} = \sigma_{ij}^D + \frac{1}{3}\sigma_{kk}\delta_{ij} \qquad \sigma_H = \frac{1}{3}\sigma_{kk} \tag{6.25}$$

$$\varepsilon_{ij}^e = \varepsilon_{ij}^{eD} + \frac{1}{3}\varepsilon_{kk}^e\delta_{ij} \qquad \varepsilon_H^e = \frac{1}{3}\varepsilon_{kk}^e \qquad \varepsilon_{ij} = \varepsilon_{ij}^e + \varepsilon_{ij}^p \tag{6.26}$$

- Elastic damage constitutive equations:

$$\varepsilon_{ij}^e = \frac{1+\nu}{E}\cdot\frac{\sigma_{ij}}{1-D} - \frac{\nu}{E}\cdot\frac{\sigma_{kk}}{1-D}\delta_{ij} \tag{6.27}$$

- Plastic damage constitutive equations:

$$d\varepsilon_{ij}^p = \frac{3}{2}\frac{\left(\sigma_{ij}^D X_{ij}^D (1-D)\right)}{\left(\sigma_{ij}^D X_{ij}^D (1-D)\right)_{eq}}\cdot dp \tag{6.28}$$

(2) Damage evolution laws:

$$dD = \begin{cases} \dfrac{\sigma_{eq}^2}{2ES(1-D)^2} R_v dp & p \geq p_D \\ 0 & p < p_D \end{cases} \tag{6.29}$$

$$D = D_c \text{ and } \quad D_c = D_{1c} \frac{\sigma_u^2}{\left(\tilde{\sigma}^*\right)^2} \leq 1 \qquad \text{mesocrack initiation} \tag{6.30}$$

where σ_u is material ultimate strength, σ_{ij}^D is the stress deviator, p_D is the threshold of accumulated plastic strain, D_{1c} and D_c are the uni-axial and multi-axial critical damage value respectively.

As for the numerical analysis of damage, the adopted approaches could be divided into following categories: (1) uncoupled analysis; (2) fully coupled analysis; (3) locally coupled analysis and (4) semi-coupled analysis. For a large-span bridge structure with complicated configuration, the stress and damage states cannot be determined from an uncoupled analysis. Stress redistribution and stress tri-axiality changes induced by the damage may be a major accelerating factor towards structural failure. It is then necessary to solve the continuum mechanics equilibrium equations in a fully coupled manner with the elasto-(visco-) plasticity coupled with damage laws. The objective of this study is to investigate the damage evolution progress to obtain the real structural stress distribution situation considering the induced damage and material deteriorating. Accumulation of structural damage, to some extent, result in changing the material parameters and mechanical behavior as well as the stress and strain redistribution. It is required to consider the damage-related factor in stress-strain field during each integration steps in nonlinear analysis procedure. From this point of view, the fully coupled method is absolutely necessary and adopted in the analysis for the purpose of getting the closer stress distribution condition to the real situation. In this sense,

theories of mesomechanics and continuum damage mechanics are absolutely necessary to the multi-scale model for subsequent damage-related analyses.

6.3.2 Numerical Implementation for Nonlinear Response Analysis

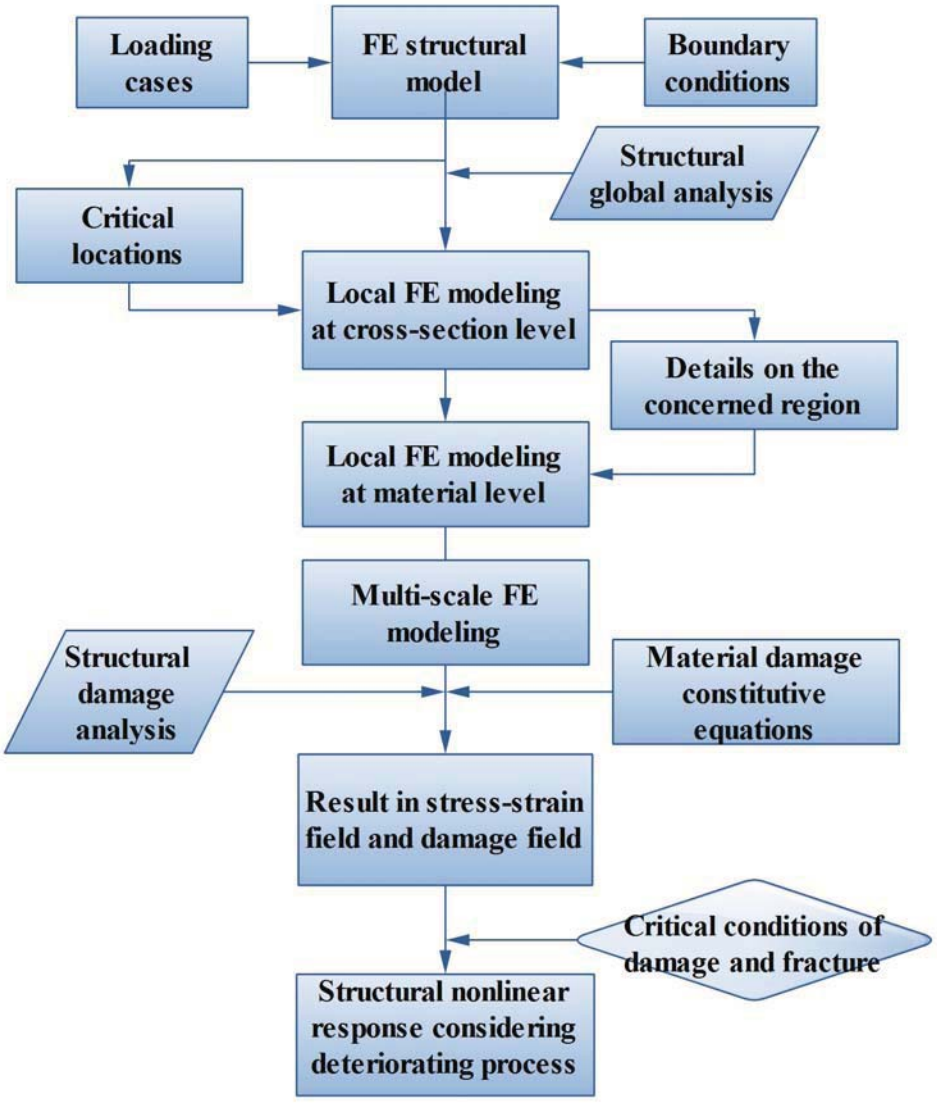

Figure 6.11 Procedure flowchart of structural nonlinear analysis by multi-scale model considering deteriorating process in term of material damage

The numerical calculation on structural dynamic response by considering damage evolution could be implemented on the basis of the general-purpose commercial

software ABAQUS, in which the function of subroutine UMAT is provided and allowed the user to define mechanical constitutive behavior of a material using the programming code for introducing new constitutive equations of the damaged material and damage evolution equations, and even make it possible to define any constitutive model of arbitrary complexity. The procedure of structural nonlinear analysis accounting for the deteriorating process in term of material damage could be described as Figure 6.11.

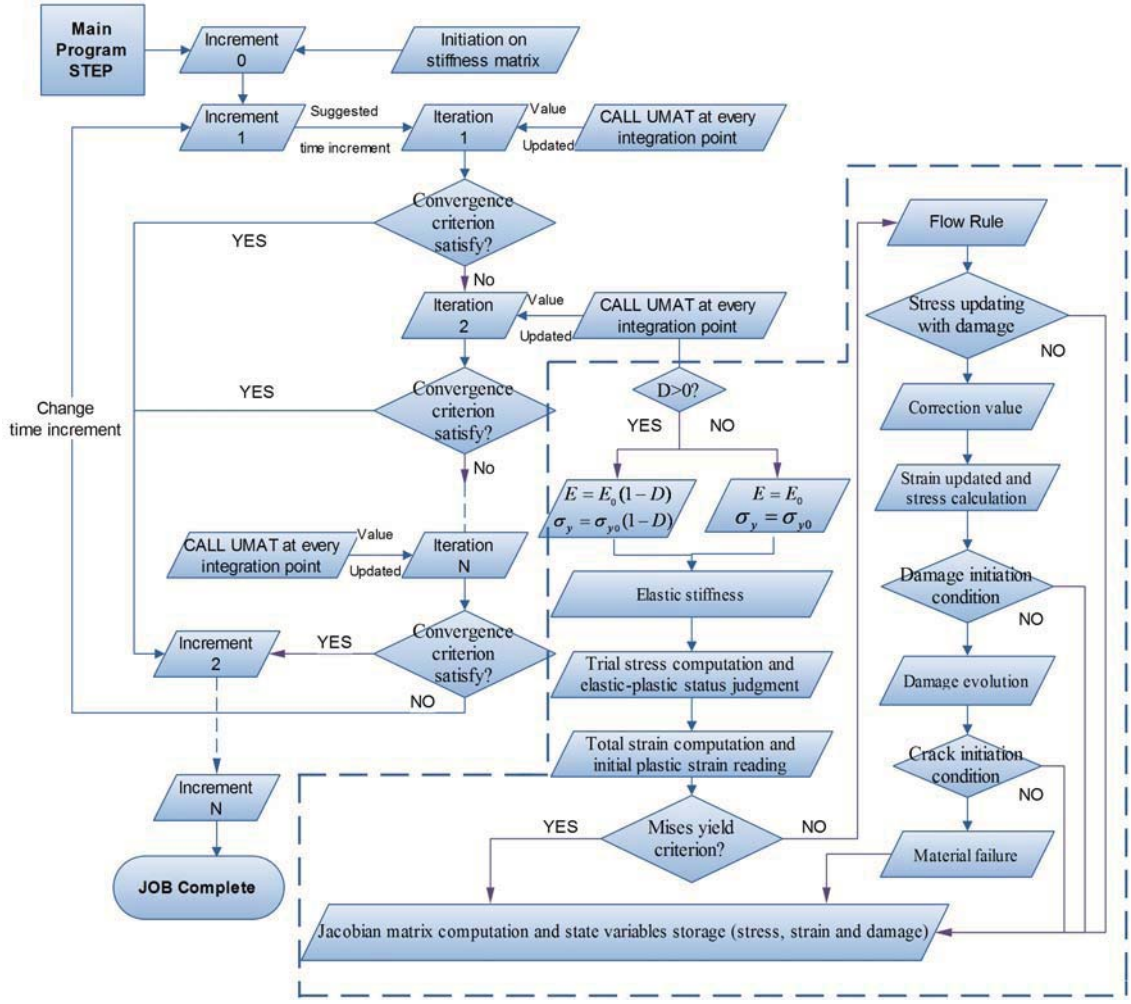

Figure 6.12 Implementation flowchart of material damage constitutive description on the basis of UMAT programming code

The damage-related material plasticity, damage threshold values and evolution laws can be incorporated into the mechanical constitutive model algorithm so that the user-defined subroutine could be called at material calculation points of elements for which the stresses and solution-dependent state variables are updated to the values at the end of each incremental step when it is called. Through the programming interface provided by ABAQUS, new damage constitutive models and numerical algorithms can be defined by user specifically and easily implemented. As shown in Figure 6.12 of implementation flowchart, the subroutine is repeatedly called (detailed process is shown inside the dashed line box) when solution-dependent state variable is needed to be updated in each iterative step. Those variables are then updated and transferred back to the main program through subroutine interface upon calling at every material integration point. The element tangent stiffness matrix and structural global stiffness matrix can be eventually modified to ensure iteration convergence and acquire correct solutions.

The detailed implementation procedure of UMAT subroutine can be divided into three steps regarding material plastic and damage state description, stress and damage increment solution, and the consistent tangent modulus matrix definition. In the first step, it is assumed to be within the elastic range so that only elastic constitutive relations are applied to compute the predictive value of stress and stress increment. If the predictive value of stress is larger than yielding strength, then material plastic and damage state can be acquired on the basis of yield

criterion, kinematic hardening rule and damage evolution law. Secondly, stress and damage increment is capable of being solved in accordance with existing strain increments and constitutive expressions. The radius return mapping algorithm based on the backward Euler method (integration algorithm) and Newton-Raphson iteration (solution algorithm) are adopted to guarantee high calculation accuracy and fast speed of convergence. Finally, the consistent tangent modulus matrix (known as Jacobian matrix) is formed and updated to replace continuum elastic-plastic modulus matrix in order to avoid the occurrence of pseudo-loading and pseudo-unloading phenomena.

6.3.3 General Procedure of Nonlinear Analysis with Multi-scale Model

Depending on the purpose of the analysis, one may choose from the possibilities of modeling a long-span bridge in one or more length scales to obtain the multi-scale model which is necessary for nonlinear history dependent systems since instantaneous material properties in the vicinity of the interconnect undergoing plastic deformation may vary in space and time due to their history dependence. On the basis of aforementioned multi-scale modeling strategy and implementation methods combined with nonlinear computing algorithms, the efficient model for carrying out the multi-scale numerical analyses of bridge response and local damage accumulation for the purpose of structural health evaluation is completed. In conclusion, the nonlinear analyzing procedure for the structural dynamic response and local damage accumulation of a long-span bridge

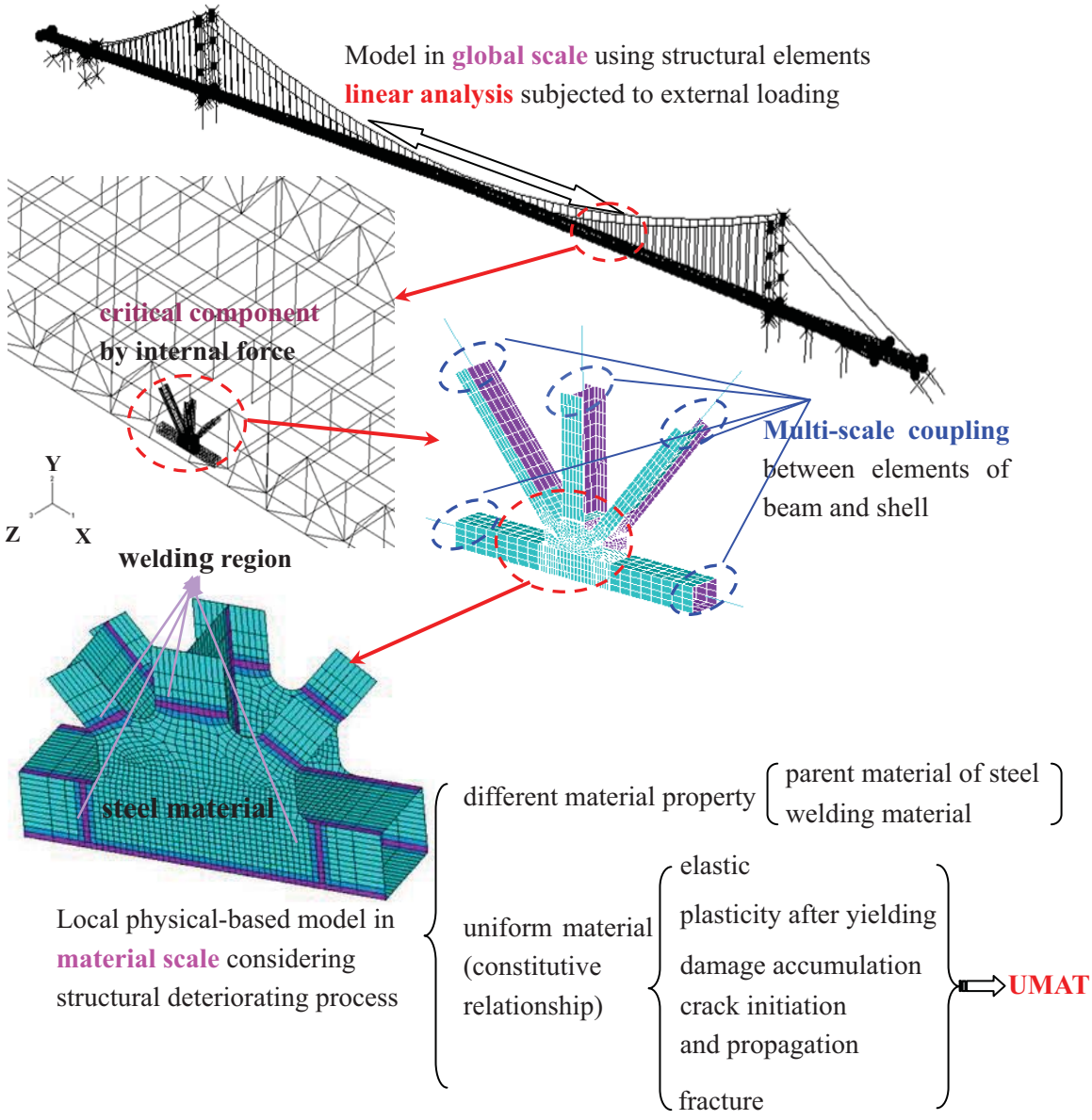

Figure 6.13 Schematic diagram of nonlinear computing algorithms using multi-scale model

could be summarized, as shown as Figure 6.13:

(1) The conventional FE model of the bridge using structural elements on a global scale is used for linear analyses of internal forces and nominal stress in the main components to determine the critical ones.

(2) The local detailed model including representation of critical components and local details is then further constructed on the component and material

scales respectively. The concerned details such as welding region, steel structural detailed configuration and so on, can be reflected in the local model, which makes it suitable for nonlinear analysis of hot-spot stress and damage-related study.

(3) The structural deteriorating process can be also simulated by the multi-scale model through considering various mechanical behavior, for instance, different material properties of steel welding, accumulative induced damage, the stress yielding to step into plasticity with various hardening laws, crack growth by introducing damage evolution or crack propagation law and even ultimate state of fracture. All those process should be feasible for numerical simulating by user-defined UMAT program.

To sum up, the multi-scale modeling strategy and methodology have been proposed and investigated. The corresponding multi-scale model of long-span suspension bridge is then developed. The multi-scale model could be extended for nonlinear analysis in combination with the nonlinear computing method to account for major effect of the damage and nonlinear influence on structural response.

The final nonlinear physical-based model is expected to be capable of simultaneously obtaining the structural response undertaking the linear analysis and local hot-spot stress distribution during deteriorating process which could be introduced a wide variety of nonlinear computing algorithms corresponding to

constitutive relationships. Up to now, the theoretical framework for nonlinear physical-based modeling of structural degradation behavior has been successfully completed.

The nonlinear computing method regarding the structural deteriorating process by introducing the material damage has been briefly introduced and attempted to explore. As a member of research team, Jiang (2010) has successfully applied the nonlinear computing method on the steel truss model fully constructed by solid elements to investigate the structural deteriorating process by introducing material damage. The external cyclic loading is artificially applied so that state between the elastic and plastic could be controlled arbitrarily. From this point of view, this nonlinear computing method combined with the desirable constitutive formulation is proven to be applicable and feasible. In this dissertation, only the damage-induced nonlinear computing algorithm is attempted to be proposed and has not implemented by case study. It has beyond the scope of this study and leaves it for the future research.

6.4 SUMMARY

The nonlinear physical-based model is considered as absolutely necessary for the fatigue damage analyses of large-span cable-supported bridge considering the deteriorating process. The developed multi-scale model of TMB can be extended for nonlinear numerical analysis. Geometric nonlinearity could be considered in

calculation while material nonlinearity is taken into account by introducing the constitutive relationship for steel material. As the case study of nonlinear calculation by multi-scale model, the linear and nonlinear seismic responses of TMB under El-Centro earthquake wave are investigated. Traveling wave has the complex and significant effects on the seismic responses of long-span bridges.

The implementation ways for damage-related nonlinear analyzing procedures have been explored by introducing the constitutive equations combined with proper damage laws to consider the structural deteriorating process. The entire nonlinear calculation procedures associated with corresponding algorithms are also proven to be feasible. However, the nonlinear computation method summarized in this study just point out a direction and corresponding implementation way as reference for further research on nonlinear fatigue damage analyses using multi-scale model. Meanwhile, the detailed implementation steps for case study are beyond the scopes of this study and left for future research.

CHAPTER 7

CONCLUSIONS AND RECOMMENDATIONS

7.1 CONCLUSIONS

The efforts performed in this thesis aims to develop an efficient numerical approach for multi-scale modeling of long-span bridges for the purpose of structural health evaluation and demonstrate its efficiency by including some analytical and experimental case studies as well as the practical engineering application. The strategies and methodologies of multi-scale modeling of long-span bridges have been successfully developed. An experimental study on the steel truss specimen in combination with the analytical comparison with different modeling methods have been carried out to validate the proposed multi-scale modeling strategy. Then it is further applied to the long-span suspension Tsing Ma Bridge to build the corresponding multi-scale model, based on which the global response of the bridge and local hot-spot stress distribution of concerned locations could be simultaneously obtained. This model can be further extended for nonlinear analysis by introducing the nonlinear computing algorithm and for the subsequent damage-related analyses.

Based on the results from this study, the specific conclusions could be obtained as follows:

1. A concurrent multi-scale model including the representations of the global structural configuration and local concerned regions in details is considered as absolutely necessary for a nonlinear time history depending system in order to evaluate the possible damage condition and the structural health state of engineering structures.

2. The multi-scale modeling strategies and methodologies are successfully developed and numerically implemented by introducing the mixed dimensional coupling method using multi-point constraint equations. General implementation procedure of multi-scale modeling is then summarized. This coupling method has been verified to be accurate and efficient when compared with results from other types of models in the analytical case study of both determinate and indeterminate structures.

3. An experimental study on a scaled down steel truss specimen with typical welded details is carried out to validate multi-scale modeling strategy and methods by laboratory test. Comparison of dynamic and static responses between the calculated results by different models indicates that the proposed multi-scale model is found to be the most efficient and accurate. Having performed the procedures of model updating and verification, the multi-scale model is considered as the baseline model to be the closest to

the prototype of the structure.

4. After the successful verification and validation of proposed multi-scale modeling strategy and implementation methods on scaled down steel truss specimen in laboratory, this coupling method is then applied to full-scale bridge structure to build the multi-scale model of TMB. By using this model, structural global response at component scale and the hot-spot stress distribution of critical locations at local scale level are obtained simultaneously so that they can be used for structural health assessment and subsequent damage-related analyses. The concurrent multi-scale modeling method has been proven to be superior as compared to the traditional two-step analyzing method.

5. In order to demonstrate the multi-scale model can be further extended for nonlinear analysis, the linear and nonlinear seismic responses of TMB under the El-Centro ground motion are investigated with consideration of geometric nonlinearity and bilinear hysteretic constitutive model. Traveling wave has complex and significant effects on the seismic responses of long-span bridges and no universal principles to describe the influence pattern so that such effects should be specifically investigated for an individual bridge. The schemes for implementation for damage-related nonlinear analyzing procedures have been explored and outlined by introducing a nonlinear computing algorithm of constitutive equations combined with proper damage laws to consider the structural deterioration

process.

6. It should be noticed that some conditions and simplifications have been assumed in the process of multi-scale modeling and numerical analyses. Only the typical widely-used coupling situation of connecting shell element with beam element is investigated in this study. Meanwhile, the simplest situation of one local model of detailed connection incorporated in multi-scale model is adopted for strategy study in this thesis. Although it is successful, the conclusions reached in this study are limited and case-specific. There are much more work in the research area should be conducted in the future because of the significant advancement made in the project.

In conclusion, the research efforts performed in this thesis have successfully proposed the efficient and accurate multi-scale modeling strategy and corresponding implementation methods. Also they are verified and validated by the analytical case study and laboratory test. After applied to real bridge structure, the developed multi-scale model of TMB is able to simultaneously provide the information about structural global response and hot-spot stress distribution of local concerned details that could be used for structural health assessment. Moreover, the feasible scheme of implementation for damage-related nonlinear analyzing procedures using multi-scale model have been explored and clearly outlined by introducing the constitutive equations combined with proper damage laws to consider the structural deterioration process. On the basis of above

achievements, it is evident that the research work involved in this study has completely accomplished the aforementioned three research objectives and also shown the explicit way for future research direction and implementation method of applying multi-scale modeling to nonlinear analyzing procedure.

7.2 RECOMMENDATIONS

Although the above proposed objectives have been successfully accomplished during the research period, it is only the first step for completing the investigation on multi-scale modeling and corresponding fatigue damage analyses for engineering structures. There are relevant research studies could be further carried out to improve the integrity, reliability and accuracy of the strategies and implementation methods. On the basis of outcomes and findings aforementioned, potential for further development of the research and the proposed course of action would be outlined as follows:

1. The adopted mixed dimensional coupling method has been proven to be able to provide satisfactory results within the allowable engineering error range. However, the analyzing accuracy at the interface amongst different dimensional structural elements could be further enhanced. In addition, the coupling algorithms are particularly applicable to coupling situation of beam elements with shell elements. In other words, other than this specific situation, there are other various coupling situations which should be

further studied in the subsequent research activities.

2. The nonlinear computing method associated with constitutive formulation of isotropic damage law has been proposed and this method is also proven to be feasible. Nevertheless, the implementation procedure of nonlinear calculation accounting for material damage could be performed on the shell element as a follow up of the present study. The corresponding UMAT codes could be further programmed to fit all kinds of elements for considering structural deteriorating process by material damage.

3. In this study, the term of “multi-scale” in this study specifically refers to different levels of length scale. However, the deterioration is actually a process in which the long-term behavior of slow degradation of material properties together with the short-term damage due to overloading, implying that the corresponding fatigue analyses should be performed in the multiple temporal scales. Therefore, another aspect of “multi-scale” definition could be transferred from space to time so that the research activities with respect to the multi-scale modeling on time-scale would be carried out in a new interest area. The ideal multi-scale formulation and procedures for the numerical analyses should be based on the model in multiple temporal and spatial scales of a large structure.

4. The corresponding general implementation procedure proposed for the large-span bridge structures and all the findings are directly drawn from the

case study of a specific suspension bridge. As for a different configuration type of cable-supported bridges, e.g. a cable-stayed bridge, the results would be varied which is deserved to carry out further investigation. Moreover, the further research could be conducted on how to make full use of the possible outcome from this study to provide useful information for authorities to make cost-effective decisions regarding inspection, maintenance and repairs in both after construction and during the design period.

5. Nominal stress on structural component and hot-spot stress distribution on critical region could be simultaneously obtained in multi-scale numerical analysis. When applied the proper loading case scenarios combined with monitoring data from the SHM, the multi-scale model could predict the stresses at the critical location where there are no sensors installed. With those stress information, the structural health status could be then accurately evaluated.

6. On the basis of preceding study, one could be trying to propose a rational and practical approach of SHA for the state or damage diagnosis of long-span steel bridges. The assessment will be similar to procedure of fatigue life assessment. Success in this endeavor is possible since nonlinear physical-based methods have significant potential in structural health assessment when compared with other linear and vibration-based methods which depend on the lower frequency global modes so that somewhat

insensitive to local damage. Therefore, on the basis of the updated nonlinear physical-based model of bridge structures and the stress information acquired by the SHM and interpreted stresses from the developed model, a rational definition of Health Assessment Indicator (HAI), instead of Damage Index (DI), describing the health state of a structure will be established for the purpose of state assessment of bridge components. Strategies for the state assessment or damage diagnosis of long-span bridges will eventually be proposed.

REFERENCE

Abdel Wahab, M. M. (2001), "Effect of modal curvatures on damage detection using model updating", *Mechanical Systems and Signal Processing*, 15(2), 439-445.

Abdel-Ghaffar, A. M., and Scanlan, R. H. (1985), "Ambient vibration studies of Golden Gate Bridge-I: suspended structure", *Journal of Engineering Structures*, 111(4), 463-482.

Adams, V. and Askenazi, A. (1999), *Building Better Products with Finite Element Analysis*, On Word Press, Santa Fe, New Mexico.

Ahmadian, H., Mottershead, J. E. and Friswell, M. I. (2002), "Physical realization of generic-element parameters in model updating", *Journal of Vibration and Acoustics*, *Transaction of ASME*, 124, 628-633.

Agerskov, H. and Nielsen, J. A. (1999), "Fatigue in steel highway bridge under random loading", *Journal of Structural Engineering*, ASCE, 125, 152-162.

Alfaro, M. V. C., Suiker, A. S. J. and Borst, R. (2011), "*Multiscale modeling of the failure behavior of fiber-reinforced laminates*", Multiscale Methods in Computational Mechanics, Lecture Notes in Applied and Computational Mechanics, R. de Borst and E. Ramm (edts.), Springer Science and Business Media B.V., 233-259.

Aktan, A. E., Catbas, F. N., Grimmelsman, K. A. and Pervizpour, M. (2002), "Development of a model health monitoring guide for major bridges", *Final*

Report to Federal Highway Administration, Dexrel Intelligent Infrastructure and Transportation Safety Institute, Dexrel University, USA.

Atkan, A. E., and Gosselin, S. R. (edt.) (2000), *Proceedings of SPIE's International Symposium on NDE and Health Monitoring and Diagnostics, Nondestructive Evaluation of Highways, Utilities and Pipelines.*

Aktan, A. E., Grimmelsman, K. A. and Helmicki, A. J. (1998), "Issues and opportunities in bridge health monitoring", *Proceeding of 2nd World Conference on Structural Control*, June 28-July 2, Kyoto, Japan, 2359-2368.

Aktan, A. E., Farhey, D. F., Brown, D. L., Dalal, V., Helmicki, A. J., Hunt, V. J., Shelley, S. J. (1996), "Condition assessment for bridge management", *Journal of Infrastructure Systems*, ASCE, 2(3), 108-117.

Aktan, A. E., Farhey, D. N., Helmicki, A. J., Brown, D. L., Hunt, V. J., Lee, K. L., Levi, A. (1997), "Structural identification for condition assessment: experimental arts", *Journal of Structural Engineering*, ASCE, 123(12), 1674-1684.

Aktan, A. E., Catbas, N., Turer, A., Zhang, Z. (1998), "Structural identification: analytical aspects", *Journal of Structural Engineering,* ASCE, 124(7), 817-829.

ANSYS Release 8.1, ANSYS Inc., 2004.

Armstrong, Bridgett, Donaghy, McCune, McKeag and Robinson (1998a), "Techniques for interactive and automatic idealization of CAD models", *Proceedings of 6th International Conference on Numerical Grid Generation in Computational Field Simulations*, July 1998, London, 643-662.

Armstrong, McCune and Robinson (1998b), "Multi-dimensional analysis modeling", *Proceedings of 6th ACME Annual Conference on Computational Mechanics in UK*, 47-50.

ASTM E 1049-85 (Reapproved 2005), *Standard Practices for Cycle Counting in Fatigue Analysis*, ASTM International.

Auweraer, H. V. D., and Peeters, B. (2003), "International research projects on structural health monitoring: an overview", *Structural Health Monitoring*, 2(4), 341-358.

Bai, Y. L., Wang, H. Y., Xia, M. F. (2005), "Statistica1 mesomechanics of solid 1inking coupled multiple space and time scales", *Applied Mechanics Reviews*, 58, 372-388.

Balageas, D. L. (edt.) (2002), "Structural Health Monitoring 2002", *Proceedings of the 1st European Workshop on Structural Health Monitoring*, DEStech, Lancaster, Pennsylvania, USA.

Baruch. M. (1978), "Optimization procedure to correct stiffness and flexibility matrices using vibration tests", *AIAA Journal*, 16(11), 1208-1210.

Bazant, Z. P., Chen, E. P. (1997), "Scaling of the structural failure", *Appl. Mech. Rev.* 50(10), 593-627

Berman, A. and Nagy, E. J. (1983), "Improvement of large analytical model using test data", *AIAA Journal*, 21(8), 1168-1173.

Bernhard A. S., Francesco P. and Dariusz G. (2011), "Multi-scale/multiphysics model for concrete", *Multiscale Methods in Computational Mechanics*, Lecture Notes in Applied and Computational Mechanics, R. de Borst and E. Ramm (edts.), Springer Science and Business Media B.V., 381-404.

Bhattacharya, B., Ellingwood, B. (1998), "Continuum damage mechanics analysis of fatigue crack initiation", *International Journal of Fatigue*, 20(9), 631-639.

Boller, C., and Staszewski, W. J. (edts.) (2004), *Structural Health Monitoring 2004*, *Proceedings of the 2nd European Workshop on Structural Health Monitoring*, DEStech, Lancaster, Pennsylvania, USA.

Boonyapinyo, V., Yamada, H. and Miyata, T. (1994), "Nonlinear structural instability of long-span cable-stayed bridges under gravity and wind loads", *Journal of Structural Engineering*, 40A, 295-308.

Brandt, A. (2001), "Multiscale scientific computation: review 2001", *Multiscale and Multiresolution Methods: Theory and Applications*, T. J. Barth, T. F. Chan, and R. Haimes, edts., Springer Verlag, Heidelberg.

Brock, J. E. (1968), "Optimal matrices describing linear systems", *AIAA Journal*, 6(7), 1292-1296.

Broughton, J. Q., Abraham, F. F. (1999), "Concurrent coupling of length scales: methodology and application", *Physics Review. B.*, 60(4), 2391-2403.

Brownjohn, J. M. W., Xia, P. Q., Hao, H., Xia, Y. (2001), "Civil structure condition assessment by FE model updating: methodology and case studies", *Journal of Finite elements in analysis and design*, 37, 761-775.

BSI, BS5400: Part 10, *Code of Practice for Fatigue*, 1982.

BSI, BS7608, *Code of Practice for Fatigue Design and Assessment of Steel Structures,* 1993.

Carden, E. P., and Fanning, P. (2004), "Vibration based condition monitoring: a review", *Structural Health Monitoring*, 3(4), 355-377.

Catbas, F. N., Atkan, A. E. (2002a), "Vibration based condition monitoring: a review", *Structural Health Monitoring*, 3(4), 355-377.

Catbas, F. N., Atkan, A. E. (2002b), "Condition and damage assessment issues and some promising indices", *Journal of Structural Engineering*, 128(8), 1026-1036.

Chaboche, J. L., Lesne, P. M. (1988), "A non-linear continuous fatigue damage model", *Fatigue and Fracture of Engineering Materials and Structures*, 11(1), 1-7.

Chan, T. H. T., Law, S. S. and Yung, T. H. (2000a), "Moving force identification using an existing pre-stressed concrete bridge", *Engineering Structures*, 22(10), 1261-1270.

Chan, T. H. T., Ko, J. M. and Li, Z. X. (2000b), "Fatigue analysis for bridge-deck sections under blocked cycles of traffic loading", *Nondestructive Evaluation of Highways, Utilities, and Pipelines IV*, *Proceedings of SPIE,* March 7-9 2000, 3995, Aktan, A.E. and Gosselin, S.R. edts., 358-369.

Chan, T. H. T., Li, Z. X., Ko, J. M. (2001a), "Fatigue analysis and life prediction of the bridges with health monitoring data-Part II: application", *International Journal of Fatigue*, 23(1), 55-64.

Chan, T. H. T., Ko, J. M., Li, Z. X. (2001b), "Fatigue evaluation for Tsing Ma Bridge using structural health monitoring data", *Proceedings of SPIE - The International Society for Optical Engineering*, 4337, Mar. 6-8 2001, 335-346.

Chan, T. H. T., Guo, L., and Li, Z. X. (2003), "Finite element modeling for fatigue stress analysis of large suspension bridges", *Journal of Sound and Vibration*, 261, 443-464.

Chan, T. H. T., Zhou, T. Q., Li, Z. X., Guo, L. (2005), "Hot spot stress approach for Tsing Ma Bridge fatigue evaluation under traffic using finite element method", *Structural Engineering and Mechanics*, 19(3), 261-279.

Chan, T. H. T., Yu, Y., Wong, K. Y., Guo, L. (2007), "A multi-scale finite element model of Tsing Ma Bridge for hot spot stress analysis", *Proceeding of International Conference on Health Monitoring of Structure, Material and Environment*, Oct.16-18, 2007, Southeast University, Nanjing, China, 130-140.

Chan, T. H. T., Yu, Y., Wong, K. Y. and Li, Z. X. (2008), "Condition-assessment-based finite element modeling of long-span bridge by mixed dimensional coupling method", *Proceedings of the 3rd World Congress on Engineering Asset Management and Intelligent Maintenance System (WCEAM-IMS 2008)*, October 27-30 2008, Beijing China, 260-270.

Chan, T. H. T., Li, Z. X., Yu, Y., Sun, Z. H. (2009), "Concurrent multi-scale modeling of civil infrastructures for analyses on structural deteriorating-Part II: model updating and verification", *Journal of Finite Element in Analysis and Design*, 45(11), 795-805.

Chan, T. H. T., Wong, K. Y., Li, Z. X. and Ni, Y. Q. (2011), "Structural Health Monitoring for Long Span Bridges-Hong Kong Experience & Continuing onto Australia", Chapter 1 in *Structural Health Monitoring in Australia*, edited by Chan, T. H. T. and Thambiratnam, D. P., Nova Publishers.

Chang, F. K. (edt.) (1997), "Structural Health Monitoring–Current Status and Perspective", *Proceedings of the 1st International Workshop on Structural Health Monitoring*, Techinomic, Lancaster, Pennsylvania, USA.

Chang, F. K. (edt.) (1999), Structural Health Monitoring 2000, *Proceedings of the 2nd International Workshop on Structural Health Monitoring*, Techinomic, Lancaster, Pennsylvania, USA.

Chang, F. K. (edt.) (2001), "Structural health monitoring–the demands and challenges", *Proceedings of the 3rd International Workshop on Structural Health Monitoring*, CRC Press, Boca Raton, Florida, USA.

Chang, F. K. (edt.) (2003), "Structural health monitoring–from diagnostics & prognostics to structural health management", *Proceedings of the 4th International Workshop on Structural Health Monitoring*, DEStech, Lancaster, Pennsylvania, USA.

Chang, F. K. (edt.) (2005), "Structural health monitoring–advancements and challenges for implementation", *Proceedings of the 5th International Workshop on Structural Health Monitoring*, Stanford University, USA.

Chang, P. C., Flatau, A. and Liu, S. C. (2003), "Review paper: health monitoring of civil infrastructure", *Structural Health Monitoring*, 2(3), 257-267.

Chen, J. C., Garba, J.,A. (1980),"Analytical model improving using modal test results", *AIAA Journal*, 18(6), 684-690.

Chen, J. C., Kuo, C. P., Garba, J. A. (1983), "Direct structural parameter identification by modal test results", *AIAA Paper*, 44-49.

Cheung, Y. K. (edt.) (2000), *Proceedings of the International Workshop on Research and Monitoring of Long Span Bridges*, Hong Kong.

Choi, S., and Stubbs, N. (2005), "Damage identification in structures using the time-domain response", *Journal of Sound and Vibration*, 275, 577-590.

Chong, L., and Ray, L. B. (2002), "Whole-istic biology," *Science*, 295(5560), 1661.

Chong, K. P. (2005), "NSF research in mechanics, computational and other areas", *Multi-scale Damage Related to Environment Assisted Cracking*, Sih, G. C.， Tu, S. T., Wang, Z, edts., 323-332.

Chong, K. P. (2007), "Nano mechanics and multi-scale problems", *Proceedings of the 5th International Conference on Nonlinear Mechanics,* June 2007, Shanghai, 13-18.

Cobb, R. G. and Liebst, B. S. (1997), "Structural damage identification using assigned partial eigenstructure", *AIAA Journal*, 35(1), 152-158.

Collins, J. D., Hart, G. C., Hasselman, T. K. and Kennedy, B. (1974), "Statistical identification of structures", *AIAA Journal*, 12(1), 185-190.

Cunha, A., Caetano, E., Delgado, R. (2001), "Dynamic tests on large cable-stayed bridge", *Journal of Bridge Engineering*, 1, 54-62,

Curtin, W. A., and Miller, R. E. (2003), "Atomistic/continuum coupling in computational materials science", *Modell. Simul. Mater. Sci. Eng.*, 11, 33-68.

Dailey, R. L. (1988), "Eigenvector derivatives with repeated eigenvalues", *AIAA Journal*, 27, 486-491.

Da´vila, C. G. (1994), "Solid-to-shell transition elements for the computation of interlaminar stresses", *Computing Systems in Engineering*, 5(2), 193-202.

Deng, Y., Li, A.Q., Ding, Y. L., Sun, J. (2008), "Damage location identification for a super-long-span cable-stayed bridge based on structural multi-scale analysis", *Journal of Disaster Prevention and Mitigation Engineering*, 28(3), 268-273.

Ding, Y. L., Li, A.Q., Miao, C. Q., Li, Z. X., Han, X. L. (2006), "Multi-level finite element modeling of long-span bridges for structural damage diagnosis and safety evaluation", *Earthquake Engineering and Engineering Vibration*, 26(2), 66-72.

Ding, Y. L., Li, A.Q., Miao, C. Q. (2007), "Multi-scale damage analysis for steel box girder of long-span cable-stayed bridges", *Engineering Mechanics*, 24(7), 99-121.

Ding, Y. L., Li, A.Q., Du, D. S., Liu, T. (2010), "Multi-scale damage analysis for a steel box girder of a long-span cable-stayed bridge", *Structure and Infrastructure Engineering*, 6(6), 725-739.

Doebling, S. W. (1996), "Minimum-rank optimal update of elemental stiffness parameters for structural damage identification", *AIAA Journal*, 34, 2615-2621.

Doebling, S. W., Farrar, C. R., Prime, M. B., Shevitz, D. W. (1996), "Damage identification and health monitoring of structural and mechanical systems from changes in their vibration characteristics: a literature review", *Los Alamos National Laboratory report*, LA-13070-MS.

Doebling, S. W., Farrar, C. R., Prime, M. B., (1998), "A summary review of vibration-based damage identification methods", *Shock and Vibration Digest*, 30(2), 91-105.

Doherty, J. E. (1987), *Nondestructive Evaluation*, in Handbook on Experimental Mechanics, A. S. Kobayashi (edts.), Society for Experimental Mechanics.

Dowling, N.E. (1972), "Fatigue failure predictions for complicated stress-strain history", *Journal of Materials*, JMLSA, 7(1), 71-87.

Downing, S. D., Socie, D. F. (1982), "Simple rainflow counting algorithms", *International Journal of Fatigue*, 4(1), 31-40.

Duan, Y. F., Xu, Y. L., Fei, Q. G., Wong, K. Y., Chan, K. W. Y., Ni, Y. Q. (2006), "Full 3D finite element model for criticality analysis of Tsing Ma Bridge", *Proceedings of International Conference on Bridge Engineering — Challenges in the 21st Century, Hong Kong.*(in CD format)

Duchêne, L. and Habraken, A. M. (2007), "Multi-scale approaches", *Advances in material forming: Esaform 10 Years on*, Springer 2007, 125-141.

Dumanoglu, A. A., and Stevern, R. T. (1989), "Seismic response of modern suspension bridges to asynchrous longitudinal and lateral ground motion", *Proc., Instn. Civ. Engrs*., London, Part 2, 73-86.

Enright, M. P., Frangopol, D. M. (1998), "Service-life prediction of deteriorating concrete bridges", *Journal of Structural Engineering*, 124(3), 309-317.

Enright, M. P., and Frangopol, D. M. (2000), "Reliability based lifetime maintenance of aging highway bridges", *Proceedings of SPIE's 6th International Symposium on NDE and Health Monitoring and Diagnostics. Nondestructive Evaluation of Highways, Utilities and Pipelines*, Aktan, A. E. and Gosselin, S. R. (edts.), International Society for Optical Engineering, Bellingham, Wash., 3995, 4-13.

Fan, R. (2009), "Multiscale methods for material failure simulations", *PhD Dissertation*, Rensselaer Polytechnic Institute, NY, USA.

Farhat, C., and Hemez, F. M. (1993), "Updating finite element dynamic models using an element-by-element sensitivity methodology", *AIAA*, 31(9), 702-711.

Farrar, C. R., and Doebling, S. W. (1999), "Damage detection-II: field application to large structures", In: Silva, J. M. M and Maia, N. M. M. (edts.), *Modal analysis and testing*, NATO Science Series, Dordrecht, Netherlands: Kluwer Academic Publishers.

Farrar, C. R., Sohn, H. and Doebling, S. W. (2000a), "Structural health monitoring at Los Alamos National Laboratory", *The 13th International Congress and Exhibition on Condition Monitoring and Diagnostic Engineering management* (COMADEM 2000), Houston, TX, USA, Dec. 3-8.

Farrar, C. R., Sohn, H. (2000b), "Pattern recognition for structural health monitoring", *Los Alamos National Laboratory Report*, Los Alamos, NM 87545.

Farrar, C. R., Doebling, S. W. (1997), "An overview of modal-based damage identification methods", *Proceedings of the DAMAS Conference*, Sheffield, UK, June 1997.

Farrar, C. R., Sohn, H., Fugate, M. L., Czarnecki, J. J. (2001a), "Integrated structural health monitoring", *SPIE's 8th Annual International Symposium on Smart Structures and materials*, Newport Beach, CA, March 4-8.

Farrar, C. R. and Sohn, H. (2001b), "Condition/damage monitoring methodologies, Invited Talk", *The Consortium of Organization for Strong Motion Observation System (COSMOS) Workshop*, Emeryville, CA, Nov. 14-15.

Farrar, C. R., and Doebling, S. W. (2001c), "Vibration-based structural damage identification", *Philosophical Transactions: Mathematical, Physical and Engineering Sciences*, 359, 131-149.

Fatemi, A., Yang, L. (1998), "Cumulative fatigue damage and life prediction theories: a survey of the state of the art for homogeneous materials", *International Journal of Fatigue*, 20(1), 9-34.

Federal Highway Administration (FHWA) (2001), "Reliability of visual inspection", *FHWA Rep. Nos. FHWA-RD-01-020 and FHWA-RD-01-021*.

Fisher, J. W., *et al*. (1980), "Fatigue behavior of full-scale welded bridge attachments", *NCHRP Report 227*, National Academy Press, Washington DC, November 1980.

Fisher, J. W., *et al*. (1983), "Steel bridge members under variable amplitude long life fatigue loading", *NCHRP Report 267*, National Academy Press, Washington D.C.

Fisher, J. W. (1984), *Fatigue and Fracture in Steel Bridges: Case Study*, John Wiley Sons.

Fisher, J. W. (1987), "Fatigue and fracture evaluation for rating riveted bridges", *NCHRP Report 302*, National Academy Press, Washington D.C.

Fisher, J. W., *et al*. (1993), "Resistance of welded details under variable amplitude long-life fatigue loading", *NCHRP Report 354*, National Academy Press, Washington D.C.

Fish, J., Shek, K. (2000), "Multiscale analysis for large scale nonlinear structures and materials", *International journal for computational Civil and Structural Engineering*, 1(1), 79-90.

Fish, J. (2007), "Discrete-to-continuum multiscale bridging", *Multiscaling in Molecular and Continuum Mechanics: Interaction of Time and Size from Macro to Nano*, Sih, G. C. (edt.), springer, 85-102.

Fish, J. (2011), "Multi-scale modeling and simulation of composite materials and structure", *Multiscale Methods in Computational Mechanics*, Lecture Notes in Applied and Computational Mechanics, R. de Borst and E. Ramm (edts.), Springer Science and Business Media B.V., 215-231.

Fleming, J. F. (1979), "Nonlinear static analysis of cable-stayed bridge structures", *Computer and Structures*, 10(4), 621-635.

Fleming, J. F., Egeseli, E. A. (1980), 'Dynamic behavior of a cable-stayed bridge", *Earthquake Engineering and Structural Dynamics*, 8(1), 1-16.

Flint, A. R., McFadyen, A. N., Lau, C. K., and Wong, K. Y. (1995), "Wind and structural health monitoring system (WASHMS) for Lantau Fixed Crossing, Part II: performance requirement for bridge instrumentation system", *Bridges into the 21st Century*, Hong Kong Institution of Engineers, Hong Kong, 661-668.

Flint and Neill Partnership (1998), *Lantau fixed crossing and Ting Kau Bridge, wind and structural health monitoring criticality and vulnerability ratings review*, Highway Department, Government of Hong Kong, January, 1998.

Fox, R. L. and Kapoor, M. P. (1968), "Rates of change of eigenvalues and eigenvectors", *AIAA Journal*, 6, 2426-2429.

Friswell, M. I. (1989), "The adjustment of structural parameters using a minimum variance estimator", *Mechanical Systems and Signal Processing*, 3, 143-155.

Friswell, M. I. and Penny, J. E. T. (1992), "The effect of close or repeated eigenvalues on the updating of model parameters from FRF data", *Journal of Vibration and Acoustics*, ASME, 114, 514-520.

Friswell, M. I. and Mottershead, J. E. (1995), "*Finite Element Model Updating in Structural Dynamics*", Kluwer Academic Publishers.

Friswell, M. I. and Penny, J. E. T. (1997), "Is damage location using vibration measurements practical?", *EUROMECH 365 International Workshop: DAMAS 97, Structural damage assessment using advanced signal processing procedures*, Sheffield, June/July 1997, 351-362.

Friswell, M. I. and Mottershead, J. E. (2001), "Physical understanding of structures by model updating", *International Conference on Structural System Identification*, September 5-7, 2001, Kassel, Germany, 81-96.

Fritzen, C. P. (1986), "Identification of mass, damping, and stiffness matrices of mechanical systems", *Journal of Vibration, Acoustics, Stress, and Reliability in Design*, 108(1), 9-16.

Fritzen, C. P., Zhu, S. (1991), "Updating of finite element models by means of measured information", *Computers and Structures*, 40(2), Nonlinear Finite Element Analysis and ADINA, 475-486.

Fritzen, C. P. and Jennewein, D. (1998), "Damage detection based on model updating methods", *Mechanical Systems and Signal Processing*, 12(1), 163-186.

Ernst, J. H. (1965), "Der E-modul von seilen unter berucksienhtigung des durchanges." *Der Bauingenieur*, 40(2), 52-55 (in German).

Gladwell, G. M. L., and Ahmadian, H. (1995), "Generic element matrices suitable for finite-element model updating", *Mechanical Systems and Signal Processing*, 601-614.

Gmur, T. C., Schordoret, A. M. (1993), "A set of three-dimensional solid to shell transition elements for structural dynamics", *Computer and Structures*, 46(4), 583-591.

Golos, K. and Ellyin, F. (1988), "A total strain energy density theory for cumulative fatigue damage", *ASME Journal of Pressure Vessel Technology*, 110, 36-41.

Gosselet, O. A. P. and Kerfriden, P. (2011), "Improved multiscale computational strategies for delamination", *Multiscale Methods in Computational Mechanics*, Lecture Notes in Applied and Computational Mechanics, R. de Borst and E. Ramm (edts.), Springer Science and Business Media B.V., 261-279.

Gu, M., Xu, Y. L., Chen, L. Z., Xiang, H. F. (1999), "Fatigue life estimation of steel girder of Yangpu cable-stayed bridge due to buffering", *Journal of Wind Engineering and Industrial Aerodynamics*, 80, 384-400.

Guo, L. (2005), "Structural-state-assessment-oriented finite element modeling of long span bridge and its application (in Chinese)", *PhD Dissertation*, Southeast University, China.

Guo, Z. X. edt. (2007), *Multi-scale materials modeling-fundamentals and applications*, Woodhead Publishing Limited.

Gurney, T. R., Maddox, S. J. (1990), "An alternative to Miners rule for cumulative damage calculation", *Proceedings IABSE Workshop Remaining Fatigue Life of Steel Structures*, Vol.59, Zurich: IABSE.

Halford, G. R. (1966), "The energy required for fatigue", *Journal of Materials*, 1, 3-18.

Hall, B. M. (1970), "Linear estimation of structural parameters from dynamic test data", *Proceedings of AIAA/ASME 11th Structures, Structural Dynamics, and Materials Conference*, 193-197.

Hemez, F. M. (1993), "Theoretical and experimental correlation between finite element models and modal tests in the context of large flexible space structures", *PhD Dissertation*, University of Colorado, Blouder.

HKS, (1998), Hibbitt, Karlsson and Screnson Inc., *ABAQUS 5.8 Theory Manual*.

Harichandran, R. S. (1999), *Spatical Variation of Earthquake Ground Motion*, Department of Civil and Environmental Engineering, Michigan State University.

Housner, J. M., Aminpoir, M. A., Davila, C. G., Schiermeier, J. E., Stroud, W. J., Ransom, J. B., Gillian, R. E., (1995), "An interface element for global/local and substructuring analysis", *Proceedings of MSC World User's Conference*, May 8-12 1995, University City, California.

Housner, G. W., Bergman, L. A., Caughey, T. K., Chassiakos, A. G., Claus, R. O., Masri, S. F., Skelton, R. E., Soong, T. T., Spencer, B. F., Yao, J. T. P. (1997), "Structural control: past, present and future (section 7, health monitoring) ", *Journal of Engineering Mechanics*, *ASCE*, 123(9), 897-971.

HY/2002/01, (2002a), "*Particular specification section 31 - Wind and Structural Health Monitoring System: Shenzhen Western Corridor*", Arup and HKSAR Highways Department.

HY/2002/26, (2002b), "*Particular Specification Section 33 - Wind and Structural Health Monitoring System: Stonecutter Bridge*", Arup and HKSAR Highways Department.

Jahn, H. A. (1948), "Improvement of an approximate set of latent roots and modal columns of a matrix by methods akin to those of classical perturbation theory", *Quarterly Journal of Mechanics and Applied Mathematics*, 1, 132-144.

Jiang, F. F. (2010), "Analysis on structural seismic response and failure process by considering damage evolution (in Chinese)", *Master Thesis*, Southeast University, China.

Jung, H. and Ewins, D. J. (1992), "Error sensitivity of the inverse eigensensitivity method for model updating", *Proceedings of the 10th International Modal Analysis Conference,* San Diego, 992-998.

Kabe, A. M. (1985), "Stiffness matrix adjustment using mode data", *AIAA Journal,* 23(9), 1431-1436.

Kachanov, L. M. (1986), *Introduction to Continuum Damage Mechanics*, Martinus Nijhoff, The Netherlands.

Kang, J. S., Park, S. K., Shin, S., and Lee, H. S. (2005), "Structural system identification in time domain using measured acceleration", *Journal of Sound and Vibration*, 288, 215-234.

Kanok-Nukulchai, W. and Guan, H. (1993), "Nonlinear modeling of cable-stayed bridges", *Journal of Structural and Steel Research*, 26, 249-266.

Kaouk, M. and Zimmerman, D. C. (1994a), "Assessment of damage affecting all structural properties", *Proceedings of the 9th VPI and SU Symposium on Dynamics and Control of Large Structures*, 445-455.

Kaouk, M. and Zimmerman, D. C. (1994b), "Structural damage assessment using a generalized minimum rank perturbation theory", *AIAA Journal*, 32(4), 836-842.

Kaouk, M. and Zimmerman, D. C. (1994c), "Structural damage detection using measured modal data and no original analytical model", *Proceedings of the 12th International Modal Analysis Conference*, 731-737.

Kaouk, M. and Zimmerman, D. C. (1995), "Structural health assessment using a partition model update technique", *Proceedings of the 13th International Modal Analysis Conference,* 445-455.

Karoumi, R. (1999), "Some modeling aspects in the nonlinear finite element analysis of cable supported bridges", *Composite Structures*, 71, 397-412.

Khandelwal, Kapil (2008), "Multi-scale computational simulation of progressive ollapse of steel frames", *PhD Dissertation*, The University of Michigan, USA.

Kiddy, J., Pines, D. (1998), "Eigenstructure assignment technique for damage detection in rotating structures", *AIAA/ASME/ASCE/AHS/ASC Structures*, Structural Dynamics & Materials Conference, v 4, 3337-3346.

Kim, H. S., Hong, S. M. (1995), "Formulation of transition elements for the analysis of coupled walls structures", *Computers and structures*, 57(2), 333-344.

Ko, J. M., Ni, Y. Q. and Chan, T. H. T. (2000), "Feasibility of damage detection of Tsing Ma Bridge using vibration measurements", *Nondestructive Evaluation of Highways, Utilities, and Pipelines IV,* Aktan A.E. and Gosselin S.R. (edts.), SPIE 3995, 370-381.

Ko, J. M., Sun, Z. G. and Ni, Y. Q. (2002), "Multi-stage identification scheme for detecting damage in cable-stayed Kap Shui Mun Bridge", *Engineering Structures*, 24, 857-868.

Ko, J. M. and Ni, Y. Q. (2005), "Technology developments in structural health monitoring of large-scale bridges", *Engineering Structures*, 27, 1715-1725.

Krajcinovic, D. and Lemaitre, J. (1987), *Continuum Damage Mechanics: Theory and Applications*, Springer, Vienna.

Krishna, P., Arya, S. and Agrawal, T. P. (1985), "Effect of cable stiffness on cable-stayed bridges", *Journal of Structural Engineering*, ASCE, 111(9), 2008-2020.

Ladeveze, P., Nouy, A., Loiseau O. (2002), "A multi-scale computational approach for contact problems", *Computer Methods in Applied Mechanics and Engineering*, 191(43), 4869-4891.

Lau, C. K., Mak, W. P. N., Wong, K. Y., Chan, W. Y. K., and Man, K. L. D. (1999), "Structural health monitoring of three cable-supported bridges in Hong Kong", *Structural Health Monitoring 2000*: *Proceedings of the 2nd International Workshop on Structural Health Monitoring*, Chang, F. K. (edt.), Technomic, Lancaster, USA, 450-460.

Lau, C. K., Wong, K. Y., and Flint, A. R. (2000), "The structural health monitoring system for cable-supported bridges in Tsing Ma control area", *Proceedings of Workshop on Research and Monitoring of Long Span Bridges*, Cheung, Y. K. (edt.), Hong Kong, 14-23.

Law, S. S., Chan, T. H. T. and Wu, D. (2001), "Efficient numerical model for the damage detection of large scale structure", *Engineering Structures*, 23, 436-451.

Lee, I. W. and Jung, G. H. (1997), "An efficient algebraic method for the computation of natural frequency and mode shape sensitivities-Part II: Multiple natural frequencies", *Computers and structures*, 62(3), 437-443.

Leger, P., Ide, I. M. and Paultre, P. (1990), "Multiple-support seismic analysis of large structures", *Computers and Structure,* 36, 1153-1158.

Lemaitre, J., Chaboche, J. L (1990), *Mechanics of Solid Materials*, Cambridge, UK: Cambridge University Press.

Lemaitre, J. (1996), *A Course on Damage Mechanics*, Springer Verlag.

Lemaitre, J., Desmorat, R. (2005), *Engineering Damage Mechanics*, Springer-Verlag,

Li, J., and Kwauk, M. (2003), "Exploring complex systems in chemical engineering-the multi-scale methodology," *Chem. Eng. Sci.*, 58(3-6), 521-535.

Li, Z. X. (1995), "Viscoplastic damage model applied to cracking of gravity dam", *Theoretical and Applied Fracture Mechanics*, 22(1), 165-170.

Li, Z. X. and Xiao, L. G. (1996), "Finite element analysis of local damage and post - failure behavior for strain-softening solid", *International Journal of Fracture*, 80(1), 85-95.

Li, Z. X., Chan, T. H. T. and Ko, J. M. (2000), "Health monitoring and fatigue damage assessment of the bridge deck sections", *Nondestructive Evaluation of Highways, Utilities, and Pipelines IV*, Proceedings of SPIE, 7-9 March 2000, 3995, Aktan, A. E. and Gosselin, S. R. (edts.), 346-357.

Li, Z. X., Chan, T. H. T., Ko, J. M. (2001a), "Fatigue analysis and life prediction of the bridges with health monitoring data-Part I: methodology and strategy", *International Journal of Fatigue*, 23(1), 45-53.

Li, Z. X., Chan, T. H. T. and Ko, J. M. (2001b), "Fatigue damage model for bridge under traffic loading: application made to Tsing Ma Bridge", *Theoretical and Applied Fracture Mechanics*, 35(1), 81-91.

Li, Z. X., Ko, J. M. and Chan, T. H. T. (2001c), "Modeling of load interaction and overload effect on fatigue damage of steel bridges", *Fatigue and Fracture of Engineering Materials and Structures*, 24(6), 379-390.

Li, Z. X., Chan, T. H. T. and Ko, J. M. (2002a), "Evaluation of typhoon induced fatigue damage for Tsing Ma Bridge", *Engineering Structures*, 24(8), 1035-1047.

Li, Z. X., Chan, T. H. T. and Ko, J. M. (2002b), "Determination of effective stress range and its application on fatigue assessment of existing bridges", *International Journal of Solids and Structures*, 39(9), 2401-2417.

Li, Z. X., Sun, Z. H., Guo, L., Chan, T. H. T., Yu, Y. (2007), "Concurrent multi-scale modeling of structures and damage analyses", *Journal of Southeast University (Natural Science Edition)* 37(2), 251-260 (in Chinese).

Li, Z. X., Chan, T. H. T., Yu, Y., Sun, Z. H. (2009), "Concurrent multi-scale modeling of civil infrastructures for analyses on structural deteriorating-Part I: modeling methodology and strategy", *Journal of Finite Element in Analysis and Design*, 45(11), 782-794.

Liao, C. L., Reddy, J. N., Engelstad, S. P. (1988), "A solid-shell transition element for geometrically nonlinear analysis of laminated composite

structures", *International Journal for Numerical Methods in Engineering*, 26, 1843-1854.

Lim, K. B., Junkins, J. L. and Wang, B. P. (1987), "Ere-examination of eigenvector derivatives", *Journal of Guidance, Control and Dynamics*, 10(6), 581-587.

Lim, T. W. (1995), "Structural damage detection using constrained eigenstructure assignment", *Journal of Guidance, Control, and Dynamics*, 18(3), 411-418.

Lim, T. W. and Kashangaki, T. A. L. (1994), "Structural damage detection of space truss structure using best achievable eigenvectors", *AIAA Journal,* 32(5), 1049-1057.

Lin, R. M., Lim, M. K., and Du, H. (1995), "Improved inverse eigensensitivity method for structural analytical model updating", *ASME Journal of Vibration and Acoustics*, 117, 192-198.

Lindner, D. K. and Goff, R. (1993), "Damage detection. location and estimation for space trusses", *SPIE Smart Structures and Intelligent Systems: Smart Structures and Materials,* 1028-1039.

Liu, W. K., Karpov, E. G., Zhang, S. and Park, H. S. (2004), "An introduction to computational nano mechanics and materials", *Computer Methods in Applied Mechanics and Engineering*, 193(1720), 1529-1578.

Lu, X. Z., Lin, X. C., Ye, L. P. (2008), "Multi-scale finite element modeling and its application in structural analysis", *Journal of Huazhong University of Science and Technology (Urban Science Edition)*, 25(4), 76-80.

Ma, J. (2006), “Multiscale simulation using the generalized interpolation material point method, discrete dislocations and molecular dynamics”, *PhD Dissertation*, Oklahoma State University, USA.

Macdonald, K. A. and Haagensen, P. J. (1999), “Fatigue design of welded aluminum rectangular hollow section joints”, *Engineering Failure Analysis*, 6, 113-130.

MACRAS, *Manual of integrated experimental modal analyzing system for mechanical and structural modal analysis*, Nanjing AnZhen Software Engineeing Limited Company, 2009

Maguire, J. R. (1999), “Condition monitoring of structures: a briefing note for clients and owners”, *Proceedings of the Institution of Civil Engineers*, ICE, Thomas Telford, London, UK, 279-280.

Manson, S. S. (1966), “Interfaces between fatigue, creep, and fracture”, *International Journal of Fracture Mechanics*, 2, 328-363.

Manson, S. S., Halford, G. R. (1981), “Practical implementation of the double linear damage rule and damage curve approach for treating cumulative fatigue damage”, *International Journal of Fracture*, 17(2), 169-195.

Manson, S. S., Halford, G. R. (1986), “Re-examination of cumulative fatigue damage analysis-an engineering perspective”, *Engineering Fracture Mechanics*, 25(5-6), 539-571.

Markus J. Buehler (2008), “Multiscale modeling and simulation methods”, *Atomistic modeling of materials failure*, Springer, 157-181.

Matsuiski, M. and Endo, T. (1969), “Fatigue of metals subjected to varying stress”, *Japan Soc. Mech. Engineering*.

McCune, R. W. (1998), "Mixed dimensional coupling and error estimation in finite element stress analysis", *PhD Dissertation*, The Queen's University of Belfast.

McCune, R. W., Armstrong, C. G., Robinson, D. J. (2000), "Mixed dimensional coupling in finite element models", *International Journal for Numerical Methods in Engineering*, 49, 725-750.

McGown, A., Wright, H. D., Michie, C. (1997a), "Integrated, multilevel condition monitoring of structures", *The Structural Engineer*, 75(6), 91-94.

McGown, A., Wright, H. D., Michie, C. (1997b), "Discussion on integrated, multilevel condition monitoring of structures", *The Structural Engineer*, 75(14), 245-247.

McGowan, P. E., Smith, S. W. and Javeed, M. (1990), "Experiments for locating damage members in a truss structure", *Proceedings of the 2nd USAF/NASA Workshop on System Identification and Health Monitoring of Precision Space Structures*, 571-615.

Michopoulos, J. G., Farhat, C., Fish, J. (2005), "Modeling and simulation of multi-physics systems", *Journal of Computing and Information Science in Engineering*, 5(2), 198-213.

Minas, C. and Inman, D. J. (1988), "Correcting finite element models with measured modal results using eigenstructure assignment methods", *Proceedings of the 6th International Modal Analysis Conference,* 583-587.

Minas, C. and Inman, D. J. (1990), "Matching finite element models to modal data", *Transactions of the ASME, Journal of Vibration and Acoustics,* 1, 84-92.

Miner, M. A. (1945), "Cumulative damage in fatigue", *Journal of Applied mechanics*, 12(3), 159-64.

Monaghan, D. J., Doherty, I. W., McCourt, D., Armstrong, C. G. (1998), "Coupling 1D beams to 3D bodies", *7th International Meshing Roundtable*. Sandia National Laboratories, Dearborn, Michigan, 285-293.

Monaghan, D. J. (2000), "Automatically coupling elements of dissimilar dimension in finite element analysis", *PhD Dissertation*, The Queen's University of Belfast.

Monti, G., Nuti, C. and Pinto, P. E. (1996), "Nonlinear response of bridges under multi-support excitation", *Journal of Structural Engineering*, ASCE, 122, 1147-1159.

Mori, Y., Ellingwood, B. R. (1993), "Reliability-based service-life assessment of aging concrete structures", *Journal of Structural Engineering,* 119(5), 1600-1621.

Moses, F., Schilling, C. G., *et al*. (1986), "Fatigue evaluation procedures for steel bridge", *NCHRP Report 299*, National Academy Press, Washington D.C.

Moss, R. M., and Matthews, S. L. (1995a), "In-service structural monitoring: a state-of the-art review", *The Structural Engineer*, 73(2), 23-31.

Moss, R. M., and Matthews, S. L. (1995b), "Discussion on in-service structural monitoring: a state-of the-art review", *The Structural Engineer*, 73(13), 214-217.

Mottershead, J. E. and Friswell, M. I. (1993), "Model updating in structural dynamics: a survey", *Journal of Sound and Vibration*, 167(2), 347-375.

Mufti, A. A. (edt.) (2002), "Structural Health Monitoring", *Proceedings of the 1st International Workshop on Structural Health Monitoring of Innovative Civil Engineering Structures*, ISIS Canada Corporation, Winnipeg, Canada.

Nackenhorst, U., Kardas, D., Helmich, T., Lenz, C. and Shan, W. Z. (2011) "Computational techniques for multiscale analysis of materials and interface", *Modelling, Simulation and Software Concepts*, E. Stephan and P. Wriggers (edts.), LNACM 57, Springer,133-167.

Nakai, H., Kitada, T., Ohminami, R. and Nishimura, T. (1985), "Elasto-plastic and finite displacement analysis of cable-stayed bridges", *Memoires of the Faculty of Engineering*, Osaka University, 26, 251-271.

Natke, H. G., Cottin, N. and Prells, U. (1994), "Problems and related counter-measures in mathematical model improvement: a survey", *Structural safety and reliability*, G. I. Schueller, M. Shinozuka, and J. T. P. Yao (edts.), Balkema, Rotterdam, The Netherlands, 821-827.

Nazmy, A. S., Abdel-Ghaffar, A. M., (1990a), "Nonlinear earthquake response analysis of long-span cable-stayed bridges: theory", *Earthquake Engineering and Structural Dynamics*, 9(1), 45-62.

Nazmy, A. S., Abdel-Ghaffar, A. M., (1990b), "Nonlinear earthquake response analysis of long-span cable-stayed bridges: applications", *Earthquake Engineering and Structural Dynamics*, 19(1), 63-76.

Nelson, R. B. (1976), "Simplified calculations of eigenvector derivatives", *AIAA Journal,* 14, 1201-1205.

Nethercott, A. (1993), "Coupling differing finite element types", *Master Thesis*, The Queen's University, Belfast, UK.

Niemi, E. (1997) “Random loading behavior of welded components”, *Proceedings of the IIW International conference on performance of dynamically loaded welded structures*. New York: Welding Research Council, 1997.

Okauchi, Isao, Miyata, Toshio, Tatsumi, Masaaki and Sasaki, Nobuyuki (1997), “Field vibration test of a long-span cable-stayed bridge using large exciters”, *Journal of Structural Mechanics and Earthquake Engineering*, 1, 1997.

Peng, X. L. (2003), “Baseline finite element model of large-span cable-stayed bridges for health monitoring (in Chinese)”, *Maser thesis*, Fuzhou University, China.

Ramm, E., Erhart, A., Hettich, T., Bruss, I., Hilchenbach, F. and Kato, J. (2011), “Damage propagation in composites: multiscale modeling and optimization”, *Multiscale Methods in Computational Mechanics*, Lecture Notes in Applied and Computational Mechanics, R. de Borst and E. Ramm (edts.), Springer Science and Business Media B.V., 281-304.

Reissner, E. (1947), “On bending of elastic plates”, *Quarterly of Applied Mathematics*, 5, 55-68.

Ren, W. X. (1997), “Nonlinear static and seismic behaviors of long span cable-stayed bridges”, *Res. Rep. No. 2*, Dept. of Civil Engineering, Nagoya Institute of Technology.

Ren, W. X., Blandford, G. E., and Harik, I. E. (2004a), “Roebling suspension bridge - I: Finite-element model and free vibration response”, *Journal of Bridge Engineering*, 9(2), 110-118.

Ren, W. X., Zong, Z. H. (2004b), "Output only modal parameter identification of civil engineering structures", *Structural Engineering and Mechanics*, 17(3-4), 429-444.

Rodden, W. P. (1967), "A method for deriving structural coefficients from ground vibration tests", *AIAA Journal*, 5, 991-1000.

Ross, R. G. Jr. (1971), "Synthesis of stiffness and mass matrices from experimental vibration modes", *SAE Conference paper,* 710787, 2627-2635.

Rudd, R. E., Broughton, J. Q. (2000), "Concurrent coupling of length scales in solid state system", *Phys Stat Sol*, 217(2), 251-291.

Rychlik, I. (1987), "A new definition of the rainflow cycle counting method", *International Journal of Fatigue,* 9(2), 119-121.

Rytter, A. (1993), "Vibration based inspection of civil engineering structures", *PhD Dissertation*, Department of Building Technology and Structural Engineering, Aalborg University.

Saraf, V. K. (1998), "Evaluation of existing RC slab bridges", *Journal of Performance Constructed Facilities*, ASCE, 12(1), 20-24.

Savaidis, G. and Vormwald, M. (2000), "Hot spot stress evaluation of fatigue in welded structural connections supported by finite element analysis", *International Journal of Fatigue,* 22, 85-91.

Schilling, C. G. *et al*. (1978a), "New method for fatigue design of bridge", *Journal of Structural Engineering*, ASCE, 104(ST3).

Schilling, C. G. *et al*. (1978b), "Fatigue of welded steel bridge members under variable-amplitude loadings", *NCHRP Report 188*, National Academy Press, Washington D.C.

Schijve, J. (1996), "Predictions on fatigue life and crack growth as an engineering problem, a state of the art survey", In *Fatigue 96'*, Oxford, Pergamon, 1149-1164.

Schiermeier, J. E., Housner, J. M., Aminpour, M. A.,Stroud, W. J. (1997), "Interface elements in global/local analysis-part 2 surface interface elements", *Proceedings of MSC World User's Conference*, Newport Beach, California, November 17-20.

Schluter, L. (1991). *Programmer's Guide for LIFE2's Rainflow Counting Algorithm*. Sandia Report SAND90-2260.

Seif, S. P. and Dilger, W. H. (1990), "Nonlinear analysis and collapse load of PC cable-stayed bridges", *Journal of Structural Engineering,* ASCE, 116(3), 829-849.

Shepherd, R., and Frost, J. D. (1995), *Failures in Civil Engineering: Structural, Foundation, and Geo-environmental Case Studies*, ASCE, New York.

SIAM Journal on Multiscale Modeling and Simulation.

Sih, G. C. and Spyropoulos, C. P. (2002), "*International Symposium of Multiscaling in Mechanics*", Sih, G. C. and Spyropoulos, C. P. edts., National Technical University of Athens Press, Athens.

Sih, G. C., Tu, S. T., Wang, Z. D. edts. (2003), *Structural Integrity and Materials Aging：Fracture Mechanics and Applications*, East China University of Science and Technology Press, Shanghai.

Sih, G. C., Tu, S. T., Wang, Z. D. edts. (2004a), *Environment Effects on Fracture and Damage：Fracture Mechanics and Applications*, Zhejiang University Press, Hangzhou.

Sih, G. C., Kermanidis, T. B., Pantelakis, S. G. edts. (2004b), *Multiscaling in Applied Science and Emerging Technology: Fundamental and Application in Mesomechanics*. University of Patras, Greece, 2004.

Sih, G. C.,Vu, T., Khanh, edts. (2005), "Materials for safety and health-mesoscopic and multiscale consideration in modern science and engineering", *Proceedings of the 7th International Conference On Mesomechanics*, August 1-4, 2005, Montreal, Canada, Montreal Library and Archives Canada Cataloguing in Publication.

Sih, G. C., Tu, S. T., Wang, Z. D. edts. (2006), *Multiscaling Associated with Structural and Material Integrity under Elevated Temperature,* East China University of Science and Technology Press, Shanghai, 2006.

Sih, G. C. edt. (2007), *Multiscaling in Molecular and Continuum Mechanics: Interaction of Time and Size from Macro to Nano*, Springer, 2007.

Sih, G. C., (2009), "Modeling of multiscale fatigue crack growth_nanomicro and micromacro transitions", *Virtual Testing and Predictive Modeling*, B. Farahmand (edt.), Springer Science and Business Media, LLC 2009, 187-219.

Sih, G. C. edt. (2010), "*The 12th International Congress on Mesomechanics*", June 21-25, Taipei, Taiwan.

Sih, G. C. edt. (2011), "*The 13th International Congress on Mesomechanics*", July 6-8, Vicenza, Italy.

Sjostrom, C. (1997), "Overview of methodologies for prediction of service life", Masters, L. W. (edt.) *Problems in Service Life Prediction of Building and Construction Materials*. Kluwer Academic Publishers, 3-20.

Smith, S. W. and Beattie, C. A. (1991), "Model correlation and damage location for large space truss structures: Secant method development and evaluation", *NASA Report* NASA-CR-188102.

Sohn, H., Farrar, C. R., Hemez, F. M., Shunk, D. D., Stinemates, D. W., and Nadler, B. R. (2004), "A review of structural health monitoring literature: 1996-2001", *Report No. LA-13976-MS*, Los Alamos National Laboratory, Los Alamos, New Mexico.

Stubbs, N., Park, S., Sikorsky, C., Choi, S. (2000), "A global non-destructive damage assessment methodology for civil engineering structures", *International Journal of Systems Science*, 31(11), 1361-1373.

Sun, Z. H. (2006), "Multi-scale modeling dealing with local details for long span steel bridges and its applications (in Chinese)", *PhD Dissertation*, Southeast University, China.

Tang, Y. Q. (2011), "Analyses on damage and dynamic response of structures under strong loads by trans-scale modeling (in Chinese) ", *Master Thesis*, Southeast University, China.

Timoshenko, S. P., Goodier, J. N. (1970), *Theory of Elasticity*, 3rd Edition, New York, McGraw-Hill Inc.

Tinsley, O. J., Prudhomme, S., Romkes, A., and Bauman, P. (2005), "Multiscale modelling of physical phenomena: adaptive control of models", *Technical Report ICES Report 05-13*, ICES, University of Texas, Austin.

The 3rd International Conference on Damage Assessment of Structures, Dublin, Ireland, 1999.

The 6th International Symposium on Nondestructive Evaluation of Aging Infrastructure, Newport Beach, CA, 2001.

The 3rd International Structural Health Monitoring Workshop, Palo Alto, CA, 2001.

Titurus, B., Friswell, M. I., and Starek, L. (2003a), "Damage detection using generic elements Part I model updating", *Computers and Structures*, 81, 2273-2286.

Titurus, B., Friswell, M. I., and Starek, L. (2003b), "Damage detection using generic elements Part II damage detection", *Computers and Structures*, 81, 2287-2299.

Ting, T. (1992), "Accelerated sub-space iteration for eigenvector derivatives", *AIAA Journal*, 30(8), 2114-2118.

Virlogeux M., (1992), "Wind design and analysis for the Normandy Bridge", *Larsen, A. (edt.) Aerodynamics of Large Bridges*. Rotterdam, Belkema, 183-216.

Wahab, M. M., Roeck, G. D. (1999), "Damage detection in bridges using modal curvatures: application to a real damage scenario", *Journal of Sound Vibration*, 226 (2), 217-235.

Weinan, E. and Bjorn, E. (2003), "Multi-scale modeling and computation", *Notices of the American Mathematical Society*, 50(9), 1062-1070.

Weinan, E, and Engquist, B. (2003), "The heterogeneous multiscale methods," *Commun. Math. Sci.*, 1(1), 87-132.

Wilson, J. C. and Gravelle, W. (1991a), "Ambient vibration measurement and a cable-stayed bridge", *Earthquake Engineering and Structural Dynamics*, 20(8), 723-747.

Wilson, J. C., Gravelle, W. (1991b), "Modeling of a cable-stayed bridge for dynamic analysis", *Earthquake Engineering and Structural Dynamics,* 20, 707-722.

Wong, K. Y., Chan, W. Y. K., Man, K. L., Mak, W. P. N., and Lau, C. K. (2000a), "Results of structural health monitoring for cable-supported bridges in Tsing Ma control area", *Proceedings of the International Workshop on Research and Monitoring of Long Span Bridges*, Cheung, Y. K. (edt.), Hong Kong, 158-172.

Wong, K. Y., Lau, C. K., and Flint, A. R. (2000b), "Planning and implementation of the structural health monitoring system for cable-supported bridges in Hong Kong", *Nondestructive Evaluation of Highways, Utilities, and Pipelines IV*, Aktan, A. E. and Gosselin, S. R. (edts.), SPIE, 3995, 266-275.

Wong, K. Y., Chan, K. W. Y., Man, K. L., Mak, W. P. N., and Lau, C. K. (2000c), "Structural health monitoring results on Tsing Ma, Kap Shui Mun and Ting Kau Bridges", *Nondestructive Evaluation of Highways, Utilities, and Pipelines IV*, Aktan, A. E. and Gosselin, S. R. (edts.), SPIE, 3995, 288-299.

Wong, K. Y., Man, K. L. and Chan, W. Y. (2001a), "Monitoring Hong Kong's bridges: real-time kinematic spans the gap", *GPS World*, 12(7), 10-18.

Wong, K. Y., Chan, K. W. Y., and Man, K. L. (2001b), "Monitoring of wind load and response for cable-supported bridges in Hong Kong", *Health*

Monitoring and Management of Civil Infrastructure Systems, Chase, S. B. and Aktan, A. E. (edts.), SPIE, 4337, 292-303.

Wong, K. Y., Man, K. L., and Chan, W. Y. (2001c), "Application of global positioning system to structural health monitoring of cable-supported bridges", *Health Monitoring and Management of Civil Infrastructure Systems*, Chase, S. B. and Aktan, A. E. (edts.), SPIE, 4337, 390-401.

Wong, K. Y. (2004), "Instrumentation and health monitoring of cable-supported bridges", *Structural Control and Health Monitoring*, 11(2), 91-124.

Wong, K. Y. (2007), "Stress and traffic loads monitoring of Tsing Ma Bridge", *Proceedings of China Bridge Congress 2007*, Chongqing, China, March 28-30 2007.

Worden, K., Farrar, C. R., Manson, G., and Park, G. (2005), "Fundamental axioms of structural health monitoring", *Structural Health Monitoring 2005-Advancements and Challenges for Implementation*, Chang, F. K. (edt.), DEStech Publications, Lancaster, Pennsylvania, 26-41.

Wu, B. J., Li, Z. X., Tang, K. K. (2007), "Multi-scale modeling and damage analyses of large civil structure-multi-scale mechanics from material to structure", *Advances in Mechanics*, 37(3), 321-336.

Wu, Z. S. and Abe, M. (edts.) (2003), "Structural health monitoring and intelligent infrastructure", *Proceedings of the 1st International Conference on Structural Health Monitoring and Intelligent Infrastructure*, A.A. Balkema, Rotterdam, Netherlands.

Xia, H., Xu, Y. L., Chan, T. H. T (2000), "Dynamic interaction of long suspension bridge with running trains", *Journal of Sound and Vibration*, 237, 263-280.

Xu, Y. L., Ko, J. M., Yu, Z. (1997), "Modal analysis of tower-cable system of Tsing Ma long suspension bridge", *Engineering Structures*, 19(10), 857-867.

Xu, Y. L., Zhu, L. D., and Xiang, H. F. (2003), "Buffeting response of long suspension bridges to skew winds", *Journal of Wind and Structures*, 6(3), 179-196.

Xu, Y., Hu, S. D. and Wang, Z. Q. (2003), "Seismic response analysis and performance evaluation of the main span of lupu bridge", *Proceedings of the 15th National Bridge and Structural Academic Conference*, 396-403.

Yeung, K. C., Lau, C. K., Wong, K. Y., Flint, A. R., and McFadyen, A. N. (1995), "Wind and structural health monitoring system (WASHMS) for Lantau Fixed Crossing Part I: system planning and design", *Bridges into the 21st Century*, Hong Kong Institution of Engineers, Hong Kong, 539-548.

Yin, A. G. (2006), "Experimental research on static and dynamic responses of bridge longitudinal truss with typical welded details (in Chinese)", *Master Thesis*, Southeast University, China.

Zak, M. (1983), "Discrete model improvement by eigenvector updating", *Journal of Engineering Mechanics,* ASCE, 109(6), 1437-1444.

Zhan, S., Ko, J. M., Xu, Y. L., Ni, Y. Q. (1999), "An uniformization method for ambient vibration modal analysis of extra large constructions", *Journal of Jinan University*, 20(1), 28-33.

Zhang, Q., Lallement, G., Fillod, R. and Piranda, J. (1987), "A complete procedure for the adjustment of a mathematical model from the identified complex modes", *Proceedings of the 5th International Modal Analysis Conference,* London, U.K., 1183-1190.

Zhang, Q. W., Chang, C. C. and Chang., T. Y. P. (2000), "Finite element model updating for structures with parametric constraints", *Earthquake Engineering and Structural Dynamics*, 29, 927-944.

Zhang, Q. W., Chang, T. Y. P. and Chang. C. C. (2001), "Finite-element model updating for the Kap Shui Mun cable-stayed bridge", *Journal of Bridge Engineering,* July/August 2001, 285-293.

Zhao, Z. W., Haldar, A. (1996), "Bridge fatigue damage evaluation and updating using non-destructive inspections", *Engineering Fracture Mechanic*, 53(5), 775-788.

Zheng, X. L., Li, Z., Shi, Y. J., Yang, Y. M., Shi, Z. J. (1996), "Fatigue performance of old bridge steel and the procedures for life prediction with given survivability", *Engineering Fracture Mechanics*, 3(2), 251-262.

Zhou, T. Q. (2003), "Hot spot stress analysis of steel bridge components and numerical simulation of fatigue damage accumulation (in Chinese)", *PhD Dissertation*, Southeast University, China.

Zhu, L. D., Xiang, H. F., Xu, Y. L. (2000), "Triple-girder model for modal analysis of cable-stayed bridges with warping effect", *Engineering Structures,* 22(10), 1313-1323.

Ziaei-Rad, S., Imregun, M. (1996), "On the accuracy required of experimental data for finite element model updating", *Journal of Sound and Vibration*, 196(3), 323-336.

Zimmerman, D. C. and Widengren, M. (1990), "Correcting finite element models using a symmetric eigenstructure assignment technique", *AIAA Journal*, 28(9), 1670-1676.

Zimmerman, D. C. and Kaouk, M. (1992), "Eigenstructure assignment approach for structural damage detection", *AIAA Journal,* 30(7), 1848-1855.

Zimmerman, D. C., and Smith, S. W. (1992), "Model refinement and damage location for intelligent structures", *Intelligent Structural Systems*, Tzou, H. S., and Anderson, G. L. (edts.), Kluwer Academic Publishers, Boston, Massachusetts, 403-452.

Zimmerman, D. C. and Kaouk, M. (1994), "Structural damage detection using a minimum rank update theory", *Journal of Vibration and Acoustics,* 116, 222-230.

Zimmerman, D. C., Kaouk, M. and Simmermacher, T. (1995), "Structural damage detection using frequency response functions", *Proceedings of the 13th International Modal Analysis Conference*, 179-184.

Zimmerman, D. C., Simmermacher, T. W., and Kaouk, M. (2005), "Model correlation and system health monitoring using frequency domain measurements", *Structural Health Monitoring*, 4, 213-227.

Zohdi, T., and Wriggers, P. (2004), "Introduction to computational micromechanics," *Lecture Notes in Applied and Computational Mechanics*. Springer, Berlin.

Zong, Z. H., Wang, T. L., Huang, Z. and Zheng, Z. F. (2002), "State-of-the-art report of bridge health monitoring", *Journal of Fuzhou University (Natural Science)*, 30(2), 127-152.